Development of a Mathematical Model to Understand, Design & Improve Oncolytic Virus Therapies

Cory Batenchuk

Thesis submitted to the

Faculty of Graduate and Postdoctoral Studies

in partial fulfillment of the requirementas

for the Doctorate in Philosophy degree in Biochemistry, Microbiology & Immunology

with a specialization in human and molecular genetics.

Department of Biochemistry, Microbiology & Immunology

Faculty of Medicine,

University of Ottawa

Abstract

Oncolytic viruses (OVs) are emerging as a potent therapeutic platform for the treatment of malignant disease. The tumor cells inability to induce antiviral defences in response to a small cytokine known as interferon (IFN) is a common defect exploited by OVs. Heterogeneity in IFN signalling across tumors is therefore a pillar element of resistance to these therapies. I have generated a mathematical model and simulation platform to study the impact of IFN on OV dynamics in normal and cancerous tissues. In the first part of my thesis, I used this model to identify novel OV engineering strategies which could be implemented to overcome IFN based resistance in tumor tissues. From these simulations, it appears that a positive feedback loop, established by virus-mediated expression of an interferon-binding decoy receptor, could increase tumor cytotoxicity without compromising normal cells. The predictions set forth by this model have been validated both qualitatively and quantitatively in in-vitro and in-vivo models using two independent OV strains. This model has subsequently been used to investigate OV attenuation mechanisms, the impact of tumor cell heterogeneity, as well as drug-OV interactions. Following these results, it became apparent that selectivity should equally be observed when overwhelming the cell with a non replicating virus. While normal tissues will clear this pseudo-infection rapidly, owing to their high baseline in antiviral products at the onset of infection, tumor cells with defective anti-viral pathways should not have readily available biomachinery required to degrade this pro-apoptotic signal. Recapitulated by the mathematical model, non-replicating virus-derived particles generated by means of UV irradiation selectively kill tumor cells in cultured cell lines and patient samples, leading to long term cures in murine models. Taken together, this thesis uses a novel mathematical model and simulation platform to understand, design & improve oncolytic virus-based therapeutics.

Table of Contents

List of Figures

List of Abbreviations

ATP: Adenosine Tri-phosphate

BST2: Bone-stromal cell antigen II

B19R: An IFN decoy receptor from vaccinia virus

CAFs: Cancer associated fibroblast

L1210: An acute lymphocytic leukemia cell line

CD33: Siglec-3

CML: Chronic myelogenous leukemia

CpG: Cytosie—phosphate—guanine

CTL: Cytotoxic T-Cells

CT26: Resistant murine colon cancer cell line

DR: Decoy receptor

dsRNA: Double-stranded ribonucleic acid

ECM: Extracellular matrix

EIF2A: Eukaryotic translation initiation factor 2A

GDEPT: Gene-directed enzyme pro-drug therapies

GFP: Green fluorescent protein

GM-CSF: Granulocyte macrophage colony stimulating factor

GM38: A normal fibroblast cell line

GO: Gene-Ontology

G-protein: Glycoprotein

HDAC: Histone Deacetylase

HDF: Human dermal fibroblast

HSCT: Hematopoietic stem cell transplantation

HSV: Herpes simplex virus

HT29: Resistant human colon cancer cell line

IAP: Inhibitors of apoptosis

ICP34.5: Infected cell protein 34.5 from herpes simplex virus

ICP47: Infected cell protein 47 from herpes simplex virus

IDE: IFN decoy-expressing

Intron A: Interferon Alpha 2b

IFN: Interferon

IRF: Interferon regulatory factor

ISG: Interferon stimulated genes

ISGF3: Interferon stimulated gene factor 3

I.T.: Intratumoral

I.V.: Intravenous

IVIS: In vivo imaging system

ISGs: Interferon stimulated genes

JAK: Janus kinase

JAKi: Janus kinase inhibitor

LacZ: β-galactosidase

Maraba: The wildtype isolate of Maraba Virus

MHC: Major Histocompatibility Complex

MDA: Microtubule-destabilizing agent

MG1: An attenuated Maraba virus strain harboring a substitution in both the glycoprotein and matrix protein substitutions.

MOI: Multiplicity of infection

M-protein: Matrix Protein

MRC5: A normal fibroblast cell line

MTD: Maximum tolerated dose

MX1: Myxovirus resistance 1

NAN: Not a Number

NFs: Normal fibroblasts

NKs: Natural killer cells

NRRPs: Non-replicating rhabdovirus-derived particles

ODE: Ordinary differential equation

OV: Oncolytic virus

PBS: phosphate-buffered saline

PDGF: Platelet-derived growth factor

PET-Scans: Positron emission tomography scan

PFU: Plaque forming units

PI: Propidium Iodine

PKR Protein kinase R

RANTES: Regulated on activation normal T cell expressed and secreted

RIG-I: Retinoic acid inducible gene I

RVs: Rhabdoviruses

SAHA: suberoyl anilide hyroxamic acid

s.d.: Standard deviation

SMAC: Second mitochondria-derived activator of caspases

ssRNA: Single- stranded ribonucleic acid

STATs: Signal transducer activators of transcription

TGFβ: Transforming growth factor β

TAP: Transporter associated with antigen presentation

TBK: Tank binding kinase

TIL: Tumor Infiltrating Leukocytes

TK: Thymidine kinase

TKI: Tyrosine kinase Inhibitor

TLP: Talimogene laherparepvec

TLR: Toll-like receptors

UV: Ultraviolet

vGF: Vaccinia growth factor

vTK: Vaccinia thymidine kinase

VSe: Virus Sensitizing agent

VSV: Vesicular Stomatitis Virus

VSVΔ51: An attenuated Vesicular Stomatitis Virus strain harboring a deletion of Methionine 51 in the Matrix protein

vvDD: Vaccinia double deleted mutant

WI38: A normal fibroblast cell line

WT: Wild type

X-Gal: 5-bromo-4-chloro-3-indolyl-β-D-galactopyranoside

Δ51: An attenuated Vesicular Stomatitis Virus strain harboring a deletion of Methionine 51 in the Matrix protein

786-0: A resistant renal carcinoma cell line

List of Symbols

[$]: Published supplementary high-throughput dataset not shown in thesis

[$$$]: Published supplementary data not shown in thesis as produced by another author

AP: Activated population

DR: decoy receptor

DR-IFN: decoy receptor-IFN complex

EC_{50}: the EC50 of IFN

γ_c: The rate of cell death

γ_{DR}: The rate of decoy degradation

γ_n: The rate of NRRP degradation

γ_V: The rate of virus degradation

γ_{IFN}: The rate of IFN degradation

IFN: interferon

IP: Infected population

$K_{Bud\ IP}$: The virus production rate from IP

$K_{Bud\ AP}$: The virus production rate from AP

K_{DR_IP}: The rate of decoy receptor production from IP

K_{DR_AP}: The rate of decoy receptor production from AP

K_f: The forward rate constant for IFN-Decoy complex formation

K_{IFNon}: The rate of IFN signaling activation

K_{IFNoff}: The rate of IFN signalling inactivation

K_{IFN1}: The IFN production rate from IP

$K_{IFN2.1}$: The IFN production rate from AP

$K_{IFN2.2}$: The IFN production rate from PP

K_{NI}: The rate of NRRP internalization

K_{NC}: The rate NRRP clearance from AP

K_r: The reverse rate constant for IFN-Decoy complex degradation

K_{VC}: The rate viral clearance from AP

$K_{vi.}$: The rate of virus infection

N: NRRPs

PP: Protected population

UP: Uninfected population

V: virus

Acknowledgements

First and foremost, I would like to thank Drs. John Bell and Mads Kaern for offering me a unique work environment where I could fulfill my personal research interests. By working on both theoretical and experimental aspects of several ongoing research projects, and being strongly influenced to work in collaboration with others, I have had the opportunity to develop a unique skill set and maintain a high level of productivity during my graduate degree. I would equally like to thank all the members with whom I have worked with over the years. This includes Drs. Rozanne Arulanandam, Fabrice LeBoeuf, Carolina Ilkow, and MD. David Conrad. Not only did these collaborations advance the presented research, but these people provided me with the necessary training to develop my skills over the course of my PhD. I would also like to thank my thesis advisory committee members, Drs. Harold Atkins, Jean-Simon Diallo, and David Stojdl, for helping guide my research and the overall structure of my thesis, as well as my wife, Katy Morin, for her support during my PhD.

Chapter I. General Introduction

1.1 The Process of Tumorigenesis

Cancer is a malignant disease resulting from unregulated & perpetual division of a defective host cell. If left untreated, these cells will undergo clonal expansion and evolve to eventually overwhelm the population within the affected organs. As the tissue accumulates these defective cells, the organ will gradually lose its function and drive the pathology of the disease. To become cancerous, the malignancy must acquire several key characteristics commonly referred to as the hallmarks of cancer (1, 2). These defects allow for the cancer cells to not only sustain perpetual growth, but evade destruction by the ensuing immune response against the tumor.

In cancer, chronic proliferation requires the rewiring of processes involved in the regulation of cell number homeostasis (3). Under normal conditions, cell abundance is defined by a plethora of growth factors and adhesion molecules which allow for the organ to relay system level information regarding cell number requirements to cell cycle control (4). These pathways, critical throughout development, allow for the organism to replenish aging cells and repair tissue following injury (4). Several of the factors involved are in fact oncogenes whose dysfunction has the potential to cause cancer. Chronic activation of these pathways ensures that the cell proliferation signalling axis is persistently "ON" in tumors. This is achieved by up-regulating the secretion of these same growth factors involved in regulating cell number homeostasis (e.g. Transforming Growth Factor β (5) & Vascular Endothelial Growth Factor (6)), and by enabling constitutive activation of their downstream target receptors (e.g. Human

Epidermal Growth Factor Receptors (7) & Platelet Derived Growth Factor Receptors (8)) or kinases (e.g. B-Rapidly Accelerated Fibrosarcoma Kinase (9) & Thymidine Kinase (10)). To ensure that continuous proliferation remains unresolved, the cell must equally inactivate tumor suppressors which would otherwise resolve the situation, in part by inducing growth arrest. Perhaps the best described mutations in growth suppressors involve those repressing the function of the tumor suppressor p53 which, when functional, would otherwise induce cell cycle arrest following the accumulation of DNA damage (11).

As the tumor evolves, cancer cells must compensate for the increased metabolic and energetic demand required for continuous proliferation. This is believed to in part be achieved by undergoing a glycolytic switch. Also known as the Warburg effect, cancer cells favour energy production along the glycolysis axis, followed by lactic acid fermentation, rather than through Krebs cycle in the mitochondria (2, 12). Although its role in cancer remains enigmatic, an emerging line of thought is that this glycolytic switch increases the abundance of key precursors required for the biosynthesis of nucleotides and amino acids while at the same time ensuring a continuous supply of energy (12). For example, several amino acids, such as Serine, Cysteine, Glycine, Tyrosine, Phenylalanine, and Alanine, have precursors generated by glycolysis (12). Furthermore, glucose-6-phosphate produced during this first step of glycolysis may be diverted to the pentose phosphate pathway to promote nucleoside biosynthesis (13). Indeed glucose-6-phosphate transformation to nucleotides via the pentose phosphate pathway is a key process in cell division which is actively repressed by the tumor suppressor p53 (14, 15). The Warburg effect, in conjunction with the activation of parallel metabolic processes, such as increased glutamine uptake and up-regulated folate metabolism, ensures that cancer cells not only meet the

energy requirements for cell division, but equally accumulates the biomaterial precursors necessary to sustain continuous cell proliferation. Without this effect, perpetual cell divisions would eventually result in cell death owing to a lack of sufficient metabolites (16).

Although the hallmarks of cancer can be bestowed by epigenetics (17) resulting from chronic activation of wound healing and developmental signalling pathways (18), these defects have the potential to be fixed within the population through gene mutation. This factor, typically viewed as the pillar element involved in the onset of cancer, is favoured by positive selection throughout tumorigenesis (19). This will ensure that the trait is fixed within the cells following loss of the epigenetic cue (20). However, novel antigens produced by gene mutation or fusion have the potential to be recognized by the immune system, resulting in destruction of the associated cancer cells (21, 22). As such, mutation accumulation requires evasion of anti-tumor immune responses throughout tumorigenesis (21, 22).

Upon the presentation of foreign antigens, the immune response recognizes the abnormality and destroys the cell with the associated defect. Classically viewed as a response to recognize and remove foreign pathogens, this process plays an important role in regulating tumor cell turnover (21). Cancer cells substantially remodel both innate and adaptive immune responses in the local tumor microenvironment to evade destruction by immuno-surveillance mechanisms (23). This is achieved by accumulating mutations within antigen presentation pathways (24, 25) as well as by secreting immunosuppressive cytokines to dampen the adaptive immune responses (26-28), and eventually generate tolerance against these foreign tumor-associated antigens (29).

Immunoediting is the term used to describe the process by which tumor cells acquire these defects (21, 22). During the initial phase of elimination, mutations and the resulting cellular

stress activate innate immune processes in tumor cells. These mechanisms trigger tumor cell death though both the activation of intrinsic apoptotic pathways as well as the recruitment of innate immune cells such as Natural Killer Cells, gamma delta T cells, and natural killer t-cells. In addition to direct promoting apoptosis, cytokines released by these cells allows for antigen presenting cells, most commonly dendritic cells, to uptake the resulting apoptotic debris and present tumor-associated antigens. Presentation of novel immunoreactive antigens resulting from gene mutation will allow for naïve T-cells to differentiate into antigen specific cytotoxic T-cells (CTLs). Following epitope presentation on tumor cells, CTLs destroy the malignancy by secreting FasL, perforins, granzymes and granulysins (30). During these early stages, cells which acquire mutations resulting in immunoreactive epitopes presented at the cell surface via the major histocompatibility complex I (MHC-I) are recognized and removed within the population. The subset of tumor cells which have survived this onslaught either do not poses immunoreactive antigens, have evolved mechanisms to evade apoptotic responses, or have acquired subtle defects which enable partial immune evasion. As this population of cancer cells expands, it gradually acquires additional defects within its antigen presentation pathway, or up-regulates ligands which activate CTL inhibitory receptors, to further decrease the ability of CTLs to recognize tumor cells and its associated antigens. This process, referred to as tumor escape, allows for a greater plasticity in the level of immunoreactive epitopes (21, 22). As such, there is a distinct positive feedback mechanism present between the fixation of gene mutations and the evasion of immuno-surveillance machinery.

The level of heterogeneity in these mutations is another critical element of tumorigenesis (19, 20, 31). During the clonal expansion process, the cancer cell lineage will be defined by the

selective pressures occurred throughout its development. The sequence of 1) gene mutations, 2) environmental pressures (e.g. chemotherapies), and 3) anti-tumor immune responses, will define shape the mutational landscape within the tumor. Given that most mutations are stochastic, the process of clonal expansion ensures that downstream lineages, which may have resulted from the same initial events, are extensively different from one another following several rounds of selection (19, 31). Not only is this heterogeneity observed between tumor types, but even within the same tumor sample. Indeed, the differences in gross chromosomal abnormalities are so profound, that the cell can acquire differential morphologies within the same tumor (e.g. (32)), and define the probability of success for the prescribed treatment regimen (33).

1.2 Impact of the Tumor Microenvironment

The emergence of heterogeneity, and the probability of treatment success, is defined by the local tumor microenvironment. During tumorigenesis, cancer cells continuously communicate with the surrounding tissue to foster the development of these hallmarks of cancer (2). This is achieved by inducing chronic activation of developmental pathways in adjacent healthy tissue, particularly those involved in wound repair. Described as a wound that cannot heal (34-36), tumors mimic the environment of a wound by secreting the same signalling molecules, leading to the recruitment of similar cell types. Consisting of up to 80% of the tumor mass (37), the tumor stroma is composed of several cell types including cancer-associated fibroblasts (35), tumor-infiltrating leukocytes (38), endothelial cells (39) and pericytes (40). Cell-to-cell communication between these compartments drives both immuno-suppression and up-

regulated metabolism in tumors (2). Tumor stoma plays a defining role in the tumors response to cancer therapies (41), the emergence of resistance (42), as well as the prognosis of cancer (43-47).

Cancer Associated Fibroblast or CAFs represent a preponderant cell type in most tumors including pancreatic (37), breast (48) and ovarian (49). CAFs play a vital role in tumor biology by regulating metastasis, immunosuppression and tumor cell proliferation (35). Under normal conditions, fibroblasts are the cell-type responsible for regulating the structural framework supporting tissues also known as the extracellular matrix (ECM). ECM homeostasis is regulated in response to various cues, such sheer stress & cytokines, which will allow for the "activation" of these fibroblasts to induce their proliferation and their synthesis of ECM structural components (50). The functional role of these "activated fibroblasts" is particularly evident during wound repair where fibroblasts provide the scaffold for incoming tissues. To ensure efficient wound closure, activated fibroblasts equally produce cytokines which regulate cell proliferation, vascularisation and angiogenesis (51, 52) as well as immunosuppression at the site of injury (53, 54). Interestingly, the cytokines produced by these fibroblasts, as well as those involved in fibroblast activation, are well documented oncogenes tightly associated with the hallmarks of cancer. Classical examples of cytokines "activating" fibroblasts include Transforming Growth Factor β (TGF-β) (55-57) and platelet-derived growth factor (PDGF) (58). Notable examples of oncogenic cytokines secreted by fibroblasts include Chemokine (C-X-C motif) ligand 12 (CXCL12) (59), Hepatocyte Growth Factor (60) and Vascular Endothelial Growth Factor (51, 61). By activating the surrounding fibroblasts through the release of small molecules such as PDGF and TGF-β, cancer cells generate not only the matrix necessary to

support tumor structure, but equally promote its vascularisation and evasion of immune responses (35, 62).

Tumor Infiltrating Leukocytes or TILs are an equally important component of the tumor microenvironment. Although many TILs are simply inhibited within tumors, notably by the cytokines produced by CAFs and cancer cells, TILs can equally drive several aspects of tumorigenesis. This includes cancer initiation (63), proliferation (64), and angiogenesis (65). However, the predominant impact of TILs on the tumor microenvironment may involve the suppression of anti-cancer immune responses by decreasing antigen recognition & presentation (66, 67). To prevent tumor antigen recognition, the tumor microenvironment actively recruits TILs such as regulatory T-cells (68) and Myeloid Derived Suppressor Cells (69) which suppress innate and adaptive immune responses. These cell types not only have the ability to modulate tumor antigen presentation (70, 71), but equally have the ability to provide inhibitory signals to natural killer cells (72, 73) and cytotoxic T-cells (74, 75) which are responsible for destroying antigen-expressing tumor cells. Alternative TILs associated with the hallmarks of cancer include infiltrating neutrophiles (63) and M2 macrophages (76) which provide the inflammatory signals responsible for the generation and recruitment of these immunosuppressive TILs (77). Similar to CAFs, under normal contexts, immunosuppressive TILs are involved in wound repair. Decreased antigen presentation is a surprising yet critical component of wound closure (78), putatively to prevent systemic shock upon injury (79, 80). TILs with defined function in blocking immune responses during wound repair include neutrophiles (81), regulatory T-cells (82), M2 macrophages (83, 84) and Myeloid Derived Suppressor Cells (85). To achieve this effect, both cancer cells and CAFs within the tumor microenvironment (86) secrete small molecules such as

TGF-β (73, 87) and Hypoxia Inducible Factor 1α (87), which promote the recruitment of these immunosuppressive subtypes (87) or by promoting TILs differentiation into these cells (88).

1.3 Oncogenic viruses are a Factor Involved in the Onset of Tumorigenesis

A historical line of thought is that chronic inflammation, resulting from continuous wounding, is a critical driving element of cancer (89-92). Although cancer is promoted by chronic inflammation induced by a variety of dietary and chemical agents, such as alcohol and tobacco, several pathogens have been equally demonstrated to cause cancer (93). Approximately 15-20% of cancers have an etiology directly relating to infectious organisms (93). These agents include parasitic infections (e.g. Schistosoma haematobium (94, 95), and liver flukes (96)), chronic bacterial infections (e.g. Helicobacter pylori (97)) and **several** viral agents (human papillomavirus (98), Epstein-Barr virus (99), Kaposi's sarcoma herpes virus (100), hepatitis viruses (101), Human T-cell leukemia virus-1 (102) and Merkel cell polyomavirus (103, 104)). Interestingly, all of these "oncogenic viruses" are associated with chronic infection. This observation fosters the notion that chronic immunosuppression is critical in tumorigenesis. Not only do these oncogenic viruses likely promote cancer by establishing an immunosuppressive hub in which tumor antigens can freely evolve, but several of their virulence factors have the ability to induce cancer cell transformation. Classical examples of transforming agents produced by viruses include large-T antigen (105) or human papillomavirus protein E7 (106), which inactivate p53 functionality in the cell. In the life cycle of the virus, these evasion factors ensure that growth remains perpetual and unresolved. Given the relationship between cancer and

chronic oncogenic virus infection, it is not surprising that most cancers have acquired defects in anti-viral pathways. Although beneficial to tumor immune evasion (22, 107), it is interesting to theorize that perhaps certain of these mutations evolved as a result of loss of selective pressures following the expression of viral evasion factors during present or prior chronic infections.

1.4 The Role of Type-I Interferons (IFNs) in Cancer Progression

The type-I IFN response is critical to both anti-viral (108) and anti-tumor immune responses (21). Type I or 'viral' IFNs are a family of ubiquitously expressed cytokines which are produced in response to infection. Upon secretion, type-I IFNs allow for the activation of various anti-viral defences (109-111) including MHC-driven antigen presentation (112, 113). Upon viral infection, a variety of signalling molecules, such as toll-like receptors (TLR), detect the presence of virus by recognizing structural components of the virus and its genome such as ssRNA (TLR7/TLR8), dsRNA (TLR3), CpG DNA (TLR9) and envelope glycoproteins (TLR2/TLR4) (114). Recognition by these receptors leads to downstream activation of a subset of transcription factors known as interferon regulatory factors (IRFs) which trigger transcription of a first wave of anti-viral defences, including the production of a type-I IFN known as IFNβ (115). Following translation and release into the extracellular environment, IFNβ binds to its target receptor and activates Janus Kinase (JAK). This kinase in turn phosphorylates and activates downstream transcription factors such as Signal Transducer Activators of Transcription (Stats) and IRFs which trigger the second wave of antiviral defences, also known as the Interferon Stimulated Genes (ISGs). ISGs, including several isoforms of IFNα, further propagate the signal in adjacent

cells, and actively seek to activate processes which will blunt infection (77, 116). ISGs decrease virus replication in infected cells through several distinct processes targeting every stage of viral replication cycle. This notably includes preventing viral genome duplication by actively degrading the it via Ribonuclease L (RNAseL) (117), blocking viral genome translation through a global inhibition of protein synthesis mitigated by protein kinase R (PKR) (117), cross-linking budding virus particles to the cell membrane via the Bone-Stromal Cell Antigen I (BST-2) (118), as well as by interfering with viral complex assembly via Myxovirus resistance 1 (MX1) (119). Although IFN is primarily viewed as a mechanisms which modulates the transcription of ISGs in adjacent cells to blunt/delay infection, type-I IFNs equally activate various immune cells in response to infection (116). Notably, type-I IFN release can promote: dendritic cell activation and antigen cross-presentation, NK-cell activation, as well as CTL expansion and differentiation (120-124).

Given its multimodal role in both cell autonomous and humoral immune responses, it is well documented that the interferon signalling pathway undergoes substantial immunoediting throughout tumorigenesis (21, 107). Both the expression level and deletion status of 1) IFN ((125) and (126) respectfully), 2) its upstream signalling molecules ((127) and (128) respectfully), as well as 3) downstream signalling targets ((129) and (130) respectfully) affect cancer prognosis. In cancer, mutations within this pathway confer a 'loss-of-function' phenotype which renders the IFN signalling cascade dysfunctional (126, 128, 130). It is though that these mutations allow the tumor to evade the priming of anti-tumor T-cell responses and recognition by innate immune cells (131). However, one can hypothesize that perhaps many of these mutations are the result of the loss of selective pressures during present or prior chronic

infections. Indeed the IFN response is a key target of evasion factors isolates from strains of virus and bacteria which are involved in both chronic infection and cancer (132-135). Over time, defects in upstream transcriptional regulators lead to a lower baseline level of IFN expression (125), or downstream signalling components (127, 129), which are both associated with poor cancer prognosis. Therefore, Interferon alpha 2b, or known in its recombinant marketed version as Intron A, has been used as a direct treatment for cancer. As reviewed in (136), IFN based treatments have been approved for several cancers including Renal Cell Carcinoma, Chronic Myelogenous Leukemia (CML), Hairy Cell Leukemia, Multiple Myeloma, Follicular Lymphoma, as well as Kaposi Sarcoma - a malignant disease with an etiology directly resulting from chronic infection with Kaposi Sarcoma Herpes Virus.

1.5 A Brief History of Chemotherapies and the Emergence of Viruses-based Therapies

During the first half of the 21st century, the majority of chemotherapies developed sought to actively target the rapid growth kinetics of cancer cells - a hallmark common to all tumors. Through the use of DNA damaging agents (137), microtubule destabilizing agents (138) and anti-metabolites (139), these drugs disrupt processes associated with distinct phases of the cell cycle to kill dividing cells. Although highly effective with many still used in the clinic up to this day (137-139), there are several complications with the use of these agents. While these drugs may initially have profound tumoricidal effects, there is eventual emergence of drug resistance during the selection process. This is achieved by expanding the population of cells which actively promoting drug efflux, acquire mutations that prevent the target from interacting with the drug, up-regulate pro-survival pathways, increase DNA repair, and activate anti-apoptotic

mechanisms (recently reviewed in (140)). Furthermore, by targeting actively dividing cells, virtually all of the therapies in this category result in immunosuppression. This effect is observed as bone marrow renewal of blood cells is a continuous process with billions of cells produced every day. Not only does immunosuppression open the door to opportunistic infections in patients, but equally has a negative impact on therapeutic outcome given that it removes immunoreactive immune cells which are responsible for maintaining the tumor at bay.

With our better understanding of the molecular details behind cancer, the recent focus of anti-cancer drug development has been targeted therapies (141). In contrast with the conventional approach, targeted therapies seek to destroy cancer by targeting specific molecules essential in tumorigenesis, and may allow the body to maintain functional immune responses. Perhaps the quintessential drug of this category is Imatinib - a selective Tyrosine Kinase Inhibitor (TKI) used for the treatment of CML (142). First approved in 2001 (143, 144), this TKI selectively targets a driving mutation in CML known as the BCR-ABL gene fusion (145). With this mutation associated with ~95% of CML cases (142), it is not surprising that this drug has revolutionized the treatment of CML. Under Imatinib treatment regimens, the 6 year survival rate is now approximately 88% (143). Although targeted therapies have been quite successful in the clinic, with drugs such as Gefitinib (146), Erlotinib (147), Bortezomib (148, 149), and Tamoxifen (150) replacing conventional therapies for alternative malignancies, their success to date does not approach that observed with Imatinib (141). This result is in part attributed to the high specificity of these drugs against the drug target. Since the drug is highly specific, only when the protein target is essential to tumor development/survival and the drug can maintain strong activity upon target mutation can the targeted therapy achieve its desired effects. Perhaps

better results could be achieved by utilizing a targeted platform which affects numerous parallel targets essential in tumor development & survival, yet leaves the immune response unharmed.

A therapy that has recently been revisited is the use of viruses to treat cancer. Although viruses have been known to selectively kill cancer for almost a century, this field of research was largely abandoned in favour of developing chemotherapeutics which actively targeted the rapid growth kinetics of dividing cells (151). This focus on small molecules may be attributed to our understanding of cancer during the first half of the 20th century as well as our manufacturing capabilities at the time. According to our current understanding of the molecular processes involved in cancer, it is interesting to note not only the parallels between virus infection and cancer, but how the hallmarks of cancer may be beneficial for virus replication. By augmenting cellular energetics, tumor cells are essentially transformed into a "soup" of nucleotides and amino acids readily available for virus replication. Indeed although the Warburg effect was first described in tumors, it is an essential component of many viral strains. Indeed, this process is actively targeted by the evasion factors of numerous viruses, noticeably though the stabilization of HIF-1a (152-155). Enhanced replication in the tumor microenvironment is further accentuated by impaired immune responses within the tumor microenvironment. By having defects in key antiviral pathways, such as the IFN responses (21, 107, 125-128, 130), tumor cells lack the appropriate machinery to overcome viral infection. Furthermore, immunosuppressive TILs, such as M2 Macrophages allow the cancer cell to sustain viral replication and improve dissemination within the tumor (156).

Another benefit to the use of viruses is that they offer a multimodal approach to kill cancer cells. Our body has evolved numerous pathways and mechanisms to overcome infection.

Although direct apoptotic processes are induced by the virus at the onset of infection (157, 158), the eventual induction of immune responses further improves the tumoricidal effects associated with these viruses. Upon infection by virus, the immune response of the local tumor microenvironment can be "reset" such that the presentation of tumor antigen is restored. This property further enhance tumor killing (158, 159). Overwhelming viral loads in certain tumors can equally activate TILs, such as tumor infiltrating neutrophiles, which allow the virus to induce vasculature shutdown within the tumor (158, 160). Taken together, viruses offer a multi-pronged approach which exploits various hallmarks of cancer, to induce both innate and adaptive immune responses which ultimately result in tumor destruction.

1.5 The Development of Oncolytic Viruses (OVs) as Anti-Cancer Platforms

Although certain isolates of virus are naturally targeted against the tumor microenvironment (161, 162), off-target replication was perhaps the greatest hurdle in the development of viruses as an anti-cancer therapy. With the advent of modern technologies, viral strains have been engineered to selectively replicate within the tumor microenvironment (163). This is achieved by removing virus evasion factors whose function is redundant with processes whose dysfunction occurs during tumorigenesis. By deleting virus evasion factors involved in up-regulating host cell metabolism (164) or evading IFN signalling (165-167), the virus is engineered to selectively replicate and spread in microenvironments where these processes are naturally defective. However, when the virus enters normal healthy tissue where these evasion factors would otherwise be required to establish infection foci, virus replication is aborted to

prevent off target replication. Over the past 25 years, over 90 clinical trials have been initiated using these oncolytic virus strains (168).

Talimogene LaherParepvec (TLP) is the first OV to provide successful interim overall survival data for a phase III clinical trials in the United States (OPTiM). Derived from Herpes Simplex Virus (HSV), this infectious agent harbours several genetic alterations which target it against the tumor microenvironment, and arm it to induce potent anti-tumor immune responses. This virus is attenuated through the deletion of two key virulence factors. First and foremost, ICP47 is deleted in TLP (167). This evasion factor blocks cytotoxic T cell recognition of infected cells by inhibiting the transporter associated with antigen presentation (TAP) (169). Given that TAP is typically defective in cancer (170-173), this deletion allows for the virus to be targeted against tumor cells where antigen presentation is defective. To improve specificity, this virus equally harbours a deletion in the neurovirulence factor ICP34.5 (167). This evasion factor is involved in blocking PKR-mediated shutdown of host cell protein synthesis by preventing PKR-mediated inhibition of Eukaryotic translation initiation factor 2A (EIF2A) (174). Given that PKR is stimulated by IFN (175), and EIF2A is involved in global translational control, this mutation allows for the virus to exploit both impaired IFN/PKR responses and the heightened EIF2α signalling status observed in many cancers (176-178). Given the pivotal role of ICP34.5 in the life cycle of the virus, the consequence of this mutation decreases the potency of this platform. This effect is partially relieved by augmenting virus-mediated expression US11 (167), a virus evasion factor with partially redundant function on PKR-EIF2A signalling (179). To "arm" the virus, granulocyte macrophage Colony Stimulating Factor (GM-CSF), was equally cloned into the genetic backbone (167). When this cytokine is secreted from infected cells, it allows for the

production and maturation of antigen presenting cells to enhance uptake and recognition of tumor associated antigens and therefore induce adaptive immune responses against the tumor (180).

JX-594 is an advanced biotherapeutic that was derived from the Wyeth vaccine strain of Vaccinia Virus (158). Similar to TLP, this virus is both attenuated & armed for killing within the tumor microenvironment, although the extent of its genetic alterations is much less extensive. To target this non-pathogenic strain of vaccinia virus against the tumor microenvironment, it harbours a single deletion of an evasion factor encoding virus Thymidine Kinase (vTK). Thymidine kinase (TK) plays a central role in cancer by upregulating nucleotide biosynthesis (181), where it is even routinely used as a diagnostic in positron emission tomography scans (PET-Scans) (181). By ablating vTK function, this virus only replicates in metabolically active cells, typically associated with elevated TK levels (182). Similar to TLP, this virus is engineered to encode for GM-CSF to improve the induction of adaptive anti-tumor immune responses. The next-generation of vaccinia virus OV platforms is known as JX-929 or vaccinia virus double deleted (vvDD) (164). By using a more pathogenic strain of vaccinia virus, termed Western Reserve, the heightened toxicity of this virus requires an additional deletion in a gene known as vaccinia growth factor (vGF). This evasion factor is responsible for activation of EGFR-RAS singling to support genome replication (183). As such, by deleting both vTK and vGF, this more pathogenic virus only infect tumor cells with defects in TK and EGFR-RAS singling, both common defects in cancer.

Oncolytic Rhabdoviruses, such as VSVΔ51 (165) and MG1 (166), are an emerging therapeutic platforms which have been derived from the Vesicular Stomatitis Virus (VSV) and

the Maraba Virus strains. While JX594 and TLP are complex DNA viruses, encoding >250 (184) and ~70 genes respectfully (185), these rhabdoviruses are simple negative ssRNA viruses which encode a total of 5 genes; all of which are structural components of the virus. These five genes are produced in a gradient with the abundance of nucleoprotein (N) > phosphoprotein (P) > matrix protein (M) > glycoprotein (G) > large protein (L) (186, 187). This gradient is a net result of the start-stop nature of the transcription of the VSV genome where stalling at integenic region may prevent the transcription of latter genes (188). Interference with the expression level or the ratio of these gene products can severally attenuate the viral strain - a strategy which has been successfully utilized to engineer safety into these oncolytic viruses (189).

Rather than producing evasion factors with a unique function, rhabdovirus evasion of host defences is ensured by physical interactions with its five structural components. For example, the virus matrix protein (M-protein) blocks the function of a nuclear pore complex protein (Nup-98) (190, 191), which mitigates nuclear-cytoplasmic mRNA transport of anti-viral defences raised against the virus (192). An alternative mechanism which can be utilized to attenuate these rhabdoviruses, and ensure selective replication in cancer cells, is to engineer loss of function mutations in these proteins to ablate their immunosuppressive function. While Methionine 51 of the M-Protein is deleted in VSVΔ51, MG1 harbours two amino acid substitutions (Q242R and L123W) which alter the function of the surface glycoprotein (G-protein) and M-protein respectfully. Both strategies result in viruses with an attenuated capacity to replicate in normal cells, as they become hypersensitive to the effects of IFN (165, 166)(166, 180)(166, 180)[166, 180]

.

Perhaps one of the greatest attributes of the Rhabdovirus family of oncolytic viruses is that they do not rely on receptor mediated endocytosis to enter the cell. In contrast with several alternative OV strains, the rhabdovirus family of viruses appear to rather rely on enthalpy-driven protein-lipid interactions for viral entry (193). After forming electrostatic interactions with the cell membrane, the virus subsequently enters the cell through clathrin-mediated endocytosis (194). Given that this process is critical for normal cell function and essential for all cell types (195), it does not appear that these viruses are restricted to a subset of tumors which express the appropriate viral receptors in contrast with alternative OV platforms (196, 197). Furthermore, it would be unexpected that tumors can gain resistance to this therapy on the basis of restricting entry into the host cell.

1.6 The Mechanisms of resistance to OV therapies.

Although OVs have shown great promise in the clinic, tumors can acquire resistance to these therapies. While it is presumed that resistance can be bestowed by a lack of receptors for the specific Oncolytic virus strain (196, 197), it is presumed that the mechanism of resistance equally reflects the nature of the genetic alteration used to develop the OV platform. In the case of the above examples, the induction of immune responses against the virus, specifically type-I IFN signalling, is a pillar mechanism of resistance (198-200). This is clearly exemplified by the oncolytic rhabdoviruses VSVΔ51 and MG1, which have been specifically developed to target the tumors defect in IFN pathway (165, 166, 201). While tumor cell lines expressing IFN have well documented resistance to these platforms (165, 166, 198-200), cell lines which are responsive, but do not express/activate IFN pathways in-vitro can acquire resistance through production of

IFN by adjacent cells or infiltrating immune populations (202). Mounting immune responses against the virus equally allow for the eventual production of neutralizing antibodies. These components neutralize the virus upon subsequent intravenous administration, and may prevent the release and spread of the virus to distant metastatic sites. Indeed, in regards to oncolytic rhabdoviruses, pre-clinical studies indicate that neutralizing antibodies are detected in animals as early as day 5 post administration(203).

Although the platforms devel(203)oped using Vaccinia and HSV encode for multiple immune evasion factors, resistance is nonetheless associated with induction of the IFN response. Similar to VSVΔ51 and MG1, TLP harbours deletions in genes which repress downstream IFN signalling elements (204). This effect is attributed to the role of ICP34.5 in blocking PKR-mediated inhibition of virus protein synthesis, a well known ISG process (175). By activating PKR in response to IFN, the cell can inactivate EIF2A-mediated protein synthesis, thereby blocking viral protein synthesis and replication (205). Further TAP, which is targeted by ICP47 in wildtype HSV, is a downstream element of IFN signalling (206).While this process may not solely account for resistance to this therapy, antibody synthesis, in part exasperated by the ICP47 deletion in the OV backbone, allows for the eventual neutralization of this platform, particularly by activation of the complement cascade which destroys the virus in a cell independent manner (207, 207, 208).

JX594 is equally affected by both IFN (182) and complement fixation (209). Both attributes may be the result of strain selection. For example, the Wyeth strain used to construct the platform has a truncated version of B18R (210), a soluble IFN decoy receptor. This defect, among others, may in contribute to the low pathogenicity of this virus. JX594 is equally sensitive

to complement fixation and destruction (211). Given that the Wyeth strain was used extensively during the small pox vaccination program, it is well documented that this virus induces potent neutralizing antibody responses. Indeed in the phase II clinical trial of JX594, neutralizing antibodies were detectable at baseline in 50% of patients and all subjects had detectable neutralizing antibody titers by day 29 (211). Although the impact of antibodies may have only marginal effects when the virus is administered intratumorally (211), virus neutralization should in principal occur when administered intravenously, or when the OV tries to spread to distant metastatic sites, thereby limiting the efficacy of this therapeutic platform.

1.7 Overcoming resistance to OV therapies

Several strategies have been devised to overcome resistance against oncolytic viruses. These can be divided into two categories: overcoming immune barriers or enhancing cytotoxicity induced by the virus. To overcome resistance resulting from immune responses against the virus, it is possible to use direct chemical antagonists of IFN. Although it is noted that such drug have a strong impact on OV replication and cytotoxicity in tumor cell lines (198), normal cell lines should inevitably be sensitized to the same degree, and compromise the safety of this approach. Although several drugs affecting different elements of the IFN signalling pathway have been demonstrated to selectively enhance replication within cancer cells (212-214), the exact mechanism of tumor selectivity remains enigmatic. It is hypothesized that such antagonists target genes and/or processes with a redundant partners in normal cells (213). As such, by blocking a pathway with a redundant partner whose function is defective in cancer, the drug will selectively

enhance replication in the tumor microenvironment (213). Another mechanism which can be utilized to overcome immune mediated resistance to these therapies is to block neutralizing antibodies raised against the oncolytic virus strain. This can be achieved through the use carrier cells(215), chemical conjugates to the virus (216) as well as inhibitors of the complement cascade (208, 217).

It is equally possible to combine OV platforms with one another to overcome immune-mediated resistance, and enhance replication within the tumor microenvironment (218). Given that both viruses are engineered to target the tumor microenvironment using distinct mechanisms, it is possible that the evasion factors secreted by one OV platforms can complement and rescue the other. Although highly promising results have been observed (218), it is difficult to imagine how regulatory agencies would react faced with the combination of two complementary viruses, given the potential for recombination between these two platforms.

An alternative means to improve the efficacy of OV regimens, is to combine OVs with chemotherapeutics that will propagate the cytotoxicity induced by the virus. One such strategy is the development of gene-directed enzyme pro-drug therapies (GDEPT) (219). By allowing the virus to express an enzyme which converts a prodrug into its active from, it is possible to enhance killing from the initial infection foci (220). Without re-engineering the virus, it is equally possible to use pro-drugs which are activated in response to the cytokines released upon infection (221). This includes the use of second mitochondria-derived activator of caspases (SMAC) mimetics in combination with OVs (221). By blocking the inhibitors of apoptosis (IAP) with SMAC mimetics, the region surrounding the infection foci becomes highly sensitized to the pro-apoptotic cytokines released upon OV infection (221). Perhaps a better understanding of

these systems, and the dynamics involved, may allow us to devise novel strategies to overcome resistance.

1.8 Modelling OV dynamics

Perhaps some of the greatest work involving the mathematical modeling and behaviour of biological systems was performed by Hodgkin & Huxley. This work awarded them the Nobel Prize in 1963. Over the course of 3 papers published back-to-back in 1952, this research group presented their work involving the instrumentations (voltage-clamp) used to measure membrane conductance (222), the first description of the role of ions channels in action potential (223), as well as the quantitative mathematical modelling of this system (224). According to data retrieved from Scopus on January 30th 2014, for both Hodgkin & Huxley, their most cited paper remains the quantitative mathematical modelling of this system (224) with over 5000 citations. By observing the biology, and understanding how these components drive the observation through mathematical modeling, Hodgkin & Huxley provided the first insight into the role of ion channels in action potential. Since this pillar discovery, the modeling of biological systems has gained much interest from the scientific community. Not only does it substantiate the biological observations, but can provide additional insight into system dynamics to be validated by future experiments, and drive the development of novel therapeutic platforms.

To understand the emergence of resistance to OV therapies, and develop better pharmaceuticals, it is essential that we model the interplay between viral infection and the activation of anti-viral responses. To date, several models have been devised to describe OV

dynamics (225-229), most of which stem from the work of Nowak & Bangham (230, 231). In their original work, the authors modified the Lotka–Volterra system of differential equations, also known the predator-prey model, to explain the interaction of "free virus" with an uninfected cell and its transition towards an infected cellular state (230, 231). These models were originally developed to investigate the replication dynamics of pathogens, such as HIV and Hepatitis B. To better describe drug treatment regimens this model was amended to include the impact of various inhibitors on virus replication (232), the induction of CTL responses (225), and the emergence of drug resistance (233). These models have been subsequently amended to investigate various OV dynamics. This includes the role of CTL responses in OV therapies (226), the impact of tumor growth and the laws of virus spread (228), the level of synergy between OVs and radiotherapy (227), as well as the role of the cell cycle in virus replication (229).

While the models developed to date have been utilized to understand the fundamental biology of OVs in tumors, little effort has been placed on understanding the differential in kinetics between normal and tumor cells to guide pipeline development. By utilizing general assumptions about the behaviour in these distinct cell types, and incorporating elements of resistance attributed to IFN anti-viral responses, it may be possible to use develop a model which can guide the engineering process. The topic of my thesis will focus on using a systems biology approach, defined as 1) Conceptualization, 2) Design, 3) Modeling, 4) Simulation, 5) Construction, 6) Probing and 7) Measuring the biological system (234), to identify novel strategies which can enhance OV cytotoxicity in the tumor compartment without compromising normal cells.

1.8 Hypothesis

1. By modeling OV replication dynamics in normal and tumor tissue, under the assumption that resistant tumor cells are associated with a greater rate of virus replication/protein expression yet overcome infection due to activation of IFN signalling, it may possible to identify IFN evasion strategies which will selectively enhance cytotoxicity in tumor cells. This model could be utilized to identify novel engineering strategies, attenuation mechanisms, the impact of tumor heterogeneity as well as the consequence of drug-OV interactions.

2. Given that pro-apoptotic responses are induced upon recognition of the viral backbone, and that the tumor microenvironment has acquired defects in degrading the virus through gene mutation or cross-talk with immunosuppressive cells, tumors may have a heightened sensitivity to virus-mediated cell death in the absence of replication, a process which may be recapitulated by my model.

1.9 Objectives

1. Develop a mathematical model, and simulation platform, to describe OV dynamics in tumor and normal tissues.

2. Implement this model to identify IFN evasion strategies which will selectively enhance cytotoxicity in tumor cells.

3. Utilize this model to explore the impact of drugs on oncolytic virus dynamics.

4. Characterize the impact of cross-talk between CAFs and cancer cells by microarray analysis and viral growth measurements.

5. Amend the model according to the observation in objective 4 to describe the impact of tumor heterogeneity on OV dynamics, specifically how resistant cancer cells are influenced by the presence of various tumor infiltrates.

6. Model the impact of inhibiting IFN signalling on the sensitivity towards a non-replicating rhabdovirus.

7. Explore the use of Non-Replicating Rhabdovirus-derived Particles (NRRPs) for the treatment of haematological diseases.

Chapter II. Model-based rational design of an oncolytic virus with improved therapeutic potential

Authors:

Fabrice Le Bœuf[1,2],*, Cory Batenchuk[1,3,4],*, Markus Vaha-Koskela[1,2], Sophie Breton[1,2], Dominic Roy[1,2], Chantal Lemay[1,2], Julie Cox[1,2], Hesham Abdelbary[1,2], Theresa Falls[1,2], Girija Waghray[1,2], Harold Atkins[1,2], David Stojdl[5], Jean-Simon Diallo[1,2], Mads Kærn[4,6,7]& John C. Bell[1,2,3]

Affiliations:
1. Center for Innovative Cancer Therapeutics, Ottawa Hospital Research Institute, Ottawa, Ontario, Canada K1H 8L6.
2. Department of Medicine, University of Ottawa, Ottawa, Ontario, Canada K1H 8L6.
3. Department of Biochemistry, Microbiology and Immunology, University of Ottawa, Ottawa, Ontario, Canada K1H 8L6.
4. Ottawa Institute of Systems Biology, University of Ottawa, Ottawa, Ontario, Canada K1H 8L6.
5. Apoptosis Research Center, Children's Hospital of Eastern Ontario, Ottawa, Ontario, Canada K1H 8L6.
6. Department of Cellular and Molecular Medicine, University of Ottawa, Ottawa, Ontario, Canada K1H 8L6.
7. Department of Physics, University of Ottawa, Ottawa, Ontario, Canada K1H 8L6.

*** These authors contributed equally to this work.**

Journal:

Nature Communication, 2013

My contribution:

I performed all aspects of modelling & microarrays data analysis in this paper which is represented in Figure 2.1, Figure 2.2, Figure 2.3d, Appendix Figure 1, Appendix Figure 2, Appendix Figure 3, Appendix Figure 4, Appendix Table 1, Appendix Table 2, Appendix Table 3, Data S1[$] & Data S2[$].

Chapter Synopsis

In the article entitled ***Model-based rational design of an oncolytic virus with improved therapeutic potential***, I developed a mathematical model and simulation platform to describe OV dynamics which I have used and further developed throughout my thesis. This model was derived by amending the original two-state model developed to described human immunodeficiency virus or hepatitis replication (230, 231) to incorporate the elements of IFN secretion & responsiveness as well as the ensuing antiviral response in tumor and normal tissue.

In this article, the parameters of the resulting four state model were adapted to describe three distinct cell types: normal cells, resistant IFN responsive tumor cells and sensitive IFN non-responsive tumor cells (**Figure 2.1**). Relative to normal cells, both tumor types were associated with an increased rate of virus replication & virus-mediated protein production due to increased biosynthetic machinery availability and repression of cell autonomous innate immune responses at the onset of infection. Sensitive tumor cells have further defects in the IFN pathway, thereby preventing the potent induction of antiviral responses. In contrast, resistant tumor cells are not associated with these defects and eventually overcome infection by activating IFN signalling pathways.

This model was simulated using a Monte Carlo strategy to identify a method by which OVs could consistently evade the IFN response to increase cytotoxicity in resistant tumor cells without compromising normal cells. After testing several evasion mechanisms (**Figure 2.2**), using parameters derived from literature or biological observations for rhabdovirus infection (**Appendix Table 1**), I arrived to the conclusion that a positive feedback-loop, generate by virus-

mediated expression of an IFN decoy receptor, would lead to tumor-specific sensitization towards the OV. According to the simulations, expression of the decoy receptor did not further sensitize normal cells, even at high doses of the virus (**Appendix Figure 1**). After the B19R IFN decoy receptor from vaccinia virus was isolated and cloned into the MG1 and Δ51 viral backbones (MG1-IDE & Δ51-IDE respectfully), I performed microarray analysis to confirm the phenotype of this virus. While the resistant renal cell adenocarcinoma cell line (786-0) mounted a potent anti-viral response against the MG1 backbone, the majority of this response was lost following expression of the decoy receptor (**Appendix Figure 2**). To confirm the tumor specific cytopathic effects associated with this engineering strategy, and quantitatively validate my model, I integrated the in-vitro dose response curves with my simulations (**Figure 2.3d, Appendix Figure 3**). Not only are tumors hypersensitive to this agent, even at extremely low doses of the oncolytic virus, but excellent quantitative agreement was observed between the model and the biological datasets. These observations effectively validate the model parameters and assumptions. Not only could this model be applied to identify methods which would improve OV platforms, but could equally be applied to investigate alternative attenuation mechanisms, such as a negative feedback-loop where wildtype VSV expresses IFNβ (**Appendix Figure 4**).

Abstract

Oncolytic viruses are complex biological agents that interact at multiple levels with both tumour and normal tissues. Antiviral pathways induced by interferon are known to have a critical role in determining tumour cell sensitivity and normal cell resistance to infection with oncolytic viruses. Here we pursue a synthetic biology approach to identify methods that enhance anti-tumour activity of oncolytic viruses through suppression of interferon signalling. On the basis of the mathematical analysis of multiple strategies, we hypothesize that a positive feedback loop, established by virus-mediated expression of a soluble interferon-binding decoy receptor, increases tumour cytotoxicity without compromising normal cells. Oncolytic rhabdoviruses engineered to express a secreted interferon antagonist have improved oncolytic potential in cellular cancer models, and display improved therapeutic potential in tumour-bearing mice. Our results demonstrate the potential of this methodology in evaluating potential caveats of viral immune-evasion strategies and improving the design oncolytic viruses.

Introduction

Oncolytic viruses (OVs) are promising anticancer therapeutics engineered or selected to infect and multiply specifically in tumour cells while having attenuated replication capacity in normal tissues (235, 236). The attenuation of OV growth in normal tissues is often due to the inability of OVs to antagonize normal cellular, interferon (IFN)-mediated antiviral responses. Many tumour cells have acquired defects in their IFN response during their malignant evolution, and are correspondingly excellent hosts for OV growth (157, 165, 201, 237, 238). However, the extent of the IFN response deficit in cancers is highly variable and can impair the efficacy of OV therapies (235). This has led to intensive efforts aiming at suppressing IFN signalling in tumour cells without compromising the antiviral programmes in normal tissues (218, 239). Although previous mathematical models have been developed to describe the kinetics of OV replication (226, 240-242), the field of OV engineering has yet to adopt approaches from Synthetic Biology, where mathematical models are often used to guide the development of biological systems. To demonstrate the potential of model-based rational design of OVs, we combined mathematical modelling and viral genome engineering to design and test strategies that might allow evasion of the IFN response in the tumour microenvironment, while maintaining safety in normal tissues.

Whether a patient receives therapeutic virus intravenously (243) or through direct intratumoural injection (244), the quantity of virus that reaches the tumour bed is vastly outnumbered by the number of target cells found in the malignancy (245). Successful OV therapies thus rely upon the ability of a relatively small number of virus particles to initiate an infection and spread within a population of cancer cells. Viruses are strictly dependent upon the biosynthetic machinery of the infected host cell to produce progeny particles. Correspondingly, cancer cells that are rapidly

dividing and have established robust biosynthetic machinery inherently produce larger numbers of virus particles when compared with cells in normal tissue, which are quiescent and have a restricted ability to synthesize new nucleic acids and proteins (164, 182). In cancer cells, this effect is exasperated by defects in immune responses, which further enhance viral replication.

In a simple model of virus infection, the distinction between viral replication kinetics in healthy and tumour tissue is characterized by differences in available biosynthetic machinery and innate immune responses (Fig. 2.1). When virus is delivered to normal tissue, it infects a limited number of cells creating a subpopulation, producing both virus progeny and IFN. As the infection proceeds, slow virus replication enables the IFN-mediated defence response to outpace virus particle production and restrict infection. Viruses that can prevent the production of IFN from infected cells, or stimulate host cell metabolism, are correspondingly expected to have an increased capacity to spread within normal tissues. Indeed pathogenic viruses incorporate both these strategies into their life cycle (246, 247). In tumours non-responsive to the antiviral effects of IFN, invading virus will co-opt the biosynthetic machinery of the cancer cell producing large numbers of virus particles. In this setting, the virus will rapidly spread and destroy the malignancy. In tumours responsive to IFN, virus spread will be favoured by the high metabolic rate of the cancer, but at the same time limited by the ability of neighbouring cells to mount an innate immune antiviral response. In this setting, it is the balance between virus production and the extent of initiation of antiviral responses that will ultimately determine the therapeutic outcome.

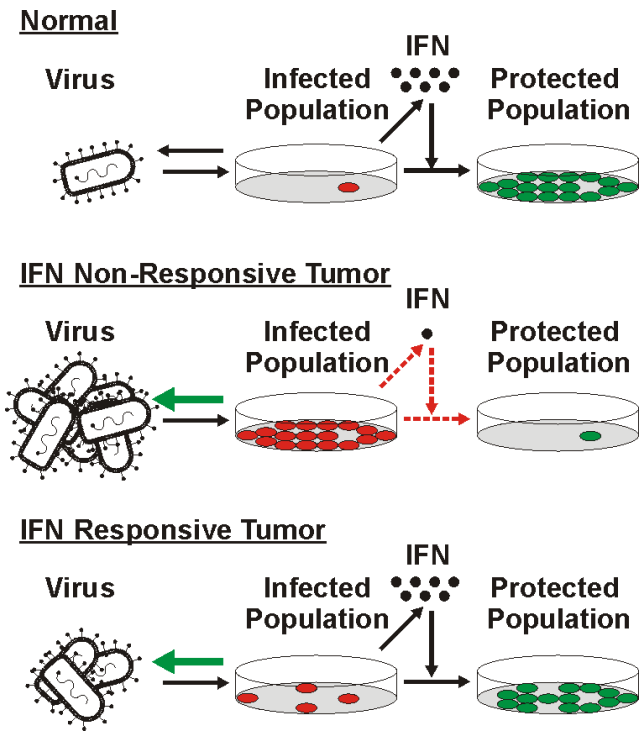

Figure 2.1 Model development.
Comparison of virus replication dynamics in three tissue types: normal cells, IFN non-responsive tumours and IFN-responsive tumours. Processes enhanced relative to normal cells are illustrated in green, whereas those impaired are illustrated in red.

Results

Model simulations of different IFN-evading strategies

To simulate virus infection and spread within tumour and normal tissue, we developed a phenomenological model describing the varied ability of different cell types to support virus proliferation. In this model, cells within an 'uninfected population' (UP) transitions into an 'infected population' (IP) upon viral infection. The number of infected cells in the IP increases over time, as virus is produced and spreads to neighbouring cells. Production of IFN from IP cells allows these cells to transition into an 'activated population' (AP) where viral defences slow virus release and further enhance IFN production. Over time, this population will gradually become a 'protected population' (PP) of cells that have cleared the infection and maintain active antiviral defence programmes (248-250).

We used this phenomenological model as the basis for simulating the outcome of different IFN-evasion strategies on three types of cells: normal cells, IFN non-responsive tumour cells and IFN-responsive tumour cells. We assumed that these cell types differ mainly in their ability to facilitate virus replication and to activate IFN. By quantifying cytotoxicity induced 72 h post infection in each of these three cell types, the simulations seek to explore how the relationship between virus replication, activation of IFN-mediated defence responses and cytotoxicity induced across the population might be exploited to design improved therapeutic strategies. Because of the heterogeneity of tumour and healthy cells, and the corresponding uncertainty associated with kinetic parameter estimates, we further employed a Monte Carlo sampling method to simulate 1E4 different combinations of kinetic parameters randomly

sampled within one order of magnitude from values reported in the literature. The outcomes of this unbiased method are probability distributions describing the susceptibility of each of the three simulated types of cells towards viral infection.

We first asked if the model could recapitulate the effects associated with an attenuating mutation in the natural wild type (WT) isolate of vesicular stomatitis virus (VSV), (wild type (WT)), which renders the virus sensitive to IFN signalling, here referred to as Δ51(165). In VSV WT, functional Matirx-protein blocks IFN production to enable viral evasion of the immune response (192). As expected, VSV WT is highly efficient in infecting and killing both normal and tumour populations (Fig. 2.2a). In agreement with experimental observations in a variety of tumour models (165, 251, 252), our simulations predict that the Δ51-attenuated virus will eradicate IFN non-responsive tumours, whereas normal populations or IFN-responsive tumours will be largely resistant (Fig. 2.2c).

We next tested two scenarios to determine whether chemical manipulation of the IFN responses of virus-infected cell could enhance the activity of Δ51 in IFN-responsive tumours, while maintaining a low impact in normal populations. Simulations of Δ51 infection in the presence of a chemical inhibitor that blocks IFN signalling (for example, a JAK inhibitor (JAKi)) predicts a toxicity profile reminiscent of infection with VSV WT (Fig. 2.2e). Although the inhibition of IFN signalling increases virus effectiveness against tumours, it also causes the normal population to become highly susceptible to infection. This outcome is also predicted to occur in simulations where the population is exposed to a biological agent that prevents IFN interaction with its cognate receptor (for example, a soluble IFN receptor antagonist; Fig. 2.2g).

We then tested the idea of coupling the production and secretion of the decoy receptor (DR) to virus replication. In this model, Δ51 is engineered to synthesize a soluble IFN binding DR only when viral gene expression is initiated, thereby creating a positive feedback loop. Positive feedback sharpens dose responses and enables all-or-none switching in cellular signalling pathways (253), and might thus drive specificity towards the tumour environment. The results obtained by simulating the cytotoxicity induced upon infection with the Δ51 IFN decoy-expressing (IDE) virus ($\Delta51_{IDE}$) were highly encouraging (Fig. 2.2i). Specifically, the simulated efficacy towards tumours was significantly increased compared with the unmodified Δ51 virus, without posing additional risk of damage to the normal population even at high doses of the virus (Appendix Figure 1).

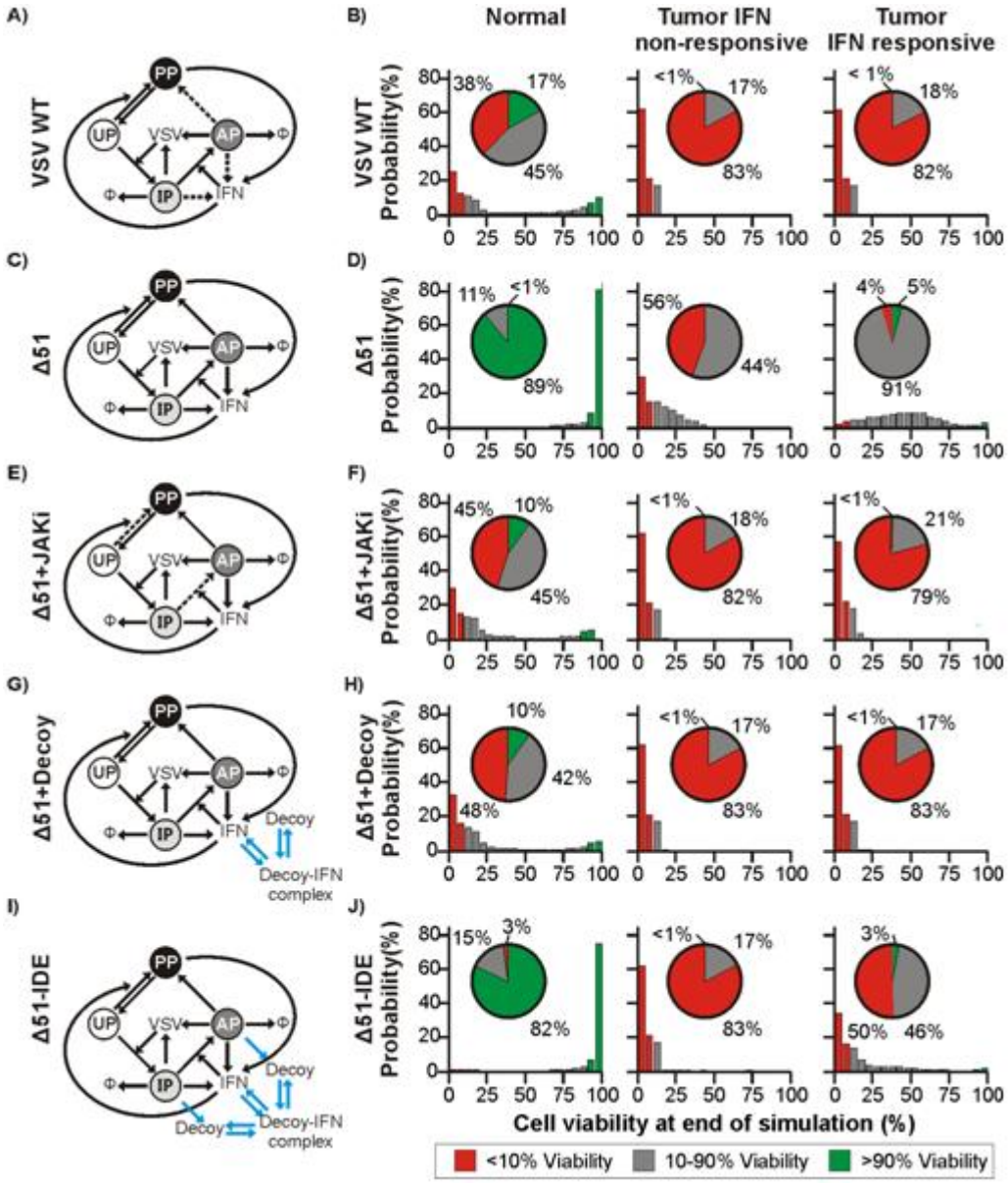

Figure 2.2. Simulation of IFN-evasion strategies on rhabdovirus-induced cytotoxicity.
The phenomenological model was amended to describe treatment with (**a**) VSV WT, (**c**) Δ51, (**e**) Δ51 in the presence of a JAKi, (**g**) Δ51 in the presence of a DR for IFN and (**i**) Δ51-mediated expression of the IFN DR ($\Delta51_{IDE}$). Colour coding highlights processes impaired (dashed) or gained (blue) relative to Δ51. Each of the above models used a Monte Carlo sampling method to generate the probability distribution of population viability following treatment with (**b**) VSV WT, (**d**) Δ51, (**f**) Δ51+JAKi (**h**), Δ51+decoy (**j**) $\Delta51_{IDE}$ for 72 h in normal cells (left) and tumours with non-responsive (tumour IFN-NR; centre) or responsive (tumour IFN-R; right) IFN signalling pathways. Colour coding, quantified in pie charts, describes the probability that each of the three cell types has a viability <10% (red), 10–90% (grey) or >90% (green) at the end of the simulation.

Experimental testing of simulation predictions in vitro

To test the model predictions, we performed experiments to compare the efficacy and specificity of Δ51 under each of the simulated IFN-evasion strategies. We previously identified the renal carcinoma cell line 786-0 as having a partially intact IFN response and being refractory to killing by Δ51 (213, 218). Correspondingly, experiments were performed by the co-treatment of IFN-responsive tumour cells (786-0) and normal fibroblast (MRC5) cells with the Δ51-GFP virus in the presence of the JAKi or exogenously added recombinant B19R-soluble IFN DR (210, 254-257). In agreement with the outcome predicted by our simulations, the presence of the chemical inhibitor increased Δ51-mediated killing of 786-0 tumour cells, but equally resulted in a loss of specificity as MRC5 normal cells became susceptible to infection (Fig. 2.3a). Similar results were obtained when the two cell types were cultured in the presence of the DR protein before Δ51 treatment (Fig. 2.3a and Supplementary Fig. S2[$$$]).

To test the prediction that virus performance can be improved by incorporating an IFN-suppressing positive feedback loop, we incorporated the B19R IFN DR into the Δ51 backbone, and a second IFN-sensitive attenuated OV derived from the Maraba virus termed MG1 (Supplementary Fig. S3[$$$]). This second rhabdovirus was used to evaluate the generality of the strategy, and because MG1 is a more aggressive rhabdovirus with more potent oncolytic activity as compared with Δ51(166). We refer to these IDE viruses as $\Delta51_{IDE}$ and $MG1_{IDE}$, respectively. After confirming the expression and activity of the DR produced from these viruses (Supplementary Fig. S3[$$$]), we performed a microarray analysis of differential genome-wide transcription upon infection. This analysis confirmed that IFN decoy expression following viral infection leads to a significant repression of the type I IFN response in IFN-producing cells

(Appendix Figure 2 and Appendix Table 1 and Supplementary Data $1^{\$}$ and $2^{\$}$). As predicted by our simulations, both $\Delta 51_{IDE}$ and $MG1_{IDE}$ viruses were associated with tumour-selective cytotoxicity. In the 786-0 tumour cell line, both strains were associated with a greater cytopathic effect than their attenuated parental virus strains. However, neither of the IDE viruses caused significant damage to MRC5 normal cell (Fig. 2.3b). We next examined the effect of varying initial virus concentrations on cell viability using both our computer model and cell culture experimentation. Remarkably, we were able to achieve excellent quantitative agreement between the model simulations and experimental data in the above cell lines (Fig. 2.3 c&d), or in alternative models (Appendix Figure 3).

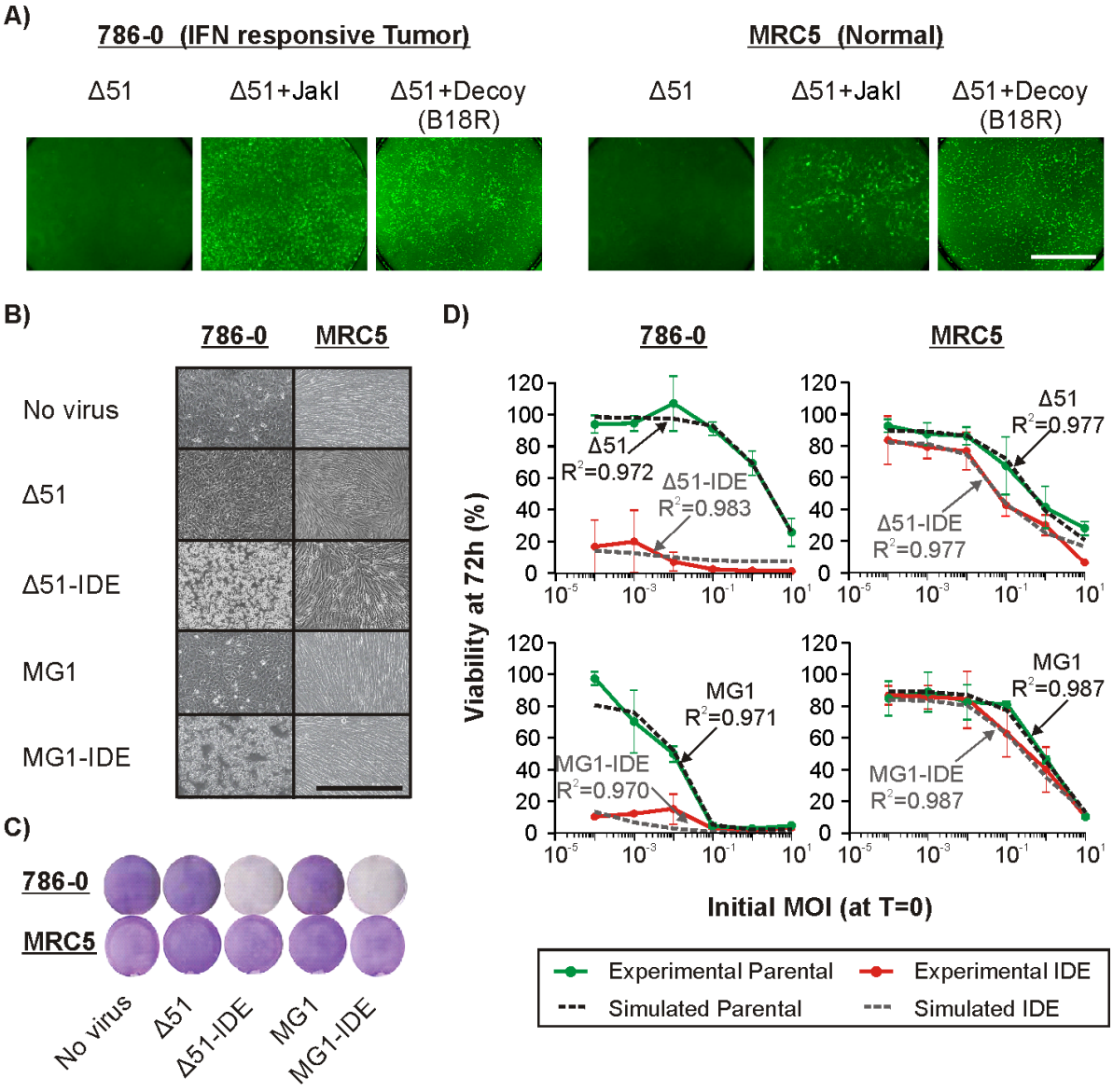

Figure 2.3. Validation of model predictions in vitro.
(**a**) Infection of resistant tumours with functional IFN defences (786-0) and normal (MRC5) cells with Δ51-GFP at a multiplicity of infection of 0.1 in the presence or absence of 10 μM of the JAKi or 0.1 μg ml−1 of the B19R DR. Microscopy images were taken 48 h post infection. Scale bar, 2 mm in length. (b) Cytopathic effects of the $\Delta 51_{IDE}$ as observed by bright-field microscopy 24 h post infection. Scale bar, 500 μm in length. (c) Cytopathic effects of the $\Delta 51_{IDE}$ as observed by crystal violet staining 72 h post infection. Images are from a 12-well plates (2.5 cm diameter). (**d**) Experimental and simulated relationship between multiplicity of infection and cellular viability 72 h post infection. Error bars represent the s.d. from triplicate technical replicates. Trends represent the simulation, which best describes the experimental results.

To establish whether spreading between the cancerous and normal cell compartments compromises safety, we performed a series of co-culture experiments. To first assess if IDE viruses have increased spreading ability, we deposited virions in the centre of a monolayer of 786-0 cells and examined cell death caused by virus spreading 48 h post infection (Fig. 2.4a). Both $\Delta 51_{IDE}$ and $MG1_{IDE}$ viruses were superior to their parental counterparts in terms of their ability to rapidly spread through a 786-0 monolayer. Quantification of the surface area affected revealed that virus penetrance was increased sevenfold for $\Delta 51_{IDE}$ and fourfold for $MG1_{IDE}$ (Fig. 2.4b). Similar results were obtained using alternative tumour cell lines and methods (Supplementary Fig. S6[$$$]). In contrast, IDE viruses had no detectable spread in normal GM38 cells. We next performed our co-culture spreading assay by adding pre-infected 786-0 cells onto a monolayer of normal fibroblasts, and monitored viability 72 h post infection by crystal violet staining. Parental WT viruses (VSV WT or Maraba) spread from the infected tumour cells into surrounding normal cell culture causing widespread off-target killing (Fig. 2.4c). On the other hand, Δ51/MG1 were restricted only to the local tumour microenvironment and had their spreading rapidly blunted by the normal cell monolayer. Finally, the $\Delta 51_{IDE}$ and $MG1_{IDE}$ viruses were indistinguishable from their attenuated parental counterparts, and lacked the ability to spread into a normal cell monolayer, suggesting that the engineered IFN-suppressing positive feedback loop does not compromise normal tissue (Fig. 2.4c).

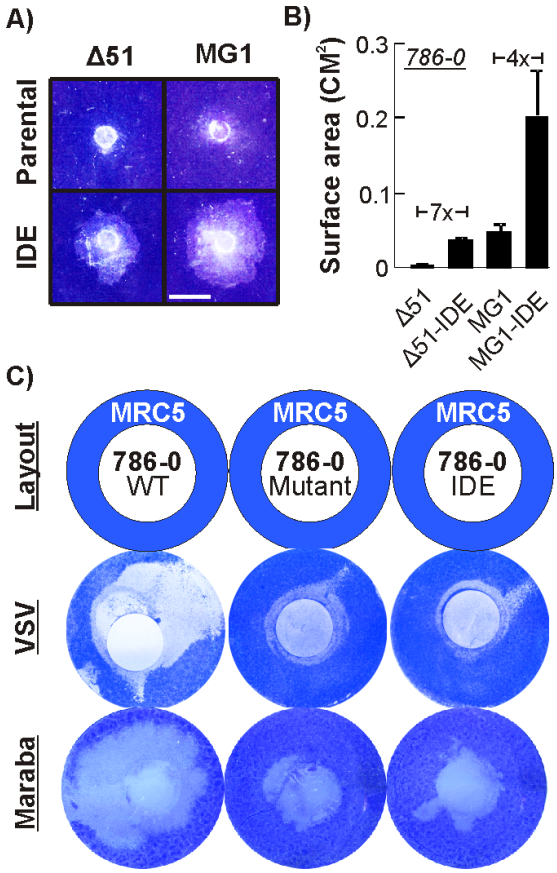

Figure 2.4. Viral spreading.
(**a**) Comparison of virus spreading by crystal violet staining in 786-0 cells. Scale bar, 2 mm in length. (**b**) Quantification of virus spreading surface. Error bars represent the s.d. from triplicate technical replicates. (**c**) Coverslip spreading assay. The 786-0 cells were plated in a dish containing round coverslip and infected at a multiplicity of infection of three during 4 h. The round coverslip was transferred on a monolayer of naive MRC5 cells and an agarose overlay was added on the top. Five days later, cells were fixed and stained with Coomassie brilliant blue. Images are from a six-well plates (3.5 cm diameter).

Efficacy and specificity of IDE viruses in vivo

To test the in vivo activity of the IDE viruses, we established subcutaneous tumours in BALB/c mice using an IFN-responsive variant of the murine CT26 colon tumour cell line. In our initial studies, animals were treated with OVs intravenously and were killed at various times to quantitate the level of virus replication in normal and tumour tissues (Fig. 2.5a). Consistent with earlier studies6, virus was cleared from normal organs whether or not it expressed an IFN decoy by day 4. However, the $\Delta 51_{IDE}$ and $MG1_{IDE}$ viruses persisted longer and grew to higher titres in the tumour tissue than in their parental counterparts.

We also tested the efficacy of $MG1_{IDE}$ in a number of tumour settings after confirming that the maximum tolerated dose was minimally affected by addition of the DR (Fig. 2.5b). In a human xenograft model using the HT29 cell line, $MG1_{IDE}$ clearly outperformed its parental MG1 strain, effecting long-term cures in ~50% of the animals (Fig. 2.5c and Supplementary Fig. $S7^{\$\$\$}$). We next established CT26–LacZ colon tumours in the lungs of BALB/c mice by intravenous (i.v.) infusion to assess the impact of IDE on metastatic tumour clearance (Fig. 2.5d). Mice were injected with CT26–LacZ i.v. and 3 days later with 1e7 plaque forming units (pfu) of virus. Mice were killed 13 days after cell injection. CT26 metastases were counted and results clearly show an increase in efficacy associated with the IDE virus. This result could be further improved in a liver metastasis model in immunocompetent mice where 100% of the mice treated with $MG1_{IDE}$ were liver tumour free (Fig. 2.5e). Taken together, these results indicate that IDE rhabdoviruses improve the therapeutic potential of OVs without compromising toxicity in normal tissue.

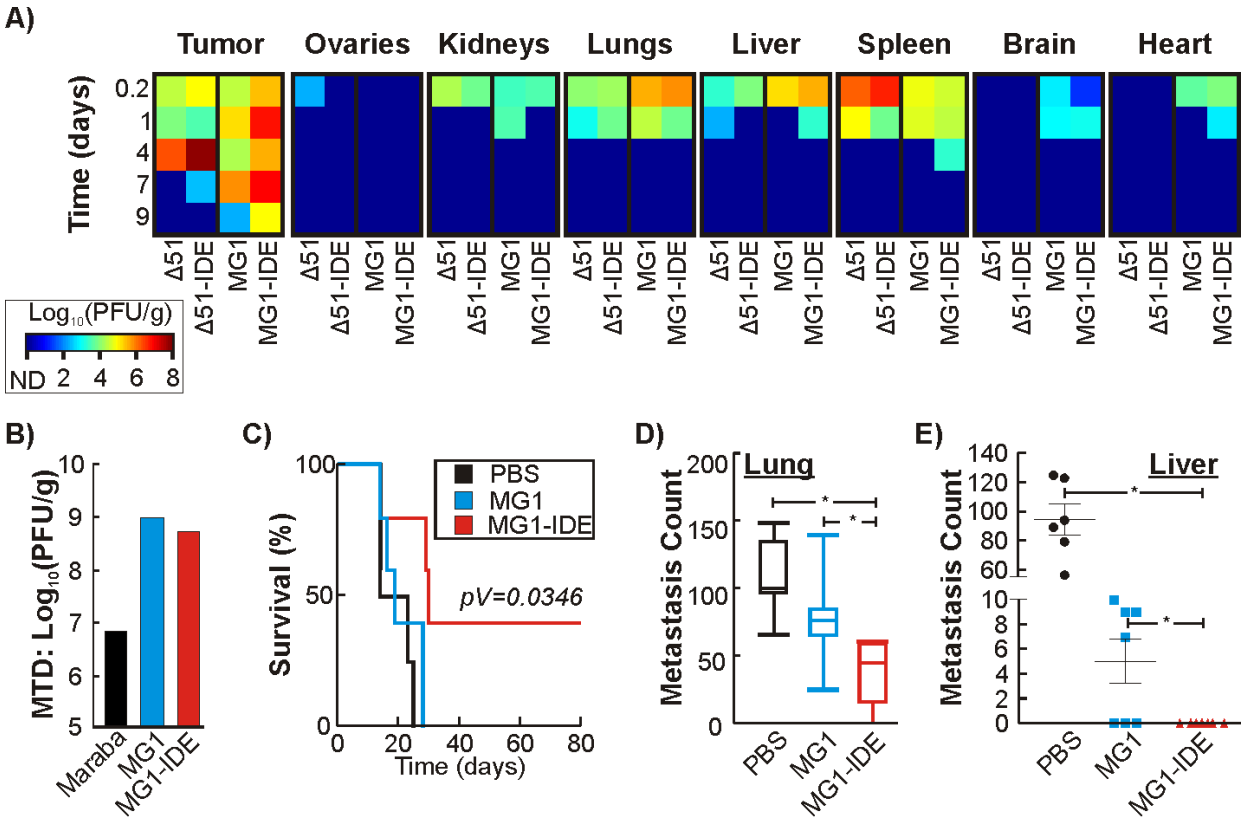

Figure 2.5. Safety and efficiency of a decoy-expressing virus in vivo.
(a) Biodistribution in CT26 tumour-bearing BALB/c mice injected with 1E8 pfu i.v. (b) maximum tolerated dose in tumour-naive BALB/c mice. (c) Survival study of immunodeficient mice bearing an HT29 subcutaneous tumour treated with 1E8 pfu injected i.v. (n=5). (d) CT26 tumour cell metastasis to the lung in BALB/c mice following treatment with 1E7 pfu injected i.v. (n=7). Box plot illustrates the sample maximum and minimum (error bars), Q1 and Q3 (box), and the median of the population (central bar). (e) CT26 tumour metastasis to the liver in BALB/c mice following treatment with 1E8 pfu injected i.v. (PBS, N=6; MG1s, N=7). *Statistical difference between groups (one-way analysis of variance, P<0.0001; two-tailed heteroscedastic t-test, P<0.05).

Discussion

OVs are advancing through late-phase randomized clinical trials, and it seems likely that one or more products will be approved in the near future (258-262). Despite encouraging clinical data, it is clear that the genetic heterogeneity of tumours will make it necessary to create novel OVs to maximize their potential as anticancer agents.

Here, we evaluated whether model-based rational design could be used to design OVs. After implementing the model to characterize various prevalidated attenuating strategies, such as the Δ51 mutation (165) or engineering VSV WT to express IFN (Appendix Figure 4) (263), we sought to predict novel methods that would increase tumour killing in IFN-responsive tumours without compromising normal tissues. Our model simulations demonstrated that an indirect positive feedback loop, generated through virus-mediated expression of a DR, should selectively enhance virus-mediated cytotoxicity within the tumour microenvironment in excellent agreement with subsequent experimental observations.

These simulations provide the theoretical framework describing the advantages of incorporating a DR into the backbone of OVs. By allowing a DR to be encoded by the virus, the functional impact of the repressor on virus kinetics is delayed, as its expression requires the establishment of a productive viral infection. Repressor-mediated enhancement of viral replication can only occur in the environment surrounding cells predisposed towards viral infection and replication. When virus particles enter adjacent normal tissue where viral replication is slow or aborted, levels of the DR should be gradually lost, thereby preventing the systematic spread of the virus in normal tissue.

By using a synthetic biology approach to rationally designed OVs, we have established a methodology that allows the potential caveats of various immune-evasion strategies to be evaluated. This method has allowed us to identify those with the greatest probability of success, and has resulted in the development of two novel oncolytic candidates.

Methods

Biological materials and reagents

Vesicular stomatitis viruses are as follows: Δ51 (165), Δ51-GFP, VSV WT and Δ51IDE. Maraba Spanish double-mutant virus MG1 and $MG1_{IDE}$ were both generated by Stojdl and colleagues (166). The following cell lines used were obtained from the American Type Culture Collection (Manassas, VA): African Green Monkey kidney (Vero), human renal cancer cells (786-0), murine colon cancer cells (CT26), human colon cancer cells (HT29), mouse melanoma cancer cells (B16), human glioma cancer cells (U251), primary human fibroblast cells (GM38) and human (MRC5). All cells were grown in DMEM (Hyclone Laboratories Inc.) with 10% FBS (Invitrogen, Burlington, ON, Canada). Recombinant B19R (VACWR200) utilized in this study was obtained from eBioscience, Inc. (San Diego, CA), and the JAKi was purchased from EMD Millipore.

Construct validation

For the cloning, mRNA expression of the IFN–DR expression from new rhabdoviruses constructs was verified by PCR. For primers used, see Supplementary Table S2[$$$].For the microarray analysis, RNA extraction was performed 24 h post infection in 786-0 cells. Duplicate samples were pooled and hybridized on Affymetrix human gene 1.0 ST arrays according to manufacturer instructions. Data analysis was performed using AltAnalyze (264). Briefly, probeset filtering implemented a DABG threshold of 70 with $P<0.05$ and utilized constitutively expressed exons. Genes differentially expressed were identified using a combination of a >1.5-fold change in expression and a significance of $P<0.05$ (Student's t-test) (Supplementary Data 1[$$$]). Gene ontology enrichments were performed using GOrilla (265) (Supplementary Data 2[$$$]). Identification of genes induced by type I IFNs was performed using the interferome database (266). For both cloning and microarray analysis, RNA was collected using an RNeasy kit (Qiagen, Toronto, Ontario, Canada).

In vitro analysis

For in vitro cell death and cytopathic effects assays, cell lines were plated in 12-well plates at 3E6 cells per well. Twenty-four hours later, cells were treated with each of the five different regimens. Seventy-two hours post infection, crystal violet (0.1%) staining was performed to visualize live cells. Bright-field images were taken with a Zeiss Axiovert S100 Inverted Microscope.

For the Alamar Blue Assay, 5E4 cells were plated in 96-well plates. After 24 h, cells were infected with each virus. Forty-eight hours post infection, 10 µl of the Alamar blue reagent (Invitrogen) was added to each well. Reading was done using the Labsystems Fluoroskan II Fluorescent Microplate Reader using the Em/Ex 590/530 nm filters.

For spreading assays, cells were plated in six-well plates at 8E5 cells per well. After 24 h, the cells were covered with a 0.7% agarose overlay containing antibiotics (Penicillin and Streptomycin) in which a small hole was made in the middle of the well where 5E3 pfu of virus was injected. After 5–6 days incubation, crystal violet staining or VSV immunostaining assessed virus spread. VSV antibodies (polyclonal antibodies from immunized mouse) targeting whole virus were utilized at a dilution of 1/800 and left for a duration of 30 min before being washed off with water.

For coverslip spreading assays, MRC5 cells were plated into a 10-cm-well dish until 100% confluence was obtained after 24 h. The 786-0 cells were plated in a six-well plates containing a sterile coverslip at a density to reach 100% confluence after 24 h. The 786-0 cells were then infected at an multiplicity of infection of five for 4 h. Coverslips were removed and placed on the dish containing MRC5 cells and were covered by a 0.5% agarose/2 × DMEM overlay. Five days later, virus spreading was assayed by crystal violet staining.

Animal experiments

All animal experiments were performed in accordance with institutional guidelines review board for animal care (John C Bell and University of Ottawa ethical board).

For safety study, biodistribution assay was performed by injecting 3E5 CT26–LacZ cells subcutaneously on the right side of a BALB/c mouse. Seven days later, tumours were administered 1e8 pfu of each virus intravenously (i.v.). Organs titred and collected 0.2, 1, 4, 7 and 9 days post infection include the brain, lungs, ovaries, spleen, liver, kidneys, heart and tumour.

The maximum tolerated dose assay was performed using a dose escalation of Maraba, MG1 and MG1IDE between 5E8 and 5E9 pfu administered i.v., and monitoring the dose keeping 100% of mice alive.

For efficacy testing in the HT29 model, 3E6 cells were injected subcutaneously in nude mice. Seven days post tumour embedding, mice were treated with PBS, MG1 or MG1IDE at 1E8 pfu administered i.v.

In the CT26–LacZ model, 1E5 CT26–LacZ cells were injected via the tail vein into BALB/c mice. Mice were treated with MG1 and MG1IDE (1e7 pfu) i.v. on day 3. Thirteen days post tumour implantation, mice were killed and the lungs were excised and stained with X-gal solution before counting.

In the liver metastases model, 1E6 CT26–LacZ cells were administered intrasplenic into BALB/c mice using intrasplenic/portal injection. Four days after, 1E8 pfu of virus was injected i.v. as treatment. Fourteen days after tumour cell injection, mice were killed and the spleen/liver were collected and stained with X-Gal before counting.

Modelling

Our model describing OV replication dynamics is represented by a subset of 8 ordinary differential equations. The first four equations describe the transition between the UP, IP, AP and PP depending on the concentration of virus and IFN in the environment. These equations are:

$$\frac{dUP}{dt} = -K_{VI} \times [V] \times [UP] - \left(\frac{-K_{IFNon}}{1+\left(\frac{[IFN]}{EC50}\right)^2} + K_{IFNon} \right) \times [UP] + K_{IFNoff} \times [PP],$$

$$\frac{dIP}{dt} = K_{VI} \times [V] \times [UP] - \left(\frac{-K_{IFNon}}{1+\left(\frac{[IFN]}{EC50}\right)^2} + K_{IFNon} \right) \times [IP] - \gamma_c \times [IP],$$

$$\frac{dAP}{dt} = \left(\frac{-K_{IFNon}}{1+\left(\frac{[IFN]}{EC50}\right)^2} + K_{IFNon} \right) [IP] - K_{VC} \times [AP] - \gamma_c \times [AP],$$

$$\frac{dPP}{dt} = \left(\frac{-K_{IFNon}}{1+\left(\frac{[IFN]}{EC50}\right)^2} + K_{IFNon} \right) [UP] + K_{VC} \times [AP] - K_{IFNoff} \times [PP].$$

The parameters used in the above equations represent the infection rate ($K_{vi.}$), the rate of IFN signaling activation (K_{IFNon}), the rate of IFN signalling inactivation (K_{IFNoff}), the EC50 of IFN (EC50), the rate of cell death (γ_c), and the rate viral clearance (K_{VC}).

The next subset of equation describe the concentration of virus (V), interferon (IFN), decoy receptor (DR) and decoy receptor-IFN complex (DR-IFN) in the media. These equations are:

$$\frac{dV}{dt} = K_{Bud\ IP} \times [IP] + K_{Bud\ AP} \times [AP] - K_{VI} \times [V] \times [UP] - \gamma_V \times [V],$$

$$\frac{dIFN}{dt} = K_{IFN1} \times [IP] + K_{IFN2.1} \times [AP] + K_{IFN2.2} \times [PP] - \gamma_{IFN} \times IFN - K_f \times [DR] \times [IFN] + K_r \times [DR - IFN],$$

$$\frac{dDR}{dt} = K_{DR\_IP} \times [IP] + K_{DR\_AP} \times [AP] - \gamma_{DR} \times [DR] - K_f \times [DR] \times [IFN] + K_R \times [DR - IFN],$$

$$\frac{dDR-IFN}{dt} = K_f \times [DR] \times [IFN] - K_r \times [DR - IFN].$$

The parameters described in the above equations represent the rate of virus budding from IP and AP ($K_{Bud\ IP}$ and $K_{Bud\ AP}$, respectfully), the infection rate ($K_{vi.}$), the rate of virus degradation (γ_V), the rate of IFN production from IP, AP and PP (K_{IFN1},$K_{IFN2.1}$ and $K_{IFN2.2}$ respectfully), the rate of IFN degradation (γ_{IFN}), the rate of decoy receptor production from IP and PP (K_{DR_IP} and K_{DR_AP} respectfully), the rate of decoy degradation (γ_{DR}), the forward rate of IFN-Decoy complex formation (K_f), and the reverse rate of complex formation (K_r). IFN responsive tumors were simulated by decreasing $K_{Bud\ IP}$ and $K_{Bud\ AP}$ 10 fold relative to normal cells. IFN non-responsive tumors were simulated by equally randomly decreasing all IFN-regulated processes (K_{IFN1}, $K_{IFN2.1}$, $K_{IFN2.2}$,K_{VC} and K_{IFNon}) 2 to 20 fold. The Monte Carlo simulation was generated by varying the parameters in the above model within a 1 log window.

Model parameter identification was performed using a simulated annealing-like method were all parameters are identical in a given cell line other than the capacity to produce IDE. All simulations were generated in Matlab using the ODE solver ode15s under default parameters imposing a none-negativity constraint. A full list of model amendments to describe each IFN evasion strategy, as well as a list of parameter values utilized in our simulations, are available in **Appendix Table 2 & Appendix Table 3** respectfully.

Chapter III. Microtubule Destabilizers Disrupt Interferon Production and Sensitize to Rhabdovirus Bystander Killing

Authors:
Rozanne Arulanandam[1,2], Cory Batenchuk[1,3,4], Chadi Zakaria[5],Julie Cox[1,3], Oliver Varette[1], Vanessa Garcia[1,3], Raunak Karmacharya[1,3], Anisha Sinha[1,3], Andrew Babawy[1,3], Theresa Falls[1,2], Andrew Chen[1], Jeff Hamill[1], Nicole Forbes[1,3], Naomi Da Silva[1,3], David Conrad[1,2], Harry Atkins[1,2], Kennneth Garson[1],Carolina Ilkow[1,2],Mads Kaern[4,6,7], Barbara Vanderhyden[1],2,Nahum Sonenberg[5], Tommy Alain[5], Fabrice Le Boeuf [1], *John Bell[1,2,3], *Jean-Simon Diallo[1,2,3]

Affiliations:
1. Center for Innovative Cancer Therapeutics, Ottawa Hospital Research Institute, Ottawa, Ontario, Canada K1H 8L6.
2. Department of Medicine, University of Ottawa, Ottawa, Ontario, Canada K1H 8L6.
3. Department of Biochemistry, Immunology and Microbiology, University of Ottawa, Ottawa, Ontario, Canada K1H 8L6.
4. Ottawa Institute of Systems Biology, University of Ottawa, Ottawa, Ontario, Canada K1H 8L6.
5. McGill University, Department of Biochemistry, Goodman Cancer Center
6. Department of Cellular and Molecular Medicine, University of Ottawa, Ottawa, Ontario, Canada K1H 8L6.
7. Department of Physics, University of Ottawa, Ottawa, Ontario, Canada K1H 8L6.
5. Apoptosis Research Center, Children's Hospital of Eastern Ontario, Ottawa, Ontario, Canada K1H 8L6.

Journal:
In submission to Nature Communications, 2014

My contribution:
I performed all aspects of modelling & microarrays data acquisition & analysis in this paper which is represented in Figure 3.3, Figure 3.6, Appendix Figure 5, Appendix Table IV and Data S1[$].

Chapter Synopsis

To further substantiate the model, in the article entitled ***Microtubule Destabilizers Disrupt Interferon Production and Sensitize to Rhabdovirus Bystander Killing***, I adapted the model to describe the impact of colchicine on virus kinetics. In the current study, we observe that microtubule destabilizing agents, such as colchicine, *enhance both the cytotoxicity and replication of OVs in tumor cells*.

After I performed microarray analysis of the response against OVs in the presence of colchicine, I concluded that while this drug did appear to block the "second wave" of antiviral defences induced by type I IFN signalling (**Figure 3.2 a&b**.), it had little to no impact on the induction of IFN mRNA in response to virus infection (**Figure 3.2 c**). Latter studies performed by Dr. Arulanandam concluded that it is not downstream IFN signalling, nor the mRNA export of IFNs, which appears to be affected but rather the rate of IFN protein secretion owing to a lag in IFN mRNA translation.

When we investigated gene processes preferentially induced by virus exclusively upon colchicine treatment, we observed a strong enrichment for genes involving the inflammatory and wound healing responses (**Appendix Figure 5**). Interestingly, many of the cytokines released upon virus infection induce the activation of pro-cell death pathways, specifically mitotic catastrophe, exclusively in the presence of colchicine. Indeed, colchicine enhanced the cytotoxicity of both replicating and non-replicating rhabdovirus particles.

To better understand the relationship between both mechanisms, I adapted the model to simulate the relationship between the lag in IFN secretion, and the induction of novel pro-cell

death pathways triggered by cytokines released from infected cells (**Figure 3.6 a**). From these simulations, induction of the pro-cell death pathways appears to be the key driving factor in tumor specific cytotoxicity (**Figure 3.5 c-d**). Although increasing the lag in IFN secretion did sensitize tumor tissue, this response was non-specific and lead to the sensitization of normal tissue. This observation is analogous with my previous conclusion regarding chemical inhibitors of IFN signalling or exogenous addition of an IFN decoy receptor in chapter II (**Figures 2.2 & 2.3**). In regards to virus replication, while the cytokine-mediated cell death pathway generally decreased the amount of virus particles released, a short lag in IFN responses had the potential to selectively enhance replication in tumor tissue (**Figure 3.5 b**). Taken together, the data in chapters III illustrates that the model can be adapted to describe and understand the impact of viral sensitizing drugs on OV kinetics.

Abstract

Oncolytic rhabdoviruses are being evaluated clinically for the treatment of cancer but are known to face a roadblock in tumors that retain the capacity to engage antiviral defences through the type I interferon (IFN) response. In this study, we show that several microtubule-destabilizing agents that have been used for decades to treat a myriad of human diseases also sensitize cancer cells to oncolytic rhabdoviruses and improve therapeutic outcomes in resistant mouse cancer models. Drug-induced microtubule destabilization leads to superior viral spread in cancer cells by disrupting Type I IFN production, through a decrease in polysome-associated mRNAs, IFN protein expression and secretion. Furthermore, cancer cells are specifically sensitized to a subset of rhabdovirus-induced cytokines following treatment with microtubule destabilizing drugs, increasing viral bystander effects. Overall, this study brings new insight in rhabdovirus biology and uncovers a novel role for microtubules in coordinating the innate cellular antiviral response, opening new avenues to improve oncolytic rhabdovirus therapeutic efficacy.

Introduction

Oncolytic viruses (OV) are self-amplifying cancer biotherapeutics that destroy malignancies without harming normal tissues. Derived from a variety of viral species, OVs are often engineered to exploit well-known hallmarks of cancer. This includes deregulated metabolism and proliferation, evasion of cell death, and inefficient antiviral signaling (267). Within the tumor, these agents destroy the malignancy by inducing direct oncolysis, stimulating anti-tumor immune responses and promoting tumor-vasculature shutdown (reviewed in (168)). While promising early and late phase clinical trials employing OVs to treat cancers continue to generate great enthusiasm, heterogeneity in the clinical response remains a challenge (168, 211, 243). To this end, it has been long recognized that improvements to therapeutic efficacy either through viral engineering or through combination therapies will be critical to the success of these platforms (168, 268).

Rhabdoviruses such as vesicular stomatitis virus (VSV) have been used pre-clinically as a backbone to generate OVs for over a decade (165, 201, 269) and are now beginning clinical evaluation (e.g. NCT01628640). While wild-type rhabdoviruses such as VSV (wtVSV) preferentially replicate in cancer cells, their tumor-selectivity can be greatly improved through genetic engineering, for example by capitalizing on the frequently defective capacity of tumors to engage antiviral programs (165, 201, 269). One of the first characterized and widely studied oncolytic strains of VSV (VSVΔ51) harbours a deletion at methionine 51 in the matrix (M) protein hindering on its ability to interact with nuclear pore proteins and to block the export of cellular anti-viral mRNAs from the nucleus to the cytoplasm (191). This stable deletion severely

attenuates VSVΔ51 in normal cells that have fully functional antiviral systems but permits robust replication in tumor cells that have lost the ability to mount an effective antiviral response.

Capitalizing on cancer-specific defects in cellular immunity makes for remarkably safe and selective therapeutics; however, this can come at a significant cost in terms of efficacy. While VSVΔ51 can cure animals of some tumors incapable of producing or responding to IFN, nearly a third of cancer cell lines are essentially normal in this capacity, severely limiting viral spread and oncolysis (201). Several genetic approaches have been explored and can be effective to overcome this roadblock. This includes using more potent viral backbones (e.g. Maraba MG-1 (166), wtVSV-IFNβ (269)) or expressing therapeutic transgenes to impair the IFN response (e.g. VSVΔ51-IDE) (270). However, the success of this strategy requires astutely navigating the delicate balance between efficacy and safety.

Alternately, pharmacological approaches to enhance OVs have also been explored and provide additional therapeutic control due to the inherently transient and tunable action of drugs. For example our group has shown that treatment of resistant tumor cells with HDAC inhibitors (HDIs) that down-regulate IFN-responsive genes (271), leads to increased oncolysis by VSVΔ51 (212). More recently, we screened a small molecule library to discover novel enhancers of VSVΔ51-mediated oncolysis. This led to the discovery of VSe1 (Viral Sensitizer 1), a novel synthetic antagonist of the cellular antiviral response that inhibits Type I IFN-induced gene transcription, analogously to HDIs (213). VSe1 was but one of fifteen viral sensitizer (VSe) compounds exhibiting VSVΔ51-enhancing activity identified. In the present study, we further characterize a subgroup of these fifteen compounds that interestingly share a common yet unexpected target. We report here that several VSe compounds are microtubule-destabilizing

agents (MDA), and set the framework for explaining how they selectively enhance oncolytic rhabdovirus activity in tumors.

Results

Microtubule-destabilizing agents enhance VSVΔ51-mediated oncolysis in a cancer-specific fashion

Literature mining performed on our published high throughput screening dataset (213) revealed that seven of fifteen VSe compounds enhancing VSVΔ51-mediated oncolysis are approved drugs that have microtubule-destabilizing activity. The compounds, their drug class, and structures are listed in Supplemental Table 1[$$$] along with their associated VSe nomenclature as previously published (213). To validate their activity, we selected representative colchicinoids (colchicine), vinka alkaloids (vinorelbine) and benzimidazoles (albendazole and parbendazole). These MDAs were tested across a range of concentrations on VSVΔ51-resistant 786-0 human renal carcinoma cells (Fig. 3.1a). Viability assays using alamar blue metabolic dye revealed that all MDAs tested enhanced cell killing elicited by a low multiplicity of infection of VSVΔ51 (MOI = 0.01, Fig 3.1a). Similar results were obtained in VSVΔ51-resistant mouse cancer cell lines (4T1 and CT26, Fig S1a-b). Treatment of cancer cells with colchicine, a drug used for autoimmune diseases such as gouty arthritis and one of the most potent MDAs tested, led to synergistic killing in combination with both VSVΔ51 and wtVSV (Fig. S1c[$$$]) and robustly enhanced the activity of Maraba MG-1 (Fig. S1d[$$$]). In contrast, MDAs did not enhance VSVΔ51-mediated oncolysis in normal human fibroblasts (GM38, Fig 3.1b).

Given MDAs and VSVΔ51 can independently have cytotoxic effects, we considered that the visible synergy between drug and rhabdoviruses could result from improved rhabdoviral spread/oncolysis, increased sensitivity to MDAs, or both. Microtubule destabilization using colchicine and other MDAs robustly increased VSVΔ51 spread and viral titers in several human and mouse cancer cell lines but not in normal fibroblasts (Fig. 3.1c-d$^{\$\$\$}$ and S1e-f$^{\$\$\$}$) consistent with a cancer-specific enhancement of viral growth. In cancerous 786-0 but not normal GM38 cells, colchicine increased VSVΔ51-GFP spread (Fig 3.1d, h) and viral protein expression (Fig 3.1e), even though the drug effectively depolymerized microtubules in both cell lines at the dose used (100 nM, Fig 3.1f). Comparing multi-step and single-step viral growth profiles suggest that in cancer cells, microtubule destabilization impacts VSVΔ51's ability to spread as opposed to its replication rate (Fig 3.1g). In contrast, a slightly negative effect of the drug on viral propagation was observed using wild-type VSV (wtVSV, Fig 3.1e, h, g). Parallel quantification of virally-expressed GFP and propidium iodine (PI) staining of dead/dying cells by flow cytometry however confirmed that while wtVSV propagation is hampered by colchicine treatment, cell death is nonetheless increased in comparison to virus or drug alone (Fig 3.1h) consistent with results from synergy assays (Fig S1d). The combination of VSVΔ51 and colchicine also led to substantially more PI positive cells than either treatment alone, although this was accompanied by substantially increased GFP-positive infected cells in sharp contrast with wtVSV (Fig 3.1h). Altogether, these data suggest that microtubule destabilization augments rhabdovirus-mediated oncolysis by promoting cell death following infection and also promotes spread in the case of IFN-sensitive rhabdovirus mutants such as VSVΔ51.

Figure 1

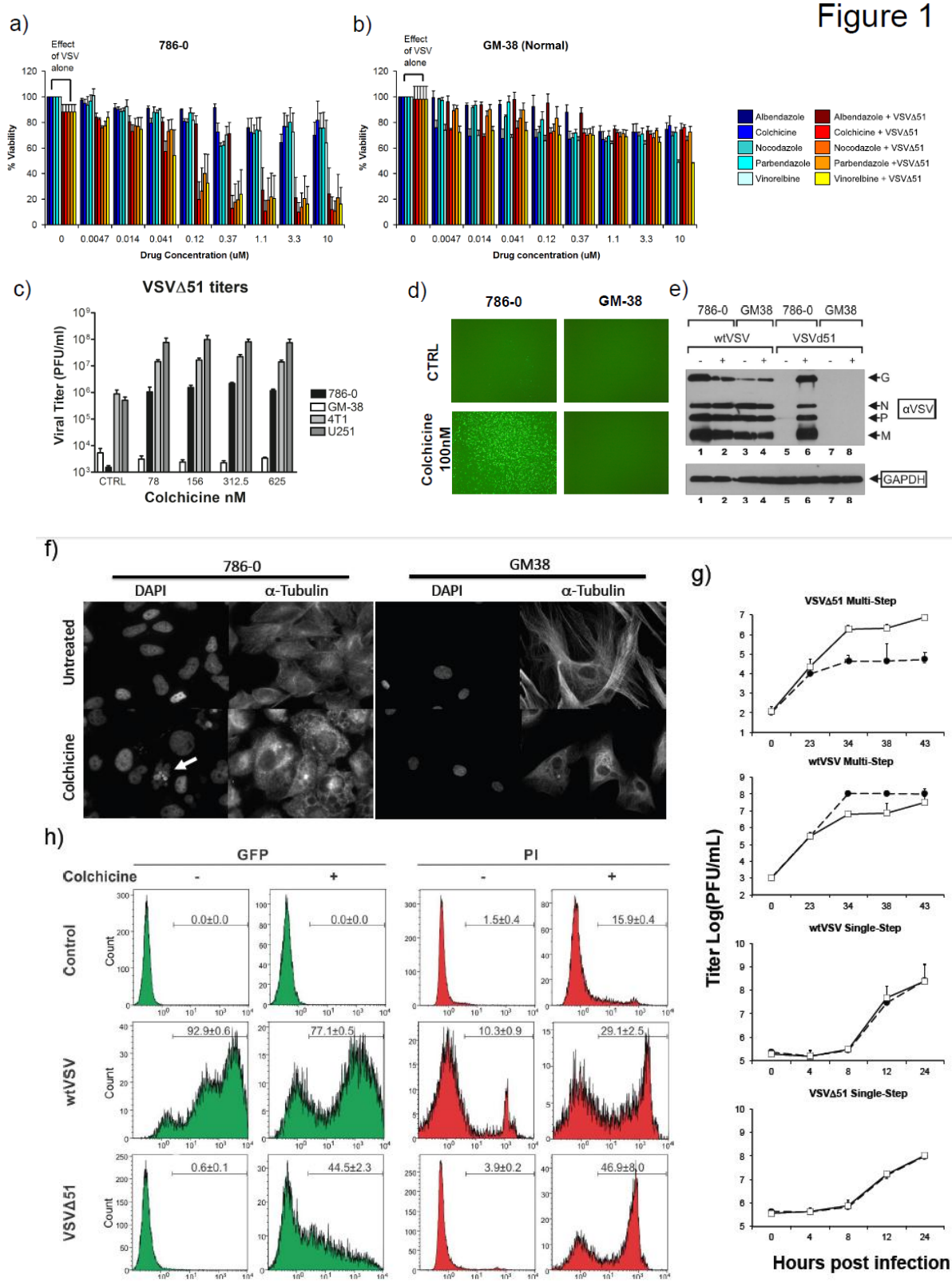
a)
786-0
Effect of VSV alone
% Viability
Drug Concentration (uM)
b)
GM-38 (Normal)
Albendazole
Colchicine
Nocodazole
Parbendazole
Vinorelbine
Albendazole + VSVΔ51
Colchicine + VSVΔ51
Nocodazole + VSVΔ51
Parbendazole +VSVΔ51
Vinorelbine + VSVΔ51
c)
VSVΔ51 titers
Viral Titer (PFU/ml)
786-0
GM-38
4T1
U251
Colchicine nM
d)
786-0
GM-38
CTRL
Colchicine 100nM
e)
786-0 GM38 786-0 GM38
wtVSV
VSVd51
G
N
P
M
αVSV
GAPDH
f)
786-0
GM38
DAPI
α-Tubulin
Untreated
Colchicine
g)
VSVΔ51 Multi-Step
wtVSV Multi-Step
wtVSV Single-Step
VSVΔ51 Single-Step
Titer Log(PFU/mL)
Hours post infection
h)
GFP
PI
Colchicine
Control
wtVSV
VSVΔ51
Count
0.0±0.0
0.0±0.0
1.5±0.4
15.9±0.4
92.9±0.6
77.1±0.5
10.3±0.9
29.1±2.5
0.6±0.1
44.5±2.3
3.9±0.2
46.9±8.0

Figure 3.1. Microtubule destabilizers enhance VSVΔ51 spread in cancer but not normal cells.

a-b) 786-0 cancer (a) and GM-38 normal (b) cells were pre-treated for 4h with microtubule destabilizing agents at concentrations indicated in x-axis then challenged with VSVΔ51 at MOI 0.01. 48h later, metabolic activity was assessed using alamar blue as a measure of cell viability. Error bars are standard error (SE) from three separate triplicate experiments. c) Cancerous human 786-0, U251, and mouse 4T1 cells as well as normal human GM-38 cells were pre-treated 4h with colchicine at the dosed indicated in x-axis and treated with VSVΔ51 MOI 0.01 for 48h at which time supernatants were collected and titered by standard plaque assay. Error bars represent SE from three independent experiments. d-e) 786-0 and GM38 cells were treated with 100nM colchicine or vehicle for 4h prior to infection with VSVΔ51-GFP at MOI 0,01. At 48h post infection, fluorescence pictures were taken (c), and cells were lysed and probed using polyclonal anti-VSV and anti-GAPDH antibodies by Western blot, where VSV G, N, P, M proteins are indicated by arrows (d). f) 786-0 cells were pretreated with colchicine 100 nM or vehicle and infected with VSVΔ51-GFP MOI 0.01 for 48h at which time cells were collected and stained with propidium iodine (PI). Cells were sorted by flow cytometry according to GFP and PI. Numbers represent the average percent cells gated ± standard deviation from three experiments. In g), 786-0 cells were pre-treated with 100nM colchicine for 4h and infected with MOI 0.01 (multi-step) or MOI 3 (single-step) of VSVΔ51 or wtVSV, and supernatants were collected at various times indicated on the x-axis and titered by standard plaque assay. In h) cancerous 786-0 and normal GM-38 fibroblasts were treated with 100nM colchicine for 24h and cells were fixed and stained using anti beta-Dapi and tubulin antibody and imaged using fluorescence microscopy under oil immersion under 63X objective. The white arrow highlights an example of cellular polynucleation induced by microtubule destabilization.

Microtubule-destabilizing agents enhance oncolytic rhabdovirus efficacy in highly resistant syngeneic and transgenic mouse tumor models

Given that colchicine, vinorelbine, and other MDAs enhanced oncolytic rhabdovirus efficacy in vitro, we performed a series of murine tumor model studies to determine whether these could also provide therapeutic benefit in vivo. We focused on the VSVΔ51 platform given that MDAs enhanced both viral spread and cancer cell killing for this strain. We first explored this in a highly aggressive syngeneic model of triple-negative breast cancer. Subcutaneous 4T1 breast tumors were implanted in syngeneic Balb/C mice and mice were treated intraperitoneally (i.p) with either PBS or colchicine (2mg/kg i.p.) and an intratumorally (i.t) with either VSVΔ51 (1E8 PFU) or PBS. We found that two once-weekly treatment cycles led to delayed tumor progression and significantly prolonged survival in mice receiving both colchicine and VSVΔ51 compared to either monotherapy (Fig. S2a$^{\$\$\$}$). Vinorelbine (8 mg/kg) was also effective, significantly prolonging survival of 4T1-tumour bearing mice in combination with VSVΔ51 (Fig. S2a$^{\$\$\$}$). A similar impact on tumor growth was observed using oncolytic Maraba MG-1 (Fig. S2b$^{\$\$\$}$) and in a syngeneic subcutaneous CT26 colon cancer model (Fig. S2c). As expected from in vitro evidence (Fig. 3.1 a-h), these effects of colchicine were associated with tumor-specific increases in VSVΔ51 growth. Using a firefly luciferase expressing VSVΔ51 and an in vivo imaging system (IVIS), we observed that 24h post-infection (i.t), 4T1-grafted animals treated with colchicine exhibited increased luminescence specifically in tumors (Fig. 3.2a). In line with this, a significant increase in VSVΔ51 titers was observed in colchicine-treated animals (Fig. 3.2b). In contrast, assessment of viral titers in normal organs including spleen, heart, liver,

lungs, kidney, and brain by standard plaque assay revealed no detectable VSVΔ51 in any organ at any time point in both PBS and colchicine-treated mice.

The efficacy of combined rhabdovirus/MDA treatment was subsequently evaluated in a highly treatment-resistant MISIIRTag transgenic ovarian cancer mouse model. These mice express SV40 Large T-antigen specifically in the ovaries and develop visible tumors at 10-11 weeks (272). In these experiments, we used VSVΔ51 expressing GM-CSF to further increase anti-tumor activity. Fig 3.2c shows that weekly treatment cycles of VSVΔ51-GM-CSF and colchicine both delivered i.p., led to significantly prolonged survival of MISIIRTag mice as compared to either monotherapy. Overall, these data suggest that combined oncolytic rhabdovirus and MDA treatment can elicit significant antitumor efficacy, prolonging survival even in highly treatment-resistant spontaneously arising tumors.

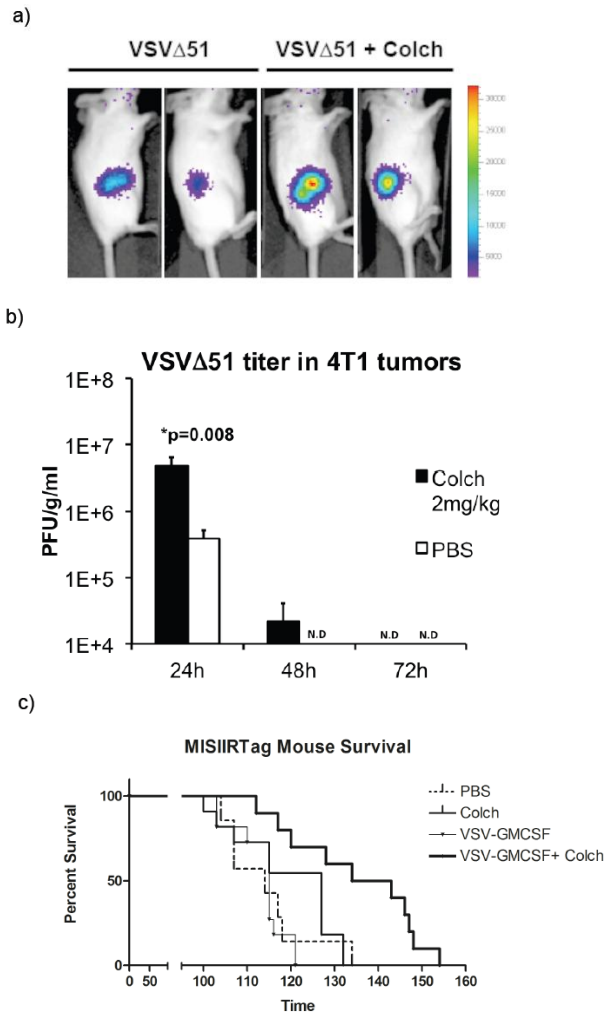

Figure 3.2. Colchicine increases VSVΔ51 spread and oncolytic activity in resistant syngeneic and transgenic tumor models.

a) 4T1 tumors were implanted in right hind flanks of syngeneic Balb/C mice and injected with 1E8 PFU of VSVΔ51-luciferase or PBS intratumorally (i.t) , and 2mg/kg colchicine or vehicle intraperitoneally (i.p), 7 days after tumor implantation. Luminescence was monitored by IVIS after 24h. b) 4T1 tumors were implanted and treated as in a) and tumors and other organs were harvested after 24, 48, and 72h. Tissues were subsequently homogenized and titered by plaque assay. Error bars indicate standard error from an average of 5 tumors. * denotes a significant difference between PBS and colchicine treated tumors ($p<0.05$, t-test). N.D denotes not detected. Virus was also undetectable in all other organs (brain, lung, liver, kidney, spleen, heart) at all time points. c) MISSIIRTag transgenic mice were treated starting at 10 weeks of age with a weekly i.p. dose of VSVΔ51-GM-CSF (1E8 PFU, n=11), PBS (n=7) colchicine (1.5 mg/kg, n=11) or VSVΔ51-GM-CSF (1E8 PFU) and colchicine (1.5mg/kg, n=10). Survival was monitored over time (days, x-axis) and animals exhibiting critical abdominal extension were euthanized according to IRB guidelines. Log Rank test indicate the combined treatment is significantly prolonged over colchicine ($p=0.0082$) and VSVΔ51-GM-CSF ($p=0.0007$) alone.

Microtubule destabilization interferes with Type-I IFN-induced gene programs

While combined MDA and oncolytic rhabdovirus treatment provided therapeutic benefit in several models, the contrasting enhancing effects on spread of VSVΔ51 and wtVSV prompted further investigation. We used gene expression microarrays to gain perspective on the mechanisms involved. Cellular RNA was extracted 24h following infection of 786-0 cells with a low MOI (0.01) of VSVΔ51 (or mock) in presence of 100 nM colchicine or vehicle and hybridized on Affymetrix human Gene 1.0 ST microarrays. Analysis of this dataset is summarized in Figure 3.3a and shows for each treatment condition the expression of a subset of 248 genes found uniquely up- or down-regulated (>2-fold, $p<0.05$) VSVΔ51 infection in absence of drug. Importantly, gene enrichment analyses using the GOrilla gene set databases (265) revealed significant enrichments in Gene Ontology (GO) terms only within the 158 genes induced by VSVΔ51 but dampened by colchicine co-treatment (genes represented in green in the top half of the heat map in Fig. 3.3 a). Significant enrichments highlighted a multitude of biological processes involved in the immune response to virus/biologicals, ultimately converging on the Type I interferon response (Figure 3.3b). Indeed, 26 of the 158 genes up-regulated by VSVΔ51 that were not similarly induced upon co-treatment with colchicine are known direct downstream targets of Type I IFN (Fig 3.3a, right inset). Removing the 26 IFN target genes from the dataset led to the loss of all significant GO-term enrichments. Altogether, this suggests that microtubule destabilization alters the genetic response of cancer cells to VSVΔ51 infection and most prominently dampens virus-induced Type I IFN gene programs.

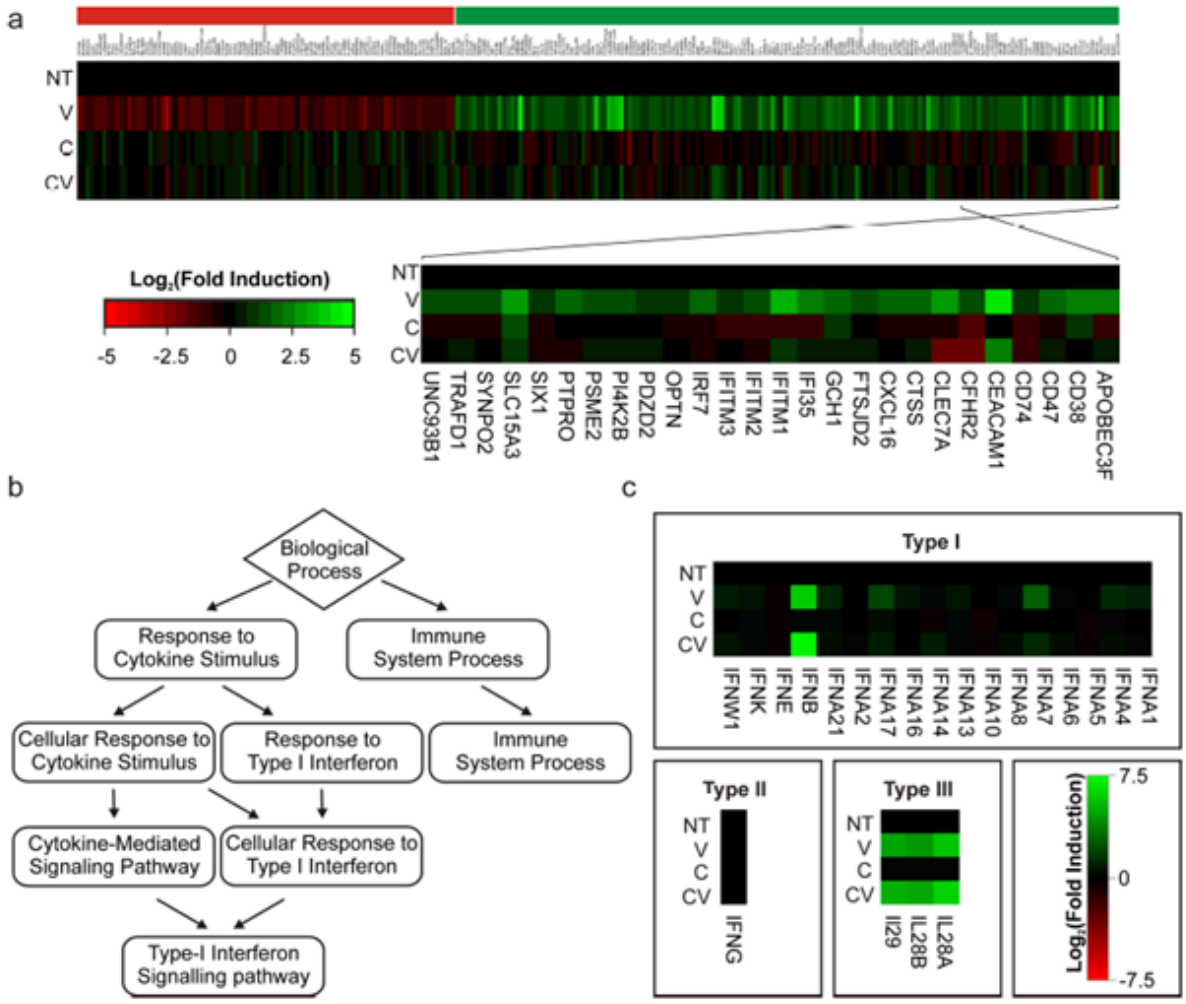

Figure 3.3. Microtubule destabilization hinders the response to Type I IFN stimulated genes induced by VSVΔ51.

a) 786-0 cells were pretreated for 4h with 100nM colchicine or vehicle and infected with VSVΔ51 at MOI 0.01 or mock infected. 24h later RNA was collected and pooled, and triplicate experiments were hybridized on Affymetrix human Gene ST 1.0 microarrays. Shown are the heat maps of all genes found to be significantly increased (green) or decreased (red) >2-fold in VSVΔ51 infected 786-0 cells as compared to control (NT) and the fold increase of the same genes VSV-infected (V), colchicine treated, and colchicine treated / virus infected (V + C) conditions. Inset shows a group of 26 Type I IFN stimulated genes that are up-regulated in V but not V + C conditions. b) Summary of gene ontology relationships for significantly enriched gene sets from analysis of microarray data presented in a). c) Microarray expression data for subset of Interferon isoforms and sub-types obtained from a).

Microtubule destabilization does not interfere with VSV or IFN-induced antiviral signaling

The type I IFN response is thought to proceed in three waves. First, activation of pattern recognition receptors such as Toll-like receptor 7 (TLR7) and Retinoic acid-induced gene I (RIG-I), through signaling via Tank binding kinase 1 / IκBα kinase (TBK-1/IKK) and transcription factor Interferon regulatory factor 3 (IRF-3), leads to increased "first wave" IFNβ transcription, translation, and secretion. Second, autocrine/paracrine signaling through IFN receptor /Janus kinase (JAK) / STAT (Signal Transducer and Activator of Transcription), leads to formation of Interferon Stimulated Gene Factor 3 (ISGF3), leading to the up-regulation of interferon stimulated genes (ISGs) including IRF-7 and "second wave" IFN-α isoforms. Third, additional ISGs are up regulated due to the combination of persistent IFN signaling and IRF-7 up-regulation (165, 273).

Microarray data suggested that microtubule destabilization inhibits the transcriptional response of direct Type I IFN targets in the context of VSVΔ51 infection. However, we did note that while some virus-induced second wave IFNα isoforms were dampened similarly to other ISGs after treatment with colchicine, first wave IFNβ mRNA induction following infection remained similar (Figure 3.3c). This suggested a possible blockage in between the first and second wave of IFN production. Supporting this, colchicine treatment did not alter IFNβ mRNA expression in either nuclear or cytoplasmic compartments, nor IRF-3 or STAT-1 nuclear shuttling and phosphorylation status shortly following VSVΔ51 infection at high MOI (3). This suggests that signaling upstream of IFNβ transcription is unaffected by microtubule destabilization (Fig. 3.4a-b). Similarly, colchicine treatment did not inhibit STAT-1 phosphorylation or alter nuclear/cytoplasmic distribution of the transcription factor following

treatment with exogenous IFNα (Fig. 3.4c), indicating fully functional IFN response through JAK/STAT. In line with this, colchicine could not overcome the antiviral effects of Type I IFNs in either 786-0 or U251 cells (Fig S3a-b[$$$]), in sharp contrast with suberoyl anilide hyroxamic acid (SAHA), an HDAC inhibitor known to effectively dampen the antiviral effects of type I IFNs (212) (Fig. S4a[$$$]). Overall, this suggests that MDAs do not modulate antiviral response pathways upstream of IFNβ mRNA transcription and cytoplasmic shuttling nor alter Type I IFN-induced JAK/STAT signaling and its antiviral effects.

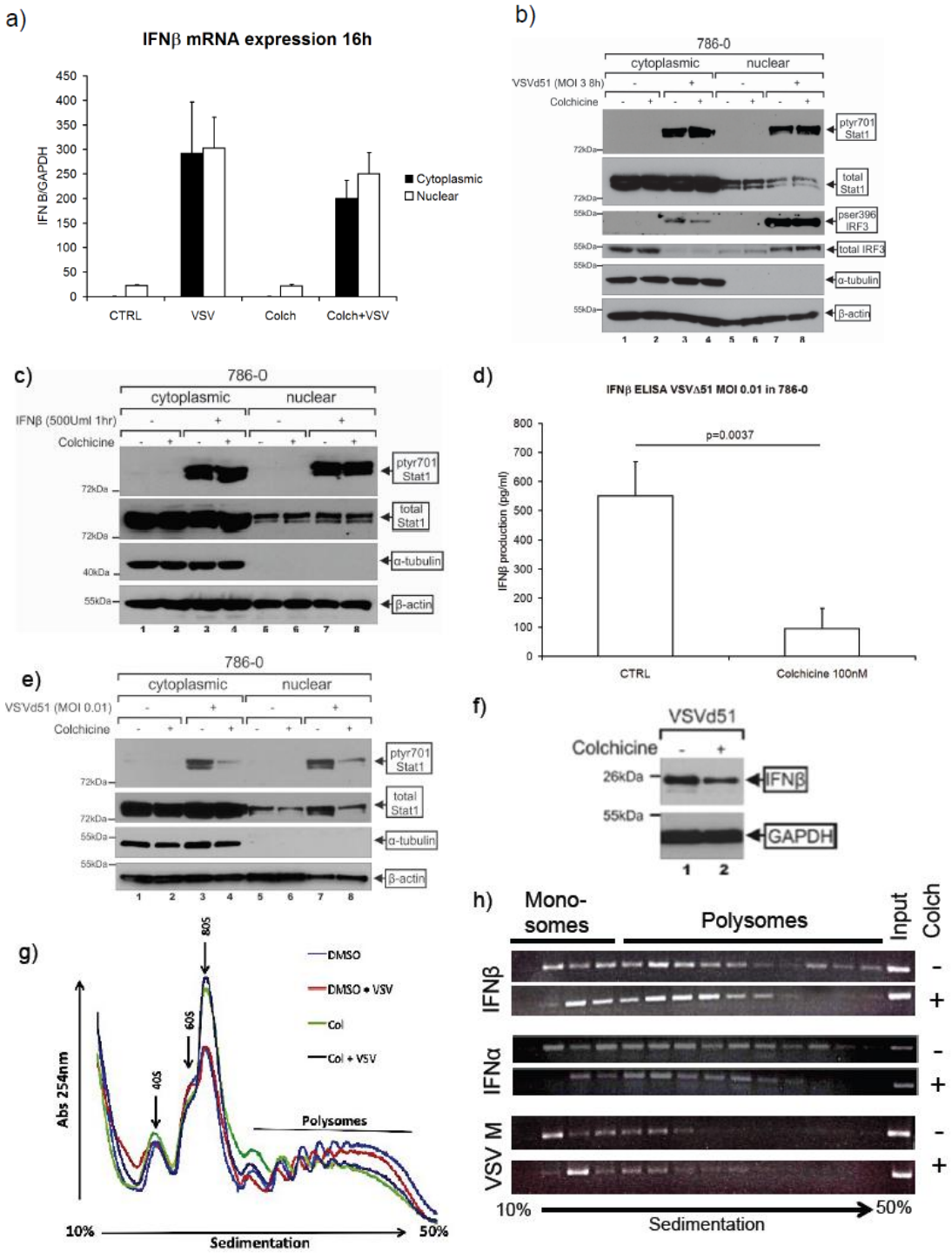
a)
IFNβ mRNA expression 16h
IFN B/GAPDH
Cytoplasmic
Nuclear
CTRL
VSV
Colch
Colch+VSV
b)
786-0
cytoplasmic
nuclear
VSVd51 (MOI 3 8h)
Colchicine
ptyr701 Stat1
total Stat1
pser396 IRF3
total IRF3
α-tubulin
β-actin
c)
786-0
cytoplasmic
nuclear
IFNβ (500Uml 1hr)
Colchicine
ptyr701 Stat1
total Stat1
α-tubulin
β-actin
d)
IFNβ ELISA VSVΔ51 MOI 0.01 in 786-0
p=0.0037
IFNβ production (pg/ml)
CTRL
Colchicine 100nM
e)
786-0
cytoplasmic
nuclear
VSVd51 (MOI 0.01)
Colchicine
ptyr701 Stat1
total Stat1
α-tubulin
β-actin
f)
VSVd51
Colchicine
IFNβ
GAPDH
g)
DMSO
DMSO + VSV
Col
Col + VSV
40S
60S
80S
Polysomes
Abs 254nm
10%
Sedimentation
50%
h)
Mono-somes
Polysomes
Input
Colch
IFNβ
IFNα
VSV M
10%
Sedimentation
50%

Figure 3.4. Microtubule destabilization leads to a decrease in Type I IFN translation and secretion.

a) 786-0 cells were pretreated for 4h with 100nM colchicine or vehicle and infected with VSVΔ51 at MOI 0.01 or mock infected. 16h later, cells were collected and separated into nuclear and cytoplasmic fractions, from which RNA was extracted and converted to cDNA. qPCR for IFNβ and GAPDH were then performed. Data reported represents the fold change in IFNβ relative to uninfected control. Error bars represent standard error from an average of three replicate experiments. b) 786-0 cells were pretreated for 4h with 100nM colchicine or vehicle and infected with VSVΔ51 at MOI 3 or mock infected. 8h later, cytoplasmic and nuclear cell fractions were collected, run on polyacrylamide gels and subject to western blotting. Blots were cut into strips for was used to probe for STAT-1, phospho STAT-1 (Tyrosine 701) , IRF-3, phospho-IRF-3 (serine 396), alpha-tubulin, and beta-actin. c) 786-0 cells were pretreated for 4h with 100nM colchicine or vehicle and treated with 500U IFNβ or mock. One hour later, cytoplasmic and nuclear cell fractions were collected and run on a polyacrylamide gel. Western blotting was used to probe for STAT-1, phospho STAT-1 (Tyrosine 701), α-tubulin, and β-actin. d) 786-0 cells were treated with 100nM colchicine or vehicle for 4h prior to infection with VSVΔ51-GFP at MOI 0.01. 24h later, supernatants were collected and IFNβ was quantified by ELISA. Error bars represent standard error from three replicate experiments and statistical significance was assessed by ANOVA. e) 786-0 cells were treated with 100nM colchicine or vehicle for 4h prior to infection with VSVΔ51-GFP MOI 0.01. After 20h,cytoplasmic and nuclear cell fractions were collected and run on polyacrylamide gel. Western blotting for was used to probe for STAT-1, phospho STAT-1 (Tyrosine 701), α-tubulin, and β-actin. f) 786-0 cells were treated as in e. After 24h, whole cell extracts were collected and IFNβ expression was assessed through Western blotting. GAPDH was used as a loading control. g) 786-0 cells were treated as in d) and after 24h, whole cell lysates were collected and run on a 10-50% sedimentation gradient. Absorbance at 254nM (RNA) was then measured over each fraction (sampling interval of 0.1 seconds). In h) RNA was subsequently extracted from each fraction and used to generate cDNA. The abundance of , IFNα, IFNβ and VSV-M in each fraction was assessed by semi-quantitative PCR. Cycle numbers were adjusted to minimize saturation and compensate for different input gene expression levels.

Microtubule destabilization decreases type I IFN secretion in part by reducing mRNA translation efficiency

Altogether, our data suggested that microtubule destabilization decouples first and second wave IFN without inhibiting the JAK/STAT signaling axis. Offering a potential explanation for this phenomenon, studies dating prior to the purification and identification of Type I IFNs reported an effect of microtubule de-stabilizers such as colchicine and vinblastine on antiviral "interferon" cytokine secretion (274, 275). We addressed this possibility directly using ELISA (enzyme-linked immunosorbent assay). Figure 3.4d shows that even though mRNA levels and subcellular distribution was unaltered (Fig 3.3c, 3.4a) treatment with colchicine caused a significant decrease in secreted IFNβ following a 24h infection with a low MOI of VSVΔ51. A time-course revealed that treatment with colchicine effectively delayed the onset IFNβ, which eventually appeared over 48h in infected cell culture supernatants (Fig. S4a$^{\$\$\$}$). Expectedly, IFN-α was equally detected at lower concentrations than in control conditions in the absence of colchicine (Fig. S4b$^{\$\$\$}$), in line with microarray mRNA expression data (Fig. 3.3c). Consistent with the observed decrease in Type I IFN secretion, we found that colchicine treatment reduced phosphorylation of STAT-1 in these conditions (Fig 3.4e). Suggesting the effect was not unique to colchicine or 786-0 cells, other MDAs also decreased IFNβ secretion 24h post-infection with VSVΔ51 (Fig S4c) and a similar impact of microtubule destabilization on IFNβ secretion was observed in U251 cancer cells (Fig. S4d$^{\$\$\$}$). However, colchicine treatment also decreased IFNβ secretion in normal MRC-5 fetal lung fibroblasts (Fig. S4d$^{\$\$\$}$), suggesting this effect is not restricted to cancer cells and that additional mechanisms may contribute to the cancer-specific enhancement in VSVΔ51 spread observed in vitro and in vivo.

Given that microtubules are known to play a role in vesicular transport and that microtubule destabilizers such as colchicine have been shown to impact the secretion of various proteins (276-280), we considered the possibility that microtubule destabilization may simply impact the ability of cells to secrete cytokines. To assess this, we looked at the impact of microtubule destabilization on overall protein secretion using S35 pulse-labelling following challenge with either VSVΔ51, G-less VSVΔ51 (which can infect but cannot exit the cell) or treatment with the TLR agonist poly I:C. Looking at visible bands obtained by autoradiogram, we observed a variety of responses to colchicine treatment following viral stimulation. Whereas the secretion of some proteins was increased by all three stimuli but reduced following treatment with colchicine (analogously to what was observed by ELISA for IFNα and β), other proteins were not impacted by any viral stimulus nor affected by colchicine (Fig S4e[$$$]). This argues against a systematic negative impact of microtubule destabilization on protein secretion. To further address this, we quantified IL-6 secretion in cell supernatants following VSVΔ51 infection in presence and absence of colchicine, given that similarly to IFNβ, this cytokine was robustly up-regulated by VSVΔ51 infection at the mRNA level based on microarray analyses (Fig. 3.3c). In sharp contrast with what was observed for Type I IFNs, these experiments revealed no significant decrease in virus-induced IL-6 secretion following treatment with colchicine (Fig. S5f[$$$]). Further arguing against systematic inhibition of protein secretion following microtubule destabilization, the secretion of mouse GM-CSF encoded by the VSVΔ51-GM-CSF virus used in mouse experiments shown in Figure 3.2c increased proportionally to viral titers following treatment of VSVΔ51-GM-CSF infected 786-0 cells with colchicine (Fig. S4g-h[$$$]).

We therefore considered the possibility that microtubule disruption leads to decreased secretion of Type I IFNs indirectly by reducing translation of their encoding mRNAs. Supporting this idea, Western blots on whole cell extracts of infected 786-0 cells revealed that intracellular IFNβ protein expression levels decrease in parallel with a reduction with protein secretion (Fig. 3.4f). To measure translation efficiency, we looked at RNA distribution in mono-ribosomes and poly-ribosomes using gradient sedimentation. Fig 3.4g shows that colchicine treatment of 786-0 cells, irrespective of infection, led to a shift in mRNA distribution from polysome (highly translated) to monosome (poorly translated) fractions albeit to a lesser extent than PP242, an mTOR (mammalian target of rapamycin) translation inhibitor (see Fig. S5a[$$$]). Assessment of mRNA abundance by semi-quantitative PCR further showed that both IFNα and IFNβ were less abundant in the highest density polysomes of colchicine-treated cells (Fig. 3.4h). In contrast, looking at VSV M revealed a slight opposite shift in abundance from monosomes to lower-density polysomes (Fig. 3.4h). Overall, this suggests that microtubule destabilization reduces mRNA translation efficiency of cellular genes such as type I IFNs, whilst nonetheless allowing translation of viral genes. However, arguing against a role of mTOR or 4E-BP in mediating the observed effects of MDAs on Type I IFN mRNA translation efficiency, we failed to observe any alterations in the expression or phosphorylation of either mTOR targets S6 or 4EBP1 (237) following treatment of 786-0 cells with colchicine (Fig. S5b[$$$]).

Multiple secreted proteins induced by VSV infection increase microtubule destabilizer-induced mitotic catastrophe and death.

While these experiments shed light on the mechanisms leading to the enhancement of VSVΔ51 spread in cancer cells, it remained unclear why MDAs could also increase rhabdovirus infection-associated death, even with wtVSV for which spread was paradoxically reduced by microtubule destabilization (Fig 3.1e,g,h). We therefore assessed whether viral triggers could be sufficient to elicit cytotoxic effects upon microtubule destabilization. To this end, we challenged colchicine or vehicle-treated 786-0 cells with a UV-inactivated wtVSV. As expected, UV-inactivated wtVSV did not affect 786-0 viability in control conditions, even at a very high MOI (200). However, UV-inactivated virus was capable of effectively killing 786-0 cells treated with colchicine (starting at MOI 50, Fig. 3.5a). This was also observed in mouse 4T1 cells, albeit starting at a higher MOI of UV inactivated virus (Fig. S6a[$$$]).

MDAs lead to cytotoxicity by inducing mitotic catastrophe and polynucleation in cells that divide rapidly and have lost key cell cycle checkpoints, key hallmarks of cancer cells (138). To gain a better understanding of the mechanisms leading to increased death in MDA-treated cells challenged with rhabdovirus, we looked at the frequency of polynuclear cells in the context of infection. We treated 786-0 cells with colchicine or vehicle and infected them with VSVΔ51-GFP at low MOI (0.01). Twenty-four hours post-infection, cells were fixed and stained with a nuclear dye (Dapi) and an anti-α-tubulin antibody. Fluorescence microscopy was then used to visualize and count GFP-positive infected cells and those exhibiting characteristic polynucleation (see Fig. 3.1f white arrow for an example at higher magnification). As expected, colchicine treatment led to increased polynuclear cells whereas infection with VSVΔ51-GFP alone did not.

Importantly, 786-0 cells exhibited a robust increase in virus-associated GFP and a near doubling in the number of polynucleated cells compared to colchicine-treated cells upon co-treatment with VSVΔ51-GFP and colchicine (Fig. 3.5b-c). In contrast, polynucleation remained low in normal GM-38 cells under these conditions (Fig. 3.5c).

Looking at the proportion of polynuclear cells in infected (GFP+) and uninfected (GFP-) cells further revealed that these were equally frequent in both populations (Fig. 3.5d). This distribution suggested the likely involvement of a secreted factor in promoting polynucleation in the colchicine-treated infected cancer cell population. To explore this idea, we used supernatants from cancer cells infected with G-less VSVΔ51-GFP. As described previously, G-less VSVΔ51-GFP can infect and replicate but cannot bud from the cytoplasmic membrane (281). We treated 786-0 cells with G-less VSVΔ51-GFP at high MOI (10) or not and collected supernatants 24h post-infection. These supernatants were applied to virus-naïve 786-0 cells treated with colchicine or vehicle and cellular polynucleation was quantified. In line with the involvement of a secreted factor, supernatants from G-less VSVΔ51-infected but not mock treated cells increased polynucleation and cell death in virus-naïve 786-0 cells treated with colchicine (Fig. 3.5 e, f). However, this did not occur when using normal GM38 cells (Fig. 3.5f).

Interestingly, the polynucleation-inducing activity of G-less VSVΔ51-infected 786-0 cell supernatants was abrogated following filtration using a 10 but not 50 or 100 kDa molecular-weight cutoff filter. This pointed to the involvement of one or more secreted factors between 50 kDa and 10 kDa (Fig 3.5e). To generate a list of candidates, we queried the microarray data. We deemed that relevant candidates should be between 10 and 50 kDa and induced by VSVΔ51 in both vehicle and colchicine-treated conditions. The short list of these candidates is shown in

supplemental Table 2[$$$]. In addition to Type I IFNs, this included several growth-promoting cytokines (e.g. Rantes, IP-10, CXCL11, IL-8 and IL-6) as well as death inducing cytokines (e.g. TNF-α and other TNF-related proteins). Type III IFNs (IL28a, IL28b, and IL29) also figured on this list. While it is likely that many of these factors work in concert to recapitulate the synergy observed between virus infection and colchicine treatment observed in 5a-f, we nevertheless evaluated the impact of a subset of cytokines on the frequency of polynuclear cells in 786-0 cells in presence of colchicine. Interestingly, we found that some cytokines such as IL-6, IL-8, IP-10 and IL-29 significantly increased the frequency of polynuclear cells in colchicine-treated 786-0 cells (Fig. 3.5g). In addition, colchicine treatment increased cell death induced by TNF-α in 786-0 but not GM-38 cells (Fig. 3.5h). Overall, this infection with rhabdoviruses in the presence of colchicine leads to cancer-specific increases in bystander polynucleation and cell death, likely through the action of multiple secreted factors and death inducing cytokines.

Figure 5

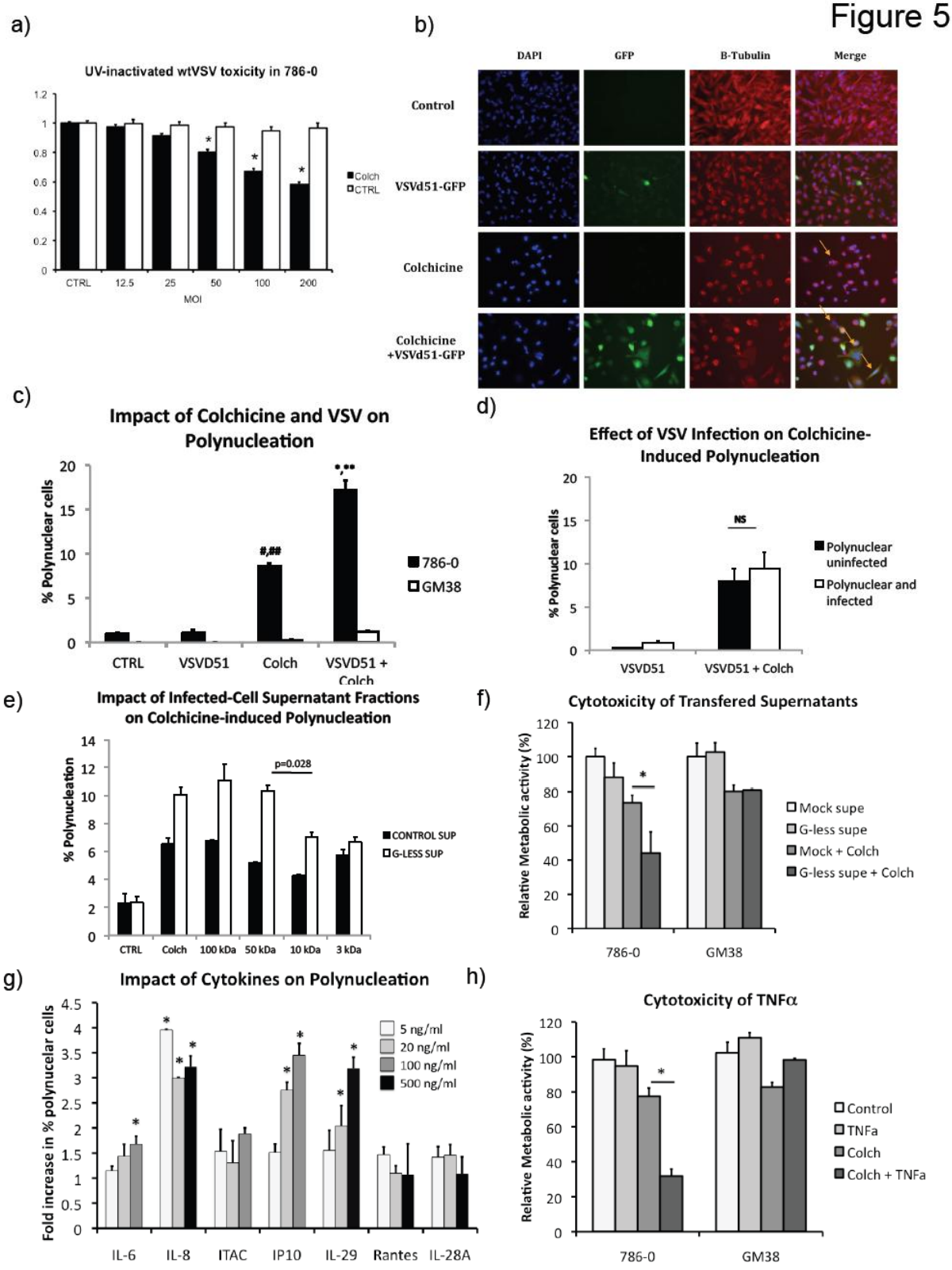
a)
UV-inactivated wtVSV toxicity in 786-0
Colch
CTRL
MOI
b)
DAPI
GFP
B-Tubulin
Merge
Control
VSVd51-GFP
Colchicine
Colchicine +VSVd51-GFP
c)
Impact of Colchicine and VSV on Polynucleation
% Polynuclear cells
786-0
GM38
CTRL
VSVD51
Colch
VSVD51 + Colch
d)
Effect of VSV Infection on Colchicine-Induced Polynucleation
NS
Polynuclear uninfected
Polynuclear and infected
e)
Impact of Infected-Cell Supernatant Fractions on Colchicine-induced Polynucleation
% Polynucleation
p=0.028
CONTROL SUP
G-LESS SUP
f)
Cytotoxicity of Transfered Supernatants
Relative Metabolic activity (%)
Mock supe
G-less supe
Mock + Colch
G-less supe + Colch
g)
Impact of Cytokines on Polynucleation
Fold increase in % polynucelar cells
5 ng/ml
20 ng/ml
100 ng/ml
500 ng/ml
IL-6
IL-8
ITAC
IP10
IL-29
Rantes
IL-28A
h)
Cytotoxicity of TNFα
Control
TNFa
Colch
Colch + TNFa

Figure 3.5. VSV-induced cell death is increased by microtubule destabilizer treatment through infection-induced secreted factors that lead to cell polynucleation and death specifically in cancer cells.

a) 786-0 cells were pre-treated for 4-hours with colchicine or DMSO and then treated were treated with described amount of non-replicating VSVwt at the described MOI. Viability was measured by alamar blue after 48h. Error bars represent standard error * denote $p<0.05$ based on ANOVA. b-c) Infection of 786-0 cancer cells and GM-38 normal cells were pre-treated with 100nM colchicine or vehicle for 4h and infected with VSVΔ51-GFP (green) at an MOI of 0.01 (or mock). 24h, cells were fixed and stained with Dapi (blue) and an anti-beta-tubulin antibody (red). Fluorescence microscopy pictures were taken and scored for number of GFP positive and polynuclear cells. a) Representative pictures obtained from 786-0 cells. Polynuclear cells are indicated with the yellow arrows. c) quantification of polynuclear cells reported as percentage of total cells. Error bars represent standard error of the average of three experiments. #,##,*,** denote a significant ($p<0.05$, ANOVA) differences between groups. # = 786-0 CTRL vs. 786-0 Colchicine-treated; ## = 786-0 colchicine-treated vs. GM38 colchicine-treated; * = 786-0 colchicine-treated vs. combined colchicine-VSVΔ51 treated; ** = combined colchicine-VSVΔ51 treated 786-0 vs. combined colchicine-VSVΔ51 treated GM38. d) 786-0 polynucleation data from b) looking at the percentage of virus-infected (GFP-positive) and uninfected (GFP-negative) cells exhibiting polynucleation. NS means not statistically different ($p>0.05$, ANOVA). e) 786-0 cells were infected with G-less VSVΔ51-GFP at MOI 10 and supernatants were collected 24h post-infection. Supernatants were then either applied directly to virus-naïve 786-0 cells treated with 100nM colchicine or vehicle, and passed through 100, 50, 10 and 3 kDa cutoff filters prior to application. 24h later, cells were fixed and stained with Dapi and beta-tubulin and polynuclear cells were counted. Error bars represent standard error of the mean of triplicates. A significant reduction in polynucleation was observed going from a 50 kDa to 10 kDa molecular cutoff filter ($p<0.05$, ANOVA). f) 786-0 and GM-38 cells were pre-treated for 4-hours with colchicine or DMSO and then treated with uninfected (mock) or G-less VSV infected cell supernatants (obtained from 786-0 or GM38 and re-applied to each respective cell line). g) 786-0 cells were pretreated with colchicine then treated with recombinant cytokines (indicated on the X-axis) at 5, 20 or 500 ng/ml. 24h later, polynuclear cells were counted. Fold increase in polynuclear cells relative to colchicine treatment alone is reported (average of triplicate) on the y-axis. h) 786-0 and GM-38 cells were pre-treated for 4-hours with colchicine or DMSO and then treated were treated with TNF or control. Viability was measured by alamar blue after 48h. Error bars represent standard error *,** denote $p<0.05$ based on ANOVA.

A mathematical model recapitulates the cancer-selective enhancement of VSVΔ51 oncolysis by microtubule destabilization through the combined effect of interferon secretion and increased by-stander killing

Overall, our results suggest that in the case of IFN-sensitive VSVΔ51, microtubule destabilization elicits a decrease in IFN secretion and an increase in by-stander cytopathic effects simultaneously. To describe the interplay between these two mechanisms, we adapted a mathematical model recently developed to investigate the impact of OV dynamics on tumor-selectivity (270). All equation parameters for this model are derived from literature or experimental observations and are identical between resistant cancer and normal cells, other than the rate of virus replication, which is set higher in tumor cells (270). In Figure 3.6a, we describe how this model was adapted from its original form by accounting for IFN secretion and the activation of an arbitrary cytokine-induced cell death pathway. In our simulations, we gradually decreased the rate of IFN secretion (K_{Sec}, red dahsed), and increased sensitivity towards the cytokine ($ED_{50\ Cyt}$, green), as to mimic the effects of MDAs. We then quantified the amount of infectious virus particles and viability at the 72h time point across all parameter pairings in tumor and normal tissues. We applied a Monte Carlo sampling method, varying the parameter estimates within a 10X window, to ensure that the results & conclusions represent a general phenomenon. All parameters, and the ranges used in these simulations, are available in Appendix Table IV.

Within this framework, simulations reveal that while decreasing IFN secretion drives more robust increases in viral titers in cancer cells to a limit, the bystander cytokine effect is highly tumor-selective and emerges as a main contributor to the overall cancer selective

cytopathic response when both effects are combined (Fig. 3.5b-d). Nonetheless, the simulations also suggest that increased bystander killing comes at the cost of reduced viral growth. Importantly, these data indicate that within a reasonable range of parameter estimates (dotted square region) it is possible to combine both effects to increase viral growth and elicit robust killing of cancer cells while keeping normal cells relatively unscathed.

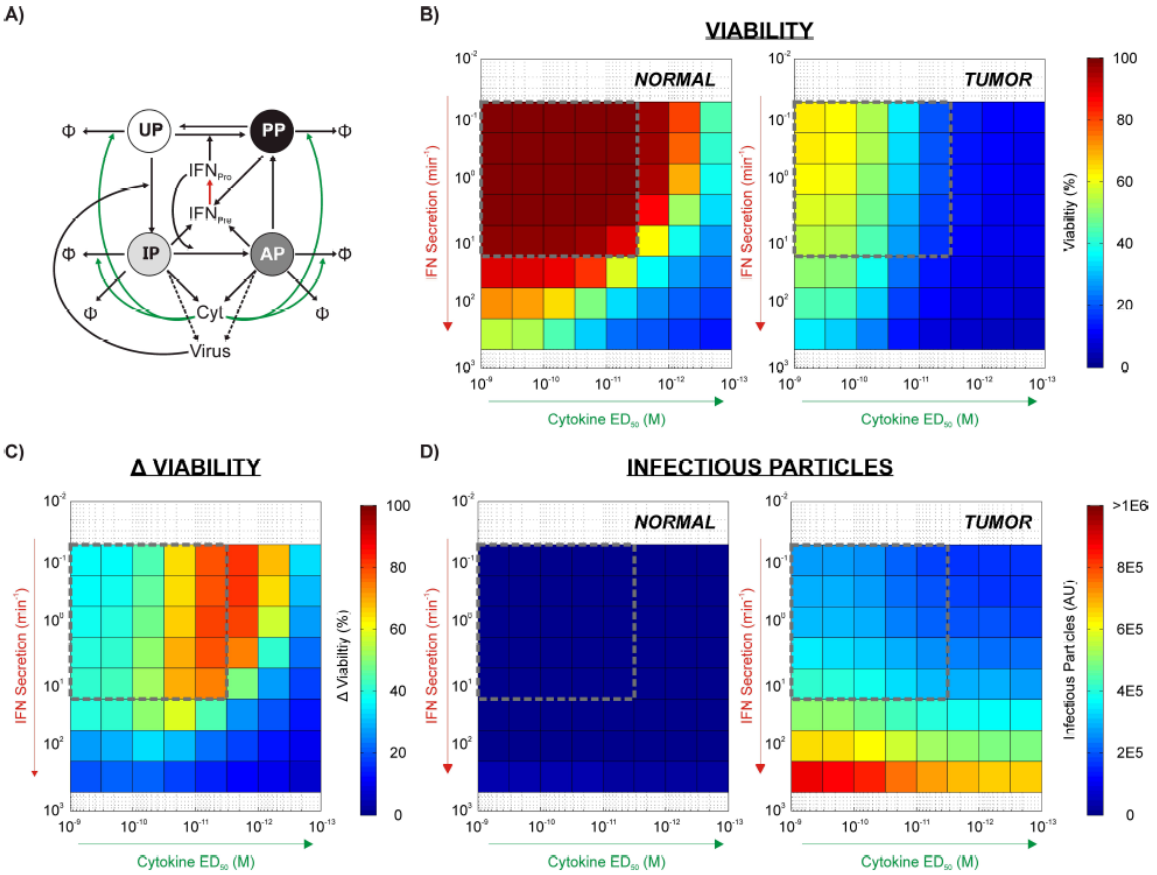

Figure 3.6. Simulation impact of decreased IFN secretion and induced cytokine-mediated polynucleation on OV dynamics.

a) Phenomenological model of VSVΔ51 kinetics in-vitro derived from the work of LeBoeuf et al 2013 11. This model describes the transition between the uninfected population (UP), infected population (IP), IFN activated population (AP), the protected population (PP) and dead cells (ϕ) as a function of IFN, virus, and production of cytotoxic cytokines. Relative to the model developed by LeBoeuf et al., this model incorporates cytotoxic cytokine production from infected cells, and the transition between intracellular and extracellular IFN to recapitulate the effects of MDAs. b) Heatmap summarizing the median viability 72h post infection in normal or tumor cells as a function of decreasing the rate of IFN release (downward in the checkerboard) and increasing the ED50 of cytotoxic cytokines (rightward in the checkerboard) induced by virus as a result of microtubule destabilization. Data illustrated represents the median value obtained over 5000 Monte Carlo simulations varying all kinetics parameter within a 1 log window. The difference between tumor and normal cells is the rate of virus replication which is set to 1 log higher in cancer cells as done in LeBoeuf et al. 2013. c) Heatmap summarizing the mean difference in viability between the normal or tumor compartments. d) Heatmap summarizing the median number of arbitrary free virus particles in the environment 72h post infection in normal or tumor cells.

Discussion

In this study, we report that MDAs synergize with oncolytic rhabdoviruses by leading to decreased antiviral Type I IFN production and increased virus-induced bystander killing. In the case of the IFN-sensitive mutant VSVΔ51, this leads to increased viral spread specifically in cancer cells (Fig. 3.1). The fact that the opposite is observed for (Fig. 3.1h) brings forth new considerations with respect to rhabdovirus biology. While rhabdovirus proteins have been reported to interact with the microtubular network (282), our data taken together suggests that intact microtubules are not essential for the life cycle of rhabdoviruses. Even though wtVSV spread is indeed hampered by MDAs (Fig. 3.1e,g,h) in agreement with previous reports (282), our results and simulations (Fig. 3.6d) rather argue a role for increased viral bystander killing in this phenomenon.

While rhabdoviruses may not require the microtubular network, many viruses such as vaccinia for example are well known to hijack the host cytoskeletal system in order to travel within the cytoplasm and to infect other cells (283). Suggesting MDAs may have virus-specific effects; we and others have observed that microtubule destabilizers robustly inhibit vaccinia growth ((284), data not shown). However, other viruses have been reported to grow at least equivalently in cells with destabilized microtubules. For example, while the mechanism was not addressed, low dose vinblastine increased the oncolytic activity of HSV without affecting viral titers *in vitro* (285). It is likely that other IFN-inducing viruses could be enhanced by MDAs by taking advantage of delayed type I IFN secretion. However, our data suggest that given this advantage is only transient (see Fig. S5a[$$$]), rapidly growing viruses such as VSV are more

likely to benefit. Ultimately, this may offer additional selectivity to the approach, reducing the possibility of opportunistic infections that could ensue from hindering the type I IFN system.

Interestingly, somewhat controversial reports dating prior to the purification and sequencing of Type I IFNs in the late seventies (286) denoted the impact of drugs such as colchicine and vinblastine on the expression and secretion of antiviral "interferon" and several other proteins (276-280). Here we show for the first time direct evidence that several MDAs inhibit Type I IFN secretion, and provide data supporting the involvement of protein translation in this phenomenon. Our results also suggest that the incorporation of Type I IFN mRNAs in high-density polysomal structures is compromised following disruption of microtubules. Interestingly, protein expression/secretion was clearly only partially inhibited following MDA treatment as determined by pulse-chase experiments. Nonetheless, a subset of secreted proteins responded analogously to type I IFNs (Fig. S5e$^{\$\$\$}$). This suggests the possibility that the efficient translation/secretion of other mRNAs may also depend on microtubules. Supporting this idea, it has been previously reported that microtubule disruption leads to loss of fibronectin mRNAs in high-density polysomes in smooth muscle cells (287). Given these observations, it is tempting to speculate that microtubules coordinate the organization of higher density polysomal structures, which may be preferentially associated with a subset of mRNAs.

One counterintuitive observation is that MDA treatment, while decreasing Type I IFN production in both cancer and normal cells (Fig 3.4d and S5d), only increases VSVΔ51 spread and oncolysis in the former. While simulations from our mathematical model suggest that decreasing IFN secretion leads to more robust increases in viral titers in cancer cells up to a certain extent, they also reveal that a significant contributing factor to the experimentally

observed cancer-selective effects of MDAs may be the parallel increase in bystander killing (Fig. 3.5). This is interesting given it provides an explanation for why other drugs such as HDAC inhibitors that have been shown to reduce IFN responsiveness while simultaneously increasing virus-induced cell death also lead to cancer-selective enhancement in OV spread (212).

Overall, our study show that MDAs can provide a significant therapeutic benefit when combined with oncolytic rhabdoviruses such as VSVΔ51 and Maraba MG-1, even in otherwise treatment-refractory transgenic mouse models of ovarian cancer (272) (see Fig. 3.2c). While MDAs have been used for decades to treat a number of human ailments including autoimmune disorders, helminthes and cancer (138, 288, 289), one common characteristic is the narrow therapeutic window associated to these agents. In the case of cancer, this has led to the development of more selective biological therapies including therapeutic antibodies and oncolytic viruses. Therefore, one downside of using classical MDAs in this context is their associated systemic toxicities. Notably, as a strategy to avoid overt toxicity of MDAs, these have been linked to monoclonal antibodies such as Herceptin, which retarget effects towards cancer cells (290). It will be interesting to test oncolytic rhabdoviruses in combination with novel and recently approved antibody-MDA conjugates for the treatment of cancer in order to take full advantage of the vastly superior selectivity of these therapeutics.

Methods

Cell lines and culture conditions

4T1 (breast), CT26 (colon), CT26-LacZ (colon), B16 (melanoma) mouse cancer cells; 786-0 (renal); U251 (glioma) human cancer cells; Vero monkey kidney cells; MRC-5 and GM-38 normal human fibroblasts, were obtained from the American Type Culture Collection (Manassas, VA). Cells were cultured in HyQ high-glucose Dulbecco's modified Eagle's medium (Hyclone, Waltham, MA) supplemented with 10 or 20% (GM-38) fetal calf serum (CanSera, Etobicoke, Ontario, Canada). All cell lines were incubated at 37 °C in a 5% CO_2 humidified incubator.

Viruses, purification and quantification

The Indiana serotype of VSV (VSVΔ51 or wild type) was used throughout this study and was propagated in Vero cells. VSVΔ51-expressing GFP, firefly luciferase, or murine GM-CSF are recombinant derivatives of VSVΔ51 described previously (165, 291). Maraba MG-1 as described in (166) was obtained from Dr. David Stojdl. All viruses were propagated on Vero cells and purified on 5–50% Optiprep (Sigma, St Louis, MO) gradient and all virus titer were quantified by standard plaque assay on Vero cells as described in (292). For experiments described in Fig. 3.4a and Supplemental Fig. 6a[$$$], wtVSV was first inactivated by UV crosslinking with a total of 3600 mJ/cm^2.

Drugs and cytokines

Colchicine, Vinorelbine, Nocodazole, Albendazole, Parbendazole, were obtained from Sigma-Aldrich (St Louis, MO) and dissolved in DMSO. IFN-α (Intron A) was obtained from Schering-Plough (Kenilworth, NJ). IFN-β was obtained from PBL Interferon Source (Piscataway, NJ). IL-6, IL-8, ITAC, IP-10, IL-29, IL-28a, and TNF-α were obtained from ProSpec Bio (East Brunswick, NJ).

In vitro treatment of cells with MDAs and rhabdoviruses

Confluent monolayers of cells were pre-treated for 2-4 hours with drugs, followed by infection with rhabdoviruses at indicated MOIs and incubation at 37 degrees Celcius in a humidified 5% CO_2 incubator for the indicated times. Fluorescent images to detect virus replication were obtained using the Axiovert S100 Fluorescence microscope (Carl Zeiss Ltd, Toronto, ON). Cell viability was assessed using an alamarBlue assay (AbD Serotec) according to manufacturers intructions by measuring fluorescence (530 nm excitation and 590 nm emission) on a Fluoroskan Ascent Microplate Fluorometer (Thermo Scientific, Hudson, NH). Virus titers were determined from cell supernatants by standard plaque assay on Vero cells (292).

Flow cytometry

786-0 cells were plated in 12-well dishes, pretreated with DMSO or 100 nM colchicine for 4 hours, followed by mock infection or infection with VSVΔ51-GFP or wtVSV-GFP at MOI 0.01. 48hours later, cells were collected, washed and resuspended in HBSS with 10% FBS and 0.01% Sodium Azide. Single cell suspensions were labeled with or without 50 µg/ml propidium

iodide (Sigma, St Louis, MO) and subjected to flow cytometry on a Beckman Coulter FC500 and data analyzed with Kaluza v1.1 software.

Rodent tumor models

Six-week-old female Balb/c mice obtained from Charles River Laboratories (Wilmington, MA) were given subcutaneous tumors by injecting 3 x~ 10^5 syngeneic 4T1 (or CT26-LacZ) cells suspended in 100 µl PBS. At the indicated times post-implantation, tumors were injected with $1x10^8$ pfu (in 50 µl PBS) of the indicated virus. Four hours later, colchicine or vinorelbine was administered i.p at the indicated dose. This was repeated a week later for a total of two treatment cycles. Tumor sizes were measured every other day using an electronic caliper. Tumor volume was calculated as = (length x $width^2$)/2. For survival studies, mice were culled when tumors had reached 1600 mm^3. For *in vivo* imaging, an In Vivo Imaging System (IVIS, Perkin Elmer, Waltham, MA) was used as described previously (218). For viral quantification described in Figure 3.2b, tumors were dissected at the indicated times and homogenized using a tissue homogenizer in PBS prior to quantification by standard plaque assay as described in (292). For the ovarian cancer model in Fig. 3.2c, T-antigen-positive MISIIRTag transgenic mice (described previously (272)) approximately 10-weeks of age were treated with weekly i.p injections of 1 x 10^8 PFU VSVΔ51-GM-CSF and colchicine 1.5 mg/kg until endpoint as determined by animal care guidelines. Doses were adjusted to body weights of individual mice to account for weight gain over time. All experiments were performed in accordance with institutional guidelines for animal care.

Microarrays and analysis

786-O cells were plated at a density of 4E5 cells in 6-well flat bottom plate (Costar). Following overnight growth, cells were treated with 100 nM colchicine or vehicle. Following a 4-hour pre-treatment, PBS or VSVΔ51at an MOI of 0.01 was added to cell cultures. Twenty-four hours post-infection, RNA was collected using an RNA-easy kit (Quiagen). Biological triplicates were subsequently pooled and hybridized to Affymetrix human gene 1.0 ST arrays. RNA quality was measured using Agilent 2100 Bioanalyzer (Agilent Technologies) prior to hybridization.

Microarray data were processed using AltAnalyze v2.0 under default parameters (264). A detection above background score >70, and a pV<0.05 were used to filter probe sets. By subsequently evaluating gene expression using constitutive probe sets shared across splice variants, our analysis focused on changes in gene transcription rates rather than alternative splicing mechanisms. Gene enrichment analyses were subsequently focused on 248 genes induced or repressed two-fold by VSVΔ51 relative to all other datasets (Z-test p<0.05, Benjamini-Hochberg correction). GO-term enrichments were evaluated using GOrilla (265) following correction for multiple hypothesis testing (Bonferonni). Pathway enrichments were evaluated using David following correction for multiple hypothesis testing (Benjamini-Hochberg). Raw and processed microarray data has been deposited in the ArrayExpress database.

Cell lysis and Western blotting

Whole cell extracts were obtained by lysing in 50 mM Hepes, pH 7.4, 150 mM NaCl, 10 mM EDTA, 10 mM $Na_4P_2O_7$, 100 mM NaF, 2 mM Na_3VO_4, protease inhibitor cocktail (Roche,) and 1% Triton X-100 as described (293). Following protein determination by Bradford

assay (BioRad Protein Assay Solution, Mississauga, Ontario), 10-20ug of clarified cell extract were electrophoresed using the NuPAGE SDS-PAGE Gel system (Invitrogen) and transferred onto a nitrocellulose membrane (Bio-Rad). Blots were blocked with 5% nonfat milk and probed with rabbit polyclonal antibodies specific for VSV (a gift from Earl Brown), or IFNβ (OAAB05131, Aviva Systems Biology, San Diego, CA), GAPDH (Abcam, Cambridge, UK) as a loading control, followed by horseradish-peroxidase conjugated rabbit or mouse secondary antibodies, respectively (The Jackson Laboratory, Bar Harbor, Maine). Bands were visualized using Supersignal West Pico Chemiluminescent substrate (ThermoScientific Pierce, Rockford IL).

Nuclear / cytoplasmic fractionation and Western blotting

Cell fractionation experiments were performed as previously described (293). Briefly, cells were washed with ice cold PBS, swelled in Hypotonic buffer (0.5 M Hepes pH 7.9, 0.1 M EGTA, 0.1 M EDTA with protease and phosphatase inhibitors), lysed with 0.1% NP-40 and cytoplasmic fractions collected by low speed centrifugation. Nuclear proteins were then extracted with hypertonic buffer (0.5 M HEPES pH 7.9, 2.5 M NaCl, 0.1 M EGTA, 0.1 M EDTA, 30% glycerol, 20 mM NaF, 1 mM Na_3VO_4, 1 mM $Na_4P_2O_7$, 1 mM DTT, and protease inhibitor cocktail) and clarified. Nuclear and cytoplasmic fractions were resolved by gel electrophoresis as above and membranes blocked with 5% BSA, cut into strips and probed for the tyrosine-701 phosphorylated (i.e. activated) form of Stat1, total Stat1, serine-396 phosphorylated IRF3 or total IRF3 (Cell Signalling/NEB, Whitby, Ontario). Antibodies against α-tubulin (Santa-Cruz, Dallas, Texas) and β-actin (Cell Signalling) were used as loading controls.

Quantitative realtime PCR

786-0 cells were pretreated for 4h with 0.1µM colchicine or DMSO, and infected with VSVΔ51 at MOI 0.01 or mock. 16h later, cells were collected and fractionated in nuclear and cytoplasmic fractions (Norgen Biotek Corp., ON, Canada). RNA extraction was performed using Qiagen QiaShredder columns and the Qiagen RNeasy kit (Qiagen, Valencia, CA, USA). 2µg RNA was converted to cDNA with Superscript II Reverse Transcriptase (Invitrogen). Real time PCR reactions were performed with the QuantiTect SYBR Green PCR kit (Qiagen) on a Rotor-gene RG-300 (Corbett Research, Australia). Optimal threshold and reaction efficiency were determined using the Rotor-gene software. Melt curves for each primer exhibited a single peak, indicating specific amplification, which was also confirmed by agarose gel. Ct values were determined using the Rotor-gene software at the optimal threshold previously determined for each gene. Gene expression relative to GAPDH was calculated using the method described by Pfaffl et al (294). Fold induction was calculated relative to the DMSO treated control for each gene. Primers were designed using Primer 3 v 4.0 (sequences available upon request).

ELISA

Cells were plated in 12-well dishes, pretreated with DMSO or 100 nM colchicine for 4 hours, followed by mock infection or infection with VSVΔ51-GFP (or VSVΔ51 GM-CSF) at indicated MOI. Cell supernatants were collected at different times post-infection, centrifuged to remove cellular debris, and protease inhibitor cocktail added. ELISA was performed with the Verikine Human or Mouse Interferon alpha and beta or mouse GM-CSF kits as appropriate (PBL Interferon Source) by following the manufacturer's instructions. Absorbance values at 450nM

were measured on a Multiskan Ascent Microplate Reader (MXT Lab Systems, Vienna, Virginia).

Polysome profiling

Cells were cultured in 15-cm dishes until confluency and then pretreated with colchicine (100 nM), or vehicle (DMSO) for 4 hours followed by infection with VSV at 0.1 MOI. Cells were washed 24 hours post infection with cold PBS containing 100 μg/mL cycloheximide, collected, and lysed in a hypotonic lysis buffer [5 mmol/L Tris-HCl (pH 7.5), 2.5 mmol/L MgCl2, 1.5 mmol/L KCl, 100 μg/mL cycloheximide, 2 mmol/L DTT, 0.5% Triton X-100, and 0.5% sodium deoxycholate). Lysates were loaded onto 10% to 50% sucrose density gradients [20 mmol/L HEPES-KOH (pH 7.6), 100 mmol/L KCl, 5 mmol/L MgCl2] and centrifuged at 36,000 rpm for 2 hours at 4°C. Gradients were fractionated, and the optical density (OD) at 254 nm was continuously recorded using an ISCO fractionator (Teledyne ISCO). RNA from each fraction was isolated using TRIzol (Invitrogen) and treated with DNaseTurbo (Ambion) according to the manufacturer's instructions. Reverse transcription PCR (RT-PCR) and semi-quantitative RT-PCR (qRT-PCR) reactions were carried out using SuperScript III First-Strand Synthesis System (Invitrogen) and SYBR Green Supermix (Qiagen) according to the manufacturer's instructions using primers for IFNβ, α and VSV M (sequences available upon request).

Immunofluorescence and assessment of Polynuclear cells

Human 786-0 renal carcinoma cells or normal human GM-38 lung fibroblasts were cultured in DMEM/10% FBS and plated in 12 well dishes with glass coverslips. Following a 2-hour 0.1 uM colchicine pretreatment (or vehicle control), wells were infected with oncolytic

VSVΔ51 expressing green fluorescent protein (GFP) at a multiplicity of infection (MOI) of 0.01 (or mock). Alternately, cells were treated with supernatants (see below) or cytokines for experiments in Figures 3.5e,g. Plates were incubated overnight and coverslips were fixed and incubated with primary and secondary antibodies to β-tubulin (ab21057, Abcam, Cambridge, UK) and mounted on slides. Coverslips were then photographed at 40X using an inverted fluorescence microscope and polynuclear/infected cells were counted from 3-5 pictures per well and a minimum of 100 cells total.

Supernatant Transfer and Filter Experiment

786-0 cells were cultured and plated as described above but were instead infected with VSVΔM51-ΔG-GFP at an MOI of 10. This virus can infect cells but cannot exit the cell due to lack of the viral G protein, thus preventing release of viral particles in the supernatant. After overnight incubation and verification of initial infection, supernatants were filtered through a 100, 50, 10, or 3 kDa filters (Millipore, Billerica, MA) or left unfiltered before being transferred to fresh 786-0 plates with or without 100 nM colchicine. Coverslips were fixed, stained and polynuclear cells counted as described above. Alternately, an alamar blue viability assay (described above) was performed.

Mathematical Modeling

The model describing OV replication dynamics in the presence of colchicine was derived from our previous work [11]. The first four equations describe the transition between the uninfected population (UP), the infected population (IP), the activated population (AP) and the protected

population (PP) depending on the concentration of virus [V], cytotoxic cytokine [Cyt] and extracellular [IFN] in the environment. These equations are:

$$\frac{dUP}{dt} = -K_{VI} \times [V] \times [UP] - \left(\frac{-K_{IFNon}}{1+\left(\frac{[IFNext]}{EC50\ IFN}\right)^2} + K_{IFNon}\right) \times [UP] + K_{IFNoff} \times [PP] - \left(\frac{-\gamma_{C\_Cyt}}{1+\left(\frac{[Cyt]}{EC50\ Cyt}\right)^2} + \gamma_{C\_Cyt}\right) \times [UP],$$

$$\frac{dIP}{dt} = K_{VI} \times [V] \times [UP] - \left(\frac{-K_{IFNon}}{1+\left(\frac{[IFNext]}{EC50\ IFN}\right)^2} + K_{IFNon}\right) \times [IP] - \gamma_c \times [IP] - \left(\frac{-\gamma_{C\_Cyt}}{1+\left(\frac{[Cyt]}{EC50\ Cyt}\right)^2} + \gamma_{C\_Cyt}\right) \times [IP],$$

$$\frac{dAP}{dt} = \left(\frac{-K_{IFNon}}{1+\left(\frac{[IFNext]}{EC50\ IFN}\right)^2} + K_{IFNon}\right) [IP] - K_{VC} \times [AP] - \gamma_c \times [AP] - \left(\frac{-\gamma_{C\_Cyt}}{1+\left(\frac{[Cyt]}{EC50\ Cyt}\right)^2} + \gamma_{C\_Cyt}\right) \times [AP],$$

$$\frac{dPP}{dt} = \left(\frac{-K_{IFNon}}{1+\left(\frac{[IFNext]}{EC50\ IFN}\right)^2} + K_{IFNon}\right) [UP] + K_{VC} \times [AP] - K_{IFNoff} \times [PP] - \left(\frac{-\gamma_{C\_Cyt}}{1+\left(\frac{[Cyt]}{EC50\ Cyt}\right)^2} + \gamma_{C\_Cyt}\right) \times [PP].$$

The parameters used in the above equations represent the infection rate ($K_{vi.}$), the rate of IFN signaling activation (K_{IFNon}), the rate of IFN signalling inactivation (K_{IFNoff}), the EC50 of IFN ($EC_{50\ IFN}$), the rate of virus-mediated cell death (γ_c), the EC50 of the cytotoxic cytokine ($EC_{50\ Cyt}$), the rate of cytokine-mediated cell death (γ_{C_Cyt}),and the rate viral clearance (K_{VC}).

The next subset of equation describe the concentration of virus, interferon, and cytotoxic cytokine in the media. These equations are:

$$\frac{dV}{dt} = K_{BudIP} \times [IP] + K_{BudAP} \times [AP] - K_{VI} \times [V] \times [UP] - \gamma_V \times [V],$$

$$\frac{dIFN_{Ext}}{dt} = K_t \times IFN_{Int} - \gamma_{IFN} \times IFN_{Ext}$$

$$\frac{dIFN_{Int}}{dt} = K_{IFNIP} \times [IP] + K_{IFNAP} \times [AP] + K_{IFNAP} \times [PP] - K_t \times IFN_{Int} - \gamma_{IFN} \times IFN_{Int}$$

$$\frac{dCyt}{dt} = K_{Cyt} \times ([IP] + [AP]) + -\gamma_{Cyt} \times IFN$$

The parameters described in the above equations represent the rate of virus budding from IP and AP (K_{BudIP} and K_{BudAP}, respectfully), the infection rate ($K_{vi.}$), the rate of virus degradation (γ_V), the rate of internal IFN production upon initial infection (K_{IFNIP}), the rate of internal IFN production following activation of IFN defenses (K_{IFNAP}), the rate of IFN transfer to the extracellular compartment ($K_{t.}$), the rate of IFN degradation (γ_{IFN}), the rate of cytotoxic cytokine production (K_{Cyt}) and the rate of cytotoxic cytokine degradation (γ_{Cyt}).

A Monte Carlo simulation was generated by varying the parameters in the above model within a 1 log window (Supplemental Table 3[$$$]). These parameters were generated from literature based evidence as described in our previous studies [11]. The difference between tumor an normal cells is K_{BudIP} and K_{BudAP}, which is set to be 1-100 fold greater in the tumor microenvironment. The Monte Carlo simulation was performed by simulating the above equations for a population of 2.5E5 cells in 1ml of media infected at an MOI=0.001, calculating virus and viability at the 72h time point for each $EC_{50\ Cyt}$ and $K_t$combination, and repeating the simulation 5000 times with novel model parameters selected within the 1 log window. All simulations were performed in Matlab using the ODE solver ode15s under default parameters imposing a none-negativity constraint.

Statistics

Unless otherwise noted (see microarray analysis), ANOVA was used to determine significance between all treatment conditions (Tukey's post-hoc test). The Log-rank test was used to determine significant differences in plots for survival studies. For all studies, significance

was considered to mean a p-value below or equal to 0.05. Graphs and Statistics were computed using Prism 5 and Excel.

ACKNOWLEDGEMENTS

This project was funded by a Terry Fox Research Institute Grant (grant # TFF 122868; by J.C.B, J.S.D, N.S, T.A) as well as a The Lotte & John Hecht Memorial Foundation Innovation Grant of the Canadian Cancer Society (grant #2012-701460; J-S.D, J.C.B, M.K.). C.B is supported by a Natural Sciences and Engineering Research Council of Canada (NSERC) studentship.N.D.S. is supported by a Vanier Scholarship. V.G. is supported by anOntario Graduate Scholarships in Science and Technology Queen Elizabetth II studentship. J.C.B. is supported by Ontario Institute for Cancer Research.

Chapter IV. Reciprocal cellular cross-talk within the tumour microenvironment enhances oncolytic virus activity

Carolina S. Ilkow1,2, Monique Marguerie1,2, Cory Batenchuck1,2, Daniela Ben Neriah1, Sophie Cousineau1, Theresa Falls1, Christiano Tanese de Souza1, Fabrice LeBoeuf1,2, Lawton Stubbert1,2, Rozanne Arulanandam1,2, and John C. Bell1,2,3

1.Centre for Innovative Cancer Therapeutics, Ottawa Hospital Research Institute, Ottawa, Canada
2Departments of Biochemistry, Immunology and Microbiology, University of Ottawa, Ottawa, Canada
3Department of Medicine, University of Ottawa, Ottawa, Canada.

Authors:
Cory Batenchuk[1,3,4], Chadi Zakaria[5],Julie Cox[1,3], Oliver Varette[1], Vanessa Garcia[1,3], Raunak Karmacharya[1,3], Anisha Sinha[1,3], Andrew Babawy[1,3], Theresa Falls[1,2], Andrew Chen[1], Jeff Hamill[1], Nicole Forbes[1,3], Naomi Da Silva[1,3], David Conrad[1,2], Harry Atkins[1,2], Kennneth Garson[1],Carolina Ilkow[1,2],Mads Kaern[4,6,7], Barbara Vanderhyden[1],2,Nahum Sonenberg[5], Tommy Alain[5], Fabrice Le Boeuf [1], *John Bell[1,2,3], *Jean-Simon Diallo[1,2,3]

Affiliations:
1. Center for Innovative Cancer Therapeutics, Ottawa Hospital Research Institute, Ottawa, Ontario, Canada K1H 8L6.
2. Department of Medicine, University of Ottawa, Ottawa, Ontario, Canada K1H 8L6.
3. Department of Biochemistry, Immunology and Microbiology, University of Ottawa, Ottawa, Ontario, Canada K1H 8L6.
4. Ottawa Institute of Systems Biology, University of Ottawa, Ottawa, Ontario, Canada K1H 8L6.

Journal:
In submission to Nature, 2013

My contribution:

I performed all aspects of microarrays data acquisition & analysis in this paper which is represented in Figure 4.2, Appendix Figure 12, Table S1[$], Table S2[$], and Data S1[$]. I also performed all simulations which are relevant to this chapter. This data, which can be found in the Appendix Figures 6-8 and Appendix Table V, are not included in the current manuscript.

Chapter Synopsis

In the manuscript entitled, ***Crosstalk between cancer cells and activated fibroblasts modulates innate antiviral responses - a critical determinant of successful virus-based therapies***, I characterized the mechanism by which Cancer Associated- Fibroblasts (CAFs) became sensitized to OV infection. By performing microarray analysis of VSVΔ51 infection in CAFs and Normal Fibroblasts (NFs) isolated from the same patient, I determined that it was not the lack of the CAFs ability to induce IFN signalling, but rather that these cells are in a repressed anti-viral state prior to OV infection (**Figure 4.2c**). Of the 88 genes repressed in CAFs, 55 were induced following OV treatment, and represent the fraction of genes targeted by type I IFNs (**Figure 4.2d**). These results were confirmed by qRT-PCR (**Figure 4.2e**), as well as in a second patient (**Appendix Figure 12**). Under the assumption that it is the anti-viral baseline which drives resistance, I performed a single-step growth curve in both CAFs and NFs with a wildtype variant of VSV capable of inhibiting mRNA export. This experiment consists of infecting cells at a high PFU to cell ratio (MOI=5), and monitoring the amount of virus produced on a per cell basis. By tracking virus-mediated gene expression by GFP (**Figure 4.2f**) and viral titers (**Figure 4.2g**) over time, this experiment demonstrates that a viral strain capable of inhibiting the induction of antiviral responses is nonetheless associated with preferential replication in CAFs. This result confirms that CAFs are in a repressed anti-viral state **prior** to infection. As such, tumor cells are associated with an augmented rate of viral genome replication and expression; the assumptions used in chapter II & III. This observation opens the door to the use of these anti-viral genes as predictive biomarkers for OV therapies.

After Dr. Ilkow determined that CAFs sensitized resistant cancer cells to infection, I performed simulations to gain further insight into the impact of tumor heterogeneity on infectivity. At steady state, tumors should have varying ratios CAFs, NFs, Resistant Cancer Cells (RCC) and Sensitive Cancer Cells (SCC). From our observations, each cell type is associated with varying degrees of IFN production, IFN responsiveness and virus production, a diversity which should affect the outcome of OV therapies. Using the model developed in chapter II, I amended the parameters to describe OV replication in each of these populations (**Appendix Table 5**). I then modified the mathematical model to examine the effects of homogenously mixing resistant cancer cells with varying ratios of these three different steady state populations (**Appendix Figure 6**). This was achieved by duplicating the equation for UP, IP, AP and PP describing the second population, and adding their contribution to the total amount of virus and IFN. I then simulated the cytotoxicity in both populations following 72h infection at varying cell-to-cell ratios. By performing a Monte-Carlo simulation similar to Chapter II/III, repeating the simulation 1000 times with different parameter pairings, my goal was to investigate the impact of the cell infiltrate in tumors derived from resistant cancer cells.

From these simulations, the greatest impact on RCCs was when they were co-cultured with NFs. When NFs were the dominant population (>75% of the population), RCCs could be fully protected against infection (**Appendix Figure 7a**). RCC could conversely sensitize NFs, when representing between >75% of the population. In contrast, CAFs had little to no impact on the level cytotoxicity in RCCs (**Appendix Figure 7b**). Although associated with a defect in IFN defences, this property failed to further enhance replication in RCCs. Increased cytotoxicity, was only observed when co-cultured with SCCs, where increasing the size of this population lead to a

continuous rise in sensitization for RCCs population, albeit to a lesser degree than the impact of NFs (**Appendix Figure 7c**). In contrast, RCC failed to transfer resistance to this population. From these simulations, I concluded that while NFs could contribute to the emergence of resistance in RCCs, when they where the dominant population, SCCs could sensitize RCCs, even when at low proportions in the population. As such, the level of cancer cell sensitivity is not only defined by its transition to an SCC phenotype, through the plethora of growth factors produced by CAFs, but equally affected by low-level infiltration from cells with varied IFN and virus output. This would suggest that the frequency of each population greatly influences treatment outcome, other than CAFs which have little to no impact on the behaviour of RCC in the absence of cell-to-cell communication converting them to a SCC phenotype.

To better understand the impact of the infiltrate, I varied the rate of virus budding (K_{Bud_IP}), the rate of IFN production (K_{IFN1}) or the degree of IFN responsiveness ($K_{IFN\ On}$), for a sub-population of infiltrating cells (5% of population) with all other parameters identical to the RCC. These simulations indicate that while increasing IFN sensitivity or production from the sub-population could drive RCC resistance, decreasing these parameters had little to no impact on cytotoxicity in RCCs (**Appendix Figure 8**). On the other hand, further increasing the rate of virus budding was the only parameter tested which alone could sensitize the predominant RCC population (**Appendix Figure 8**). It would therefore appear that sensitive cancer cells sensitize the local region by releasing large amounts of virus particles, and not inherently by their defect in IFN production. This observation explains why CAFs, had little to no impact on RCC behaviour, as their rate of virus production and release was assumed to be equivalent.

Abstract

Signalling between cancer cells and the normal stromal cells that support them is known to negatively impact the activity of a variety of chemically based anti-cancer therapies. Here we demonstrate that in the case of oncolytic virus based therapeutics, crosstalk between cancer associated fibroblasts (CAFs) and cancer cells leads to enhanced infectivity. TGF-β produced by tumour cells re-programs supporting cancer associated fibroblasts dampening their steady state level of anti-viral transcripts and rendering them sensitive to virus infection. We found that in turn, CAFs produce high levels of fibroblast growth factor 2 (FGF-2) initiating a signaling cascade in cancer cells that leads to a decrease in RIG-I expression and impedes the ability of the malignant cell to sense and respond to an invading virus therapeutic. In pancreatic cancer patient explants, the expression of FGF-2 correlated with susceptibility to infection with oncolytic viruses and resistant patient samples could be sensitized by the addition of FGF-2 in vitro and in vivo.

Introduction

Tumours are complex ecosystems composed of networks of interacting "normal" and malignant cells. It is now recognized that cytokine mediated crosstalk between normal stromal cells, like cancer associated fibroblasts (CAFs), vascular endothelial cells, immune cells and cancer cells influences all aspects of tumor biology including growth, metastasis, angiogenesis, and local immunosuppression (295). CAFs represent the most abundant stromal cell type in many tumors including renal, ovarian, breast and pancreatic carcinomas (296). In many settings, metabolic coupling and paracrine communication between cancer cells and CAFs can determine the impact and resistance to a variety of cancer therapeutics (297-299)(297-299)[297-299]

(42, 297-301). We are developing virus based anti-cancer therapeutics (211, 243) and sought to determine if CAFs impact the ability of oncolytic viruses (OVs) to infect and destroy cancer cells within the tumour bed. In the present study, we tested the hypothesis that factors secreted by the tumor stroma modulate, at least in part, OV replication within the tumor. We discovered that, in contrast with primary normal fibroblasts, CAFs support the replication of therapeutic viruses and can enhance the sensitivity of tumour cells to OV infection. The increase in virus infectivity appears to arise from cross talk between the FGF2 and interferon regulated pathways.

Results

Stromal Cell Secreted Factors Sensitize Cancer Cells to Oncolytic Virus Infection

To test for interactions between tumour and stromal cells that could influence the replication of oncolytic viruses, we compared and contrasted infections in mono or co-cultures.

Human renal cell carcinoma cells engineered to express the red fluorescent protein (dsRED-786-0) were cultured alone or in the presence of untagged cancer associated fibroblasts. An oncolytic version of Vesicular Stomatitis Virus encoding green fluorescent protein (VSVΔ51-GFP) was used to infect either the dsRED-786-0 tumour cell line, cancer associated fibroblasts or co-cultures of the two. At the indicated times, cultures were examined and the extent of virus infection and spread determined by the expression of green fluorescent protein (GFP). Under the conditions used here, the 786-0 cell line is relatively refractory to VSV infection however pure CAF cultures, isolated from two distinct lung cancer patients, showed some level of sensitivity to virus infection. Interestingly in the CAF:786-0 co-cultures there appeared to be significantly more GFP expression (Figure 4.1a) an observation that was substantiated by titering of virus produced from infected cultures (Figure 4.1b). From these experiments it was difficult to determine if the increase in virus replication in cellular co-cultures occurred in both the tumour and CAFs so a more detailed quantitation was carried out using flow cytometric analysis of individual infected cells (Figure. 4.1c,d). This analysis revealed the in co-cultures there was approximately a 700% increase in OV infection of 786-0 cells and up to 500% increase in OV infection of CAFs compared to infection of either cell alone. Fetal fibroblasts (e.g.WI-38 cells) are known to display many of the markers associated with cancer associated fibroblasts (302-305) and also sensitized 786-0 cells to infection with VSV (Supplemental Figure 1a,b,c[$$$]). We tested two other human cancer cell lines and found that both a human pancreatic line (MiaPaca-2) and an ovarian cell line (OVCAR8) could be rendered more sensitive to virus infection when cultured in the presence of CAFs (Supplemental Figures 1d,e[$$$]). Furthermore the effect was not restricted to VSV as the replication of a thymidine kinase deleted vaccinia virus, currently undergoing clinical development (211, 243), also showed enhanced tumour replication in the

presence of CAFs (Supplemental Figures 2a,b,c and d[$$$]). To determine if virus sensitization was due to the secretion of paracrine factors or required cell:cell contact, we used transwell cultures wherein the upper chamber contained either a pancreatic tumour cell line (MiaPaca-2), fetal fibroblasts (WI-38) or CAFs isolated from a human pancreatic tumour (Figure 4.1e). The transwell cultures were grown for 72 hours and then the upper chamber removed and the lower tumor cell culture infected with an oncolytic VSV-GFP strain (Figure 4.1e and f) or an oncolytic vaccinia-GFP strain (Supplemental Figure 2e and f[$$$]). From fluorescent imaging, bright field microscopy (Figure 4.1e) or virus titering (Figure 4.1f) it was apparent that MiaPaca-2 cells in the lower chamber were substantially sensitized to oncolytic virus infection when exposed to conditioned medium from fetal fibroblasts or CAFs.

The transition from a normal fibroblast (NF) state to a cancer associated fibroblast is an epigenetically regulated phenomena known to result from exposure of NFs to tumour secreted factors like TGF-β (35, 302, 306).We obtained normal human fibroblasts from a non-tumour site and cultured them with or without conditioned media obtained from cancer cell cultures to create genetically identical cultures of normal and cancer associated fibroblasts. The phenotype of NFs and CAFs was confirmed by immunoblot analysis against alpha smooth muscle actin (αSMA), a specific marker for activated fibroblasts (302, 303) (Supplementary Figure. 5a[$$$]). Conditioned media from NFs is unable to enhance VSV growth in 786-0 cells whereas conditioned media from TGF-β activated NFs increased virus production by almost 100 fold (Figure 4.1 g). Taken together these experiments suggest that a factor specifically produced by CAF cultures is capable of sensitizing cancer cells to virus infection.

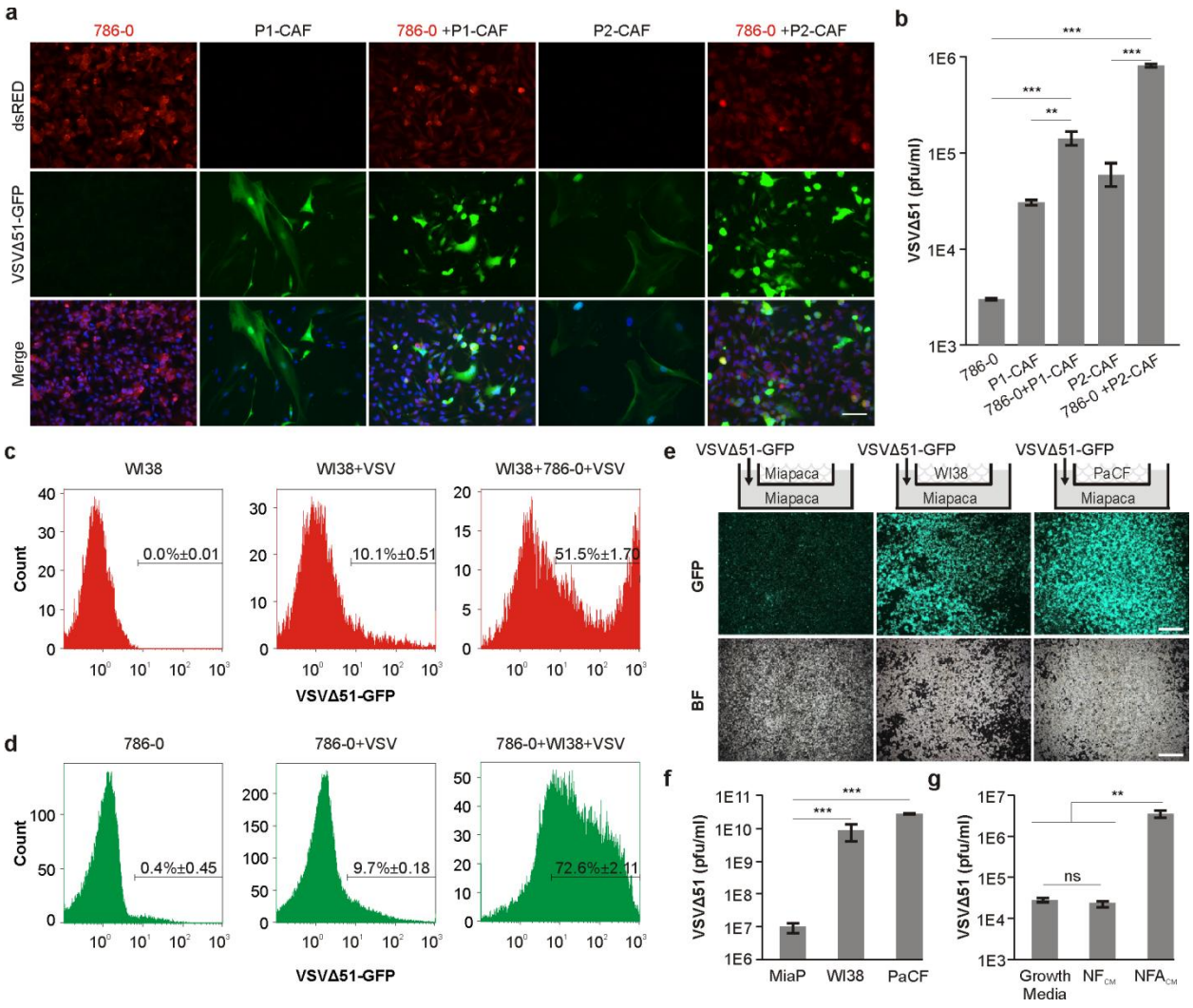
a
786-0
P1-CAF
786-0 +P1-CAF
P2-CAF
786-0 +P2-CAF
dsRED
VSVΔ51-GFP
Merge
b
VSVΔ51 (pfu/ml)
1E6
1E5
1E4
1E3
***
**
786-0
P1-CAF
786-0+P1-CAF
P2-CAF
786-0 +P2-CAF
c
WI38
WI38+VSV
WI38+786-0+VSV
Count
0.0%±0.01
10.1%±0.51
51.5%±1.70
VSVΔ51-GFP
d
786-0
786-0+VSV
786-0+WI38+VSV
Count
0.4%±0.45
9.7%±0.18
72.6%±2.11
VSVΔ51-GFP
e
VSVΔ51-GFP
Miapaca
WI38
PaCF
GFP
BF
f
VSVΔ51 (pfu/ml)
MiaP
WI38
PaCF
g
VSVΔ51 (pfu/ml)
ns
Growth Media
NF$_{CM}$
NFA$_{CM}$

Figure 4.1. Paracrine factors secreted by cancer cells and activated fibroblasts enhance oncolytic virus replication

a, Monotypic cultures or co-cultures of dsRED-768-0 and CAFs derived from two patients (P1 and P2) were infected with VSVΔ51-GFP at a multiplicity of infection (MOI) of 0.01. At 24 hours cells were fixed and nuclei were stained with DAPI. Scale bar=100 μm. **b,** VSVΔ51 titers from mono- or co-cultures were determined by plaque assay at 24 hours post-infection. **c,** dsRED-786-0 cells cultured alone or in combination with WI38 fibroblasts were infected with VSVΔ51-GFP (MOI=0.01, 24 h) and processed for flow cytometry analysis. Plots were obtained from gated dsRED positive cells. **d,** WI38 fibroblasts cultured alone or in combination with dsRED-786-0 cells were infected with VSVΔ51 expressing GFP (MOI=0.01, 24 hr) and processed for flow cytometry analysis. Plots were obtained using dsRED negative fibroblasts. Plots shown are representative of at least three independent experiments. **e,** MiaPaca cells were cultured alone or in combination with activated fibroblasts grown on transwell inserts. After 72 hours, inserts were removed and MiaPaca cells were infected with VSVΔ51-GFP (MOI=0.001, 24 hr). **e,** Representative GFP and bright-field (BF) images are shown. **f,** Cell associated supernatants from MiaPaca cells grown and infected, as described in (g), were collected and virus titers were determined. **g,** 786-0 cells were cultured with regular growth medium (GM) or in conditioned media from normal GM38 fibroblasts (NFCM) or activated fibroblasts (NFACM). After 72 hours, cells were infected with VSVΔ51 (MOI=0.01, 24 hr). Production of infectious virus particles was assessed by plaque assay. Error bars show ± s.e.m. of triplicate infections.

Cancer-associated fibroblasts are uniquely sensitive to virus-based therapy

As demonstrated previously (182, 213), normal GM38 foreskin fibroblasts are refractory to infection by oncolytic viruses but when these cultures were passaged continuously in the presence of cancer cell-conditioned medium or TGFβ1 they eventually become sensitive to OV infection (Supplementary Figures 4a,b,c[$$$] and 6a,b,c,d,e[$$$]). This model system suggested that perhaps CAFs isolated from tumours have increased sensitivity to OV infection when compared to their normal counterparts. We obtained CAF and NF cultures from two lung cancer patients and tested the sensitivity of these cells to OV infection. CAFs are significantly more sensitive than their NF counterparts to infection with tumour selective viruses VV-GFP, VSVΔ51-GFP, and Maraba MG1 virus (Figure 4.2a&b). These data suggested to us that normal stromal cells growing in the presence of tumour cells have re-programmed their transcriptional response to virus infection and render them sensitive to infection compared to their normal counterparts. To test this idea, we used microarray analysis to compare and contrast the cellular transcriptional response following virus infection of NF and CAF cultures isolated from the same patient. In the absence of infection, a total of 87 genes are repressed in CAFs compared to genetically identical NFs (Supplementary Table 1[$$$]). Gene-Ontology (GO) term analysis of these genes revealed that the primary processes repressed in CAFs in the absence of infection are innate antiviral responses and Type I interferon (IFN-I) signaling circuits (Figure. 4.2c). Following infection, 63% of these repressed genes (55/87) were induced to levels equivalent to, or greater than, those observed in NFs. Partitioning of these genes according to their induction status by IFN-I (see Materials and Methods) revealed that all of the repressed genes targeted by IFNs were induced following VSVΔ51 infection (Figure. 4.2d & e). Using two pairs of donor-matched NFs and

CAFs, we validated these observations by performing quantitative real-time PCR (qPCR) of key anti-viral response genes (DDX58, OAS2L, RSAD2, BST2, and IFI44L). In patient 1, these genes were repressed 20 to 2000 fold in CAFs, and 3 to 84 fold in patient 2 (Figure 4.2f and Appendix Figure 12). Conversely, all of these genes were induced 70-4600 fold in both patients following infection with VSVΔ51. This is in sharp contrast with NFs, where these genes were maintained at a high baseline and induced at best 2 fold following infection (Figure. 4.2f and Supplementary Figure.5b[$$$]). Taken together, this data indicates that CAFs are in a repressed antiviral state prior to infection but retain the capacity to produce or respond to IFNs. In contrast, NFs maintain a high antiviral state at baseline, and do not require dramatic induction of antiviral genes to slow or block virus infection.

In this view, even a virus that has the capacity to prevent induction of IFN signaling should nonetheless be associated with a greater burst of replication in CAFs. As such, we performed single-step growth curves in patient-derived samples using a wild-type isolate of VSV (VSV-WT) encoding GFP to monitor infection. This natural isolate of VSV maintains a functional M-protein which blocks mRNA export of anti-viral defense gene products, including IFNs, through direct inhibition of the nucleoporin NUP98 (190, 191). While both CAFs & NFs are infected by VSV-WT (Figure. 4.2g), virus replication was severely diminished in NFs compared to CAFs likely due to a high baseline of expression of anti-viral defense genes in normal cells (Figure. 4.2 g,h). In sum, these findings provide evidence for a re-wired anti-viral response program in CAFs where an initial burst of virus replication allows the virus to outpace activation of antiviral defenses.

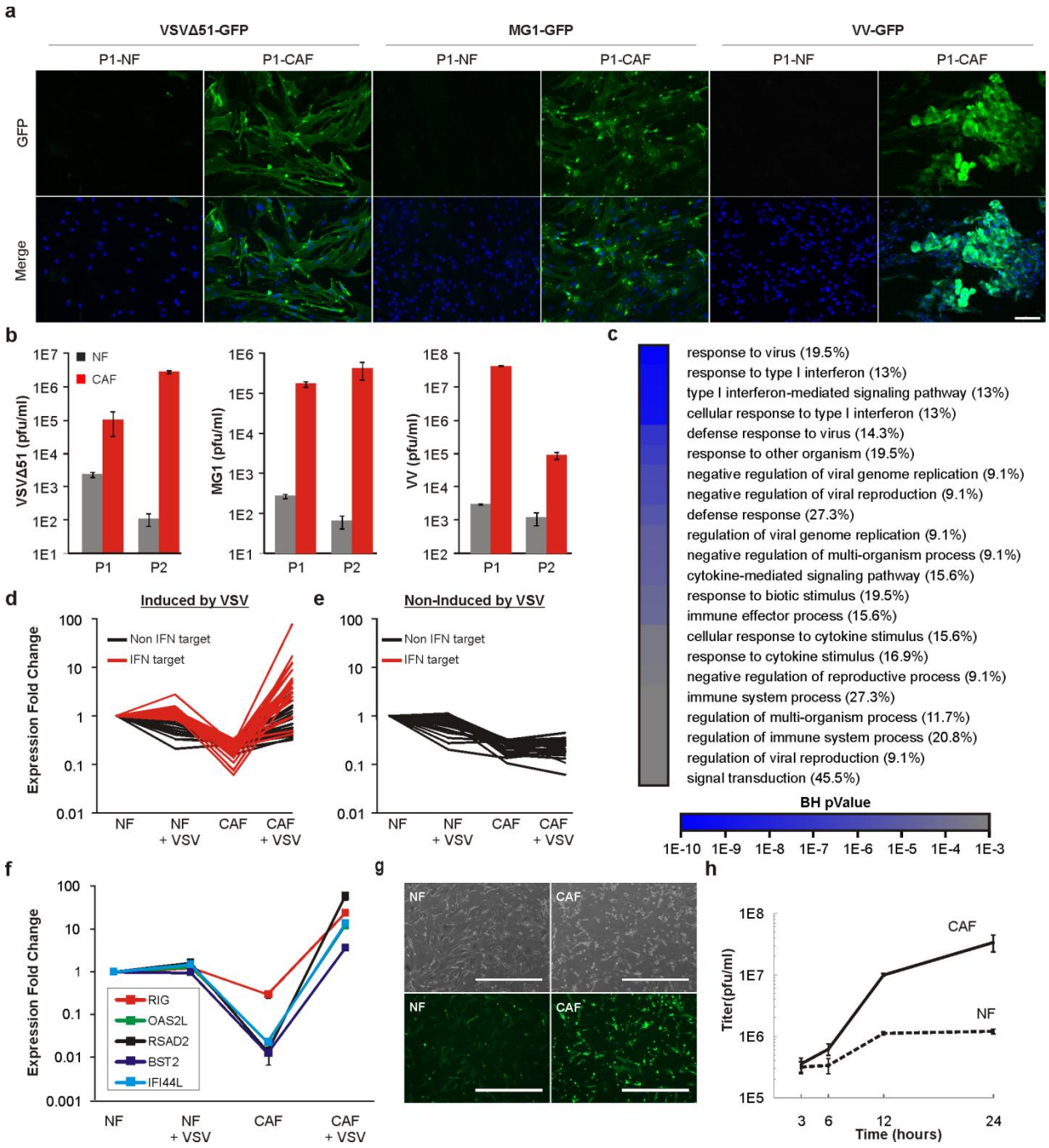
a
VSVΔ51-GFP
MG1-GFP
VV-GFP
P1-NF
P1-CAF
GFP
Merge
b
NF
CAF
VSVΔ51 (pfu/ml)
MG1 (pfu/ml)
VV (pfu/ml)
P1
P2
c
response to virus (19.5%)
response to type I interferon (13%)
type I interferon-mediated signaling pathway (13%)
cellular response to type I interferon (13%)
defense response to virus (14.3%)
response to other organism (19.5%)
negative regulation of viral genome replication (9.1%)
negative regulation of viral reproduction (9.1%)
defense response (27.3%)
regulation of viral genome replication (9.1%)
negative regulation of multi-organism process (9.1%)
cytokine-mediated signaling pathway (15.6%)
response to biotic stimulus (19.5%)
immune effector process (15.6%)
cellular response to cytokine stimulus (15.6%)
response to cytokine stimulus (16.9%)
negative regulation of reproductive process (9.1%)
immune system process (27.3%)
regulation of multi-organism process (11.7%)
regulation of immune system process (20.8%)
regulation of viral reproduction (9.1%)
signal transduction (45.5%)
BH pValue
1E-10 1E-9 1E-8 1E-7 1E-6 1E-5 1E-4 1E-3
d
Induced by VSV
e
Non-Induced by VSV
Non IFN target
IFN target
Expression Fold Change
NF
NF + VSV
CAF
CAF + VSV
f
RIG
OAS2L
RSAD2
BST2
IFI44L
g
h
Titer(pfu/ml)
Time (hours)

Figure 4.2. Cancer-associated fibroblasts, but not normal fibroblasts, are sensitive to virus-based therapy due to re-wired anti-viral networks

a, Microscopy images from NFs and CAFs, derived from the same cancer patient, infected with VSVΔ51-GFP (MOI=0.1, 24 hr) or MG1-GFP (MOI=0.1, 24 hr) or oncolytic VV-GFP (MOI=0.1, 48 hr). Nuclei were stained with DAPI. Scale bar=100μm. **b,** NFs and CAFs derived from two cancer patients were infected as described in (a), and plaque assays for VSVΔ51, MG1 and VV were conducted. **c,** GO-term analysis of biological processes associated with genes repressed in CAFs vs. NAFs. Genes selected for analysis are the subset of genes repressed over three-fold in CAFs (n=87/25465). Illustrated GO-terms represent all those significantly different (hypergeometric test pValue<0.001) after correction for multiple hypothesis testing (Benjamini–Hochberg). **d,** Fold change in gene expression as a function of previously documented induction by type I IFNs for genes repressed in CAFs but induced over three-fold by VSVΔ51. **e,** Fold change in gene expression as a function of previously documented induction by type I IFNs for genes repressed in CAFs but not induced by VSVΔ51 (less than three-fold). Induction by type I IFNs was established when one or more microarray datasets within the interferome database documented induction by type I IFNs. **f,** Quantitative real-time polymerase chain reaction (qRT-PCR) of select genes categorized as repressed in CAFs (>3 fold) and induced (>3fold) by VSVΔ51 according to the microarray analysis. qRT-PCR was performed on CAFs and NAFs obtained from cancer Patient 1 infected or not with VSVΔ51 for 18hours. **g,** NFs and CAFs derived from Patient 1 were infected with VSV wild-type expressing GFP and microscopy images were taken after 24 hours post-infection. Scale bar=100 μm. **h,** Single-step growth curve analysis of VSV-WT in NFs and CAFs. Error bars indicate standard deviation among replicates.

FGF-2 enhances virus replication and oncolysis in cancer cells

To identify the secreted factor(s) that mediate the sensitization of 786-0 cells to viral oncolysis, we tested a defined set of cytokines and growth factors known to be commonly expressed within the tumour milieu (35, 59, 296, 307-310). While all of the candidate cytokines tested were able to activate signaling pathways within 786-0 cells (Supplementary Figure 7c[$$$]) only FGF-2 was able to significantly enhance VSV replication (Supplementary Fig 7b[$$$]). As described above, TGFβ1 treatment of normal fibroblasts can sensitize them to oncolytic virus infection however it has no impact on the ability of 786-0 cells to support virus growth. VSVΔ51 multi-step growth curves in 768-0 cells showed that FGF2-dependent virus sensitization increases the rate of virus replication and the maximum amount of virus yield per cell (Supplementary Figure.8d[$$$]). The virus sensitizing activity of FGF-2 was diminished in a dose dependent fashion with specific neutralizing antibodies (Supplementary Figure.8c[$$$]). The activity of FGF-2 was independent of the oncolytic virus tested (Figure 4.3a,b), occurred in several different cancer cell lines (Figure 4.3c & Supplementary Figure.8e[$$$]) and was not simply a consequence of an in increase cell proliferation following growth factor stimulation (Supplementary Figure 7e[$$$]). Interestingly FGF2 was unable to enhance VSVΔ51 replication in normal GM38 fibroblasts (Figure 4.3c) but did enhance virus replication in GM-38 cells that had been transformed to a "cancer associated fibroblast-like" state by TGFβ treatment (Figure 4.3c). The closely related growth factor FGF1, although able to stimulate phosphorylation of ERK in a FGF-receptor dependent fashion and increase cell proliferation (Supplementary Figure 7c,d,e[$$$]) does not lead to sensitization of 786-0 cells to VSV infection (Supplementary Figure 8 a,b,d,e[$$$]). Co-culture systems were analyzed to determine if FGF-2 was responsible for establishing the pro-viral state in cancer cells. In both,

patient-derived CAFs and those induced by TGFβ-mediated transformation, FGF2 expression was higher than in its corresponding NF counterparts (Figure. 4.3d) and was maintained upon co-culture with cancer cells (Figure. 4.3e). To confirm the role of FGF2, we selectively blocked FGF2 signalling by transfecting specific small interfering RNAs (siRNAs) directed against the FGF-2 transcript into activated fibroblasts (Supplementary Figure.10a,b[$$$]). Knockdown of endogenous FGF2 transcripts in activated fibroblasts led to a significant attenuation of VSVΔ51 replication in CAF-cancer cells co-cultures (Figure. 4.3f,g and Supplementary Figure.10c[$$$]). Co-cultures containing FGF2-silenced fibroblasts produced VSVΔ51 titers that were approximately ten-fold lower than control (Figure. 4.3g). Similar results were observed when the impact of CAF-cancer cell co-culture was analyzed by flow cytometry (Supplementary Figure.10d,e[$$$]).

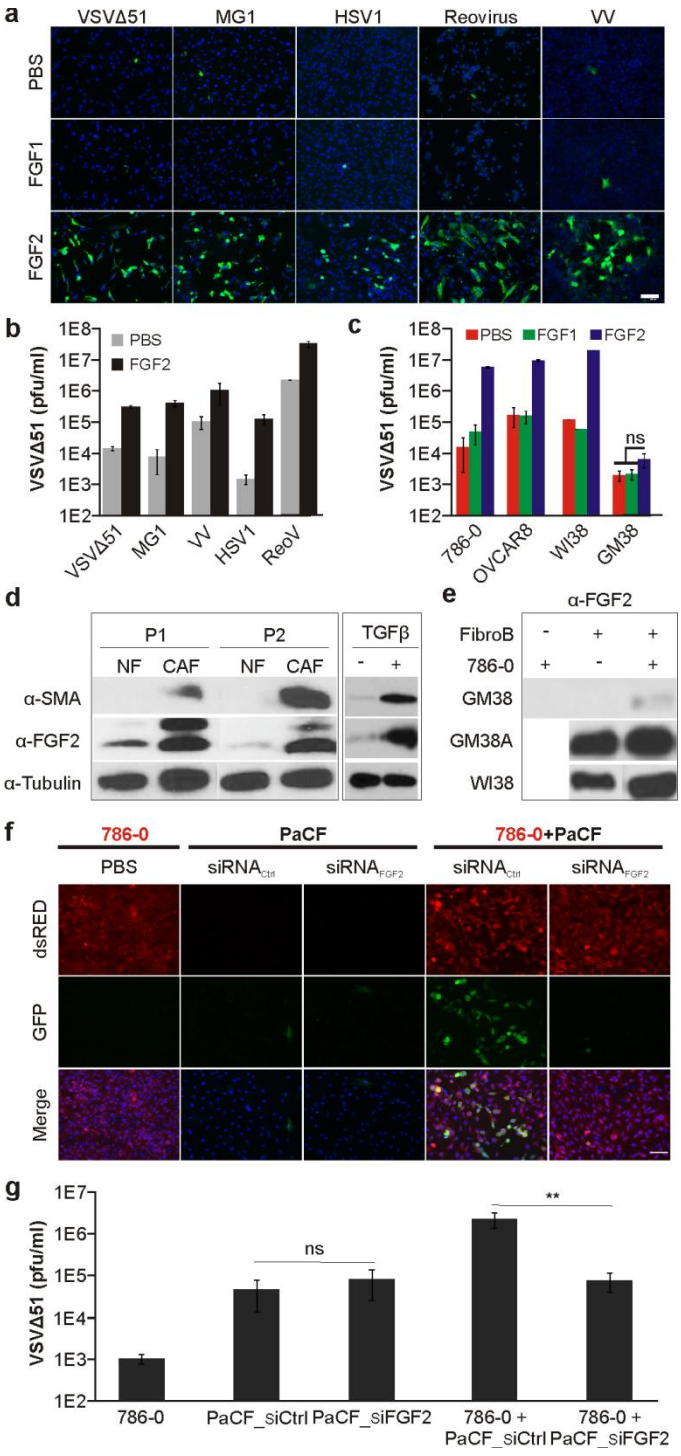
a
VSVΔ51
MG1
HSV1
Reovirus
VV
PBS
FGF1
FGF2
b
VSVΔ51 (pfu/ml)
PBS
FGF2
VSVΔ51
MG1
VV
HSV1
ReoV
c
PBS
FGF1
FGF2
ns
786-0
OVCAR8
WI38
GM38
d
P1
P2
NF
CAF
TGFβ
α-SMA
α-FGF2
α-Tubulin
e
α-FGF2
FibroB
786-0
GM38
GM38A
WI38
f
786-0
PaCF
786-0+PaCF
PBS
siRNACtrl
siRNAFGF2
dsRED
GFP
Merge
g
VSVΔ51 (pfu/ml)
ns
**
786-0
PaCF_siCtrl
PaCF_siFGF2
786-0 + PaCF_siCtrl
786-0 + PaCF_siFGF2

Figure 4.3. FGF2 induces replication of various clinically relevant oncolytic viruses in a panel of cancer cells and activated fibroblasts

a, Representative fluorescent images from 786-0 cells pre-treated with 20 ng/ml of FGF1 or FGF2 and subsequently infected with various OVs. Scale bar,100μm. **b,** 786-0 cells were treated and infected as indicated in (a), and virus yields assessed by plaque assay**. c,** The indicated human cancer cell lines and normal fibroblast were treated with FGF1 or FGF2 prior VSVΔ 51 infection (MOI=0.01). Means of virus yields from three independent experiments were calculated and plotted. Error bars are shown as standard deviation. **d,** Total cell lysates from patient derived NFs and CAFs or from GM38 treated with TGFβ1 or vehicle control were collected, and immunoblot analyses using αSMA, FGF2, and Tubulin antibodies were performed. **e,** Levels of secreted FGF2 from monotypic cultures or co-cultures of dsRED-768-0 cells and various fibroblast were assessed by western blot analysis. f and g, Pancreatic fibroblasts were treated with siRNA scramble control (siSC) or siRNA for FGF2 (siFGF2) for 24 hours, and then co-incubated with dsRED-786-0 cells for 60 hours. Mono- or co-cultures were infected with VSVΔ 51 (MOI=0.01). **f,** Shown are representative microscopy images 24 hours post-infection. Nuclei were stained with DAPI. Scale bar, 100 μm. **g,** Values represent the mean ±s.e.m. titer of VSVΔ51 from triplicate experiments.

FGF-2 modulates antiviral IFN responses by down-regulating RIG-I signalling

Since FGF-2 enhances the replication of a variety of oncolytic viruses we investigated whether it was able to dampen normal interferon mediated anti-viral activity. The rate of INF-I secretion by untreated- or FGF2-treated cells upon VSVΔ51 infection was monitored. FGF2 specifically delays the expression of INFβ (Supplementary Figure. $9^{\$\$\$}$) in response to virus. In addition, we found that when challenged with INFα, FGF2 treated cells were still significantly more sensitive to OV replication than mock or FGF1-treated cells. Specifically, virus yields were almost 100 fold higher in these samples (Supplementary Figure. $10^{\$\$\$}$). The ability to recognize cytosolic viruses, and activate IFN-I responses, depends on the RIG-I like receptor (RLR) family of proteins (311-313). One of the best-characterized RLRs is RIG-I, which detects short double-stranded viral RNA species in the cytosol of infected cells and triggers signaling pathways that induces the expression of IFNs and IFN-stimulated genes (ISGs). We examined whether FGF2 impacts RIG-I expression levels by immunoblot analysis and indirect immunofluorescence. Results shown in Figure 4.4a,b revealed a significant reduction on RIG-I protein expression in FGF2-treated cells. In parallel, we also observed decreased RIG-I expression in cancer cells cultivated with activated fibroblasts grown in a transwell chamber (Figure. 4.4c,d).

RIG-I responses are orchestrated by the mitochondrial antiviral signaling protein, MAVS. Upon viral infection, MAVS adopts a conformational change in response to RIG-I activation, leading to its oligomerization and subsequent activation of downstream regulators (314). A direct consequence of oligomerization is the activation, and nuclear translocation, of transcriptional

activators including interferon regulatory factor 1 (IRF1) (315, 316). We observed that pretreatment of cancer cells with FGF2 not only reduced oligomerization of MAVS upon VSVΔ51 infection (Figure. 4.4e), but equally blocked IRF1 nuclear translocation (Figure. 4.4f,g).

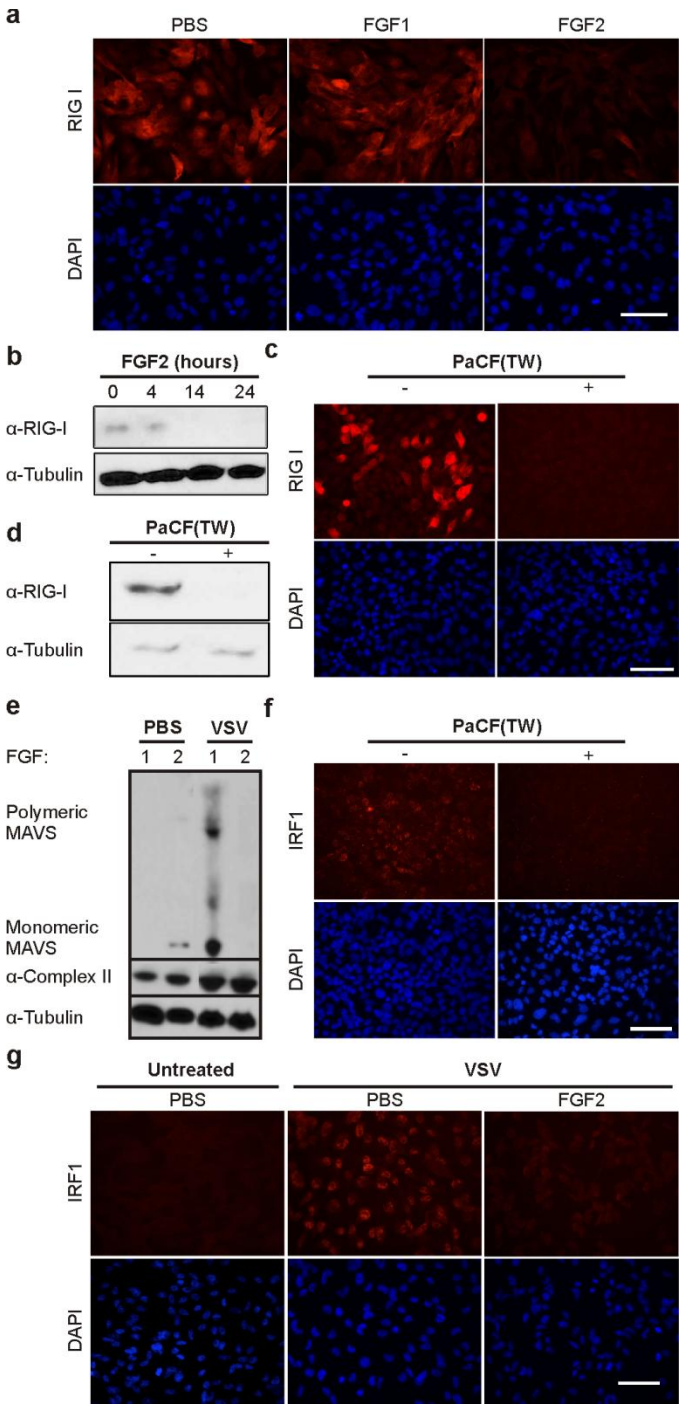
a
PBS
FGF1
FGF2
RIG I
DAPI
b
FGF2 (hours)
0 4 14 24
α-RIG-I
α-Tubulin
c
PaCF(TW)
- +
RIG I
DAPI
d
PaCF(TW)
- +
α-RIG-I
α-Tubulin
e
PBS VSV
FGF: 1 2 1 2
Polymeric MAVS
Monomeric MAVS
α-Complex II
α-Tubulin
f
PaCF(TW)
- +
IRF1
DAPI
g
Untreated
VSV
PBS
PBS FGF2
IRF1
DAPI

Figure 4.4. Modulation of anti-viral responses by FGF2

a, 786-0 cells were treated with FGF1 or FGF2 (20 ng/ml) for 24 hr prior to indirect immunofluorescence staining with RIG-I antibodies.Nuclei were stained with DAPI. Scale bar, 60 μm. **b,** Western bot analysis for RIG-I and Tubulin (loading control) in 786-0 cells treated with FGF2 (20 ng/ml) for the indicated periods of time. **c,** MiaPaca cells were co-cultured with pancreatic fibroblasts in transwellinserts (TW) for 72 hr. Cells were then fixed and processed for indirect immunofluorescence-staining using RIG-I antibodies. Nuclei were stained with DAPI. Scale bar, 60 μm. **d,** MiaPaca cells were cultured as indicated in c. Levels of RIG-I protein in total cell lysates were assayed by immunoblot analysis with RIG-I specific antibodies. The blot was re-probed with antibodies for Tubulin as a loading control. **e,** 786-0 cells were treated with FGF1 and FGF2 (20 ng/ml) prior to mock or VSVΔ51 infection (MOI=0.1, 24 hr). Crude mitochondria were isolated and then crosslinked with 1,6-bismaleimidohexane (BMH) prior to analyses by western blot with antibodies specific to MAVS and complex II (loading control). **f and g,** Analysis of nuclear translocation of IRF1 protein following VSVΔ51 infection (MOI=1, 12 hr) in MiaPaca cells, co-cultured with Pancreatic fibroblast (f) or in 786-0 cells pretreated with FGF1 or FGF2 (20 ng/ml) (g). Scale bar, 60 μm. Images are representative of at least three independent experiments.

Co-engraftment of fibroblasts with cancer cells significantly enhances virus replication in tumors

To investigate the in-vivo effect of crosstalk between the CAF and the cancer cell compartments on OV replication, we generated human pancreatic tumor grafts containing MiaPaca-2 cells alone (MiaPaca tumors) or in combination with activated pancreatic fibroblasts (MiaPaca+PaCF tumors) in SCID mice. Due to the fibrotic nature of pancreatic cancers (PaC) and the important role of CAFs in resistance to conventional therapy in this disease (35, 37, 299, 317-319), we focused our in vivo studies on pancreatic cancer models. Immunohistochemical analysis of MiaPaca+PaCF tumors showed a high density of α-SMA and FGF2 positive cells relative to control MiaPaca tumors (Supplementary Figure.12b[$$$]). Upon co-engraftment with CAFs, MiaPaca tumors became highly sensitized to VSVΔ51 infection. The presence of CAFs substantially enhanced VSVΔ51-Luciferase replication in the tumor as indicated by higher virus titers (Figure.4.5a), and increased transgene activity (Figure.4.5b). This was not due to differential tumor growth between groups since at the time of virus treatment; there was no significant size difference between both models (Supplementary Figure.12a[$$$]). Similar to our in-vitro observations, it appears that this result is attributed to a repressed anti-viral state. Detailed immunohistochemical analysis using antibodies to visualize viral proteins, RIG-I and CAF markers showed that the infection usually occurs in areas of tumor enriched in fibroblasts and deprived of RIG-I expression (Figure. 4.5c and Supplementary Figure.13[$$$]). Similar results were observed when infecting tumor explants ex-vivo (Supplementary Figure.14[$$$]), indicating that neither improved virus delivery, nor immune recruitment, is the main cause of CAF-dependent OV sensitization of tumors in-vivo.

FGF2 induces sensitivity to oncolytic virus therapy in tumor grafts

To determine whether FGF2 plays a significant role in sensitizing tumors to virus-based therapy, we monitored VSVΔ51-Luciferase delivery in SCID mice harboring bilateral MiaPaca-2 tumors pre-treated or not with intratumoral injections of recombinant FGF2 protein (Supplementary Figure.15a[$$$]). FGF2 increased VSVΔ51-Luciferase titers by more than tenfold in MiaPaca tumors (Figure. 4.5d), as well as viral luciferase transgene expression (Figure. 4.5e). Similar results were observed in OVCAR8 and 786-0 xenograft models (Supplementary Figure.15b,c[$$$]). Consistent with the notion that FGF2 impairs RIG-I responses, virus infection co-localized in areas enriched in FGF2 and poor in RIG-I staining (Figure. 4.5f). Once again, infection of tumor explants ex-vivoindicate that FGF2-mediated sensitization is not the result of improved virus delivery, nor immune recruitment, but rather of impaired innate immune responses associated with RIG-I circuit inhibition (Supplementary Figure.17[$$$]),

Patient samples were next examined to establish the role FGF2 signalling in OV therapies. After obtaining pancreatic cancer patient-derived tumor grafts, we selected samples on the criteria of low (P025, P009, P033 and P034) or high (P013, P019, P023, and P032) FGF2 protein expression level (Figure. 4.5g), and infected them ex-vivo with VSVΔ51. Using FGF2 as a biomarker for OV infection, we observed that patients with high FGF2 expression were much more susceptible to infection (Figure. 4.5h). To confirm the role of FGF2 in OV-sensitization in two patient-derived samples, tumors were embedded in NOD-SCID mice and treated or not with recombinant FGF2. Similar to our MiaPaca-2 xenograft model, FGF2-pretreatment was markedly efficient in sensitizing these tumors to VSVΔ51, enhancing replication over 100-fold (Figure. 4.5i).

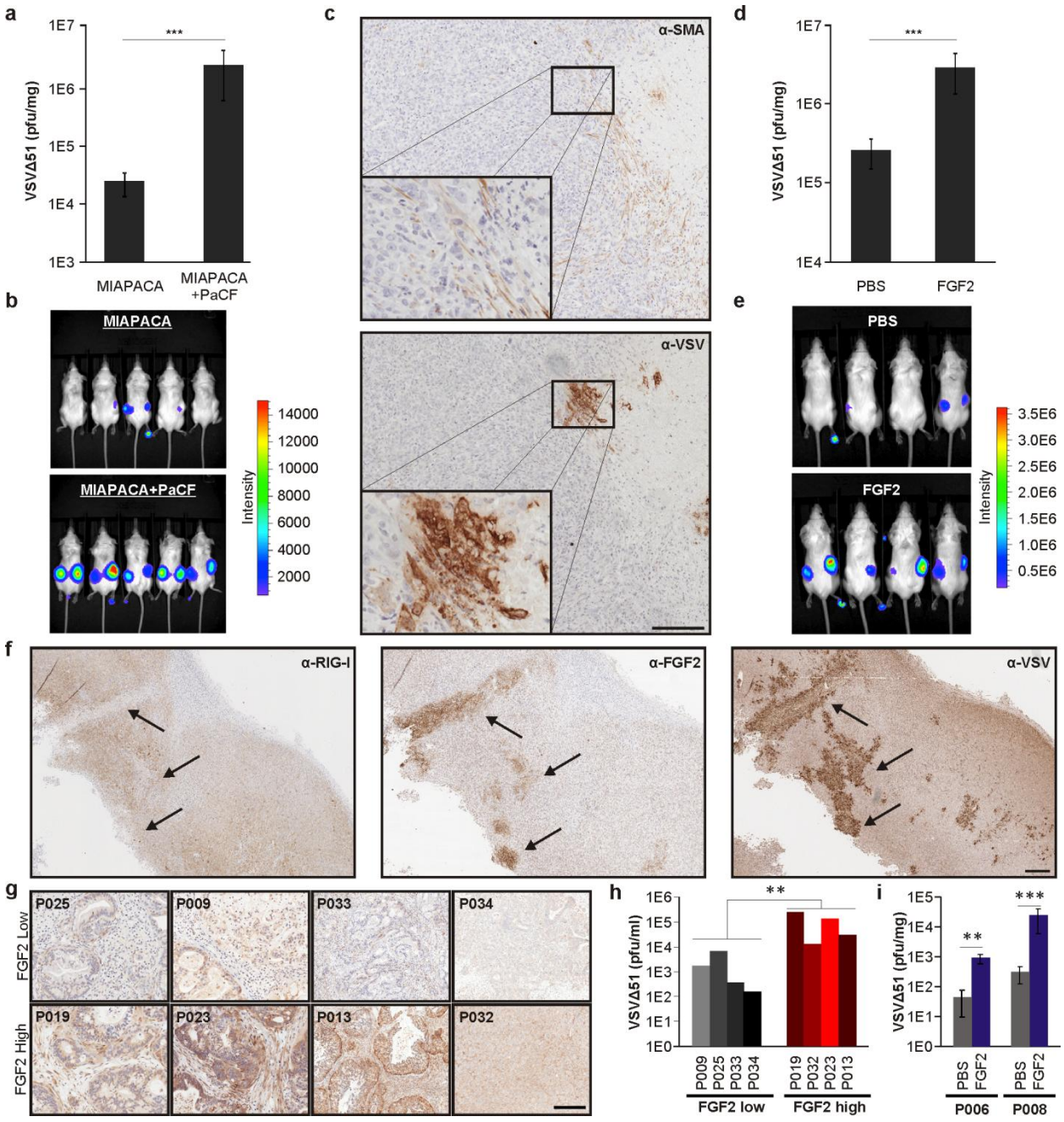
a
VSVΔ51 (pfu/mg)
1E7
1E6
1E5
1E4
1E3
***
MIAPACA
MIAPACA +PaCF
b
MIAPACA
MIAPACA+PaCF
Intensity
14000
12000
10000
8000
6000
4000
2000
c
α-SMA
α-VSV
d
VSVΔ51 (pfu/mg)
1E7
1E6
1E5
1E4
***
PBS
FGF2
e
PBS
FGF2
Intensity
3.5E6
3.0E6
2.5E6
2.0E6
1.5E6
1.0E6
0.5E6
f
α-RIG-I
α-FGF2
α-VSV
g
FGF2 Low
FGF2 High
P025
P009
P033
P034
P019
P023
P013
P032
h
VSVΔ51 (pfu/ml)
1E6
1E5
1E4
1E3
1E2
1E1
1E0
**
P009
P025
P033
P034
P019
P032
P023
P013
FGF2 low
FGF2 high
i
VSVΔ51 (pfu/mg)
1E5
1E4
1E3
1E2
1E1
1E0
**
***
PBS
FGF2
PBS
FGF2
P006
P008

Figure 4.5. Cancer-associated fibroblasts and FGF2induce sensitivity to OV therapy in xenograft models and in tumor grafts derived from Pancreatic cancer patients

a, VSVΔ51-luciferase (1E7 pfu) was delivered IV into SCID mice bearing bilateral MiaPaca or MiaPaca+PaCF tumors. After 72 hours, tumors were homogenized and virus was titrated by plaque assay. Data are means ±s.e.m. (*n*=7-9 per group). **b,** Representative bioluminescence images of (a). **c,** Tumor tissues from (a) were stained with antibodies specific for VSV and αSMA. Higher magnifications of the areas outlined are shown. Scale bar, X μm. **d,** VSVΔ51-luciferase (1E7 pfu) was delivered IV into SCID mice bearing MiaPaca tumors previously supplemented with FGF2 (3 ug) or vehicle control. After 72 hours, tumors were homogenized and titrated by plaque assay. Data are means ±s.e.m (*n*=7-9 per group). **e,** Representative bioluminescence images of (e). **f,** Immunohistochemical assessment of FGF2,RIG-I and VSVΔ51 from (e). **g,** Immunohistochemical assessment of endogenous FGF2 expression in tumor grafts derived from Pancreatic cancer patients. Tumors were arbitrarily classified based on a pattern of low or high FGF2 protein expression. **h,** Tumor cores from low or high FGF2 expression group were infected with VSVΔ51 ex-vivo (1E4 pfu). Supernatants were titrated 48 hours post-infection. **i,**VSVΔ51-luciferase (1E8 pfu) was delivered IV into NOD-SCID mice bearing bilateral tumors derived from Pancreatic cancer patients (P006 and P008), which were previously supplemented with FGF2 (3 ug) or vehicle control. After 72 hours, virus titers were assessed. Data are means ±s.e.m. among replicates (*n*=5 per group).

Conclusion

In the present study, we showed that communication between cancer cells and CAFs is a driving factor involved in targeting virus-based therapies against tumors. From our findings, it appears that cancer cells have the ability to educate surrounding normal fibroblasts to reprogram their gene landscape to improve immune evasion. Microarray data from NFs and CAFs derived from cancer patients revealed that CAFs have markedly lower expression of gene products involved in defense responses against pathogens, and are strikingly more sensitive to OV attack when compared to their normal counterparts. Although contributions from other soluble factors within the tumor microenvironment cannot be excluded, our findings imply that TGFβ1 is a key factor involved in promoting this molecular switch in fibroblasts. Conversely, we found that FGF2 is in part responsible for deregulating anti-viral circuits within cancer cells by CAFs, and together create a hub for optimal virus replication. Indeed, providing FGF2 to the tumor milieu was sufficient to dampen RIG-I protein expression levels and augment OV replication across several tumor models. In this regard, it is perhaps not surprising that many viruses have evolved virulence factors that are orthologous to FGF2 (e.g. Baculoviruses (320-322)) or that induce production of FGF2 (e.g. Rhinoviruses (323)).

The key question that arises from our findings is why do these paracrine factors promote a global pro-viral state within the tumor milieu? Interestingly, both factors are secreted during wound healing (324-328), a process that is becoming recognized as a key-driving factor of tumorigenesis heal (34-36). In regards to immunity, wound healing activates immunosuppressive processes to activate anti-inflammatory pathways and prevent systemic inflammation (79-80) which are likely rewired to be persistent in the tumor microenvironment. As tumors evolve to

full-blown malignancy they likely eliminate/inactivate the function of certain interferon gene products, but by doing so compromise their innate cellular anti-viral responses to varying degrees. Schreiber's group showed that one of the most common genetic changes in the tumor as it transitions to a stealth phenotype is the loss of expression of genes in the interferon pathway (21, 107). This key characteristic may not only be used for designing targeted therapies, but may equally serve as a predictive marker for stratifying patients for their responses to OVs. In light of our preclinical data in pancreatic cancer patient-derived tumor grafts and human xenograft models, we argue that FGF2 could have a potential prognostic value for virotherapy in PCa tumors.

Acknowledgments

This work was funded by the Terry Fox Research Foundation and the Canadian Institutes of Health Research. C.S.I. is the recipient of a Fellowship award from the Alberta Innovative Health Solutions. J.C.B. is supported by the Ontario Institute for Cancer Research and the Ottawa Regional Cancer Foundation. C.B. is funded by the Natural Sciences and Engineering Research Council of Canada. We thank the exceptional technical support of Catia Cemeus and Dominique Vaillant as well as members of the Bell, Auer, Atkins and Diallo laboratories for feedback on this project.

Author Contributions

C.S.I, M.M, C.B., D.B.N, S.C., F.L., and L.S. conducted *in vitro* experiments. C.S.I, T.F., C.T.S., and D.B.N. performed mouse experiments. C.S.I, M.M, C.B., and J.C.B. designed the study and wrote the manuscript.

Methods

Reagents

The following reagents were purchased from the respective suppliers: General laboratory chemicals from Sigma Chemical Co. (St. Louis, MO); Media, horse serum and fetal bovine serum (FBS) for cell culture from Life Technologies-Invitrogen, Inc (Carlsbad, CA). MiaPaca-2, OVCAR8, 786-0, Vero, U2OS, L929, and WI38 cells from the American Type Culture Collection (Manassas, VA). Human normal GM00038 foreskin fibroblasts (abbreviated as GM38) and human fetal pancreatic fibroblasts (PaCF) were obtained from the Coriell Cell Repositories (Camden, NJ) and Vitro Biopharma (Golden, CO), respectively. Normal and cancer-associated fibroblasts (CAFs) derived from lung carcinoma patients.

Cell culture and viruses

786-0, OVCAR8, U2OS, Vero, PaCF, WI38 and CAFs were cultured in Dulbecco's minimal essential medium (DMEM) containing 10% fetal bovine serum (FBS), and 1 mM HEPES. MiaPaca-2 cells were cultured in DMEM supplemented with 10% FBS and 2% horse serum.

GM38 fibroblasts and patient-derived normal fibroblasts (NFs) were cultured in DMEM containing 2% FBS, and 1 mM HEPES. Cells were incubated at 37ºC in a humidified atmosphere with 5% CO_2 and 80% humidity. Engineering and rescuing of the interferon sensitive version of VSV, termed VSVΔ51, has been described before (165). The oncolytic version of Maraba virus, named MG1, was previously described (166). HSV-1 N212 expressing GFP (329, 330) was a gift from Dr. Karen Mossman lab (McMaster University, Canada).The oncolytic version of Vaccinia virus encoding GFP was previously described (331). Reovirus was a gift of Dr. Patrick Lee (Dalhousie University, Halifax, Canada). All virus stocks were diluted with cell culture media and then added to cells that had been washed with phosphate-buffered saline (PBS). Cells were incubated with the virus inoculum for 1-3 hours at 37ºC after which time the inoculum was replaced with normal growth media. Infected cultures were kept at 37ºC until experimental analysis.

Cancer cell and fibroblast co-cultures

For direct in-vitro co-culture, cancer cells were plated with fibroblasts at a ratio 1 to 3 respectively in reduced-serum medium (2% FBS). The cultures were incubated for 3 days after which cells were infected with the indicated OV for 24 hours (Rabdoviruses) or 48 hours (VV, HSV-1, and Reovirus). For indirect co-culture, cancer cells were seeded in the bottom dish and activated fibroblasts were grown in cell culture transwellinserts (0.4 μm pore, BD Falcon, San Jose, CA). Similarly for conditioned media transferring experiments, cancer cells or fibroblasts were grown in reduced-serum medium (2% FBS) for 3 days. The supernatants were then

collected, filtered and applied immediately to the indicated cancer cells or fibroblasts and grown for 2 days before infection or viable cell counting by Trypan blue staining.

Cell treatment with various growth factors and cytokines

786-0, OVCAR8, MiaPaca-2 or WI38 cells were grown until 80% confluent in DMEM containing 2%FBS and treated with FGF1 (20 ng/ml), or FGF2 (20 ng/ml) or EGF (50 ng/ml) or TGFβ1 (10 ng/ml) or TGFβ2 (10 ng/ml), SDF1 (50 ng/ml), IL6 (50 ng/ml), or IL8 (50 ng/ml). All growth factors and cytokines were obtained from R&D systems (Minneapolis, MN). Twenty hours post-treatment, cells were infected with indicated oncolytic virus for 24 hours (Rhabdoviruses) or 48 hours (VV, HSV-1 and Reovirus).

FGF1 and FGF2 signaling was abrogated by pretreating cells with a FGF receptor 1 inhibitor, PD173074 (25 µM, Sigma-Aldrich). Similarly, FGF2 activity was diminished by adding a specific anti-FGF2 neutralizing antibody at the final concentration of 2 µg/ml to 50 µg/ml (R&D systems, Minneapolis, MN).

Analysis of cell proliferation and cell death

Cell viability was calculated by trypan blue exclusion assay using a ViCell automated viable cell analyzer (Beckman Coulter, Fullerton, CA). Cell death was measured with aCytotoxicity assay measuring *lactate dehydrogenase* (LDH) released as per the manufacture's protocol (Promega,

Madison, WI). All experimental conditions included three biological replicates and all experiments were independently repeated at least three times and reported by mean values.

Enzyme-linked immunosorbent assay (ELISA)

786-0 cells were pretreated with FGF2 (20 ng/ml) or vehicle control (PBS) 24 hours before infection with VSVΔ51 (MOI=0.01). Supernatants were collected at indicated time points and secreted IFN-β quantified using a Verikine human IFN-β ELISA kit as per manufacture's instruction (PBL Interferon Source, Piscataway, NJ).

siRNA transfections

For FGF2-specific silencing, WI38 or Pancreatic fibroblasts were transfected with small interfering RNAs (10 μM)against FGF2 (siGENOME Smart pool for human FGF2 siRNA, Thermo Scientific) or with non-targeting siRNA (siGENOME non-targeting control, Thermo Scientific). Transfections were carried out according to manufacture's protocol (Lipofectamine®RNAiMAX, Life Technologies). Interference of target gene expression was confirmed by immunoblot analysis using FGF2 antibodies as described below.

Plaque assays

For Rhabdoviruses, vero cells ($5x10^5$ cells) were infected with serial dilutions of virus containing samples in 35 mm dishes for 1 hour. Cells were then washed and overlaid with warm 0.5% (w/v) agarose in culture medium and incubated for 1 day. Viral plaques were visualized by staining with 0.05% (w/v) crystal violet in 17% (v/v) methanol for 2 hours at room temperature.

For Vaccinia virus, U20S cells ($7.5x10^5$) were infected with serial dilutions of virus containing samples in 35 mm dishes for 2 hour. Cells were then washed and overlaid with warm 1.2% (w/v) methylcellulose in culture medium and incubated for 3 days. Viral plaques were visualized by staining with 0.05% (w/v) crystal violet in 17% (v/v) methanol for 2 hours at room temperature.

For Reovirus, L929 cells ($1x10^6$) were infected with serial dilutions of virus-containing samples in 35 mm dishes for 3 hours. Cells were then washed and overlaid with warm 1% (w/v) agar (Sigma) in culture medium and incubated for 3 days. Viral plaques were visualized by adding neutral red to 0.01% (w/v) final concentration.

For oncolytic HSV-1, samples containing HSV1 were serially diluted and titered on U2OS cells as previously described (330).

Measurement of virus infection by flow cytometry

Monotypic or co-culture of dsRED 786-0and fibroblasts were incubated for 3 daysand then infected with VSVΔ51-GFP (MOI=0.01, 24 h) or VV-GFP (MOI=0.01, 48 h) before analysis by flow cytometry (Cyan ADP 9, Beckman Coulter, Fullerton, CA). For each sample at least 10,000 events were acquired. dsRED fluorescence was detected through the FL-2 channel equipped with a 585-nm filter and eGFP fluorescence was measured using the FL-1 channel equipped with a 489-nm filter. Data was analyzed using Kaluza Flow Cytometry Analysis software (Beckman Coulter). The percentage of infected cancer cellswas equated to the percentage of dsRED positive cells that were also GFP-positive. On the contrary, the number of VSVΔ51-GFP or VV-GFP positive fibroblasts was equated to the percentage of negative dsRED cells that were positive for GFP. Results are representative of three independent experiments.

Indirect immunofluorescence microscopy

Cells cultured on glass coverslips were infected with VSVΔ51 (MOI=0.01) or MG1 (MOI=0.01) or oncolytic VV (MOI=0.01) or oncolytic HSV-1 (MOI=0.01) or Reovirus (MOI=1). After 24 or 48 hours post-infection, cells were fixed in 4% paraformaldehyde for 20 min, followed by quenching with PBS containing 50 mM ammonium chloride. Cell membranes were permeabilized with PBS containing 0.2% Triton-X-100 for 5 min before incubation with primary and secondary antibodies. All the washes were done in PBS containing 0.1 mM $CaCl_2$ and 1 mM $MgCl_2$.

VSV and MG1 proteins were detected with rabbit anti-VSV (BreitbachMolTher. 2011). Reovirus was detected using a rabbit anti-Reovirus T3 antibody (gift from Dr. Earl Brown, University of Ottawa, Canada). IRF1 and RIG-Iwere detected using a mouse anti-RIG-I (ENZO Life Sciences) and a specific mouse monoclonal antibody for IRF1 (Abcam) respectively. Primary antibodies were detected with Alexa Fluor 594 chicken anti-mouse, Alexa Fluor 488 donkey anti-rabbit, and/or Alexa Fluor 488 donkey anti-mouse, or Alexa 594 goat anti-rabbit (Molecular Probes, Invitrogen, Carlsbad, CA). Coverslips were mounted onto microscope slides using ProLong Gold antifade reagent with 4'-6-Diamidino-2-phenylindole (Molecular probes, Invitrogen). Samples were then examined using a Zeiss Imager.M1 microscope or a Zeiss Axioskop2 microscope equipped with anAxioCamHRm digital camera (Zeiss, Germany).

Immunohistochemistry

Formalin-fixed paraffin-embedded tumors were sectioned (8 μm) for immunohistochemistry. After rehydration, sections were treated with sodium citrate (pH: 6.0) for 17.5 min in a pressured

cooker and cooled for 30 min for antigen retrieval. Sections were then blocked with 10% goat serum for 1 hour at room temperature and then incubated with rabbit antibodies to human FGF2 (Santa Cruz Biotechnology, Dallas, TX), to VSV (BreitbachMolTher. 2011), to alpha smooth muscle actin (Abcam, Cambridge, MA) or to RIG-I (ENZO Life Sciences, Farmingdale, NY) overnight at 4ºC. Dilution and specificity of each antibody were confirmed by omission of the primary antibody. The secondary antibodies used were biotinylated goat antibody to rabbit or mouse IgG (Vector Laboratories, Burlingame, CA). Sections were briefly counter stained with Hematoxylin.

Immunoblot analysis

Cells ($2x10^5$) in 35 mm culture dishes were infected with the indicated OV and/or treated with indicated cytokine and then incubated for 24 hours at 37^oC prior to lysis. Cells were lysed in 1% NP-40, 150 mMNaCl, 2 mM EDTA, 50 mMTris, pH 7.4 containing Complete™ EDTA-free protease inhibitors (Roche). Cell lysates were clarified by centrifugation at 10,000 x g for 10 minutes at 4°C. Secreted FGF2 was recovered from conditioned media using StrataClean Resin (Agilent Technologies, Santa Clara, CA). Briefly, conditioned media was incubated for 2 hours with beads (10 % v/v) and then pelleted by centrifugation at 500 x g for 2 min at 4°C. Bound proteins were eluted by heating at 95°C for 5 minutes in sample buffer. Proteins were then separated by SDS-PAGE and transferred to polyvinylidene fluoride (PVDF) membranes (Immobilon-P Millipore, Bedford, MA). Membranes were incubated for 1 hour at room temperature with the following antibodies and dilutions: 1:3000 rabbit anti-VSV,1:1000 goat anti-tubulin (Abcam), 1:1000 rabbit anti-GAPDH (Abcam), 1:1000 rabbit anti-ERK (Santa Cruz), or 1:1000 mouse anti-phospho ERK (Santa Cruz), or 1:1000 mouse anti-FGF2 (Santa

Cruz) or 1:1000 mouse anti-FGF2 (Millipore, Temecula, CA). After three washes with Tris-Buffered-Saline-Tween (TBS-T), the membranes were incubated with goat anti-rabbit, goat anti-mouse or bovine anti-goat horseradish peroxidase-conjugated IgG (Jackson ImmunoResearch Laboratories, Inc.) for 1 hour. Membranes were washed four times with TBS-T and immunoreactive proteins were detected using Supersignal West Pico chemiluminescent substrate (Pierce Biotechnology, Rockford, IL) followed by exposure to X-ray film (Fuji Photo Film Co, LTD, Tokyo, Japan).

Mitochondria isolation and crosslinking

786-0 cells ($1x10^6$ cells)treated with growth factor control (FGF1, 20 ng/ml) or with FGF2 (20 ng/ml) were cultured for 12 hours, followed by VSVΔ51 infection (MOI=1) for 12 hours. Cells were then homogenized in ice-cold mitochondria isolation buffer containing 200 mMmannitol, 70 mM sucrose, 10 mMHepes, and 1 mM EGTA (pH: 7.5) using a dounce homogenizer with a loose fitting pestle. Unbroken cells and nuclei were pelleted by centrifugation at 500 x*g* for 10 min at 4˚C. The supernatants were then centrifuged at 10,000 x *g* for 20 min at 4˚C to obtain crude mitochondrial pellets that were cross-linked with 10 mMbis (maleimido) hexane (BMH; Thermo Fisher Scientific, Wilmington, DE) for 30 min at room temperature. Samples then were separated on 4-12% polyacrylamide gels (BioRad, Hercules, CA) and processed for immunoblotting with rabbit polyclonal antibodies to MAVS (Abcam, Cambridge, MA) and Complex II Subunit 30 KDa (MitoSciences, Eugene, OR).

Affymetrix microarrays analysis and quantitative real time PCR

NFs or CAFs ($1x10^6$ cells) were seeded in a 6 well dish to allow adherence overnight. The following day, cells were treated with VSVΔ51 at an MOI=0.01 or left untreated. Eighteen hours following treatment, total RNA was extracted using an RNAeasykit (Qiagen Inc., Valencia, CA) according to the manufacture's protocol and triplicate samples were pooled prior to hybridization. Sample quality was verified on abioanalyzer (Agilent Technologies), processed and hybridized to a GeneChip Human Gene 1.0 ST Array according to manufacturer instructions. Data was processed using AltAnalyze (264)under default parameters. Probeset filtering implemented a DABG threshold of 70 with $pV<0.05$. Only constitutively expressed exons for a given locus were utilized to quantify gene expression. Gene ontology enrichments were performed using Gorilla (265) and identification of genes induced by Type-Iinterferons was performed using data obtained from the interferome database (266). All microarray data are deposited in the NCBI Gene Expression Omnibus (GEO).qRT -PCR was performed on the non-pooled triplicate samples. Following conversion to cDNA by Superscript RT II (Invitrogen, Carlsbad, CA), qRT-PCR was carried out using Sybergreen (Invitrogen) according to the manufacturer's instructions. Analyses were performed on a Rotor-Gene RG-3000A machine (Corbett Research) according to the manufacture's recommended protocols. The primer pairs specific for various gene products used in our experiments are listed in Supplementary Table $1^{\$\$\$}$. qRT-PCR measurements were normalized to the *GAPDH* gene using the Pfaffl method (294).

Animal and xenograft studies

All animal studies were approved by the institutional animal care and committee of the University of Ottawa and carried out in accordance with guidelines of the National Institutes of

Health and the Canadian Council on animal care. SCID and NOD-SCID mice were purchased from Charles River Laboratories (Wilmington, MA). For assessments of the acute effect of activated fibroblasts in virus-based therapy, human pancreatic cancer xenograft models were established in SCID mice by subcutaneously injecting MiaPaca-2 cells alone ($1x10^7$ cells) or MiaPaca cells ($5x10^6$ cells) in combination with human activated pancreatic fibroblasts ($5x10^6$ cells). Tumor growth was assessed weekly using calipers. When tumor sizes reached 1.2-1.4 cm in diameter, mice received VSVΔ51 encoding Luciferace at a dose of 1E6 pfu by I.V. injection. Luminescence imaging of mice was performed 48 and 72 hours post-virus delivery using the IVIS imaging System Series 200(Xenogen Corporation). Data acquisition and analysis was performed using Living Image v2.5 software. Mice were sacrificed 72 hours after virus treatment and tumors were removed for histological analysis and virus quantification by plaque assay.

To determine the effect of recombinant FGF2 on virus replication within the tumor, MiaPaca-2 ($1x10^7$ cells), Ovcar8 ($7.5x10^6$ cells) or 786-0 ($1x10^7$ cells) bilateral tumors were generated in SCID mice. Tumor growth was assessed weekly using calipers. When tumor sizes reached 1.2-1.4 cm in diameter, mice received a single intratumoral injection of recombinant FGF2 (3 ug) or vehicle control (PBS). Twenty-four hours later, a dose of 1E7 pfu VSVΔ51-Luciferace was delivered by I.V. injection. At 48 and 72 hours post-virus delivery the mice were injected intraperitoneally with D-luciferin (Molecular Imaging Products Company) and imaged using the IVIS imaging System Series 200 (Xenogen Corporation). The mice were sacrificed after the last IVIS imaging and tumors were removed for histological analysis and virus quantification by plaque assay.

Establishment of Patient-derived Pancreatic tumor grafts

All tissue samples were collected with informed consent from individuals being treated/diagnosed at the Ottawa Hospital General Campus under a protocol approved by the Institutional Ethics Board. Fresh or frozen tumor samples were subcutaneously implanted in NOD-SCID mice with 100 μlof Cultrex® high protein concentration basement membrane extract (Trevigen,Gaithersburg, MD). Tumor growth was measured weekly. When tumors reached 1-1.5 cm^3, animals were sacrificed and tumors were excised for ex-vivo infection or for histological analysis. For ex-vivo infection, tumors were cut into 2 by 2 mm cores and infected with VSVΔ51 (1E4 pfu) for 48 hours. Subsequently, the secreted infectious particles were titered by plaque assay. For *in-vivo* experiments, when tumors reached 1-1.2 cm^3, VSVΔ51 (1E7 pfu/mouse) was injectedI.V. Forty-eight hours later the animals were euthanized and tumor-associated infectious virus particles were quantified by plaque assay.

Statistical analyses

Analyses of microarray studies are described above.In-vitro studies of cell viability and cell proliferation were performed at least twice and data is reported as mean values. In-vitro, ex-vivo and in-vivo infections were carried out a minimum of three times and data is reported as ±s.e.m. Statistical analysis was performed on raw data by one-way analysis of variance or Student's t test (two-tailed). *p*-values< 0.05 was considered significant.

Chapter V. Non-replicating rhabdovirus-derived particles (NRRPs) eradicate acute leukemia by direct cytolysis and induction of anti-tumor immunity

Authors:
Cory Batenchuk* a,b,c, Fabrice Le Boeuf* a,c, Lawton Stubbert a,c, Theresa Falls a,c, Harold L. Atkins a,c,e, John C. Bell# a,b,c, David P. Conrad# a,c,d,e

Affiliations:
a Ottawa Hospital Research Institute, Center for Cancer Therapeutics, Ottawa, Ontario, Canada.
b Department of Biochemistry, Immunology and Microbiology, University of Ottawa, Ottawa, Ontario, Canada.
c Department of Medicine, University of Ottawa, Ottawa, Ontario, Canada.
d Department of Cellular and Molecular Medicine, University of Ottawa, Ottawa, Ontario, Canada.
e Blood and Marrow Transplant Program, The Ottawa Hospital, Ottawa, Ontario, Canada.
* and #: equal contribution to this work.

Journal:
Blood Cancer Journal (NPG), 2013

My contribution:
I contributed to all aspects of this paper other than the data represented in Figure 5.2B, 5.4 & 5.5 B/C.

Chapter Synopsis

In the article entitled ***Non-replicating rhabdovirus-derived particles (NRRPs) eradicate acute leukemia by direct cytolysis and induction of antitumor immunity***, I studied the use of NRRPs as a treatment strategy in acute leukemia's. According to the data in chapter III, tumor specific cell death induced by colchicine treatment was driven by cytokines produced upon infection even in the absence of viral replication. Similarly, data produced by Dr. David Conrad indicated that tumor cells infected with non-replicating virus particles could be used as a "vaccine" to generate potent anti-immune responses (**Figure 5.5a**). The hypothesis that non-replicating viruses could be used to preferentially kill cancer cells is justified by the biological observations in chapter IV where cells within the tumor microenvironment had a lower baseline of anti-viral defences prior to viral insult. This data, in conjunction with the observation that many cancer cell lines fail to activate anti-viral defences upon infection (165), suggests that tumors should be associated with a greater probability of inducing virus-mediated pro-apoptotic pathways when the cells are overwhelmed with NNRPs.

To illustrate this phenomenon, I amended the model developed in Chapter II by removing virus replication dynamics (**Figure 5.3a**). Simulations with this model indicate that as the cell undergoes tumorigenesis, and loses its capacity to clear the virus template, the cell remains in an infected state for a longer period of time, and is inherently associated with a greater probability of dying in response to NRRPs (**Figure 5.3b**). I then generated NRRPs by means of low-dose UV irradiation, and demonstrated this agent is associated with selective toxicity against transformed cells (**Figure 5.1**). Given the non-contiguous nature of leukemia, which negates the spreading advantage of a live OV platform, NRRPs may offer an alternative approach for the

treatment of haematological malignancies which through controlled dosing, could improve therapeutic efficacy.

Similar to transformed cells, acute leukemia's were hypersensitive to NRRPs relative to normal cells (**Figure 5.2**). This phenotype was equally observed in fresh samples obtained from patients suffering from multidrug resistant Chronic Myelogenous Leukemia (**Figure 5.4**). To highlight the proposed mechanism of action, I pre-treated normal cells, or IFN non-responsive leukemic cells, with IFN to raise the baseline in antiviral defences. While normal cells were further protected following addition of IFN, leukemic cells failed to benefit from this cytokine (**Figure 5.3**). When integrated with our mathematical model, using the same strategy as described in Chapter II (**Figure 2.3d**), the differential impact of NRRPs across tumor and normal tissues, could be accurately recapitulated by our model. Under the assumption that particle loss occurs throughout the irradiation procedure, the differential sensitivity to NRRPs between tumor and normal cells could be accurately recapitulated by my model when tumor cells have acquired defect in IFN signalling (**Appendix Figure 9**). Work later performed by Dr. David Conrad further elucidated the in-vivo mechanism of action. He demonstrated that NRRPs induced potent anti-tumoral immune responses and increased the release of immuno-stimulatory cytokines (**Figure 5.5**). Although cytokine supernatant transfer did not confer the apoptotic phenotype in leukemic cells in-vitro, it is anticipated that these cytokines play an important role in inducing anti-tumor immune responses. Taken together, this platform offers a unique approach to treat hematological malignancies, where irradiated viruses function as an evolutionary refined, stable, soluble, multipronged TLR-agonist which induces direct cytolysis and potently activates anti-tumoral immune responses.

Abstract

Rhabdoviruses (RVs) are currently being pursued as anticancer therapeutics for various tumor types, notably leukemia. However, modest virion production and limited spread between non-contiguous circulating leukemic cells requires high-dose administration of RVs, which exceeds the maximum tolerable dose of the live virus. Furthermore, in severely immunosuppressed leukemic patients, the potential for uncontrolled live virus spread may compromise the safety of a live virus approach. We hypothesized that the barriers to oncolytic virotherapy in liquid tumors may be overcome by administration of high-dose non-replicating RVs. We have developed a method to produce unique high-titer bioactive yet non-replicating rhabdovirus-derived particles (NRRPs). This novel biopharmaceutical is multimodal possessing direct cytolytic and immunomodulatory activity against acute leukemia. We demonstrate that NRRP resistance in normal cells is mediated by intact antiviral defenses including interferon (IFN). This data was substantiated using murine models of blast crisis. The translational promise of NRRPs was demonstrated in clinical samples obtained from patients with high-burden multidrug-resistant acute myeloid leukemia. This is the first successful attempt to eradicate disseminated cancer using a non-replicating virus-derived agent, representing a paradigm shift in our understanding of oncolytic virus-based therapies and their application toward the treatment of acute leukemia.

Introduction

Rhabdoviruses (RVs), such as vesicular stomatitis virus (VSV) and Maraba, are currently being explored as anticancer therapeutics (165, 166, 332, 333). Through cell lysis and activation of antitumor immune responses (157, 334), live RVs are multitasking self-amplifying cytolytic agents. In tumors, viral propagation is enabled by disrupted metabolic activities (164, 335) and impaired antiviral programs (168, 235). Typically, oncolytic viruses are genetically altered to reduce virus replication in healthy tissue, constraining viral spread to the tumor microenvironment. Although live RVs are being pursued to treat a wide variety of tumor types, their application in hematopoietic malignancies is complicated by several factors. Limited virion production and reduced spread between leukemic cells requires high-dose viral therapy to overcome these inefficiencies. However, uncontrolled live virus spread and off-target effects in normal tissue compromise the safety of this approach, particularly in immunosuppressed patients (336).

In the RV field, all oncolytic platforms developed to date utilize a replication-competent virus that spreads between tumor cells (165, 166, 332, 333). The dogma pillar to these therapies is that virus replication is a prerequisite for treatment efficacy (337-339). Indeed, reports describing the use of live replication/expression-competent RV as a direct virotherapy for cancer, typically compare efficacy with non-expressing virus controls where no measurable efficacy is observed (165, 340). In these studies, the control virus is treated with a substantial dose of ultraviolet (UV) irradiation to intentionally generate an inert bioparticle. We posited that if one could devise a method to generate non-replicating particles, which maintain both oncolytic and

immunogenic properties, many of the above barriers in the treatment of hematopoietic malignancies may be overcome.

Results

Generation of high-titer NRRPs

We theorized that UV photonic damage of RVs could be used to generate a non-replicating particle that retained bioactivity. In the past, high-dose UV irradiation has been used to ablate the RV genome rendering a biologically inert virus (165, 340). We hypothesized that when applied at moderated doses, UV irradiation could be used to generate a quasiparticle where replication is lost yet biological activity is maintained. To investigate this possibility, samples of purified VSV-expressing green fluorescence protein (GFP) were exposed to a wide range of UV irradiation intensities and the biological effects of this treatment were examined. When irradiated at a low dose (250mJ/cm2), VSV-eGFP lost its expression capabilities, yet maintained potent cytotoxicity against our immortalized production cell line (Vero; Figures 5.1a and b). Titering for virus following UV treatment confirmed that the resulting particles were unable to replicate in these cells in sharp contrast with live virus infection (Figure 5.1c). This effect was equally observed when using other members of the RV family including Maraba (Supplementary Figure $1^{\$\$\$}$).

Dose–response curves provide a better understanding of the relationship between cytotoxicity and the irradiation procedure. In these experiments, we observed that only a narrow window of UV fluence allows for the NRRP to maintain cytotoxicity against immortalized cells

(Figure 5.1d), and that this effect requires a particle to cell ratio >10 (Figure 5.1e). By comparing and contrasting with normal neonatal human dermal fibroblats (Figures 5.1d and e), it appears that cytotoxicity is tumor specific. Indeed, normal cells appear to require at least a 10 times higher dose to become sensitive to NRRP-mediated cytotoxicity.

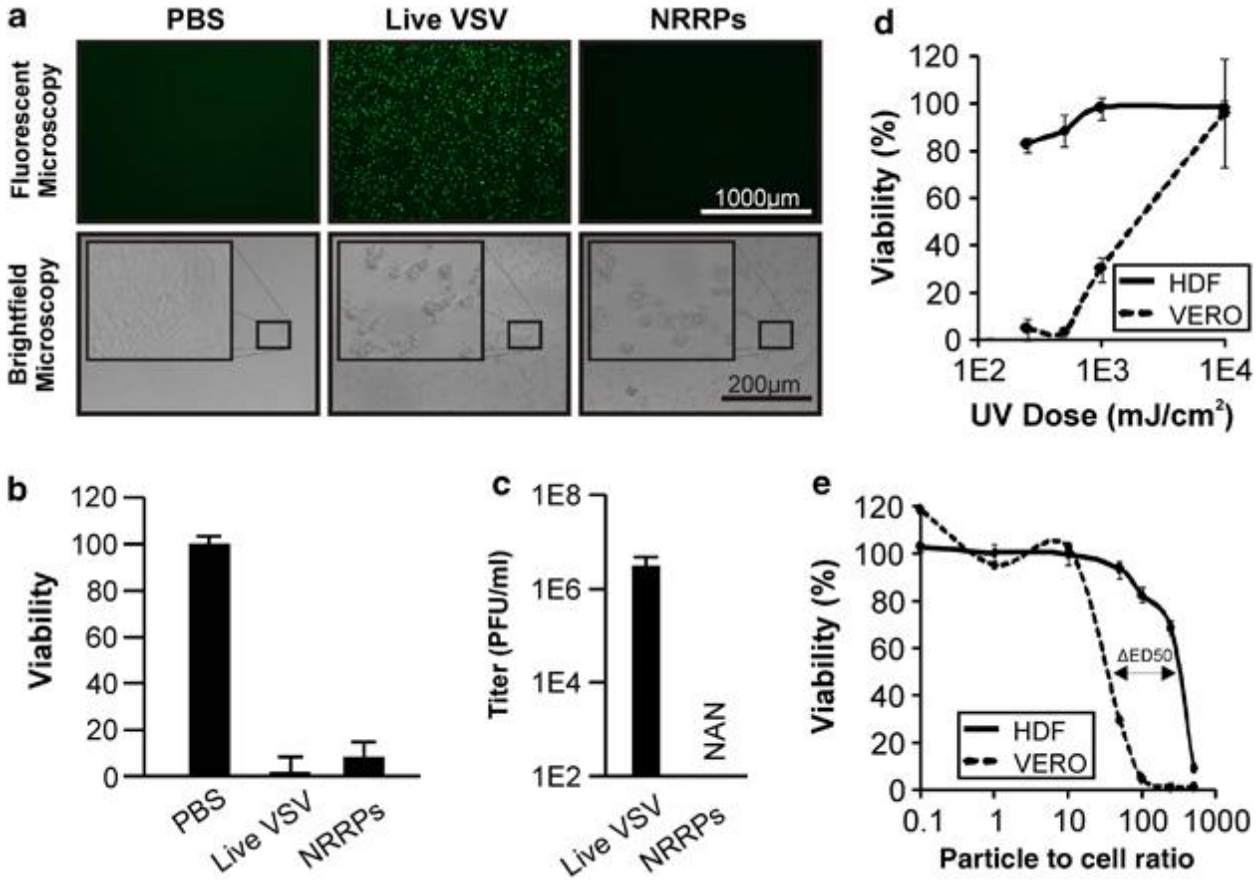

Figure 5.1. NRRP-mediated cytotoxicity in immortalized cells.
(a) Fluorescent and brightfield images of Vero cells treated with PBS, live VSV-GFP and NRRPs taken at 24 and 72 h after exposure, respectively. The multiplicity of infection (MOI) used in these experiments was set at 100 particles per cell. (b) Resazurin quantification of viability in Vero cells treated with PBS, live VSV-GFP or NRRPs 72 h after exposure. The MOI used in these experiments was set at 100 particles per cell. (c) Viral titers produced from the above experiments. NAN is defined as not a number, as no virions were detected. (d) Impact of UV dosage on NRRP-mediated cytotoxicity. All doses illustrated had no detectable GFP signal following UV-induced NRRP generation. This experiment used 100 particles per cell. Viability was quantified using the resazurin assay 72 h after treatment. (e) Impact of particle to cell ratio on the cytotoxicity induced by NRRPs in Vero and HDFN cells. The UV dosage of this experiment was set at 250 mJ/cm2. Viability was quantified using the resazurin assay 72 h after treatment. Error bars represent the s.d. between technical triplicate replicates.

NRRPs are an efficient treatment against leukemic cells in vitro

We next examined whether acute leukemic cells were equally associated with an increased sensitivity to NRRPs. In these experiments, we first compared the cytotoxicity induced in the acute lymphoblastic L1210 cell line with that observed in normal human dermal fibroblast cells. Whereas the normal cell line was resistant to NRRPs, L1210 cells were eradicated by NRRP treatment (Figure 5.2a). The classic apoptotic phenotype was observed in leukemic cells characterized by a reduced cell diameter, a shrivelled appearance with numerous apoptotic bodies and fragmented nuclear content. To validate the cell death mechanism, we quantified the level of apoptosis in L1210 cells by flow cytometry. In these experiments, we observed potent apoptosis in NRRP-treated samples 30 h after treatment, where ~84% of population was in an early- or late-stage apoptosis (Figure 5.2b). Cytotoxicity was next quantified using a standard resazurin assay in a panel of human and murine cell lines representative of hematological malignancies and normal tissue. In these experiments, acute leukemias were highly susceptible to NRRP-mediated cell death while preserving the viability of normal cells (Figure 5.2c, Supplementary Figure 2[$$$]).

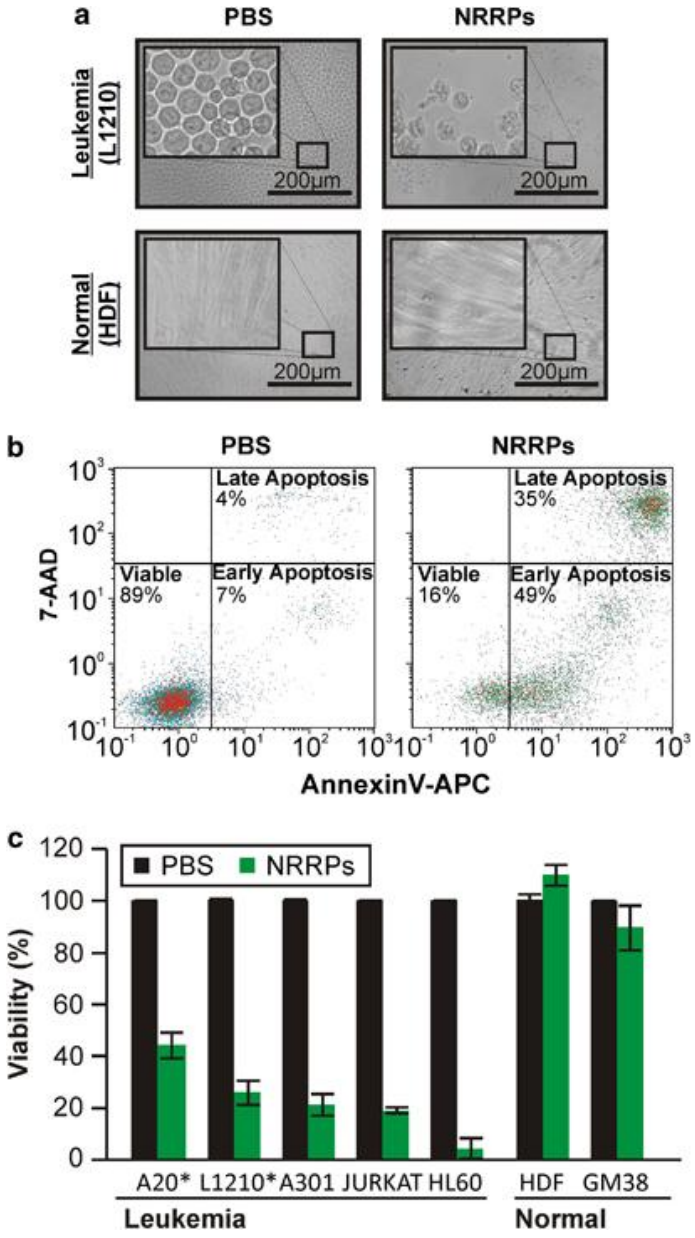

Figure 5.2. NRRP-mediated cytotoxicity in leukemic cells.
(a) Brightfield images of L1210 and human dermal fibroblast (HDF) cells treated with PBS or NRRPs (particle to cell ratio=100), 72 h after treatment. (b) Flow cytometry analysis of Annexin-V-APC and 7-AAD staining in L1210 cells treated with PBS or NRRPs for 30 h. (c) Resazurin quantification of viability in leukemic and normal cell lines. Murine cell lines are denoted by *.

Modeling depicting NRRPs' antitumor specificity

To investigate the mechanism by which specificity against tumor cells is achieved, we simulated the cytotoxicity induced by NRRPs in normal and tumor cells. Recently, we have developed a population-based model describing the relationship between cytotoxicity and live oncolytic virus replication dynamics in normal and tumor cells (270). According to this model (Figure 5.3a), an infection cycle begins as the uninfected population of cells (UP) encounters virions. This allows the population to become infected, where in the context of live virus, virions and the cytokine known as IFN are released into the environment. As IFN gradually increases, the population of cells activates antiviral signaling (AP), which over time allows this population to clear the viral infection and become protected against further insult (PP). To adapt this model to NRRPs, we removed virus replication dynamics from the model, and simulated the relationship between NRRP-mediated cytotoxicity and the extent of defects in IFN-signaling pathways, a process known to occur in ~80% of cancers (165). These defects were simulated by decreasing the rate of IFN production, the rate of activation of IFN signaling and the rate of NRRP clearance between tumor and normal cells. To ensure that this observation is systematic, a Monte Carlo simulation platform was utilized. Here, all kinetic parameters were varied within a 1 log window surrounding estimates derived from literature or experimental evidence (Appendix Table 6) (270). Following simulation across 1000 random parameter pairings (Figure 5.3b), we observed that as the cancer cells lose their ability to signal or respond to IFN, these cells become more sensitive to NRRP-mediated cytotoxicity. To validate this observation, we investigated the impact of IFN on NRRP-mediated cytotoxicity in normal (human dermal fibroblast) and leukemic (L1210) cells. Interestingly, although Intron A (recombinant IFN) could further

increase normal cell protection against NRRP insult (Figure 5.3c), it had no detectable impact on leukemic cells (Figure 5.3d).

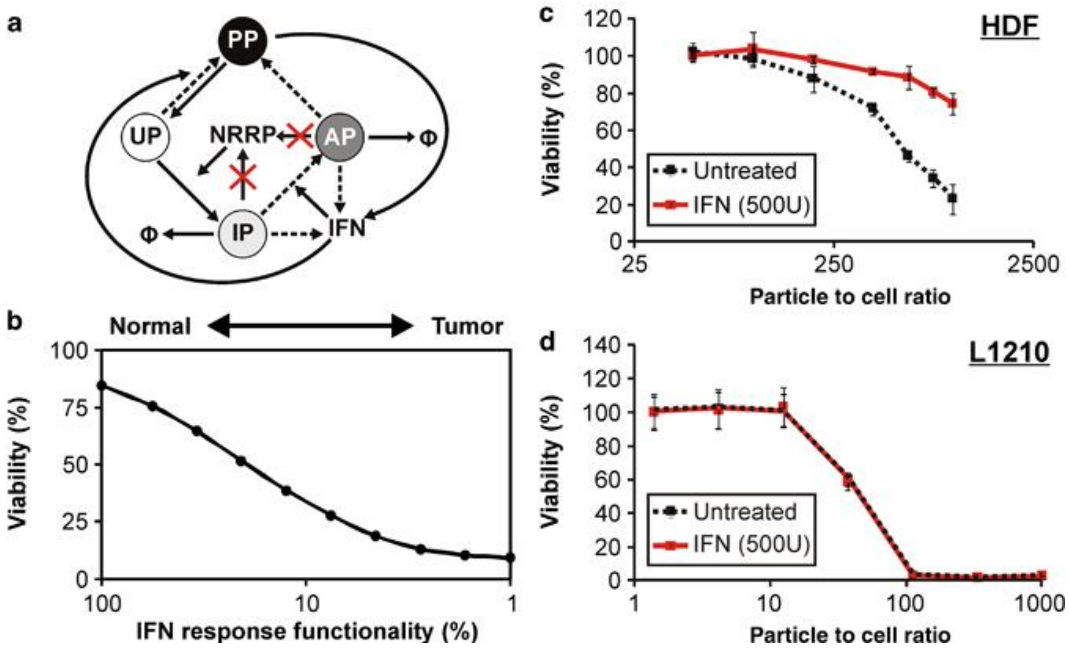

Figure 5.3. NRRPs specifically target tumor cells with defects in antiviral signaling pathways.
(a) Phenomenological model developed by Le Boeuf et al.(270) amended to simulate NRRPs cytotoxicity in normal cells and tumors with defects in antiviral signaling pathways. Kinetics removed from the Le Boeuf model to describe NRRP dynamics are marked in red. Hashed lines describe the IFN defects associated with tumor cells. (b) Simulated relationship between defects in the antiviral signaling pathways and viability 72 h after treatment with NRRPs. Trend represents the median value obtained over 1000 Monte Carlo simulations (see Materials and Methods). Defects in IFN-signaling pathways were simulated by decreasing the rate of IFN production, the rate of activation of IFN signaling and the rate of NRRP clearance from 100 to 1% of their original value in normal cells. (c) In vitro relationship between particle to cell ratio and viability 72 h after treatment with NRRPs in normal human dermal fibroblast (HDF) cells in the presence or absence of IFN. (d) In vitro relationship between particle to cell ratio and viability 72 h after treatment with NRRPs in leukemic L1210 cells in the presence or absence of IFN.

NRRP activity in AML blast crisis

The translational potential of the NRRP platform was investigated in human clinical samples. Peripheral blood mononuclear cells were obtained from two patients with high-burden acute blast crisis. The patients had circulating blasts with a CD33+ phenotype. Both had previously received extensive treatment for chronic myeloid leukemia and developed multidrug resistance. Similar to our observation in L1210 blast cells, patient samples cultured to enrich for the CD33+ fraction developed obvious NRRP-induced apoptosis with classic morphology (Figure 5.4a). Indeed, the leukemic CD33+ cells within this population avidly bound the apoptotic marker Annexin-V (Figure 5.4b). Use of the non-cultured patient samples was used to evaluate the specificity of this response. In both patients, the preponderant leukemic CD33+ population was ablated following NRRP treatment, leaving normal cells to dominate the sample (Figure 5.4c). To ensure that NRRPs do not affect normal white blood cells, the bone marrow mononuclear cells isolated from a healthy donor were treated with phosphate-buffered saline (PBS) or NRRPs. At both early (18 h) and late (65 h) time points, NRRPs did not appear to induce apoptosis within these samples (Figures 5.4d and e).

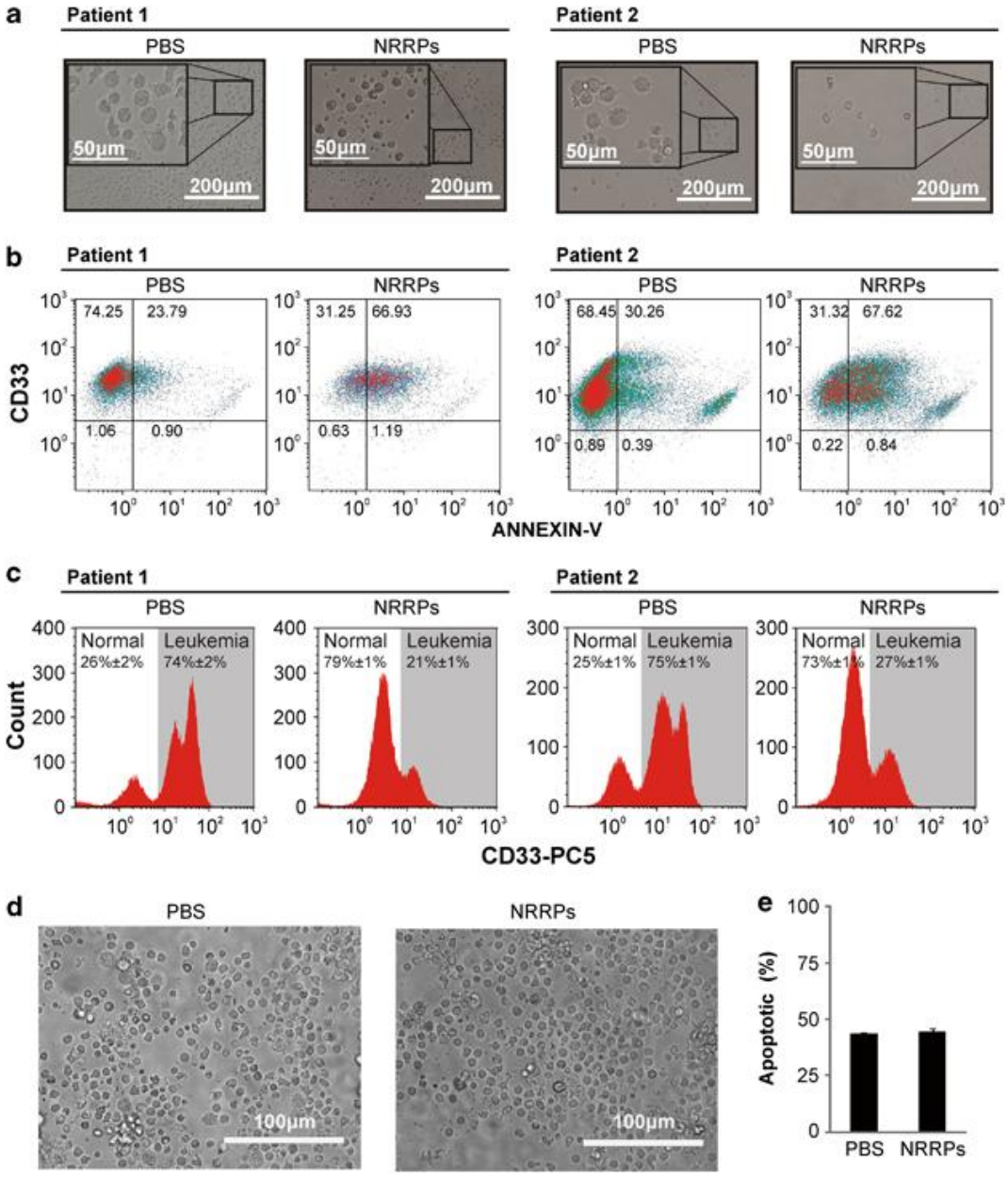

Figure 5.4. Treatment of chronic myeloid leukemia (CML)-blast crisis patient samples with NRRPs.

(a) Brightfield microscopy images of two CML-blast crisis patient samples treated with PBS or NRRPs. (b) Representative flow cytometry diagram of Annexin-V and CD33 staining in two CML-blast crisis patient samples treated with PBS or NRRPs (particle to cell ratio=100) 48 h after treatment. The CD33+ blast population was enriched by long-term culture of these cells. (c) Flow cytometry of CD33 staining in two non-enriched CML-blast crisis patient samples treated with PBS or NRRPs. (d) Brightfield microscopy images of a healthy bone marrow sample treated with PBS or NRRPs for 18 h. (e) Quantification of Annexin-V staining in the healthy bone marrow sample treated with PBS or NRRPs for 65 h.

NRRPs antileukemic activity in vivo

A murine model of leukemic blast crisis was used to evaluate the potential of NRRPs as a therapeutic agent. In brief, on day 1, DBA/2 mice were challenged with 1×10^6 dose of L1210 blast cells. The following day, mice began a regimen of 3×10^9 NRRPs administered intravenously for 3 consecutive days, and survival was monitored. In parallel, separate cohorts of mice were treated with live VSV at the MTD of 2×10^6 viruses per injection (341) or PBS under the same treatment schedule. NRRP-treated mice achieved 80% survival up to day 40, representing a significant advantage versus those treated with PBS ($P \leq 0.0045$) or live virus ($P \leq 0.044$). Indeed, mice treated with PBS or live virus, all succumbed to overwhelming leukemia (Figure 5.5a). NRRPs were well tolerated and administered at the maximal feasible dose for this particular experiment, which represented a 1500 times higher dose than the MTD of live virus. Given that acute leukemia frequently disseminates to the central nervous system, and that wild-type VSV is highly neurotoxic, intracranial injections of NRRPs and live virus were performed. Although mice could tolerate the maximum production dose for intracranial injections of 1×10^8 NRRPs, all mice rapidly succumbed to a 1×10^4 dose of live virus.

Prompted by the superlative efficacy and differential MTD afforded by the NRRP therapy, we wondered whether the recipient's immune system is activated following NRRP administration. To answer this, the peripheral blood serum was collected from L1210 tumor-bearing mice 20 h after treatment with PBS or NRRPs (Figure 5.5b). In this analysis, we observed that multiple cytokines typically known to recruit and differentiate T cells are induced and circulating following NRRP treatment. Examples of such immunomodulatory cytokines (342-344) significantly induced by NRRP treatment include leukemia inhibitory factor,

interleukin-2, interleukin-4, monocyte chemotactic protein-1, regulated on activation normal T cell expressed and secreted (RANTES), and macrophage inflammatory protein-1α (Figure 5.5b).

To confirm immune system stimulation, in particular T-cell activation, we adopted a vaccine strategy as previously described (291). Experimentally, this platform consists of injecting apoptotic cells into immunocompetent animals and measuring protective adaptive immunity against subsequent tumor challenge. We adopted this classical experimental approach to explore whether NRRPs trigger immunogenic apoptosis (345). Two cohorts of DBA/2 mice (syngeneic to L1210) received three weekly intravenous doses of 1×10^6 γ-irradiated L1210 cells pre-treated with NRRPs. Another cohort received the same number of γ-irradiated L1210 cells. One week following this regimen, a L1210 leukemic challenge (1×10^6 cells) was administered via tail vein, and survival was recorded. The cohort receiving NRRP-treated L1210 cells had 80% protection after the leukemic challenge, which was otherwise uniformly lethal in the untreated L1210-treated cohorts (Figure 5.5c). Surviving mice were kept for >150 days to ensure long-lasting protection. These results are consistent with the notion that NRRP-treated acute leukemic cells undergo immunogenic apoptosis.

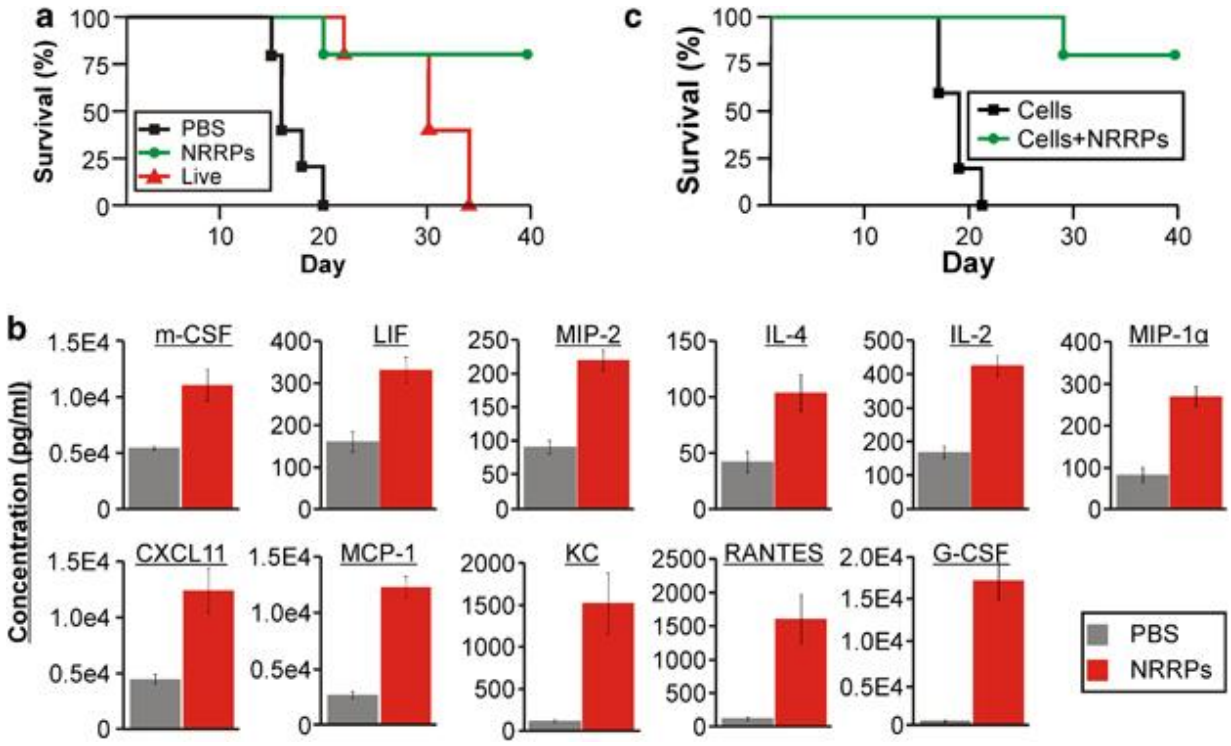

Figure 5.5. NRRPs eradicate acute leukemia by inducing immunogenic apoptosis.
(a) Survival in a murine model of immunogenic apoptosis. Before L1210 challenge on day 1, mice received three weekly doses of γ-irradiated L1210 cells preincubated or not with NRRPs. (b) Luminex-based quantification of cytokines induced by NRRPs in L1210-bearing mice. All cytokines illustrated are induced over twofold by NRRPs and are statistically significant (non-paired t-test pV<0.05). pV has been corrected to account for multiple hypothesis testing (Benjamini and Hochberg method). (c) Survival in a murine-blast crisis treatment model. Following L1210 challenge on day 1, mice received three daily doses of NRRPs (3 × 109) or PBS.

Discussion

This is the first successful attempt to eradicate disseminated cancer using non-replicating virus-derived particles, and represents a paradigm shift in the field of oncolytic virus-based therapeutics. Through in silico and in vitro testing, we demonstrate that NRRPs, analogous to live virus, are tumor selective, given that they exploit defects in innate immune pathways common to most tumors. However, this platform is unencumbered by the principle safety concern associated with live virus replication, that is, the potential for uncontrolled viral spread in immunocompromised patients. Indeed, the superior safety margin afforded by the NRRP platform was exemplified by the observation that high-titer intracranial NRRP administration was well tolerated by murine recipients.

The outcome for the majority of adult patients suffering from acute lymphoblastic or acute myeloid leukemia remains dismal (346, 347). For a minority of patients, allogeneic hematopoietic stem cell transplantation (HSCT) after myeloablative conditioning is potentially curative; however, this procedure is associated with frequent adverse events and significant treatment-related mortality (346). For many patients with chronic-phase CML, targeted tyrosine kinase inhibitor therapy offers excellent disease control (348). However, when progression into acute blast crisis occurs, very limited therapeutic options exist owing to development of multidrug resistance and the rapid kinetics of this form of recalcitrant leukemia (349). Clearly, new and innovative therapeutic approaches are urgently required.

Here we establish that NRRPs exhibit both direct cytolytic and potent immunogenic properties in multiple acute leukemia models. A peculiar form of programmed cell death

involves the induction of adaptive immune responses against the dying cell. This process, commonly referred to as immunogenic apoptosis, is essential to the efficacy of several current chemotherapeutics24 and is required for host defence against viral infection (350) including live RVs (351). Our in vivo results indicate that a similar process is induced by NRRPs and is a driving factor for treatment efficacy.

More relevant are the observations that multidrug-resistant primary myeloblasts from patients with CML in acute blast crisis are forced into apoptosis and finally eradicated by NRRP treatment. In addition, non-leukemic white cells procured from healthy bone marrow were not adversely affected. This observation suggests that despite the potent tumoricidal activity of NRRPs, the leukopenia commonly observed after standard induction and consolidation chemotherapy could be avoided by using NRRP-based regimens. This would likely significantly decrease treatment-related adverse events. Further, given the preservation of normal white blood cells during leukemic cytoreduction by NRRPs, the simultaneous induction of an effective antileukemic immune response may be attainable for the majority of patients who are not candidates for high-dose radiochemotherapy and HSCT. With the induction of immunogenic apoptosis by NRRPs, a broad array of immunomodulatory cytokines are released by the recipient's intact immune system, and this likely contributes to development of the effective adaptive antitumor immune activity—a critical component to achieving durable curative responses.

This work demonstrates a feasible biotechnology that produces high-titer NRRPs—an essential requirement for wide-scale clinical advancement. We are currently validating the MTD of NRRPs in several animal models, and are developing good laboratory practice safety

measures to ensure stringent confirmation of the non-replicating nature of these bioactive particles. We expect that the pathway to approval should be less onerous than current live RV platforms under development by our laboratory and others. This promising multimodal therapeutic platform is poised for early-phase clinical trials.

Methods

Cells

L1210, A20, A301, Jurkat, HL60 cell lines were from American Type Culture Collection (Manassas, VA, USA), and maintained in suspension culture, Dulbecco's modified Eagle's medium-high glucose (HyClone, Logan, UT, USA), with 10% fetal calf serum (CanSera, Etobicoke, ON, Canada), at 37°C and 5% CO2. Cells in culture were maintained at a concentration between 0.5 and 1.0×10^6 cells/ml. Vero cells (kidney epithelial cells extracted from an African green monkey), GM38 (normal human fibroblast cell line) and human dermal fibroblast-adherent cells were from American Type Culture Collection and propagated in same culture media used for the suspension cell lines. Normal bone marrow cells acquired from STEMCELL Technologies Inc. (Vancouver, BC, Canada) were obtained from a healthy volunteer and consented to an approved institutional review board protocol. Acquisition of human leukemic patient samples was approved by the institutional review board of the Ottawa Hospital Research Ethics Board. All patients provided written informed consent for the collection of samples and subsequent analysis.

Virus

The Indiana serotype of VSV and wild-type Maraba used throughout this study were propagated in Vero cells, as previously described (201). VSV titration was performed using serial dilutions in Dulbecco's modified Eagle's medium. Hundred microlitres of each dilution was applied to a confluent monolayer of Vero cells for 45 min. Subsequently, the plates were overlaid with 0.5% agarose in Dulbecco's modified Eagle's medium with 10% fetal bovine serum, and the plaques were grown for 24 h. Carnoy's fixative (methanol:acetic acid in a 3:1 ratio) was then applied directly on top of the overlay for 5 min. The overlay was removed and the fixed monolayer was stained with 0.5% crystal violet for 5 min, after which the plaques were counted.

Viability assays

Viability assays were done in a 96-well plate format. Cells were plated at specific density and treated with live VSV virus or non-replicating rhabdovirus-derived particles (NRRPs). After 72 h, cytotoxicity was assessed by adding 25 µl of alamar blue reagent, (AbD Serotec, Raleigh, NC, USA).

Modeling

The model used to describe NRRPs specificity against cells with defects in antiviral signaling pathways was adapted from our previous work described in Le Boeuf et al.(270) In brief, this model is represented by a subset of six ordinary differential equations describing the transition

between the cell populations (UP, IP, AP and PP) depending on the concentration of NRRPs (N) and interferon (IFN) in the environment. These equations are:

$$\frac{dUP}{dt} = -K_{NI} \times [N] \times [UP] - \left(\frac{-K_{IFNon}}{1+\left(\frac{IFN}{EC50}\right)^2} + K_{IFNon} \right) \times [UP] + K_{IFNoff} \times [PP],$$

$$\frac{dIP}{dt} = K_{NI} \times [N] \times [UP] - \left(\frac{-K_{IFNon}}{1+\left(\frac{IFN}{EC50}\right)^2} + K_{IFNon} \right) \times [IP] - \gamma_c \times [IP],$$

$$\frac{dAP}{dt} = \left(\frac{-K_{IFNon}}{1+\left(\frac{IFN}{EC50}\right)^2} + K_{IFNon} \right) [IP] - K_{NC} \times [AP] - \gamma_c \times [AP],$$

$$\frac{dPP}{dt} = \left(\frac{-K_{IFNon}}{1+\left(\frac{IFN}{EC50}\right)^2} + K_{IFNon} \right) [UP] + K_{NC} \times [AP] - K_{IFNoff} \times [PP].$$

The parameters used in the above equations represent the internalization rate (K_{NI}.), the rate of IFN-signaling activation (K_{IFNon}), the rate of IFN-signaling inactivation ($K_{IFN\ off}$), the EC50 of IFN (EC_{50}), the rate of cell death (γ_C) and the rate NRRP clearance (K_{NC}).

The next subset of equation describes the dynamics of NRRPs (N) and IFN whereby:

$$\frac{dN}{dt} = -K_{NI} \times [N] \times [UP] - \gamma_n \times [N],$$

$$\frac{dIFN}{dt} = K_{IFN1} \times [IP] + K_{IFN2.1} \times [AP] + K_{IFN2.2} \times [PP] - \gamma_{IFN} \times IFN.$$

The parameters described in the above equations represent the rate of NRRP internalization (K_{NI}), NRRP degradation (γ_n), IFN production from IP, AP and PP (K_{IFN1}, $K_{IFN2.1}$ and $K_{IFN2.2}$, respectively) and IFN degradation (γ_{IFN}).

The Monte Carlo simulation was performed by randomly varying the above parameters within a 1 log window (see Appendix Table 5) surrounding physiological parameter derived from literature and experimental evidence (270). Simulations were performed in Matlab using ODE15s imposing a non-negativity constraint. Trends described in Figure 5.3b represent the median value over 1000 simulations. The number of cells used in these simulations was 2.5E5, the media volume was set at 1 ml and the particle to cell ratio was set at 100. In these simulations, defects in IFN-signaling pathways were simulated by decreasing KIFN1, KIFN2.1, KIFN2.2, KVC and KIFN on from 100 to 1% of their original value.

Flow cytometry

Anti-CD33-PerCP Cy5.5 and Anti-CD33-PC5 antibodies obtained from eBioscience (San Diego, CA, USA) were used. Annexin-V and 7-AAD viability dye were obtained from eBioscience and performed according to manufacturer's instructions. Flow cytometry was acquired using a CyAn ADP (Beckman Coulter, Brea, CA, USA). Analysis was performed using the Kaluza software version 1.1 (Beckman Coulter).

Cytokine array

Bio-Plex Pro mouse luminex-based multiplex cytokine assay (Bio-Rad, Hercules, CA, USA) was performed on mouse serum 20 h after NRRP treatment. The assay was performed according to the manufacturer's instructions.

Murine experiments

For the L1210 vaccination strategy, cohorts of DBA/2 mice (Charles River, Wilmington, MA, USA) received three weekly intravenous doses of 1×10^6 γ-irradiated L1210 cells pre-treated , or not, with NRRPs. One week following this regimen, a L1210 leukemic challenge (1 × 106 cells) was administered via tail vein, and survival was followed. Mice were euthanized upon development of predetermined signs of advanced leukemia end points. For the L1210 treatment strategy, DBA/2 mice were challenged with 1×10^6 dose of L1210 blast cells. The following day, mice began a regimen of 3×10^9 NRRPs administered intravenously for 3 consecutive days, or treated with live VSV at the maximum tolerable dose (MTD) of 2×10^6 viruses per injection, and survival was followed. Institutional guidelines and review board for animal care (The Animal Care and Veterinary Service of the University of Ottawa) approved the above animal studies.

5. General Discussion

Throughout my thesis, I have worked on several projects, continuously incorporating new elements to further model development. Similar to the original work performed by the group of Dr. Nowak, my research lead me to amend the model to describe a wide array of different scenarios. In his research, Dr. Nowak expanded his original model to describe **1)** alternative viral strains (230), **2)** anti-viral drug therapies (232), **3)** the emergence of anti-viral drug-resistance (233) as well as **4)** the incorporation of CTL responses (225). In the context of OVs, I amended my model to describe the impact of **1)** IFN antagonists (**Figure 2.2 e-h**), **2)** next-generation OV engineering strategies such (**Figure 2.2 f**), **3)** attenuation mechanisms such as negative feedback and NRRPs (**Appendix Figure 4 and Figure 5.3**), **4)** virus sensitizers (**Figure 3.5**), as well as **5)** tumor heterogeneity (**Appendix Figure 7 & 8**). Taken together, this model has allowed me to gain insight into a number of different aspects of OV dynamics.

5.1 Insight from modeling the mechanism of action of virus sensitizers

First and foremost, the model and biological observations suggest that the use of direct IFN antagonists is not a valid means to improve cytolysis mediated by oncolytic rhabdoviruses. Although others have reported that drugs such as JAK inhibitors increase OV replication in cancer cells (352), it is noted that they do not compare the impact to normal tissue nor do they demonstrate efficacy in-vivo. According to my model & simulations, decreasing the potency or the bioavailability of IFN does not selectively enhance RV cytolysis in the tumor microenvironment. Although tumor cell preferentially increase RV release, as the potency of IFN

is lost, normal cells become highly sensitized to RVs replication, and severely compromises the safety of this approach as ISGs serve as the key defence mechanism against these pathogens in normal cells. Experiments using an IFN decoy receptor as well as a JAK inhibitor (**Figure 2.4a**) confirmed that the impact of directly inhibiting IFN signaling is not specific to tumor cells.

This observation opens up the question: how do virus-sensitizing drugs specifically enhance killing within the tumor microenvironment? To date, several drugs including Vorinostat (212), sunitinib (214) and 3,4-dichloro-5-phenyl-2,5-dihydrofuran-2-one (213), have been demonstrated to selectively enhance OV-mediated cytotoxicity and replication in tumor cells. In the article by Dr. Diallo (213), it is postulated that virus sensitizers may target a pathway or process with redundant function in normal cells. Indeed, the mechanism of action of certain virus sensitizers has been demonstrated to be associated with this effect. For example, the impact of sunitinib on OV therapies has been demonstrated to be the result of inhibited PKR/RNAse L signalling (214, 353). By targeting these two downstream elements of IFN signalling (117), sunitinib treatment lead to improved OV-mediated cytotoxicity in the tumor microenvironment (214). As normal cells can potentially overcome infection through parallel downstream IFN targets, such as BST2 (118) and MX1 (119), tumor cells which overcome infection by PKR, but have defects in these parallel pathways, may be further sensitized to OV infection.

5.2Positive-feedback - a key process to achieve tumor selective cytotoxicity

The mechanism which is perhaps one of the more specific according to my simulations is the engineering of positive feedback loops in OVs. In my thesis, I showed that attenuated RV

strains are greatly enhanced when engineered to produce a decoy receptor for IFN. This observation reflects the general biophysical principal where positive feedback can be used as a commitment strategy which drastically sharpens dose response curves (253). The mechanism of action is directly attributed to positive feedback between virus replication and inhibition of IFN responses. Given the heightened rate of virus replication and genome expression in tumor cells, the decoy receptor is expressed in more cells and to a higher degree. This in turn feeds back onto the system to further enhance the spread and stability of OV genome expression. However, once the virus enters adjacent tissue where genome expression is decreased, the decoy receptor is expressed to a lesser degree, and thereby allows the normal cells to shutdown the positive feedback loop (**Figure 2.4**).

One may wonder why we have not simply re-generated wild-type virus by allowing the attenuated virus to encode for the decoy receptor. The role of B19R as an IFN scavenger is functionally analogous to the role of the wildtype M protein, which has been engineered to be defective in VSVΔ51 and MG1 (165, 166). While functionally homologous, the M protein and the B19R positive-feedback mechanisms differ on key points. Following uncoating of the virus within the cell, the M-protein directly inhibits nuclear export of cellular mRNAs and blocks the IFN response against rhabdovirus infection (190). In contrast, B19R is a soluble factor that acts as a scavenger for IFN extracellularly, and is only expressed following replication of virus in infected cells. As such, the primary difference between the two mechanisms is the temporal delay associated with each evasion strategy. By cloning the IFN decoy receptor between genes G and L, which are expressed to lesser degrees in latent phases of the virus life cycle, we ensure that the virus must establish a productive infection prior to inhibiting IFN signalling.

Consequently, the attenuation resulting from the VSVΔ51 or MG1 backbones is the first "gate-keeper" control for safety and only when the virus can establish a sustainable infection will the decoy be expressed. A further delay is incorporated by using a factor which is secreted in the extracellular environment. Dilution in the extracellular environment provides an additional roadblock in the delay in B19R functionality relative to intracellular M-Protein which functions in a smaller volume, and inherently has a greater probability of interacting with, and inhibiting, its target.

The notion that the decoy receptor is secreted into the extracellular environment is a critical element of the success of this therapeutic platform. Not only does it further delay commitment to the positive feedback loop, but use of secreted factors allow for the positive feedback signal to be relayed to adjacent cells. This effectively allows the virus to communicate information to surrounding cells, which are potentially resistant to the OV therapy. As such, this construct exploits sensitive cancer cells within the tumor to establish interferon suppression "hubs" which produce the decoy receptor, and improve delivery throughout the tumor. In contrast, if intracellular antagonists of the IFN pathway had been used, such as ICP0 which promotes TLR degradation (354) or E3L which block IRF activation (355), we would not expect to have the same extent of information relay. Furthermore, I expect more of a pleiotropic effect in different tumor microenvironments with B19R since IFN is a central pathway essential to the activation of antiviral defences with little to no redundancy, in contrast with ICP0 or E3L.

5.3 Sensitization of stroma within the tumor microenvironment.

From my work regarding the cross talk between cancer cells and CAFs, I conclude that within the tumor microenvironment CAFs are in a repressed antiviral state at the onset of infection, but do not lack the capacity to activate anti-viral defences following infection. The net result of this lower baseline in anti-viral defences is a "burst" in viral activity at the onset of infection prior to the activation of immune responses. This mechanism supports the assumptions of my model in chapters II & III, where tumor cells are associated with a greater rate of virus expression and genome expression at the onset of infection. While I derived the model under the assumption that metabolic defects enhance OV replication and genome expression, it is noted that a decreased level of anti-viral defences at the onset of infection will achieve the same effect. The rate of virus replication and protein release is defined by both the rate of genome replication and its degradation. When I quantified virus replication and expression using a single step growth curve (**Appendix Figure 6**), both rates were enhanced in CAFs. The general mantra for the OV field is that sensitive cancer cells fail to activate anti-viral defences in response to virus (165). In contrast, this data suggests that the baseline level of activity in this pathway determines the level of sensitivity to OV therapies. This observation is of particular interest since the baseline status of IFN signalling components obtained from patient biopsies may serve as a predictive biomarker marker of OV responses.

To understand the implications of using these anti-viral genes as a predictive biomarker, it is essential that we determine the impact of tumor infiltration by these various cell types. From my simulations (**Appendix Figure 7**), it appears that infiltration by normal fibroblasts (NFs) can enhance protection of resistant cancer cells (RCCs), but only when they are the preponderant

population within the region. Although unlikely in most regions of the tumor given that crosstalk between RCC and NFs converts NFs to CAFs, it is conceivable that nascent regions of the tumor, such as the rim, gain resistance through these effects. Sensitive cancer cells (SCCs) on the other hand could influence the behaviour of resistant cancer cell even when at low proportions within the population. CAFs on the other hand had little to no impact on the behaviour of RCCs in the absence of cross talk. By analyzing the impact of kinetic parameters describing virus and IFN production, it became clear how a low level cell infiltrate could influence the behaviour of RCCs (**Appendix Figure 8**). While cells with an increased rate of IFN production or responsiveness could exclusively drive resistance, cells with an increased rate of viral release could drive sensitization. This result was not interchangeable. Cells with a decreased rate of IFN production or responsiveness could not drive sensitization, and cells with a decreased rate of viral release could not drive resistance when the cell type was at low proportions within the population. Indeed, according to the simulations, NFs which are assumed to only be associated with a decreased rate of virus release could not influence the behaviour of RCCs when present at low proportion within the population. Furthermore, CAFs which are associated with a defect in IFN production relative to RCCs had no impact on the behaviour of this population. From these simulations I conclude that it is the balance between SCCs and NFs in the tumor which will ultimately determine therapeutic success. If the region has SCCs, the tumor will be sensitized to OVs if there is not the presence of a low level infiltration by an IFN producing subtype, such normal fibroblasts or even plasmacytoid dendritic cells which are in fact the major cell type responsible for type-I IFN production (356). Of course, if the SCC has acquired defects rendering it non-responsive to IFN it can still serve as a virus production hub. Therefore I conclude that it is not the global level of expression of these IFN-based biomarkers which will

likely determine treatment success, but rather the extent of contact between sensitive and resistant cells.

An element which was not incorporated into my model, yet highly relevent to this subject, involves spatial organization. Although I assumed homogenous mixing under these simulations, this assumption is perhaps a bit contrived in vivo in the sense that a tumor is composed of a number of different relatively homogenous regions resulting from the clonal expansion process. In my model, the effects of spatial compartmentalization could be generated by varying the rate of virus and IFN diffusion between the compartments proportionally to the amount of cell contact. While this is conceptually an interesting phenomenon, this effect is critical in the use of these cell types as biomarkers for these therapies. Specifically, when obtaining patient biopsies for biomarker analysis, we must consider not only the general frequency of each cell type, but equally incorporate spatial elements. This may be evaluated using immunohistochemistry to determine the number of sensitive regions/sites in the patient, and developing an appropriate scoring scheme.

5.4 NRRPs - an alternative to conventional OV therapies

According to the model and biological observations with colchicine, tumors are exquisitely sensitive to viruses, even in the absence of replication. Defect in tumor cells result in a lower baseline in anti-viral defences, and can even prevent their induction in response to IFN or OVs (165). According to the model, by decreasing the rate at which anti-viral processes are activated, the cell remains in a "pseudo-infected" cellular state for a greater period of time. By

lacking the appropriate defence machinery at the onset of infection, tumor cells persist anti-viral apoptotic signals for a greater period of time. This allows cancer cells to be exquisitely sensitive to the apoptotic signals induced in response to NRRPs as cancer cells cannot overcome the pseudo-infection. To validate this proposed mechanism of action, I pre-treated normal and tumor cells with IFN to activate anti-viral defences prior to infection with NRRPs. In these experiments, I observed that normal fibroblasts could be further protected against NRRP insult (**Figure 5.3c**). In contrast, the effect of NRRPs on tumor cells was not affected by the presence or absence of IFN (**Figure 5.3d**). This affect is most likely due to mutations in this cell line which are well known to affect IFN signalling (357).

NRRPs generated by means of UV irradiation are well known to maintain partial genome replication/expression (358). Given the start-stop replication cycle of VSV (188), western blot indicates that early proteins are still expressed in infected cells while the latter genes fail to transcribe and accumulate in infected analysis similar to previous studies (358). When the cell cannot mount an appropriate defense to overcome this pseudo-infection, NRRPs will trigger intrinsic apoptotic pathways induced through TLR-ligation (359) and functional wildtype matrix production (360, 361) - a response which may be further potentiated by cytokines released in response to this pseudo-infection (362). Although we typically view VSV as primarily inducing apoptosis, when I followed the cellular response to NRRP infection by time lapse microscopy, I was quite surprised to note the number of cell death mechanisms induced by this agent (**Appendix Figure 10**). Over the 48h time course, I observed not only the release of apoptotic bodies (**Appendix Figure 10a**) and apoptosis (**Appendix Figure 10b**) but equally cytokinesis

failure (**Appendix Figure 10c**) as well as necrosis (**Appendix Figure 10d**) following NRRP treatment.

In-vivo, the preferential induction of tumor cell death is further accentuated by inducing immunogenic responses raised against the tumor (**Figure 5.5c)**. This response is most likely the result of priming cytotoxic T-Cell responses following DC uptake of apoptotic bodies, and the subsequent recognition of tumor antigens. Indeed, UV-inactivated VSV is well known to activate CTL responses against tumor cells (363), presumably as recognition of viral pathogens up-regulate antigen presentation (112). Cytokines naturally released in response to virus will potentiate this effect. In this regard, NRRPs may equally offer several advantages over live OV platforms. In contrast with complex OV therapies, such as those derived from HSV and vaccinia, NRRPs do not encode for a plethora of immune evasion factors. I would therefore presume that the process of generating anti-tumor immune responses is much more potent for this platform. Not only do the tumor cells have the ability to activate several immunogenic processes, but even the apoptotic bodies released upon NRRP infection should be more potent. Given the lack of replication, apoptotic bodies resulting from NRRP infection should not harbour excessive amounts of viral epitopes. After DCs uptake and present the contents of these apoptotic bodies, CTLs should have a greater probability of reacting with, and generating immune responses against, tumor antigens.

An alternative mechanism of cell death which was investigated is the impact of pro-apoptotic cytokines secreted upon infection with NRRPs. While many cytokines were released in response to NRRPs in-vivo, it is conceivable that the in-vitro cytotoxicity was partially attributed to this effect. As such, I would have had to amend my model by allowing infected cells to

produce a cytotoxic cytokine, similar to the impact of colchicine in chapter III. However, when I explored this mechanism, it did not appear that cytokines were responsible for the lethality in-vitro. When I transferred supernatants from NRRP infected cells, filtered with a 100 KD filter to remove any virus particle, I was unable to transfer lethality to a population of healthy cells. Given that most cytokines are small proteins (100KD or less), I concluded that direct apoptosis appears to be the primary mechanism of cell death, and did not include cytokine cytotoxicity in my model. Perhaps lethality may be transferred through cell-to-cell contact or release apoptotic bodies containing virus antigens and stress-associated ligands, an interesting topic to be investigated in future studies.

The primary advantage of NRRPs over conventional OV therapies is associated with the absence of replication, and is of particular importance in haematological malignancies. In blood cancers, the capacity of OV spread between cancer cells is severely compromised by the non-contiguous nature of the disease and poor replication in these cells. As such, to ensure that the majority of cells encounter a live OV particle, the virus must be administered at high doses. In such treatment regimens, the MTD of a live replicating OV platform is limited by adverse effects resulting from uncontrolled replication in normal and tumor tissue. For RVs, high dose administration, or tumor dissemination to vital immunocompromised organs, may potentially induce neuropathy (364, 365), hypercytokinemia (366) and tumor lysis syndrome (365). Given that cancer patients are in various immuno compromised states, and have varying levels of disease burden, the MTD is determined by the location and extent of virus replication, which varies immensely from one patient to the next. Indeed, haematological malignancy infiltrate into the brain greatly reduces the MTD for live RV platforms (366). In contrast, we observed that

NRRPs could be safely administered at high doses intracranially. By physically controlling the total dose administered to a patient, we offer an additional layer of control in regulating adverse effects. As such, we can administer higher doses of the therapy to improve treatment efficacy (**Figure 5.5a**).

Although NRRPs are associated with several advantages in haematological malignancies, they are nonetheless associated with well known disadvantages. The first and foremost relates to the amount of particle required. Currently, in-vitro experiments were performed with high-dosing of NRRPs. Efficacy in-vitro was often achieved at a PFU to cell ratio greater than 50. In contrast, an attenuated VSV platform is typically in the range of ~0.2 PFU per cell (165). The amount of NRRPs required to treat a patient would be unparalleled. This would not only generate roadblocks from a production standpoint, but would equally raise regulatory concerns, particularly in the amount of contaminating foreign DNA following NRRP manufacturing. Yet upon administration of NRRPs in mice bearing acute leukemia, disease was successfully eradicated at doses translatable to the human scale. The total dose administered to the mice was 3×3E9 NRRP, which is only 3 fold greater than the 6 ×5E8 live MG1 dose used by our group in previous studies (166). This result reflects the fact that in-vivo, the majority of the anti-tumor response is generated by immunologic responses, and may not require the same amount of NRRP stimulus.

Furthermore, I anticipate that I will be able to improve NRRP yields by reducing the amount of particle loss which occurs during the irradiation procedure. To have good agreement between the mathematical model and biological datasets (**Appendix Figure 9**), I had to assume substantial particle loss. If not, the EC50 in tumor cells was typically in the range of 0.5-5.

Indeed, during the initial optimization procedure, reducing the turbidity and sample volume allowed for reduced UV doses to be utilized, thereby reduced ED50 of NRRPs. It is therefore concluded that under the current irradiation procedure, I most likely obtain a poison-like distribution of NRRP activity in the resulting particles where the majority of particles are dysfunctional to ensure that ALL do not replicate. To mitigate this effect, I am investigating the use of GMP approved irradiators which through fluid mechanics ensure consistent particle irradiation, thereby minimizing the amount of UV dosing required.

The other concern with the use of NRRPs is their application in solid malignancies since NRRPs cannot spread between contiguous cells in contrast with live OV platforms. As such, by only reaching the cells surrounding the leaky vasculature upon IV delivery, or the area at the injection site upon IT delivery, few tumor cells will be in physical contact with the NRRP. While I do agree that this issue is problematic, interesting results have been observed in solid malignancies treated with NRRPs. Upon both IV and IT administration to subcutaneous CT26-LacZ murine colon tumors in immunocompetent Balb/c mice, NRRPs delivered a measureable degree of efficacy (**Appendix Figure 11**). These results were even comparable to its live OV counterpart (VSVΔ51) according to our historical studies (291). Given that this model is perhaps a bit contrived, in the sense that CT26-LacZ is a highly immunogenic homogenous tumor thorough LacZ expression, I was nonetheless quite surprised to see results comparable to the live OV counterpart (291) , and not only the wildtype strain from which the NRRP was derived. This result would strongly suggest that the ability to induce anti-tumor immunity, resulting in the induction of CTL and vascular shutdown responses, are quintessential elements of treatment outcome in solid malignancies. While live OV platforms inevitably will infect a greater bulk of

the population, and perhaps have more heterogonous immune responses, I believe that I can optimize our dosing strategy to achieving similar results.

5.5 Model assumptions & limitations.

The model developed in my thesis, although simple, accurately describes in-vitro cytotoxicity, and is highly amenable to describe new phenomena. However, there are nonetheless certain disadvantages intricate to its simplicity. Similar to the work of Nowak and others (225, 225, 228, 230, 231, 242), the viral term in my equations does not accurately represent the total amount of infectious virus particle present in the media, but rather the amount of "free virus" which are available to infect an adjacent cell. During the infection cycle, virus particles released by a cell will preferentially infect surrounding cells. As such, the site of infection expands radially to form infection plaques. There is substantial particle "loss" owing to preferential co-infection by two or more particles in adjacent cells and particle retention at the cell surface. The rate of overall infection is limited by the diffusion coefficient of the virus particle. To mitigate this effect, I had to use a rate of virus release (k_{Bud_IP}&k_{Bud_AP}) which was much smaller than the actual rate of particle release. Therefore, Free Virus << Real Virus obtained from biological datasets.

While it may be possible to design a partial differential equation which encompasses both virus diffusion and time elements, there would nonetheless still be issues with describing virus replication dynamics as virus budding is a time delay exponential process. In other word, it takes a certain period of time for the cell to accumulate sufficient viral material to enable particle

replication & release, which once attained, is an exponential process. To describe the virus according to these dynamics, and accurately estimate the amount of virus particles in the media, I believe that it is essential that I represent the infection cycle as a stochastic process, where each cell is associated with a unique set of parameters, and the solution evolves discretely over time. Not only would this model allow us to encompass diffusion elements, but allow us to better describe the spatial effects of heterogeneous populations.

Another pitfall of my current platform is the absence of a non-zero steady state following infection. While the solution is quasi-steady by the 72h time point, the lack of cell division ensures that the solution reaches 0 at infinity. Although previous models encompass cell division kinetics to compute the steady state parameters, I do not believe that growth kinetics occur within the short time frame used in my simulations. While the cell death events will eventually need to be repopulated, the cells most likely to be relieved from growth arrest and repopulate the available area are those most likely dying from virus infection or are in a growth inhibited state due to the effects of IFN in a short-time frame model. As an alternative to reach a steady state solution, I could have removed the parameter describing inactivation of antiviral defences (K_{IFN_off}). However, I believed that removal of this element would not accurately recapitulate the biology of our system. The negative feedback loop, generated by suppressors of cytokine signalling, is an essential element of virus dynamics, which I believe contributes to the population's decision to succumb to infection. Given that the parameters used in my simulations are derived from biologically relevant estimates, the platform was derived to accurately describe short-term kinetics such as cytotoxicity at the 72h time point, and cannot be used to describe long term kinetics such a tumor relapse or memory t-cell responses. Once again, if a stochastic

model was utilized, I could have allowed for adjacent cells without active IFN defences to undergo cell division and repopulate the area following infection. This is perhaps the best model development for the foreseeable future.

Appendix

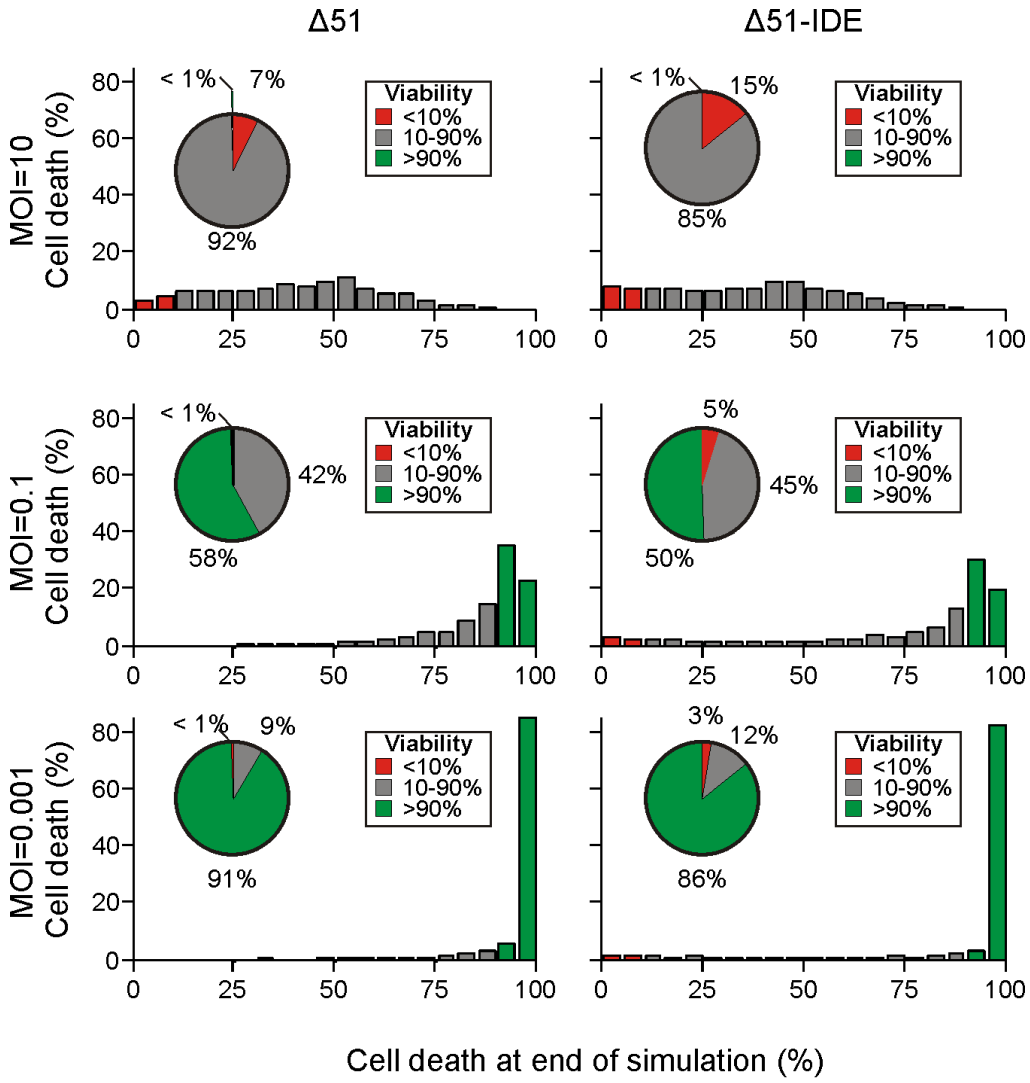

Appendix Figure 1. Simulated difference between Δ51 and Δ51-IDE at varying MOI in a population of normal cells.

Histogram illustrates the distribution of simulated viability after a 72 hour at the described MOI. Results were obtained over 1E3 Monte Carlo randomizations. Color coding, quantified in pie charts, describes the probability that the normal cell population has a viability <10% (red), 10-90% (grey) or >90% (green) at the end of the simulation.

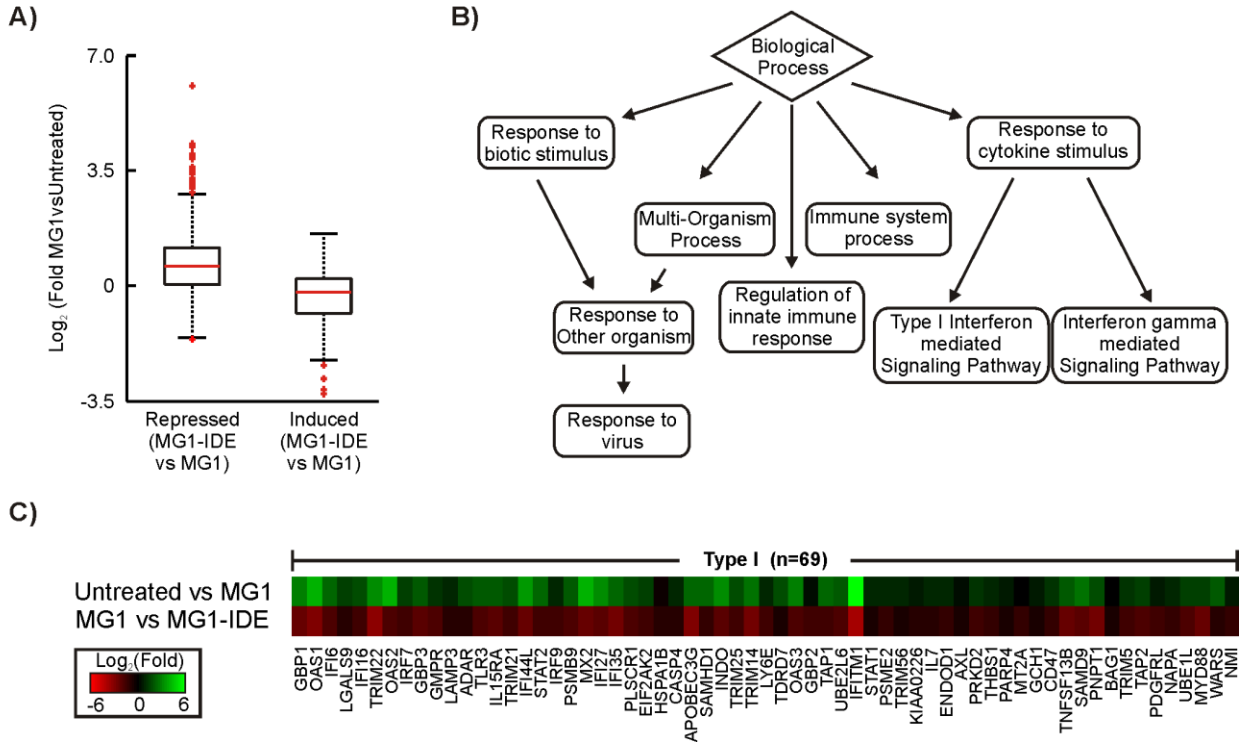

Appendix Figure 2. Microarray validation of IDE expressing rhabdoviruses.
A) Box plot illustrating the log of the fold change in gene expression induced by MG1 infection for loci sub-classified as induced or repressed by IDE expression. Genes repressed by $MG1_{IDE}$ relative to MG1, are typically induced upon MG1 infection (pV<4.39E-027, Wilcoxon signed-rank test) and those induced by $MG1_{IDE}$ are typically repressed upon MG1 infection (pV<1.89E-6; Wilcoxon signed-rank test). Box plot illustrates the sample maximum and minimum (error bars), Q1 and Q3 (box), the median of the population (red bar) and samples outliers (+). **B)** Gene-ontology enrichments for genes sub-classified as induced by the MG1 and repressed by IDE. Schematic illustrates a summary of the processes identified at a pValue threshold of 0.0001 following correction for multiple hypothesis testing (Bonferroni). **C)** Heatmap illustrating the fold change in gene expression for genes induced by the MG1 virus relative to control and repressed by subsequent treatment with the decoy expressing virus which are sub-classified as induced by type-I interferon's.

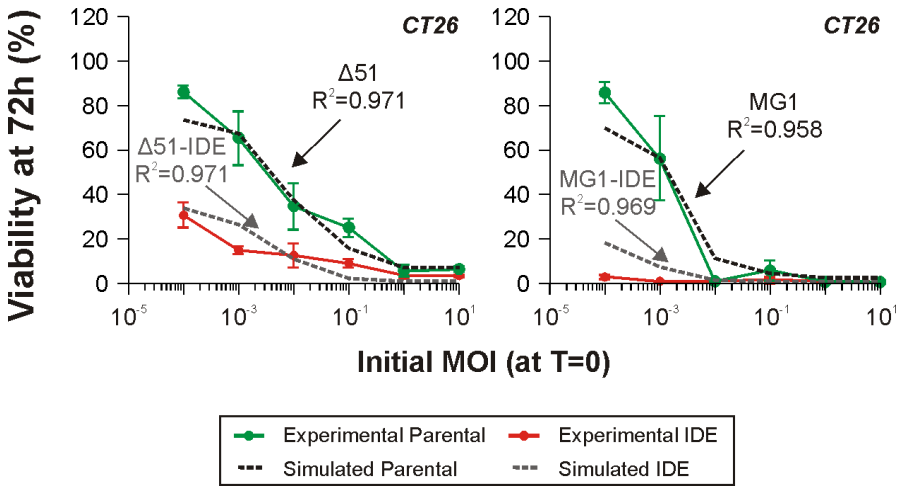

Appendix Figure 3. Experimental and simulated relationship between MOI and cellular viability 72 hours post-infection in CT26 murine colon cancer cells.

The experimental dose response curve was generated by infecting 2.5E5 cells at increasing MOI and assessing cellular viability 72 hours post-infection through an AlamarBlue assay. Viability is defined as the strength in signal intensity relative to control. Error bars represent the standard deviation obtained over triplicate experiments. Trends represent the simulation which best describes the experimental results. In these simulations, all parameters are identical between viral strains in a given cell lineage except for the capacity to produce the decoy receptor.

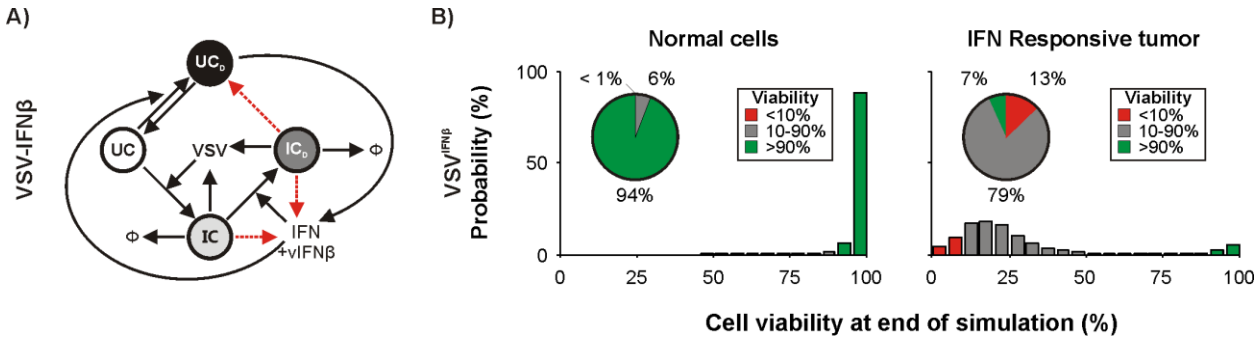

Appendix Figure 4. Simulated impact of a wildtype rhabdovirus (VSV) encoding IFNβ.
A) Development of the model to describe the infection cycle of VSV-IFNβ. According to this model all parameters are identical to the VSV model other than the capacity to produce IFNβ by VSV (vIFNβ), which was assumed to be equivalent to the rate of interferon decoy receptor production. B) Histograms illustrate the distribution of viability across a population of 1E5 normal (left) and IFN responsive tumor (right) cells following 72 hour infection. Results were obtained over 1E4 Monte Carlo randomizations. Color coding, quantified in pie charts, describes the probability that the described cell population has a viability <10% (red), 10-90% (grey) or >90% (green) at the end of the simulation.

Appendix Table I. Summary describing the overlap between genes induced by MG1 and repressed by DE and vice-versa. pValues describe the likelihood of significant overlap (Wilcoxon signed-rank test)

.

	Induced by Maraba and Repressed by IDE	Repressed by Maraba and Induced by IDE
Total Genes	n=25084	
Maraba vs Untreated	Induced (n=1463)	Repressed (n=2862)
IDE vs Maraba	Repressed (n=358)	Induced (n=175)
Overlap	n=149	n=49
Enrichment	7.14	2.45
pValue	1.66E-88	1.46E-09

Appendix Table II. Amendments performed to recapture differences between viral genotypes.

Genotype	Modification	Explanation
Δ51	$K_{DR\_IP} = 0$ $K_{DR\_AP} = 0$	Removed decoy receptor kinetics.
VSV	$K_{IFN1} = 0.1 - 1\% \times K_{IFN1}$ $K_{IFN2.1} = 0.1 - 1\% \times K_{IFN2.1}$ $K_{VC} = 0.1 - 1\% \times K_{VC}$ $K_{DR\_IP} = 0$ $K_{DR\_AP} = 0$	Wildtype M-protein impairs IFN signaling and defense mechanisms by blocking mRNA export in infected cells (165). Equally removed decoy receptor kinetics.
Δ51+JakI	$K_{IFN\ on} = 0.1 - 1\% \times K_{IFN\ on}$ $K_{DR\_IP} = 0$ $K_{DR\_AP} = 0$	The Jak inhibitor prevents activation of IFN signaling by inhibiting IFN signaling. Equally removed decoy receptor kinetics.
Δ51+Decoy	$K_{DR\_IP} = 0$ $K_{DR\_AP} = 0$ Initial Decoy=1-10pM	Removed decoy receptor production to substitute for a pre-determined concentration of the decoy receptor.
$\Delta 51_{DE}$	None	None

Appendix Table III. List of parameters estimates for Chapter II.

Parameter	Estimate	Range Utilized
K_{VI}	See below *	7.5E-5 to7.5E-4 ($V^{-1}h^{-1}$)
$EC50$	1.5pM (367)	0.25e-12 to 2.5e-12 (M)
$K_{IFN\ on}$	<ln(2)/1h (368)	ln(2)/(0.2 to 2.0) (h^{-1})
K_{IFNoff}	ln(2)/20h (369)(369)(369)[369]	ln(2)/(5 to 50) (h^{-1})
γ_c	ln(2)/8-10h (370)	ln(2)/(2.5 to 25) (h^{-1})
K_{VC}	ln(2)/(2-5h) (371)	ln(2)/(1 to 10) (h^{-1})
$K_{Bud\ IP}$	See below **	0.5 to 5 (V/h)
$K_{Bud\ AP}$	See below **	K_{Bud_IP} × 0.1 to 1% (V/h)
K_{IFN1}	See below *****	K_{IFN2}× 10 to 100% (M/h)
$K_{IFN2.1}/K_{IFN2.2}$	2.5E-17 M/cell/h*** (i.e. 15000 molecules/cell/h)	8.3e-18 to 8.3e-17 (M/cell/h) (i.e. 5000-50000 molecules/cell/h)
γ_{IFN}	ln(2)/(5.3 h) *in vivo*(372)	ln(2)/(5 to 50) (h^{-1})
K_f	1E7 $M^{-1}s^{-1}$ (367) (i.e. 4E10 ($M^{-1}h^{-1}$)	1 e10 to 10e10 ($M^{-1}h^{-1}$)
K_r	K_d=13.5 pM (246)	$K_r = K_f \times K_d$; whereK_d=2.5E-12 to 25E-12 (M)
K_{DR_IP}	See below ******	K_{Bud_IP}× 4.15E-16 to 4.15E-15 (M)
K_{DR_AP}	See below******	$K_{DR\_AP\_} = K_{DR\_IP} \times K_{Bud\ AP}/K_{Bud\ IP}$
γ_{DR}	ln(2)/(14.8 h) *in vivo* (373)	ln(2)/(5 to 50) (h^{-1})
γ_v	ln(2)/20 h *in PBS*******	ln(2)/(2.5 to 25) (h^{-1})

* Adjusted such that upon infection of 2.5E5 cells at an MOI=1, 99% of the viral particles have infected their target cell within 0.5-5 hours. A result recapturing experimental observations(374).

** Adjusted such that infection at an MOI of 0.05 over a 72 hour period leads to death of ~95% (±5% standard deviation) of the tumor cells within the population in the absence of IFN signaling. A result similar to our experimental evidence (data not shown).

*** Derived from experimental evidence measuring IFN production over time (data not shown).

**** Except for VSV wildtype.

***** Unknown value, based on notion that IFN signaling can induce a positive feedback(115) and inherently must be slower than or equivalent to the maximal rate of IFN production once positive feedback is induced.

****** This value is based on the assumption that decoy production is proportional to G-Protein production by the virus. Each functional viron contains ~1205 molecules of viral G-protein (187) and x 500 due to defective interfering particle lossess. This value was in turn converted to mol/l.

******* Derived from experimental measurements measuring VSV titer in PBS at 37oC (data not shown).

a)

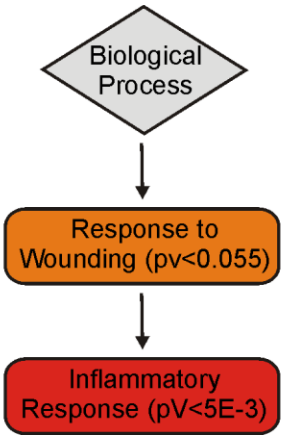

b)

CCL3 - chemokine (c-c motif) ligand 3
CCL3L3 - chemokine (c-c motif) ligand 3-like 3
CCL20 - chemokine (c-c motif) ligand 20
CCRL2 - chemokine (c-c motif) receptor-like 2,
CHUK - conserved helix-loop-helix ubiquitous kinase,
CSF1R - colony stimulating factor 1 receptor
Il8 - interleukin 8
IRAK2 - interleukin-1 receptor-associated kinase 2
PRKCZ - protein kinase c, zeta
PTGS2 - prostaglandin-endoperoxide synthase 2
TNFAIP3 - tumor necrosis factor, alpha-induced protein 3
TNFAIP6 - tumor necrosis factor, alpha-induced protein 6
TNIP3 - tnfaip3 interacting protein 3

Appendix Figure 5. Gene-ontology (GO) enrichments for genes induced exclusively by VSV in the presence of colchicine.

a) GO-processes enriched within the dataset of 167 genes induced by VSV exclusively in the presence of colchicine.

b) Genes induced by VSV exclusively in the presence of colchicine associated with both the inflammatory response and response to wounding gene ontology's.

Appendix Table IV. List of parameters estimates for Chapter III.

Parameter	Range Utilized
K_{vi}*	1E-4 to 1E-3
K_{IFNon}*	ln(2)/0.25h to ln(2)/2.5h
K_{IFNoff} *	ln(2)/10h to ln(2)/100h
γ_c *	ln(2)/5h to ln(2)/ 50h
$EC_{50\ IFN}$*	2.5E-13 to 2.5E-12
$EC_{50\ Cyt}$**	*Varied from 1E-9 to 1E-13***
γ_{C_Cyt} ***	ln(2)/5h to ln(2)/50h
K_{VC} *	ln(2)/0.5h to ln(2)/5h
$K_{Bud\ IP}$ *	0.05 to 0.5 virus/cell/h in normal cells or 0.5 to 5 virus/cell/h in tumor cells
$K_{Bud\ AP}$ *	0.1% to 1% × $K_{Bud\ IP}$
γ_V *	ln(2)/5h to ln(2)/50h
$K_{IFN\ IP}$ *	10 to 100% × $K_{IFN\ AP}$
$K_{IFN\ AP}$ *	5000 to 50000 molecules per cell per hour or 8.3E-17 M/cell/h to 8.3E-18 M/cell/h
K_t **	*Varied from ln(2)/0.05h to ln(2)/50h***
γ_{IFN} *	ln(2)/5h to ln(2)/50h
γ_{Cyt} ***	ln(2)/5h to ln(2)/50h
K_{Cyt} ***	5000 to 50000 molecules per cell per hour or 8.3E-17 M/cell/h to 8.3E-18 M/cell/h

** Range set from estimate described in LeBoeuf et al, 2013*
*** Parameters used in the simulation, varied within a larger range to mimic the effects of colchicine*
**** Derived from biological observation.*
***** Unknown cytokine parameter - set to the value utilized for IFN kinetics*

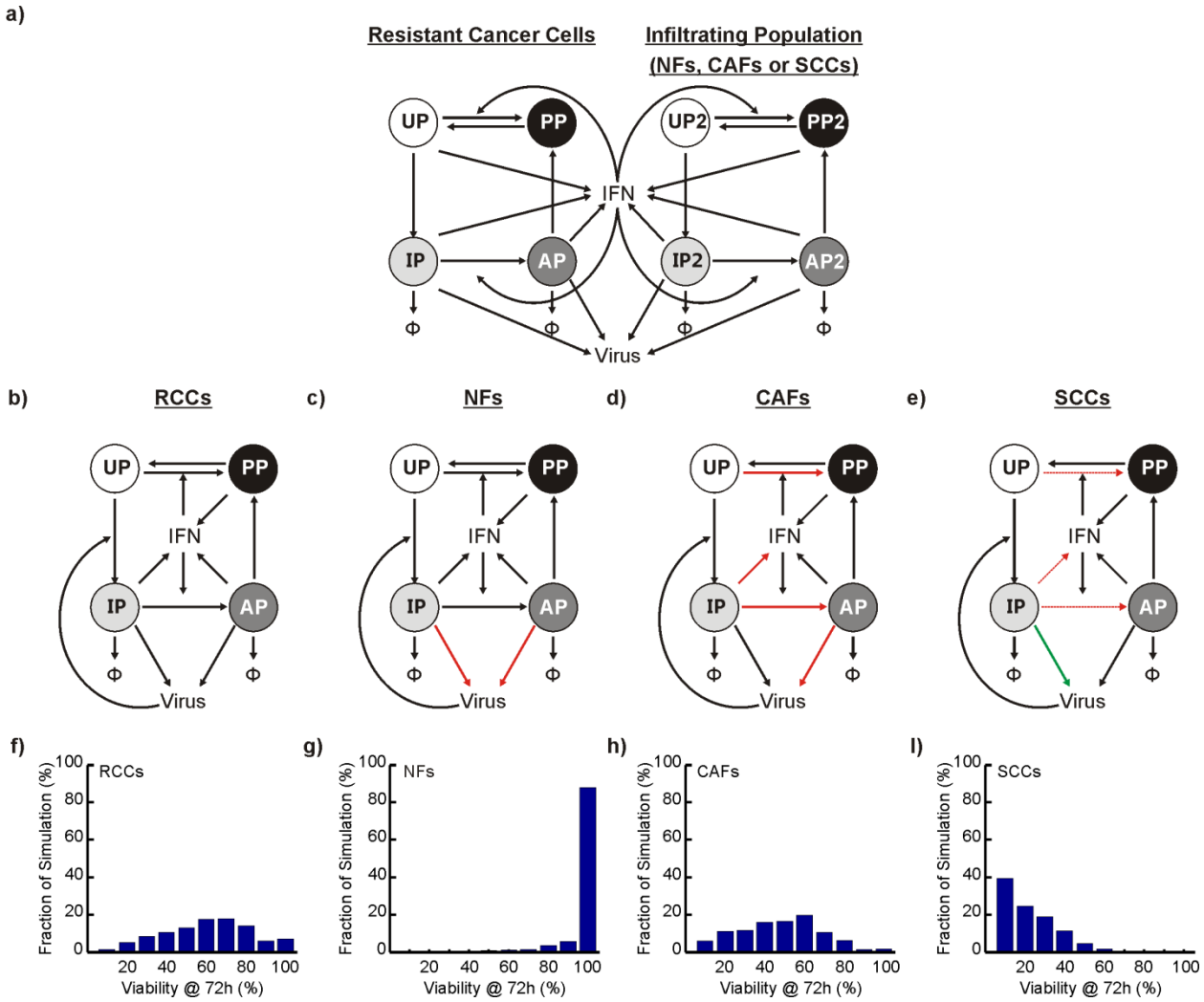

Appendix Figure 6. Modelling tumor heterogeneity.
a)The phenomenological model was amended to describe the interaction between a b) resistant cancer cell (RCC) population, and an infiltrating population of composed of c) normal fibroblasts (NFs), d) cancer-associated fibroblasts (CAFs) or e) sensitive cancer cells (SCCs). Red lines indicate processes impaired relative to RCCs. Green line indicate processes enhanced relative to RCCs. The histograms of f) RCC, g) NF h) CAF and i) SCC viability at the 72h time point in the absence of co-culture highlights the impact of these parameter alterations. These distributions summarize the results obtained over 1000 Monte Carlo simulations. See appendix table IV for details.

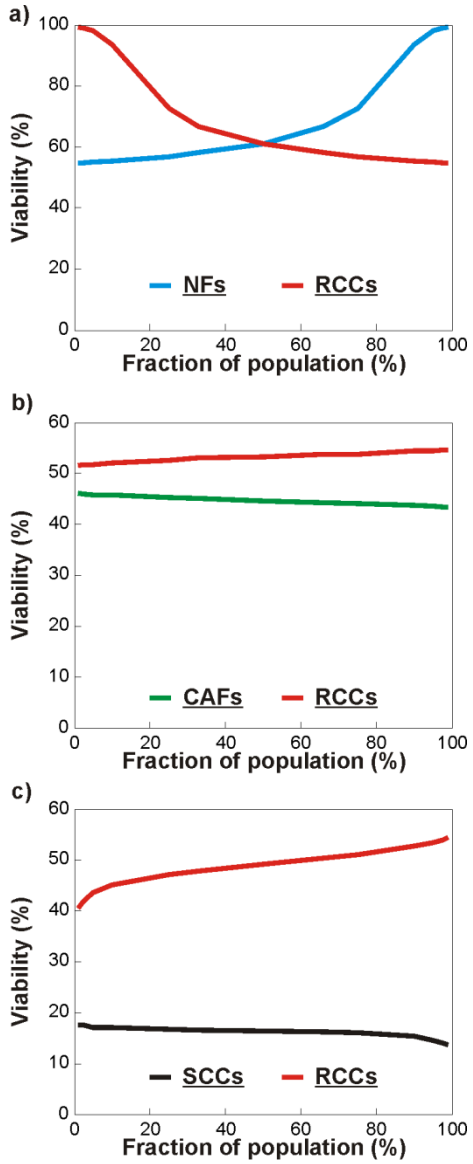

Appendix Figure 7. The impact of tumor heterogeneity on the viability of resistant tumor cells.

a) Distribution of cell viability of RCC and NF upon co-culture. Graph represents the median viability obtained over 1000 Monte-Carlo simulation as a function of the RCC **or** NF fraction within the population. b) Distribution of cell viability of RCC and CAF upon co-culture. Graph represents the median viability obtained over 1000 Monte-Carlo simulation as a function of the RCC **or** CAF fraction within the population. c) Distribution of cell viability of RCC and SCC upon co-culture. Graph represents the median viability obtained over 1000 Monte-Carlo simulation as a function of the RCC **or** SCC fraction within the population.

Appendix Table V. List of parameters estimates for Chapter IV. Table describes values for resistant tumor cells.

Parameter	Range Utilized
K_{VI}	1E-4 to 10E-4 ($V^{-1}h^{-1}$)
$EC50$	0.25e-12 to 2.5e-12 (M)
$K_{IFN\ on}$****	ln(2)/(0.2 to 2.0) (h^{-1})
K_{IFNoff}	ln(2)/(10 to 90) (h^{-1})
γ_c	ln(2)/(2.5 to 22.5) (h^{-1})
K_{VC}	ln(2)/(1 to 10) (h^{-1})
$K_{Bud\ IP}$*	0.5 to 5 (V/h)
$K_{Bud\ AP}$ **	K_{Bud_IP} × 0.1 to 1% (V/h)
K_{IFN1}***	K_{IFN2}× 10 to 100% (M/h)
$K_{IFN2.1}/K_{IFN2.2}$	8.3e-18 to 8.3e-17 (M/cell/h) (i.e. 5000-50000 molecules/cell/h)
γ_{IFN}	ln(2)/(5 to 50) (h^{-1})
γ_v	ln(2)/(5 to 50) (h^{-1})

* Range is 10x lower for normal fibroblasts and 2.5x higher for sensitive cancer cells
**Range is 10x lower for normal fibroblasts and cancer associated fibroblasts
*** Range is 1-10x lower for cancer associated fibroblasts and 10-100x lower for sensitive cancer cells
**** Range is 1-10x lower for cancer associated fibroblasts and 10-100x lower for sensitive cancer cells

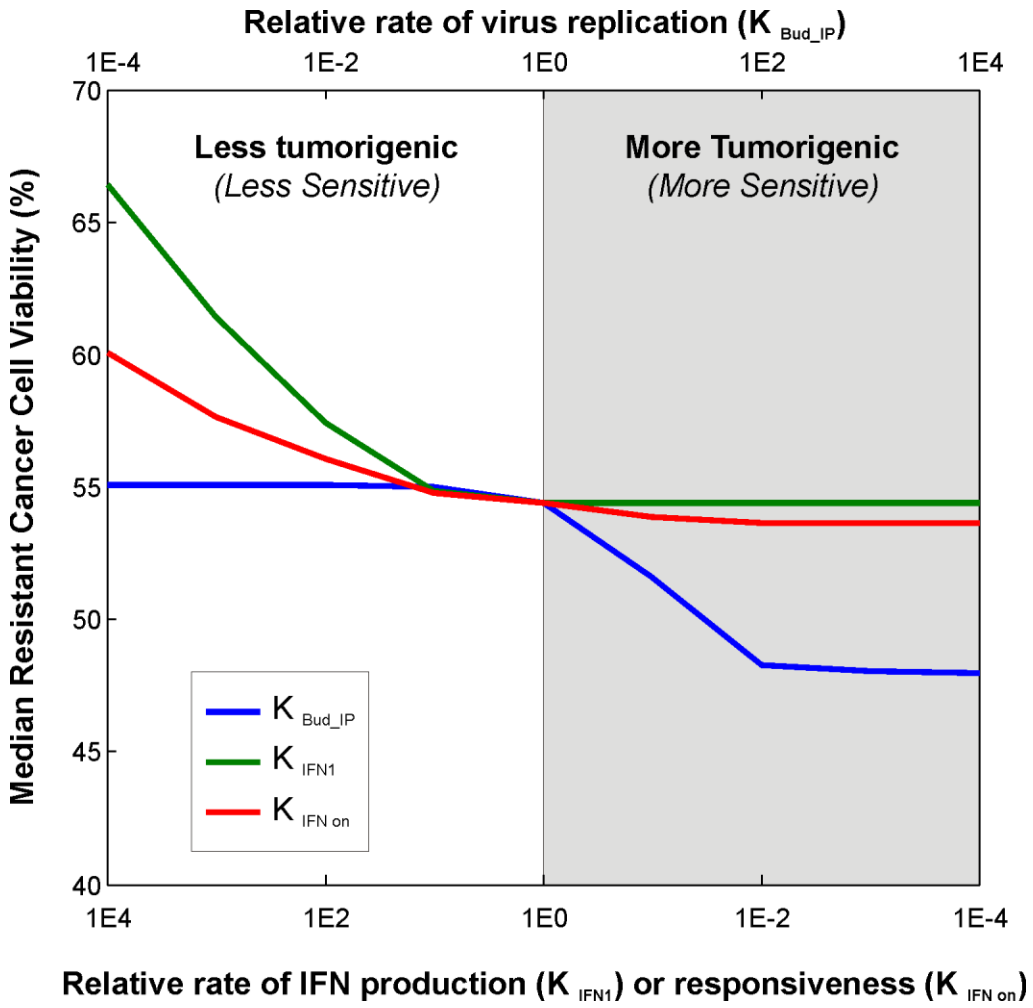

Appendix Figure 8. The impact of tumor cell infiltrate parameters on the viability of resistant tumor cells.

Simulations were performed by varying the parameter of virus budding (K_{Bud_IP}), the rate of IFN production (K_{IFN1}) or the degree of IFN responsiveness ($K_{IFN\ On}$) in the tumor cell infiltrate at a fixed rate relative to the resistant cancer cells. In these simulations, the ratio of infiltrate to resistant cancer cells was set at 1:20. Resistant cancer cell viability at the 72h time point. A Monte Carlo simulation (n=1000) was performed using the range of parameters described in Appendix Table V used to describe resistant cancer cells.

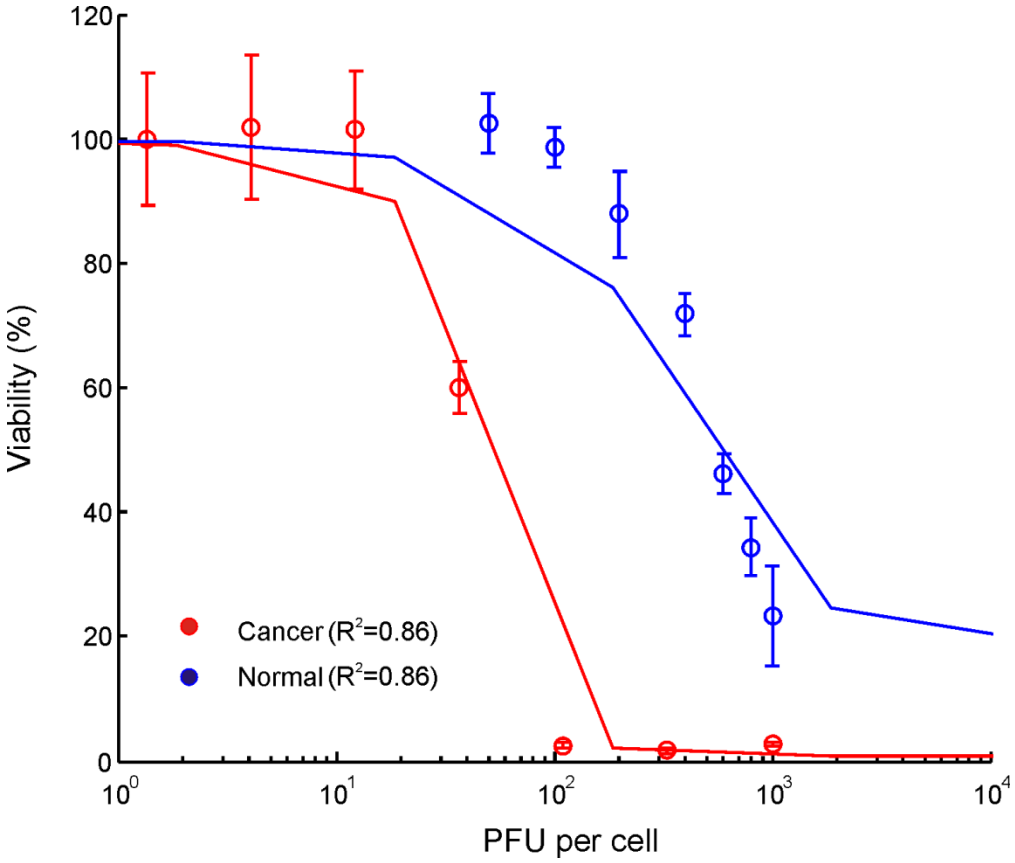

Appendix Figure 9. Experimental and simulated relationship between NRRP concentration and cellular viability 72 hours post-infection in normal (HDFN) and acute leukemic (L1210) cells.

The experimental dose response curve was generated by infecting 2.5E5 cells at increasing MOI and assessing cellular viability 72 hours post-infection through an AlamarBlue assay. Viability is defined as the strength in signal intensity relative to control. Error bars represent the standard deviation obtained over triplicate experiments. Trends represent the simulation which best describes the experimental results. Model parameter identification was performed using the simulated annealing-like method described in chapter II. In these simulations, all parameters are identical between the two cell lineages other than the capacity to produce IFN (K_{IFN1}, $K_{IFN2.1}$&$K_{IFN2.2}$), the rate of NRRP clearance (K_{NC}) and the rate of activation of antiviral defence (K_{IFNon}). In these simulations, the ratio of functional to dysfunctional NRRP particles was varied from 1:0 to 1:1000.

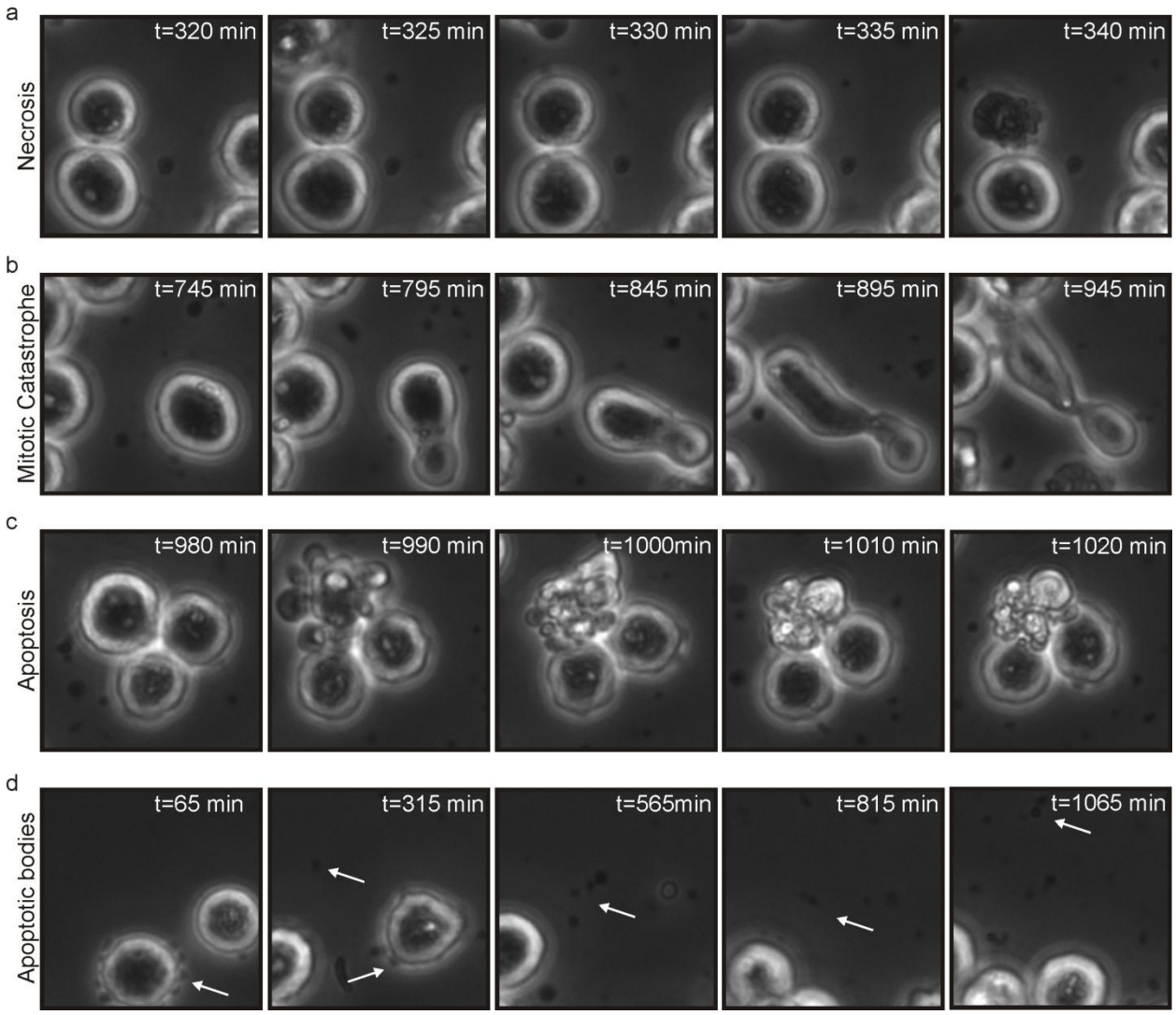

Appendix Figure 10. Time microscopy of death events following NRRP treatment.
For all experiments, the murine multiple myeloma cell line (MPC-11) was treated with NRRPs at a PFU to cell ratio of 100. Following incubation for 1h, and centrifugation to pellet the cells at the bottom of the well, the above experiments were monitored over a 48h hour period. Time indicated in top left hand corner indicates the time following the onset of infection. Images acquired.

Appendix Table VI. List of parameters estimates for Chapter VI.

Parameter	Range Utilized
K_{NI}	7.5E-5 to7.5E-4 ($V^{-1}h^{-1}$)
$EC50$	0.25e-12 to 2.5e-12 (M)
$K_{IFN\ on}$	ln(2)/(0.2 to 2.0) (h^{-1})
K_{IFNoff}	ln(2)/(5 to 50) (h^{-1})
γ_c	ln(2)/(2.5 to 25) (h^{-1})
K_{NC}	ln(2)/(0.25 to 2.5) (h^{-1})
K_{IFN1}	K_{IFN2}× 10 to 100% (M/h)
$K_{IFN2.1}$&$K_{IFN2.2}$	8.3e-18 to 8.3e-17 (M/cell/h) (i.e. 5000-50000 molecules/cell/h)
γ_{IFN}	ln(2)/(5 to 50) (h^{-1})
γ_N	ln(2)/(2.5 to 25) (h^{-1})

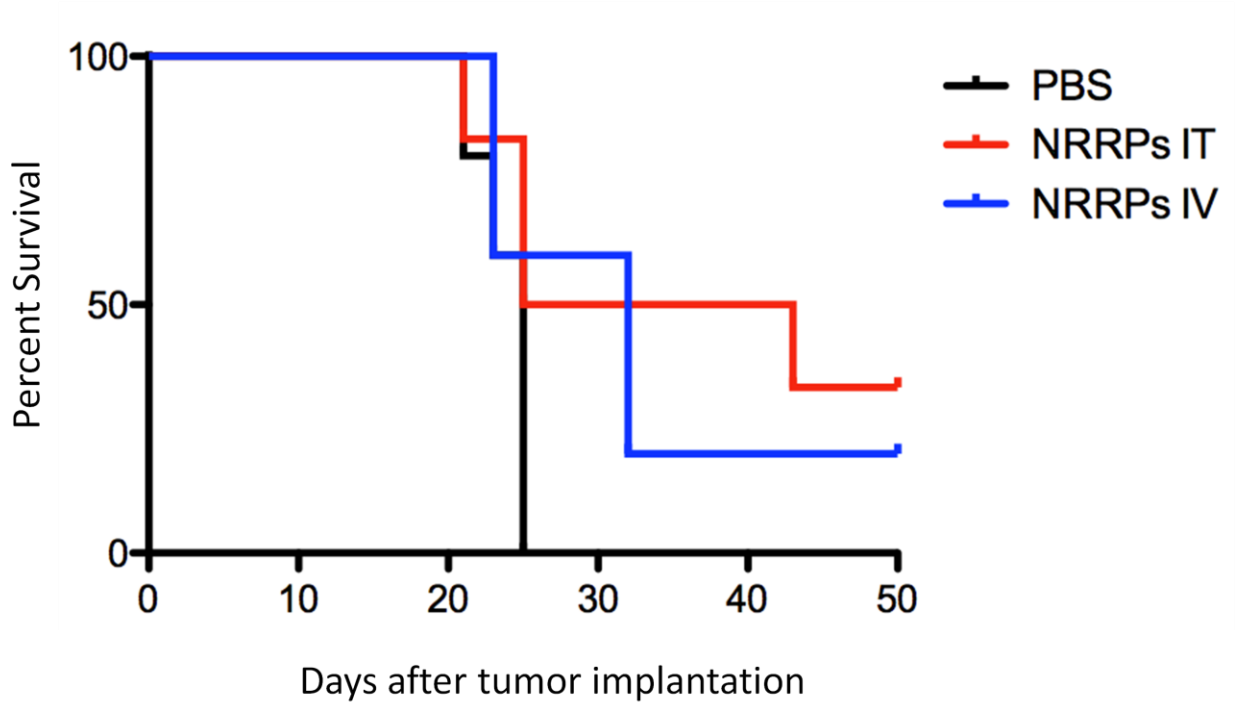

Appendix Figure 11. Survival in a CT26-LacZ murine subcutaneous colon cancer model following NRRP treatment.
On day 1, 15 mice were injected with 3.1E5 CT26-LacZ cells on the right flank. On days 16, 18 and 21, mice received a 2E9 dose of NRRPs administered IV or IT or a PBS control.

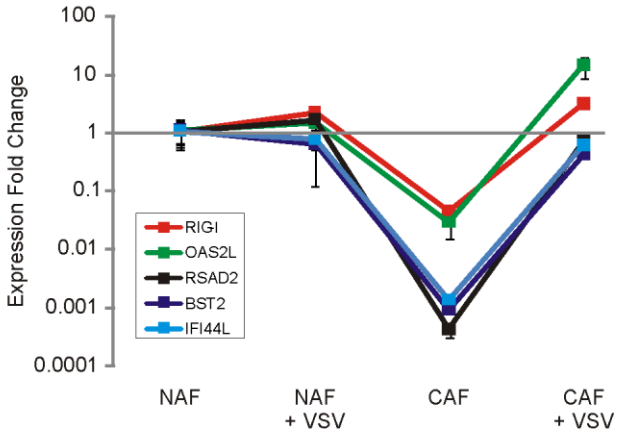

Appendix Figure 12. Quantitative real-time polymerase chain reaction (qRT-PCR) of IFN targets in the second patient identified by qRT-PCR.

qRT-PCR was performed on a subset of select genes categorized as repressed in CAFs (>3 fold) and induced (>3fold) by VSVΔ51 according to the microarray analysis. qRT-PCR was performed on CAFs and NAFs obtained from cancer Patient 2 infected or not with VSVΔ51 for 18hours and normalized to GAPDH levels using the Faffel method

References

1. Hanahan, D. and R.A. Weinberg 2000. The hallmarks of cancer. Cell. 100, 57-70.

2. Hanahan, D. and R.A. Weinberg 2011. Hallmarks of cancer: The next generation. Cell. 144, 646-674.

3. Witsch, E., M. Sela and Y. Yarden 2010. Roles for growth factors in cancer progression. Physiology. 25, 85-101.

4. Pellettieri, J. and A. S. Alvarado 2007. Cell turnover and adult tissue homeostasis: From humans to planarians. 83-105.

5. Massagué, J., S.W. Blain and R.S. Lo 2000. TGF-B signaling in growth control, cancer, and heritable disorders. Cell. 103, 295-309.

6. Hicklin, D. J. and L.M. Ellis 2005. Role of the vascular endothelial growth factor pathway in tumor growth and angiogenesis. Journal of Clinical Oncology. 23, 1011-1027.

7. Ciardiello, F. and G. Tortora 2008. Drug therapy: EGFR antagonists in cancer treatment. N. Engl. J. Med. 358, 1160-1174+1096.

8. Hirota, S., A. Ohashi, T. Nishida, K. Isozaki, K. Kinoshita, Y. Shinomura and Y. Kitamura 2003. Gain-of-function mutations of platelet-derived growth factor receptor alpha gene in gastrointestinal stromal tumors. Gastroenterology. 125, 660-667.

9. Davies, H., G.R. Bignell, C. Cox, P. Stephens, S. Edkins, S. Clegg, J. Teague, H. Woffendin, M.J. Garnett, W. Bottomley, N. Davis, E. Dicks, R. Ewing, Y. Floyd, K. Gray, S. Hall, R. Hawes, J. Hughes, V. Kosmidou, A. Menzies, C. Mould, A. Parker, C. Stevens, S. Watt, S. Hooper, R. Wilson, H. Jayatilake, B.A. Gusterson, C. Cooper, J. Shipley, D. Hargrave, K. Pritchard-Jones, N. Maitland, G. Chenevix-Trench, G.J. Riggins, D.D. Bigner, G. Palmleri, A. Cossu, A. Flanagan, A. Nicholson, J.W.C. Ho, S.Y. Leung, S.T. Yuen, B.L. Weber, H.F. Seigler, T.L. Darrow, H. Paterson, R. Marais, C.J. Marshall, R. Wooster, M.R. Stratton and P.A. Futreal 2002. Mutations of the BRAF gene in human cancer. Nature. 417, 949-954.

10. Madhusudan, S. and T.S. Ganesan 2004. Tyrosine kinase inhibitors in cancer therapy. Clin. Biochem. 37, 618-635.

11. Vousden, K. H. and D.P. Lane 2007. p53 in health and disease. Nature Reviews Molecular Cell Biology. 8, 275-283.

12. Lopez-Lazaro, M. 2008. The warburg effect: Why and how do cancer cells activate glycolysis in the presence of oxygen? Anti-Cancer Agents in Medicinal Chemistry. 8, 305-312.

13. Watson, D. G., F. Tonelli, M. Alossaimi, L. Williamson, E. Chan, I. Gorshkova, E. Berdyshev, R. Bittman, N.J. Pyne and S. Pyne 2013. The roles of sphingosine kinases 1 and 2 in regulating the warburg effect in prostate cancer cells. Cell Signal. 25 (4), 1011-1017.

14. Gottlieb, E. 2011. P53 guards the metabolic pathway less travelled. Nat. Cell Biol. 13, 195-197.

15. Jiang, P., W. Du, X. Wang, A. Mancuso, X. Gao, M. Wu and X. Yang 2011. P53 regulates biosynthesis through direct inactivation of glucose-6-phosphate dehydrogenase. Nat. Cell Biol. 13, 310-316.

16. Wise, D. R. and C.B. Thompson 2010. Glutamine addiction: A new therapeutic target in cancer. Trends Biochem. Sci. 35, 427-433.

17. Ellis, L., P.W. Atadja and R.W. Johnstone 2009. Epigenetics in cancer: Targeting chromatin modifications. Molecular Cancer Therapeutics. 8, 1409-1420.

18. Baek, J. Y., S.M. Morris, J. Campbell, N. Fausto, M.M. Yeh and W.M. Grady 2010. TGF-b inactivation and TGF-a overexpression cooperate in an in vivo mouse model to induce hepatocellular carcinoma that recapitulates molecular features of human liver cancer. International Journal of Cancer. 127, 1060-1071.

19. Podlaha, O., M. Riester, S. De and F. Michor 2012. Evolution of the cancer genome. Trends in Genetics. 28, 155-163.

20. Greaves, M. and C.C. Maley 2012. Clonal evolution in cancer. Nature. 481, 306-313.

21. Dunn, G. P., C.M. Koebel and R.D. Schreiber 2006. Interferons, immunity and cancer immunoediting. Nature Reviews Immunology. 6, 836-848.

22. Dunn, G. P., A.T. Bruce, H. Ikeda, L.J. Old and R.D. Schreiber 2002. Cancer immunoediting: From immunosurveillance to tumor escape. Nat. Immunol. 3, 991-998.

23. Grivennikov, S. I., F.R. Greten and M. Karin 2010. Immunity, inflammation, and cancer. Cell. 140, 883-899.

24. Steidl, C., S.P. Shah, B.W. Woolcock, L. Rui, M. Kawahara, P. Farinha, N.A. Johnson, Y. Zhao, A. Telenius, S.B. Neriah, A. McPherson, B. Meissner, U.C. Okoye, A. Diepstra, D.B. Van, M. Sun, G. Leung, S.J. Jones, J.M. Connors, D.G. Huntsman, K.J. Savage, L.M. Rimsza, D.E. Horsman, L.M. Staudt, U. Steidl, M.A. Marra and R.D. Gascoyne 2011.

MHC class II transactivator CIITA is a recurrent gene fusion partner in lymphoid cancers. Nature. 471, 377-383.

25. Rimsza, L. M., R.A. Roberts, T.P. Miller, J.M. Unger, M. LeBlanc, R.M. Braziel, D.D. Weisenberger, W.C. Chan, H. Muller-Hermelink, E.S. Jaffe, R.D. Gascoyne, E. Campo, D.A. Fuchs, C.M. Spier, R.I. Fisher, J. Delabie, A. Rosenwald, L.M. Staudt and T.M. Grogan 2004. Loss of MHC class II gene and protein expression in diffuse large B-cell lymphoma is related to decreased tumor immunosurveillance and poor patient survival regardless of other prognostic factors: A follow-up study from the leukemia and lymphoma molecular profiling project. Blood. 103, 4251-4258.

26. Morisaki, T., M. Katano, A. Ikubo, K. Anan, M. Nakamura, K. Nakamura, H. Sato, M. Tanaka and M. Torisu 1996. Immunosuppressive cytokines (IL-10, TGF-B) genes expression in human gastric carcinoma tissues. J. Surg. Oncol. 63, 234-239.

27. Asselin-Paturel, C., H. Echchakir, G. Carayol, F. Gay, P. Opolon, D. Grunenwald, S. Chouaib and F. Mami-Chouatb 1998. Quantitative analysis of Th1, Th2 and TGF-B1 cytokine expression in tumor, TIL and PBL of non-small cell lung cancer patients. International Journal of Cancer. 77, 7-12.

28. Wittke, F., R. Hoffmann, J. Buer, I. Dallmann, K. Oevermann, S. Sel, T. Wandert, A. Ganser and J. Atzpodien 1999. Interleukin 10 (IL-10): An immunosuppressive factor and independent predictor in patients with metastatic renal cell carcinoma. Br. J. Cancer. 79, 1182-1184.

29. Ugel, S., E. Peranzoni, G. Desantis, M. Chioda, S. Walter, T. Weinschenk, J. Ochando, A. Cabrelle, S. Mandruzzato and V. Bronte 2012. Immune tolerance to tumor antigens occurs in a specialized environment of the spleen. Cell Reports. 2, 628-639.

30. Lettau, M., H. Schmidt, D. Kabelitz and O. Janssen 2007. Secretory lysosomes and their cargo in T and NK cells. Immunol. Lett. 108, 10-19.

31. Yates, L. R. and P.J. Campbell 2012. Evolution of the cancer genome. Nature Reviews Genetics. 13, 795-806.

32. Komaki, K., N. Sano and A. Tangoku 2006. Problems in histological grading of malignancy and its clinical significance in patients with operable breast cancer. Breast Cancer. 13, 249-253.

33. Turner, N. C. and J. Reis-Filho 2012. Genetic heterogeneity and cancer drug resistance. The Lancet Oncology. 13, e178-e185.

34. Riss, J., C. Khanna, S. Koo, G.V.R. Chandramouli, H.H. Yang, Y. Hu, D.E. Kleiner, A. Rosenwald, C.F. Schaefer, S. Ben-Sasson, L. Yang, J. Powell, D.W. Kane, R.A. Star, O. Aprelikova, K. Bauer, J.R. Vasselli, J.K. Maranchie, K.W. Kohn, K.H. Buetow, W.M.

Linehan, J.N. Weinstein, M.P. Lee, R.D. Klausner and J.C. Barrett 2006. Cancers as wounds that do not heal: Differences and similarities between renal regeneration/repair and renal cell carcinoma. Cancer Res. 66, 7216-7224.

35. Kalluri, R. and M. Zeisberg 2006. Fibroblasts in cancer. Nature Reviews Cancer. 6, 392-401.

36. Schafer, M. and S. Werner 2008. Cancer as an overhealing wound: An old hypothesis revisited. Nature Reviews Molecular Cell Biology. 9, 628-638.

37. Erkan, M., C. Reiser-Erkan, C.W. Michalski, B. Kong, I. Esposito, H. Friess and J. Kleeff 2012. The impact of the activated stroma on pancreatic ductal adenocarcinoma biology and therapy resistance. Curr. Mol. Med. 12, 288-303.

38. Lanca, T. and B. Silva-Santos 2012. The split nature of tumor-infiltrating leukocytes: Implications for cancer surveillance and immunotherapy. OncoImmunology. 1, 717-725.

39. Dudley, A. C. 2012. Tumor endothelial cells. Cold Spring Harbor Perspectives in Medicine. 2.

40. Cheng, L., Z. Huang, W. Zhou, Q. Wu, S. Donnola, J.K. Liu, X. Fang, A.E. Sloan, Y. Mao, J.D. Lathia, W. Min, R.E. McLendon, J.N. Rich and S. Bao 2013. Glioblastoma stem cells generate vascular pericytes to support vessel function and tumor growth. Cell. 153, 139-152.

41. Hegde, P. S., A.M. Jubb, D. Chen, N.F. Li, Y.G. Meng, C. Bernaards, R. Elliott, S.J. Scherer and D.S. Chen 2013. Predictive impact of circulating vascular endothelial growth factor in four phase III trials evaluating bevacizumab. Clinical Cancer Research. 19, 929-937.

42. Sun, Y., J. Campisi, C. Higano, T.M. Beer, P. Porter, I. Coleman, L. True and P.S. Nelson 2012. Treatment-induced damage to the tumor microenvironment promotes prostate cancer therapy resistance through WNT16B. Nat. Med. 18, 1359-1368.

43. Dave, S. S., G. Wright, B. Tan, A. Rosenwald, R.D. Gascoyne, W.C. Chan, R.I. Fisher, R.M. Braziel, L.M. Rimsza, T.M. Grogan, T.P. Miller, M. LeBlanc, T.C. Greiner, D.D. Weisenburger, J.C. Lynch, J. Vose, J.O. Armitage, E.B. Smeland, S. Kvaloy, H. Holte, J. Delabie, J.M. Connors, P.M. Lansdorp, Q. Ouyang, T.A. Lister, A.J. Davies, A.J. Norton, H. Muller-Hermelink, G. Ott, E. Campo, E. Montserrat, W.H. Wilson, E.S. Jaffe, R. Simon, L. Yang, J. Powell, H. Zhao, N. Goldschmidt, M. Chiorazzi and L.M. Staudt 2004. Prediction of survival in follicular lymphoma based on molecular features of tumor-infiltrating immune cells. N. Engl. J. Med. 351, 2159-2169.

44. Huh, J. W., J.H. Lee and H.R. Kim 2012. Prognostic significance of tumor-infiltrating lymphocytes for patients with colorectal cancer. Archives of Surgery. 147, 366-371.

45. Yamashita, M., T. Ogawa, X. Zhang, N. Hanamura, Y. Kashikura, M. Takamura, M. Yoneda and T. Shiraishi 2012. Role of stromal myofibroblasts in invasive breast cancer: Stromal expression of alpha-smooth muscle actin correlates with worse clinical outcome. Breast Cancer. 19, 170-176.

46. Fujita, H., K. Ohuchida, K. Mizumoto, K. Nakata, J. Yu, T. Kayashima, L. Cui, T. Manabe, T. Ohtsuka and M. Tanaka 2010. a-smooth muscle actin expressing stroma promotes an aggressive tumor biology in pancreatic ductal adenocarcinoma. Pancreas. 39, 1254-1262.

47. Des Guetz, G., B. Uzzan, P. Nicolas, M. Cucherat, J.-. Morere, R. Benamouzig, J.-. Breau and G.-. Perret 2006. Microvessel density and VEGF expression are prognostic factors in colorectal cancer. meta-analysis of the literature. Br. J. Cancer. 94, 1823-1832.

48. Aboussekhra, A. 2011. Role of cancer-associated fibroblasts in breast cancer development and prognosis. Int. J. Dev. Biol. 55, 841-849.

49. Mhawech-Fauceglia, P., D. Wang, D. Samrao, G. Kim, K. Lawrenson, T. Meneses, S. Liu, A. Yessaian and T. Pejovic 2013. Clinical implications of marker expression of carcinoma-associated fibroblasts (CAFs) in patients with epithelial ovarian carcinoma after treatment with neoadjuvant chemotherapy. Cancer Microenvironment., 1-7.

50. Tomasek, J. J., G. Gabbiani, B. Hinz, C. Chaponnier and R.A. Brown 2002. Myofibroblasts and mechano: Regulation of connective tissue remodelling. Nature Reviews Molecular Cell Biology. 3, 349-363.

51. Fukumura, D., R. Xavier, T. Sugiura, Y. Chen, E.-. Park, N. Lu, M. Selig, G. Nielsen, T. Taksir, R.K. Jain and B. Seed 1998. Tumor induction of VEGF promoter activity in stromal cells. Cell. 94, 715-725.

52. Berthod, F., J. Symes, N. Tremblay, J.A. Medin and F.A. Auger 2012. Spontaneous fibroblast-derived pericyte recruitment in a human tissue-engineered angiogenesis model in vitro. J. Cell. Physiol. 227, 2130-2137.

53. Donnelly, J. J., M.S. Xi and J.H. Rockey 1993. A soluble product of human corneal fibroblasts inhibits lymphocyte activation. enhancement by interferon-gamma. Exp. Eye Res. 56, 157-165.

54. Haniffa, M. A., X.-. Wang, U. Holtick, M. Rae, J.D. Isaacs, A.M. Dickinson, C.M.U. Hilkens and M.P. Collin 2007. Adult human fibroblasts are potent immunoregulatory cells and functionally equivalent to mesenchymal stem cells. Journal of Immunology. 179, 1595-1604.

55. Roberts, A. B., M.B. Sporn and R.K. Assoian 1986. Transforming growth factor type B: Rapid induction of fibrosis and angiogenesis in vivo and stimulation of collagen formation in vitro. Proc. Natl. Acad. Sci. U. S. A. 83, 4167-4171.

56. Desmouliere, A., A. Geinoz, F. Gabbiani and G. Gabbiani 1993. Transforming growth factor-B1 induces a-smooth muscle actin expression in granulation tissue myofibroblasts and in quiescent and growing cultured fibroblasts. J. Cell Biol. 122, 103-111.

57. Vaughan, M. B., E.W. Howard and J.J. Tomasek 2000. Transforming growth factor-b1 promotes the morphological and functional differentiation of the myofibroblast. Exp. Cell Res. 257, 180-189.

58. Glim, J. E., F.B. Niessen, V. Everts, M. van Egmond and R.H.J. Beelen 2013. Platelet derived growth factor-CC secreted by M2 macrophages induces alpha-smooth muscle actin expression by dermal and gingival fibroblasts. Immunobiology. 218, 924-929.

59. Orimo, A., P.B. Gupta, D.C. Sgroi, F. Arenzana-Seisdedos, T. Delaunay, R. Naeem, V.J. Carey, A.L. Richardson and R.A. Weinberg 2005. Stromal fibroblasts present in invasive human breast carcinomas promote tumor growth and angiogenesis through elevated SDF-1/CXCL12 secretion. Cell. 121, 335-348.

60. Jia, C. -., T.-. Wang, W. Liu, B.-. Fu, X.F. Hua, G.-. Wang, T.-. Li, X. Li, X.-. Wu, Y. Tai, J. Zhou, G.-. Chen and Q. Zhang 2013. Cancer-associated fibroblasts from hepatocellular carcinoma promote malignant cell proliferation by HGF secretion. PLoS ONE. 8.

61. De Francesco, E. M., R. Lappano, M.F. Santolla, S. Marsico, A. Caruso and M. Maggiolini 2013. HIF-1α/GPER signaling mediates the expression of VEGF induced by hypoxia in breast cancer associated fibroblasts (CAFs). Breast Cancer Research. 15.

62. Silzle, T., G.J. Randolph, M. Kreutz and L. Kunz-Schughart 2004. The fibroblast: Sentinel cell and local immune modulator in tumor tissue. International Journal of Cancer. 108, 173-180.

63. Gregory, A. D. and A.M. Houghton 2011. Tumor-associated neutrophils: New targets for cancer therapy. Cancer Res. 71, 2411-2416.

64. Yu, X., H. Li and X. Ren 2012. Interaction between regulatory T cells and cancer stem cells. International Journal of Cancer. 131, 1491-1498.

65. Wakita, D., K. Sumida, Y. Iwakura, H. Nishikawa, T. Ohkuri, K. Chamoto, H. Kitamura and T. Nishimura 2010. Tumor-infiltrating IL-17-producing yo T cells support the progression of tumor by promoting angiogenesis. Eur. J. Immunol. 40, 1927-1937.

66. Scarlett, U. K., M.R. Rutkowski, A.M. Rauwerdink, J. Fields, X. Escovar-Fadul, J. Baird, J. Cubillos-Ruiz, A.C. Jacobs, J.L. Gonzalez, J. Weaver, S. Fiering and J. Conejo-Garcia 2012. Ovarian cancer progression is controlled by phenotypic changes in dendritic cells. J. Exp. Med. 209, 495-506.

67. Lindau, D., P. Gielen, M. Kroesen, P. Wesseling and G.J. Adema 2013. The immunosuppressive tumour network: Myeloid-derived suppressor cells, regulatory T cells and natural killer T cells. Immunology. 138, 105-115.

68. Curiel, T. J., G. Coukos, L. Zou, X. Alvarez, P. Cheng, P. Mottram, M. Evdemon-Hogan, J. Conejo-Garcia, L. Zhang, M. Burow, Y. Zhu, S. Wei, I. Kryczek, B. Daniel, A. Gordon, L. Myers, A. Lackner, M.L. Disis, K.L. Knutson, L. Chen and W. Zou 2004. Specific recruitment of regulatory T cells in ovarian carcinoma fosters immune privilege and predicts reduced survival. Nat. Med. 10, 942-949.

69. Nagaraj, S., K. Gupta, V. Pisarev, L. Kinarsky, S. Sherman, L. Kang, D.L. Herber, J. Schneck and D.I. Gabrilovich 2007. Altered recognition of antigen is a mechanism of CD8+ T cell tolerance in cancer. Nat. Med. 13, 828-835.

70. Cederbom, L., H. Hall and F. Ivars 2000. CD4+CD25+ regulatory T cells down-regulate co-stimulatory molecules on antigen-presenting cells. Eur. J. Immunol. 30, 1538-1543.

71. Veldhoen, M., H. Moncrieffe, R.J. Hocking, C.J. Atkins and B. Stockinger 2006. Modulation of dendritic cell function by naive and regulatory CD4 + T cells. Journal of Immunology. 176, 6202-6210.

72. Ghiringhelli, F., C. Menard, M. Terme, C. Flament, J. Taieb, N. Chaput, P.E. Puig, S. Novault, B. Escudier, E. Vivier, A. Lecesne, C. Robert, J.-. Blay, J. Bernard, S. Caillat-Zucman, A. Freitas, T. Tursz, O. Wagner-Ballon, C. Capron, W. Vainchencker, F. Martin and L. Zitvogel 2005. CD4+CD25+ regulatory T cells inhibit natural killer cell functions in a transforming growth factor-b-dependent manner. J. Exp. Med. 202, 1075-1085.

73. Zhou, H., L. Chen, Y. You, L. Zou and P. Zou 2010. Foxp3-transduced polyclonal regulatory T cells suppress NK cell functions in a TGF-B dependent manner. Autoimmunity. 43, 299-307.

74. Chen, M. -., M.J. Pittet, L. Gorelik, R.A. Flavell, R. Weissleder, H. Von Boehmer and K. Khazaie 2005. Regulatory T cells suppress tumor-specific CD8 T cell cytotoxicity through TGF-B signals in vivo. Proc. Natl. Acad. Sci. U. S. A. 102, 419-424.

75. Ostrand-Rosenberg, S. 2010. Myeloid-derived suppressor cells: More mechanisms for inhibiting antitumor immunity. Cancer Immunology, Immunotherapy. 59, 1593-1600.

76. Mantovani, A., T. Schioppa, C. Porta, P. Allavena and A. Sica 2006. Role of tumor-associated macrophages in tumor progression and invasion. Cancer Metastasis Rev. 25, 315-322.

77. Bunt, S. K., L. Yang, P. Sinha, V.K. Clements, J. Leips and S. Ostrand-Rosenberg 2007. Reduced inflammation in the tumor microenvironment delays the accumulation of myeloid-derived suppressor cells and limits tumor progression. Cancer Res. 67, 10019-10026.

78. Ayala, A., W. Ertel and I.H. Chaudry 1996. Trauma-induced suppression of antigen presentation and expression of major histocompatibility class II antigen complex in leukocytes. Shock. 5, 79-90.

79. Church, D., S. Elsayed, O. Reid, B. Winston and R. Lindsay 2006. Burn wound infections. Clin. Microbiol. Rev. 19, 403-434.

80. Munford, R. S. and J. Pugin 2001. Normal responses to injury prevent systemic inflammation and can be immunosuppressive. American Journal of Respiratory and Critical Care Medicine. 163, 316-321.

81. Nathan, C. 2006. Neutrophils and immunity: Challenges and opportunities. Nature Reviews Immunology. 6, 173-182.

82. Burzyn, D., W. Kuswanto, D. Kolodin, J.L. Shadrach, M. Cerletti, Y. Jang, E. Sefik, T.G. Tan, A.J. Wagers, C. Benoist and D. Mathis 2013. A special population of regulatory T cells potentiates muscle repair. Cell. 155, 1282-1295.

83. Willenborg, S., T. Lucas, G. Van Loo, J.A. Knipper, T. Krieg, I. Haase, B. Brachvogel, M. Hammerschmidt, A. Nagy, N. Ferrara, M. Pasparakis and S.A. Eming 2012. CCR2 recruits an inflammatory macrophage subpopulation critical for angiogenesis in tissue repair. Blood. 120, 613-625.

84. Murray, P. J. and T.A. Wynn 2011. Protective and pathogenic functions of macrophage subsets. Nature Reviews Immunology. 11, 723-737.

85. Noel, G., Q. Wang, S. Schwemberger, C. Hanson, N. Giacalone, L. Haar and C.K. Ogle 2011. Neutrophils, not monocyte/macrophages, are the major splenic source of postburn IL-10. Shock. 36, 149-155.

86. Comito, G., E. Giannoni, C.P. Segura, P. Barcellos-de-Souza, M.R. Raspollini, G. Baroni, M. Lanciotti, S. Serni and P. Chiarugi 2013. Cancer-associated fibroblasts and M2-polarized macrophages synergize during prostate carcinoma progression. Oncogene.

87. Fridlender, Z. G., J. Sun, S. Kim, V. Kapoor, G. Cheng, L. Ling, G.S. Worthen and S.M. Albelda 2009. Polarization of tumor-associated neutrophil phenotype by TGF-B: "N1" versus "N2" TAN. Cancer Cell. 16, 183-194.

88. Corzo, C. A., T. Condamine, L. Lu, M.J. Cotter, J.-. Youn, P. Cheng, H.-. Cho, E. Celis, D.G. Quiceno, T. Padhya, T.V. McCaffrey, J.C. McCaffrey and D.I. Gabrilovich 2010. HIF-1a regulates function and differentiation of myeloid-derived suppressor cells in the tumor microenvironment. J. Exp. Med. 207, 2439-2453.

89. Baniyash, M., M. Sade-Feldman and J. Kanterman 2013. Chronic inflammation and cancer: Suppressing the suppressors. Cancer Immunology, Immunotherapy., 1-10.

90. McKay, C. J., P. Glen and D.C. McMillan 2008. Chronic inflammation and pancreatic cancer. Best Practice and Research in Clinical Gastroenterology. 22, 65-73.

91. Li, Y., J. Zhang and H. Ma 2013. Chronic inflammation and gallbladder cancer. Cancer Lett.

92. Boland, C. R. 2010. Chronic inflammation, colorectal cancer and gene polymorphisms. Digestive Diseases. 28, 590-595.

93. Anand, P., A.B. Kunnumakkara, C. Sundaram, K.B. Harikumar, S.T. Tharakan, O.S. Lai, B. Sung and B.B. Aggarwal 2008. Cancer is a preventable disease that requires major lifestyle changes. Pharm. Res. 25, 2097-2116.

94. Botelho, M., P. Oliveira, J. Gomes, F. Gartner, C. Lopes, C.D. Costa and J.C. MacHado 2009. Tumourigenic effect of schistosoma haematobium total antigen in mammalian cells. Int. J. Exp. Pathol. 90, 448-453.

95. Rosin, M. P., S.E. Din, A.J. Ward and W.A. Anwar 1994. Involvement of inflammatory reactions and elevated cell proliferation in the development of bladder cancer in schistosomiasis patients. Mutation Research - Fundamental and Molecular Mechanisms of Mutagenesis. 305, 283-292.

96. Maxwell Parkin, D., H. Ohshima, P. Srivatanakul and V. Vatanasapt 1993. Cholangiocarcinoma: Epidemiology, mechanisms of carcinogenesis and prevention. Cancer Epidemiology Biomarkers and Prevention. 2, 537-544.

97. Parsonnet, J., G.D. Friedman, D.P. Vandersteen, Y. Chang, J.H. Vogelman, N. Orentreich and R.K. Sibley 1991. Helicobacter pylori infection and the risk of gastric carcinoma. N. Engl. J. Med. 325, 1127-1131.

98. Walboomers, J. M. M., M.V. Jacobs, M.M. Manos, F.X. Bosch, J.A. Kummer, K.V. Shah, P.J.F. Snijders, J. Peto, C.J.L.M. Meijer and N. Munoz 1999. Human papillomavirus is a necessary cause of invasive cervical cancer worldwide. J. Pathol. 189, 12-19.

99. Young, L. S. and A.B. Rickinson 2004. Epstein-barr virus: 40 years on. Nature Reviews Cancer. 4, 757-768.

100. Nador, R. G., E. Cesarman, A. Chadburn, D.B. Dawson, M.Q. Ansari, J. Said and D.M. Knowles 1996. Primary effusion lymphoma: A distinct clinicopathologic entity associated with the kaposi's sarcoma-associated herpes virus. Blood. 88, 645-656.

101. Chen, C. -., H.-. Yang, J. Su, C.-. Jen, S.-. You, S.-. Lu, G.-. Huang and U.H. Iloeje 2006. Risk of hepatocellular carcinoma across a biological gradient of serum hepatitis B virus DNA level. J. Am. Med. Assoc. 295, 65-73.

102. Kitajima, I., T. Shinohara, J. Bilakovics, D.A. Brown, X. Xu and M. Nerenberg 1992. Ablation of transplanted HTLV-I tax-transformed tumors in mice by antisense inhibition of NF-kB. Science. 258, 1792-1795.

103. Shuda, M., H. Feng, J.K. Hyun, S.T. Rosen, O. Gjoerup, P.S. Moore and Y. Chang 2008. T antigen mutations are a human tumor-specific signature for merkel cell polyomavirus. Proc. Natl. Acad. Sci. U. S. A. 105, 16272-16277.

104. Feng, H., M. Shuda, Y. Chang and P.S. Moore 2008. Clonal integration of a polyomavirus in human merkel cell carcinoma. Science. 319, 1096-1100.

105. DeCaprio, J. A., J.W. Ludlow, J. Figge, J.-. Shew, C.-. Huang, W.-. Lee, E. Marsilio, E. Paucha and D.M. Livingston 1988. SV40 large tumor antigen forms a specific complex with the product of the retinoblastoma susceptibility gene. Cell. 54, 275-283.

106. Dyson, N., P.M. Howley, K. Munger and E. Harlow 1989. The human papilloma virus-16 E7 oncoprotein is able to bind to the retinoblastoma gene product. Science. 243, 934-937.

107. Dunn, G. P., A.T. Bruce, K.C.F. Sheehan, V. Shankaran, R. Uppaluri, J.D. Bui, M.S. Diamond, C.M. Koebel, C. Arthur, J.M. White and R.D. Schreiber 2005. A critical function for type I interferons in cancer immunoediting. Nat. Immunol. 6, 722-729.

108. Katze, M. G., Y. He and M. Gale Jr. 2002. Viruses and interferon: A fight for supremacy. Nature Reviews Immunology. 2, 675-687.

109. Baglioni, C., P.A. Maroney and D.K. West 1979. 2' 5' oligo(A) polymerase activity and inhibition of viral RNA synthesis in interferon-treated HeLa cells. Biochemistry (N. Y.). 18, 1765-1770.

110. Floyd-Smith, G. 1988. (2'-5')A(n)-dependent endoribonuclease: Enzyme levels are regulated by IFNa, IFNb, and cell culture conditions. J. Cell. Biochem. 38, 13-21.

111. Haller, O. and G. Kochs 2002. Interferon-induced mx proteins: Dynamin-like GTPases with antiviral activity. Traffic. 3, 710-717.

112. Halloran, P. F., J. Urmson, d.M. Van and P. Autenried 1989. Regulation of MHC expression in vivo. II. IFN-a/b inducers and recombinant IFN-alpha modulate MHC antigen expression in mouse tissues. Journal of Immunology. 142, 4241-4247.

113. Makridis, C., C. Juhlin, G. Akerstrom, K. Oberg, J. Rastad, B. Greger and M. Rothmund 1994. MHC class I and II antigen expression and interferon a treatment of human midgut carcinoid tumors. World J. Surg. 18, 481-487.

114. Boehme, K. W. and T. Compton 2004. Innate sensing of viruses by toll-like receptors. J. Virol. 78, 7867-7873.

115. Honda, K. and T. Taniguchi 2006. IRFs: Master regulators of signalling by toll-like receptors and cytosolic pattern-recognition receptors. Nature Reviews Immunology. 6, 644-658.

116. Gonzalez-Navajas, J. M., J. Lee, M. David and E. Raz 2012. Immunomodulatory functions of type i interferons. Nature Reviews Immunology. 12, 125-135.

117. Sadler, A. J. and B.R.G. Williams 2008. Interferon-inducible antiviral effectors. Nature Reviews Immunology. 8, 559-568.

118. Perez-Caballero, D., T. Zang, A. Ebrahimi, M.W. McNatt, D.A. Gregory, M.C. Johnson and P.D. Bieniasz 2009. Tetherin inhibits HIV-1 release by directly tethering virions to cells. Cell. 139, 499-511.

119. Verhelst, J., E. Parthoens, B. Schepens, W. Fiers and X. Saelensa 2012. Interferon-inducible protein Mx1 inhibits influenza virus byinterfering with functional viral ribonucleoprotein complex assembly. J. Virol. 86, 13445-13455.

120. Montoya, M., G. Schiavoni, F. Mattel, I. Gresser, F. Belardelli, P. Borrow and D.F. Tough 2002. Type I interferons produced by dendritic cells promote their phenotypic and functional activation. Blood. 99, 3263-3271.

121. Curtsinger, J. M., J.O. Valenzuela, P. Agarwal, D. Lins and M.F. Mescher 2005. Cutting edge: Type I IFNs provide a third signal to CD8 T cells to stimulate clonal expansion and differentiation. Journal of Immunology. 174, 4465-4469.

122. Kolumam, G. A., S. Thomas, L.J. Thompson, J. Sprent and K. Murali-Krishna 2005. Type I interferons act directly on CD8 T cells to allow clonal expansion and memory formation in response to viral infection. J. Exp. Med. 202, 637-650.

123. Thompson, L. J., G.A. Kolumam, S. Thomas and K. Murali-Krishna 2006. Innate inflammatory signals induced by various pathogens differentially dictate the IFN-I dependence of CD8 T cells for clonal expansion and memory formation. Journal of Immunology. 177, 1746-1754.

124. Spadaro, F., C. Lapenta, S. Donati, L. Abalsamo, V. Barnaba, F. Belardelli, S.M. Santini and M. Ferrantini 2012. IFN-a enhances cross-presentation in human dendritic cells by modulating antigen survival, endocytic routing, and processing. Blood. 119, 1407-1417.

125. Saidi, R. F., F. Williams, B. Silberberg, V.K. Mittal, S.G. ReMine and M.J. Jacobs 2006. Expression of interferon receptors in pancreatic cancer: Identification of a novel prognostic factor. Surgery. 139, 743-748.

126. Diaz, M. O., C.M. Rubin, A. Harden, S. Ziemin, R.A. Larson, M.M. Le Beau and J.D. Rowley 1990. Deletions of interferon genes in acute lymphoblastic leukemia. N. Engl. J. Med. 322, 77-82.

127. Ogasawara, S., G. Tamura, C. Maesawa, Y. Suzuki, K. Ishida, N. Satoh, N. Uesugi, K. Saito and R. Satodate 1996. Common deleted region on the long arm of chromosome 5 in esophageal carcinoma. Gastroenterology. 110, 52-57.

128. Yi, Y., H. Wu, Q. Gao, H.-. He, Y.-. Li, X.-. Cai, J.-. Wang, J. Zhou, Y.-. Cheng, J.-. Jin, J. Fan and S.-. Qiu 2013. Interferon regulatory factor (IRF)-1 and IRF-2 are associated with prognosis and tumor invasion in HCC. Annals of Surgical Oncology. 20, 267-276.

129. Gordziel, C., J. Bratsch, R. Moriggl, T. Knösel and K. Friedrich 2013. Both STAT1 and STAT3 are favourable prognostic determinants in colorectal carcinoma. Br. J. Cancer. 109, 138-146.

130. Ren, Y., Y. Zhang, R. Liu, D. Fenstermacher, K. Wright, J. Teer and J. Wu 2013. JAK1 truncating mutations in gynecologic cancer define new role of cancer-associated protein tyrosine kinase aberrations. Scientific Reports. 3, e3042.

131. Fuertes, M. B., S.-. Woo, B. Burnett, Y.-. Fu and T.F. Gajewski 2013. Type I interferon response and innate immune sensing of cancer. Trends Immunol. 34, 67-73.

132. Taylor, D. R. 2000. Hepatitis C virus: Evasion of the interferon-induced antiviral response. Journal of Molecular Medicine. 78, 182-190.

133. Barnard, P., E. Payne and N.A.J. McMillan 2000. The human papillomavirus E7 protein is able to inhibit the antiviral and anti-growth functions of interferon-a. Virology. 277, 411-419.

134. Wu, L., E. Fossum, C.H. Joo, K.-. Inn, Y.C. Shin, E. Johannsen, L. Hutt-Fletcher, J. Hass and J.U. Jung 2009. Epstein-barr virus LF2: An antagonist to type I interferon. J. Virol. 83, 1140-1146.

135. Luther, J., S.Y. Owyang, T. Takeuchi, T.S. Cole, M. Zhang, M. Liu, J. Erb-Downward, J.H. Rubenstein, C.-. Chen, A.V. Pierzchala, J.A. Paul and J.Y. Kao 2011. Helicobacter pylori DNA decreases pro-inflammatory cytokine production by dendritic cells and attenuates dextran sodium sulphate-induced colitis. Gut. 60, 1479-1486.

136. Bracarda, S., A.M.M. Eggermont and J. Samuelsson 2010. Redefining the role of interferon in the treatment of malignant diseases. Eur. J. Cancer. 46, 284-297.

137. Cheung-Ong, K., G. Giaever and C. Nislow 2013. DNA-damaging agents in cancer chemotherapy: Serendipity and chemical biology. Chemistry and Biology. 20, 648-659.

138. Jordan, M. A. and L. Wilson 2004. Microtubules as a target for anticancer drugs. Nature Reviews Cancer. 4, 253-265.

139. Kaye, S. B. 1998. New antimetabolites in cancer chemotherapy and their clinical impact. Br. J. Cancer. 78, 1-7.

140. Holohan, C., S. Van Schaeybroeck, D.B. Longley and P.G. Johnston 2013. Cancer drug resistance: An evolving paradigm. Nature Reviews Cancer. 13, 714-726.

141. Martini, M., L. Vecchione, S. Siena, S. Tejpar and A. Bardelli 2012. Targeted therapies: How personal should we go? Nature Reviews Clinical Oncology. 9, 87-97.

142. Druker, B. J., S. Tamura, E. Buchdunger, S. Ohno, G.M. Segal, S. Fanning, J. Zimmermann and N.B. Lydon 1996. Effects of a selective inhibitor of the Ab1 tyrosine kinase on the growth of bcr-Ab1 positive cells. Nat. Med. 2, 561-566.

143. Druker, B. J., M. Talpaz, D.J. Resta, B. Peng, E. Buchdunger, J.M. Ford, N.B. Lydon, H. Kantarjian, R. Capdeville, S. Ohno-Jones and C.L. Sawyers 2001. Efficacy and safety of a specific inhibitor of the BCR-ABL tyrosine kinase in chronic myeloid leukemia. N. Engl. J. Med. 344, 1031-1037.

144. Cohen, M. H., G. Williams, J.R. Johnson, J. Duan, J. Gobburu, A. Rahman, K. Benson, J. Leighton, S.K. Kim, R. Wood, M. Rothmann, G. Chen, K.M. U, A.M. Staten and R. Pazdur 2002. Approval summary for imatinib mesylate capsules in the treatment of chronic myelogenous leukemia. Clinical Cancer Research. 8, 935-942.

145. Druker, B. J., S. Tamura, E. Buchdunger, S. Ohno, G.M. Segal, S. Fanning, J. Zimmermann and N.B. Lydon 1996. Effects of a selective inhibitor of the Ab1 tyrosine kinase on the growth of bcr-Ab1 positive cells. Nat. Med. 2, 561-566.

146. Fukuoka, M., S. Yano, G. Giaccone, T. Tamura, K. Nakagawa, J.-. Douillard, Y. Nishiwaki, J. Vansteenkiste, S. Kudoh, D. Rischin, R. Eek, T. Horai, K. Noda, I. Takata, E. Smit, S. Averbuch, A. Macleod, A. Feyereislova, R.-. Dong and J. Baselga 2003. Multi-institutional randomized phase II trial of gefitinib for previously treated patients with advanced non-small-cell lung cancer. Journal of Clinical Oncology. 21, 2237-2246.

147. Tsao, M. -., A. Sakurada, J.-. Cutz, C.-. Zhu, S. Kamel-Reid, J. Squire, I. Lorimer, T. Zhang, N. Liu, M. Daneshmand, P. Marrano, G. Da Cunha Santos, A. Lagarde, F. Richardson, L. Seymour, M. Whitehead, K. Ding, J. Pater and F.A. Shepherd 2005. Erlotinib in lung cancer - molecular and clinical predictors of outcome. N. Engl. J. Med. 353, 133-144.

148. Richardson, P. G., B. Barlogie, J. Berenson, S. Singhal, S. Jagannath, D. Irwin, S.V. Rajkumar, G. Srkalovic, M. Alsina, R. Alexanian, D. Siegel, R.Z. Orlowski, D. Kuter, S.A. Limentani, S. Lee, T. Hideshima, D.-. Esseltine, M. Kauffman, J. Adams, D.P. Schenkein

and K.C. Anderson 2003. A phase 2 study of bortezomib in relapsed, refractory myeloma. N. Engl. J. Med. 348, 2609-2617.

149. Hideshima, T., P. Richardson, D. Chauhan, V.J. Palombella, P.J. Elliott, J. Adams and K.C. Anderson 2001. The proteasome inhibitor PS-341 inhibits growth, induces apoptosis, and overcomes drug resistance in human multiple myeloma cells. Cancer Res. 61, 3071-3076.

150. Piccart-Gebhart, M. J., M. Procter, B. Leyland-Jones, A. Goldhirsch, M. Untch, I. Smith, L. Gianni, J. Baselga, R. Bell, C. Jackisch, D. Cameron, M. Dowsett, C.H. Barrios, G. Steger, C.-. Huang, M. Andersson, M. Inbar, M. Lichinitser, I. Láng, U. Nitz, H. Iwata, C. Thomssen, C. Lohrisch, T.M. Suter, J. Rüschoff, T. Süto, V. Greatorex, C. Ward, C. Straehle, E. McFadden, M.S. Dolci and R.D. Gelber 2005. Trastuzumab after adjuvant chemotherapy in HER2-positive breast cancer. N. Engl. J. Med. 353, 1659-1672.

151. Kelly, E. and S.J. Russell 2007. History of oncolytic viruses: Genesis to genetic engineering. Molecular Therapy. 15, 651-659.

152. Chen, I. -., T. Aoki, Y.-. Huang, I. Hirono, T.-. Chen, J.-. Huang, G.-. Chang, C.-. Lo and H.-. Wang 2011. White spot syndrome virus induces metabolic changes resembling the warburg effect in shrimp hemocytes in the early stage of infection. J. Virol. 85, 12919-12928.

153. Delgado, T., P.A. Carroll, A.S. Punjabi, D. Margineantu, D.M. Hockenbery and M. Lagunoff 2010. Induction of the warburg effect by kaposi's sarcoma herpesvirus is required for the maintenance of latently infected endothelial cells. Proc. Natl. Acad. Sci. U. S. A. 107, 10696-10701.

154. Mazzon, M., N.E. Peters, C. Loenarz, E.M. Krysztofinska, S.W.J. Ember, B.J. Ferguson and G.L. Smith 2013. A mechanism for induction of a hypoxic response by vaccinia virus. Proc. Natl. Acad. Sci. U. S. A. 110, 12444-12449.

155. Darekar, S., K. Georgiou, M. Yurchenko, S.P. Yenamandra, G. Chachami, G. Simos, G. Klein and E. Kashuba 2012. Epstein-barr virus immortalization of human B-cells leads to stabilization of hypoxia-induced factor 1 alpha, congruent with the warburg effect. PLoS ONE. 7.

156. Guo, Z. S., V. Parimi, M.E. O'Malley, P. Thirunavukarasu, M. Sathaiah, F. Austin and D.L. Bartlett 2010. The combination of immunosuppression and carrier cells significantly enhances the efficacy of oncolytic poxvirus in the pre-immunized host. Gene Ther. 17, 1465-1475.

157. Parato, K. A., D. Senger, P.A.J. Forsyth and J.C. Bell 2005. Recent progress in the battle between oncolytic viruses and tumours. Nature Reviews Cancer. 5, 965-976.

158. Kirn, D. H. and S.H. Thorne 2009. Targeted and armed oncolytic poxviruses: A novel multi-mechanistic therapeutic class for cancer. Nature Reviews Cancer. 9, 64-71.

159. Elamany, R. and M. Cascallo 2009. Oncolytic viruses from the perspective of the immune system. Future Microbiology. 4, 527-536.

160. Breitbach, C. J., J.M. Paterson, C.G. Lemay, T.J. Falls, A. McGuire, K.A. Parato, D.F. Stojdl, M. Daneshmand, K. Speth, D. Kirn, A.J. McCart, H. Atkins and J.C. Bell 2007. Targeted inflammation during oncolytic virus therapy severely compromises tumor blood flow. Molecular Therapy. 15, 1686-1693.

161. Reddy, P. S., K.D. Burroughs, L.M. Hales, S. Ganesh, B.H. Jones, N. Idamakanti, C. Hay, S.S. Li, K.L. Skele, A.J. Vasko, J. Yang, D.N. Watkins, C.M. Rudin and P.L. Hallenbeck 2007. Seneca valley virus, a systemically deliverable oncolytic picornavirus, and the treatment of neuroendocrine cancers. J. Natl. Cancer Inst. 99, 1623-1633.

162. Stoeckel, J. and J.G. Hay 2006. Drug evaluation: Reolysin - wild-type reovirus as a cancer therapeutic. Curr. Opin. Mol. Ther. 8, 249-260.

163. Bischoff, J. R., D.H. Kirn, A. Williams, C. Heise, S. Horn, M. Muna, L. Ng, J.A. Nye, A. Sampson-Johannes, A. Fattaey and F. McCormick 1996. An adenovirus mutant that replicates selectively in p53-deficient human tumor cells. Science. 274, 373-376.

164. McCart, J. A., J.M. Ward, J. Lee, Y. Hu, H.R. Alexander, S.K. Libutti, B. Moss and D.L. Bartlett 2001. Systemic cancer therapy with a tumor-selective vaccinia virus mutant lacking thymidine kinase and vaccinia growth factor genes. Cancer Res. 61, 8751-8757.

165. Stojdl, D. F., B.D. Lichty, B.R. TenOever, J.M. Paterson, A.T. Power, S. Knowles, R. Marius, J. Reynard, L. Poliquin, H. Atkins, E.G. Brown, R.K. Durbin, J.E. Durbin, J. Hiscott and J.C. Bell 2003. VSV strains with defects in their ability to shutdown innate immunity are potent systemic anti-cancer agents. Cancer Cell. 4, 263-275.

166. Brun, J., D. McManus, C. Lefebvre, K. Hu, T. Falls, H. Atkins, J.C. Bell, J.A. McCart, D. Mahoney and D.F. Stojdl 2010. Identification of genetically modified maraba virus as an oncolytic rhabdovirus. Molecular Therapy. 18, 1440-1449.

167. Liu, B. L., M. Robinson, Z.-. Han, R.H. Branston, C. English, P. Reay, Y. McGrath, S.K. Thomas, M. Thornton, P. Bullock, C.A. Love and R.S. Coffin 2003. ICP34.5 deleted herpes simplex virus with enhanced oncolytic, immune stimulating, and anti-tumour properties. Gene Ther. 10, 292-303.

168. Russell, S. J., K.-. Peng and J.C. Bell 2012. Oncolytic virotherapy. Nat. Biotechnol. 30, 658-670.

169. Hill, A., P. Juovic, I. York, G. Russ, J. Bennink, J. Yewdell, H. Ploegh and D. Johnson 1995. Herpes simplex virus turns off the TAP to evade host immunity. 411-415.

170. Kaklamanis, L., A. Townsend, I. Doussis-Anagnostopoulou, N. Mortensen, A.L. Harris and K.C. Gatter 1994. Loss of major histocompatibility complex-encoded transporter associated with antigen presentation (TAP) in colorectal cancer. Am. J. Pathol. 145, 505-509.

171. Gostout, B. S., G.A. Poland, E.S. Calhoun, Y.R. Sohni, R.L. Giuntoli II, R.M. McGovern, J.A. Sloan, S.S. Cha and D.H. Persing 2003. TAP1, TAP2, and HLA-DR2 alleles are predictors of cervical cancer risk. Gynecol. Oncol. 88, 326-332.

172. Chen, H. L., D. Gabrilovich, R. Tampe, K.R. Girgis, S. Nadaf and D.P. Carbone 1996. A functionally defective allele of TAP1 results in loss of MHC class I antigen presentation in a human lung cancer. Nat. Genet. 13, 210-213.

173. Kamarashev, J., S. Ferrone, B. Seifert, R. Böni, F.O. Nestle, G. Burg and R. Dummer 2001. Tap1 down-regulation in primary melanoma lesions: An independent marker of poor prognosis. International Journal of Cancer. 95, 23-28.

174. Cassady, K. A., M. Gross and B. Roizman 1998. The second-site mutation in the herpes simplex virus recombinants lacking the y134.5 genes precludes shutoff of protein synthesis by blocking the phosphorylation of eIF-2a. J. Virol. 72, 7005-7011.

175. Kanai, R., C. Zaupa, D. Sgubin, S.J. Antoszczyk, R.L. Martuza, H. Wakimoto and S.D. Rabkin 2012. Effect of y34.5 deletions on oncolytic herpes simplex virus activity in brain tumors. J. Virol. 86, 4420-4431.

176. Wang, S., I.B. Rosenwald, M.J. Hutzler, G.A. Pihan, L. Savas, J.-. Chen and B.A. Woda 1999. Expression of the eukaryotic translation initiation factors 4E and 2a in non-hodgkin's lymphomas. Am. J. Pathol. 155, 247-255.

177. Wang, S., R.V. Lloyd, M.J. Hutzler, I.B. Rosenwald, M.S. Safran, N.A. Patwardhan and A. Khan 2001. Expression of eukaryotic translation initiation factors 4E and 2a correlates with the progression of thyroid carcinoma. Thyroid. 11, 1101-1107.

178. Rosenwald, I. B., S. Wang, L. Savas, B. Woda and J. Pullman 2003. Expression of translation initiation factor eIF-2a is increased in benign and malignant melanocytic and colonic epithelial neoplasms. Cancer. 98, 1080-1088.

179. Poppers, J., M. Mulvey, D. Khoo and I. Mohr 2000. Inhibition of PKR activation by the proline-rich RNA binding domain of the herpes simplex virus type 1 Us11 protein. J. Virol. 74, 11215-11221.

180. Dranoff, G. 2002. GM-CSF-based cancer vaccines. Immunol. Rev. 188, 147-154.

181. Aufderklamm, S., T. Todenhöfer, G. Gakis, S. Kruck, J. Hennenlotter, A. Stenzl and C. Schwentner 2012. Thymidine kinase and cancer monitoring. Cancer Lett. 316, 6-10.

182. Parato, K. A., C.J. Breitbach, F. Le Boeuf, J. Wang, C. Storbeck, C. Ilkow, J.-. Diallo, T. Falls, J. Burns, V. Garcia, F. Kanji, L. Evgin, K. Hu, F. Paradis, S. Knowles, T.-. Hwang, B.C. Vanderhyden, R. Auer, D.H. Kirn and J.C. Bell 2012. The oncolytic poxvirus JX-594 selectively replicates in and destroys cancer cells driven by genetic pathways commonly activated in cancers. Molecular Therapy. 20, 749-758.

183. Martin, S., D. T. Harris and J. Shisler 2012. The C11R gene, which encodes the vaccinia virus growth factor, is partially responsible for MVA-induced NF-κB and ERK2 activation. 9629-9639.

184. Shchelkunov, S. N. 1995. Functional organization of variola major and vaccinia virus genomes. Virus Genes. 10, 53-71.

185. McGeoch, D. J., M.A. Dalrymple, A.J. Davison, A. Dolan, M.C. Frame, D. McNab, L.J. Perry, J.E. Scott and P. Taylor 1988. The complete DNA sequence of the long unique region in the genome of herpes simplx virus type 1. J. Gen. Virol. 69, 1531-1574.

186. Villarreal, L. P., M. Breindl and J.J. Holland 1976. Determination of molar ratios of vesicular stomatitis virus induced RNA species in BHK21 cells. Biochemistry (N. Y.). 15, 1663-1667.

187. Thomas, D., W.W. Newcomb and J.C. Brown 1985. Mass and molecular composition of vesicular stomatitis virus: A scanning transmission electron microscopy analysis. J. Virol. 54, 598-607.

188. Whelan, S. P. J. and G.W. Wertz 2002. Transcription and replication initiate at separate sites on the vesicular stomatitis virus genome. Proc. Natl. Acad. Sci. U. S. A. 99, 9178-9183.

189. van den Pol, A. N. and J.N. Davis 2013. Highly attenuated recombinant vesicular stomatitis virus VSV-12'GFP displays immunogenic and oncolytic activity. J. Virol. 87, 1019-1034.

190. Von Kobbe, C., J.M.A. Van Deursen, J.P. Rodrigues, D. Sitterlin, A. Bachi, X. Wu, M. Wilm, M. Carmo-Fonseca and E. Izaurralde 2000. Vesicular stomatitis virus matrix protein inhibits host cell gene expression by targeting the nucleoporin Nup98. Mol. Cell. 6, 1243-1252.

191. Faria, P. A., P. Chakraborty, A. Levay, G.N. Barber, H.J. Ezelle, J. Enninga, C. Arana, J. Van Deursen and B.M.A. Fontoura 2005. VSV disrupts the Rae1/mrnp41 mRNA nuclear export pathway. Mol. Cell. 17, 93-102.

192. Enninga, J., D.E. Levy, G. Blobel and B.M.A. Fontoura 2002. Role of nucleoporin induction in releasing an mRNA nuclear export block. Science. 295, 1523-1525.

193. Carneiro, F. A., M.L. Bianconi, G. Weissmüller, F. Stauffer and A.T. Da Poian 2002. Membrane recognition by vesicular stomatitis virus involves enthalpy-driven protein-lipid interactions. J. Virol. 76, 3756-3764.

194. Sun, X., V.K. Yau, B.J. Briggs and G.R. Whittaker 2005. Role of clathrin-mediated endocytosis during vesicular stomatitis virus entry into host cells. Virology. 338, 53-60.

195. McMahon, H. T. and E. Boucrot 2011. Molecular mechanism and physiological functions of clathrin-mediated endocytosis. Nature Reviews Molecular Cell Biology. 12, 517-533.

196. Noyce, R. S. and C.D. Richardson 2012. Nectin 4 is the epithelial cell receptor for measles virus. Trends Microbiol. 20, 429-239.

197. Sugiyama, T., M. Yoneda, T. Kuraishi, S. Hattori, Y. Inoue, H. Sato and C. Kai 2013. Measles virus selectively blind to signaling lymphocyte activation molecule as a novel oncolytic virus for breast cancer treatment. Gene Ther. 20, 338-347.

198. Escobar-Zarate, D., Y.-. Liu, L. Suksanpaisan, S.J. Russell and K.-. Peng 2013. Overcoming cancer cell resistance to VSV oncolysis with JAK1/2 inhibitors. Cancer Gene Ther. 20, 582-589.

199. Paglino, J. C. and d.P. van 2011. Vesicular stomatitis virus has extensive oncolytic activity against human sarcomas: Rare resistance is overcome by blocking interferon pathways. J. Virol. 85, 9346-9358.

200. Moerdyk-Schauwecker, M., N.R. Shah, A.M. Murphy, E. Hastie, P. Mukherjee and V.Z. Grdzelishvili 2013. Resistance of pancreatic cancer cells to oncolytic vesicular stomatitis virus: Role of type I interferon signaling. Virology. 436, 221-234.

201. Stojdl, D. F., B. Lichty, S. Knowles, R. Marius, H. Atkins, N. Sonenberg and J.C. Bell 2000. Exploiting tumor-specific defects in the interferon pathway with a previously unknown oncolytic virus. Nat. Med. 6, 821-825.

202. Liu, Y. -., L. Suksanpaisan, M.B. Steele, S.J. Russell and K.-. Peng 2013. Induction of antiviral genes by the tumor microenvironment confers resistance to virotherapy. Scientific Reports. 3.

203. LeBlanc, A. K., S. Naik, G.D. Galyon, N. Jenks, M. Steele, K.W. Peng, M.J. Federspiel, R. Donnell and S.J. Russell 2013. Safety studies on intravenous administration of oncolytic recombinant vesicular stomatitis virus in purpose-bred beagle dogs. Hum Gene Ther Clin Dev. 24(4), 174-181.

204. Leib, D. A., T.E. Harrison, K.M. Laslo, M.A. Machalek, N.J. Moorman and H.W. Virgin 1999. Interferons regulate the phenotype of wild-type and mutant herpes simplex viruses in vivo. J. Exp. Med. 189, 663-672.

205. Gale Jr., M. and M.G. Katze 1998. Molecular mechanisms of interferon resistance mediated by viral-directed inhibition of PKR, the interferon-induced protein kinase. Pharmacology and Therapeutics. 78, 29-46.

206. Rouyez, M. -., M. Lestingi, M. Charon, S. Fichelson, A. Buzyn and I. Dusanter-Fourt 2005. IFN regulatory factor-2 cooperates with STAT1 to regulate transporter associated with antigen processing-1 promoter activity. Journal of Immunology. 174, 3948-3958.

207. Ikeda, K., T. Ichikawa, H. Wakimoto, J.S. Silver, T.S. Deisboeck, D. Finkelstein, G.R. Harsh IV, D.N. Louis, R.T. Bartus, F.H. Hochberg and E. Antonio Chiocca 1999. Oncolytic virus therapy of multiple tumors in the brain requires suppression of innate and elicited antiviral responses. Nat. Med. 5, 881-887.

208. Ikeda, K., H. Wakimoto, T. Ichikawa, S. Jhung, F.H. Hochberg, D.N. Louis and E.A. Chiocca 2000. Complement depletion facilitates the infection of multiple brain tumors by an intravascular, replication-conditional herpes simplex virus mutant. J. Virol. 74, 4765-4775.

209. Sampath, P., J. Li, W. Hou, H. Chen, D.L. Bartlett and S.H. Thorne 2013. Crosstalk between immune cell and oncolytic vaccinia therapy enhances tumor trafficking and antitumor effects. Molecular Therapy. 21, 620-628.

210. Alcamí, A., J.A. Symons and G.L. Smith 2000. The vaccinia virus soluble alpha/beta interferon (IFN) receptor binds to the cell surface and protects cells from the antiviral effects of IFN. J. Virol. 74, 11230-11239.

211. Heo, J., T. Reid, L. Ruo, C.J. Breitbach, S. Rose, M. Bloomston, M. Cho, H.Y. Lim, H.C. Chung, C.W. Kim, J. Burke, R. Lencioni, T. Hickman, A. Moon, Y.S. Lee, M.K. Kim, M. Daneshmand, K. Dubois, L. Longpre, M. Ngo, C. Rooney, J.C. Bell, B.-. Rhee, R. Patt, T.-. Hwang and D.H. Kirn 2013. Randomized dose-finding clinical trial of oncolytic immunotherapeutic vaccinia JX-594 in liver cancer. Nat. Med. 19, 329-336.

212. Nguyen, T. L. -., H. Abdelbary, M. Arguello, C. Breitbach, S. Leveille, J.-. Diallo, A. Yasmeen, T.A. Bismar, D. Kirn, T. Falls, V.E. Snoulten, B.C. Vanderhyden, J. Werier, H. Atkins, M.J.V. VÃ¤hÃ¤-Koskela, D.F. Stojdl, J.C. Bell and J. Hiscott 2008. Chemical targeting of the innate antiviral response by histone deacetylase inhibitors renders refractory cancers sensitive to viral oncolysis. Proc. Natl. Acad. Sci. U. S. A. 105, 14981-14986.

213. Diallo, J. -., F.L. Boeuf, F. Lai, J. Cox, M. Vaha-Koskela, H. Abdelbary, H. MacTavish, K. Waite, T. Falls, J. Wang, R. Brown, J.E. Blanchard, E.D. Brown, D.H. Kirn, J. Hiscott, H.

Atkins, B.D. Lichty and J.C. Bell 2010. A high-throughput pharmacoviral approach identifies novel oncolytic virus sensitizers. Molecular Therapy. 18, 1123-1129.

214. Jha, B. K., B. Dong, C.T. Nguyen, I. Polyakova and R.H. Silverman 2013. Suppression of antiviral innate immunity by sunitinib enhances oncolytic virotherapy. Molecular Therapy. 21, 1749-1757.

215. Mader, E. K., Y. Maeyama, Y. Lin, G.W. Butler, H.M. Russell, E. Galanis, S.J. Russell, A.B. Dietz and K.-. Peng 2009. Mesenchymal stem cell carriers protect oncolytic measles viruses from antibody neutralization in an orthotopic ovarian cancer therapy model. Clinical Cancer Research. 15, 7246-7255.

216. Fisher, K. D. and L.W. Seymour 2010. HPMA copolymers for masking and retargeting of therapeutic viruses. Adv. Drug Deliv. Rev. 62, 240-245.

217. Magge, D., Z.S. Guo, M.E. O'Malley, L. Francis, R. Ravindranathan and D.L. Bartlett 2013. Inhibitors of C5 complement enhance vaccinia virus oncolysis. Cancer Gene Ther. 20, 342-350.

218. Le Boeuf, F., J.-. Diallo, J.A. McCart, S. Thorne, T. Falls, M. Stanford, F. Kanji, R. Auer, C.W. Brown, B.D. Lichty, K. Parato, H. Atkins, D. Kirn and J.C. Bell 2010. Synergistic interaction between oncolytic viruses augments tumor killing. Molecular Therapy. 18, 888-895.

219. Greco, O. and G.U. Dachs 2001. Gene directed enzyme/prodrug therapy of cancer: Historical appraisal and future prospectives. J. Cell. Physiol. 187, 22-36.

220. Dias, J. D., I. Liikanen, K. Guse, J. Foloppe, M. Sloniecka, I. Diaconu, V. Rantanen, M. Eriksson, T. Hakkarainen, M. Lusky, P. Erbs, S. Escutenaire, A. Kanerva, S. Pesonen, V. Cerullo and A. Hemminki 2010. Targeted chemotherapy for head and neck cancer with a chimeric oncolytic adenovirus coding for bifunctional suicide protein FCU1. Clinical Cancer Research. 16, 2540-2549.

221. Beug, S., V. Tang, E. LaCasse, H. Cheung, C. Beauregard, J. Brun, J. Nuyens, N. Earl, M. St-Jean, J. Holbrook, H. Dastidar, D. Mahoney, C. Ilkow, F. Le Boeuf, J. Bell and R. Korneluk 2014. Smac mimetics and innate immune stimuli synergize to promote tumor death. Nature Biotechnology. 32, 182-190.

222. Hodgkin, A. L., A.F. Huxley and B. Katz 1952. Measurement of current-voltage relations in the membrane of the giant axon of loligo. J. Physiol. (Lond.). 116, 424-448.

223. Hodgkin, A. L. and A.F. Huxley 1952. The components of membrane conductance in the giant axon of loligo. J. Physiol. (Lond.). 116, 473-496.

224. HODGKIN, A. L. and A.F. HUXLEY 1952. A quantitative description of membrane current and its application to conduction and excitation in nerve. J. Physiol. (Lond.). 117, 500-544.

225. Wodarz, D., M.A. Nowak and C.R.M. Bangham 1999. The dynamics of HTLV-I and the CTL response. Immunol. Today. 20, 220-227.

226. Wodarz, D. 2001. Viruses as antitumor weapons: Defining conditions for tumor remission. Cancer Res. 61, 3501-3507.

227. Dingli, D., M.D. Cascino, K. JosiÄ‡, S.J. Russell and Z. Bajzer 2006. Mathematical modeling of cancer radiovirotherapy. Math. Biosci. 199, 55-78.

228. Wodarz, D. and N. Komarova 2009. Towards predictive computational models of oncolytic virus therapy: Basis for experimental validation and model selection. PLoS ONE. 4.

229. Crivelli, J. J., J. Földes, P.S. Kim and J.R. Wares 2012. A mathematical model for cell cycle-specific cancer virotherapy. Journal of Biological Dynamics. 6, 104-120.

230. Nowak, M. A., S. Bonhoeffer, A.M. Hill, R. Boehme, H.C. Thomas and H. Mcdade 1996. Viral dynamics in hepatitis B virus infection. Proc. Natl. Acad. Sci. U. S. A. 93, 4398-4402.

231. Nowak, M. A. and C.R.M. Bangham 1996. Population dynamics of immune responses to persistent viruses. Science. 272, 74-79.

232. Bonhoeffer, S., R.M. May, G.M. Shaw and M.A. Nowak 1997. Virus dynamics and drug therapy. Proc. Natl. Acad. Sci. U. S. A. 94, 6971-6976.

233. Nowak, M. A., S. Bonhoeffer, G.M. Shaw and R.M. May 1997. Anti-viral drug treatment: Dynamics of resistance in free virus and infected cell populations. J. Theor. Biol. 184, 203-217.

234. Cheng, A. A. and T. K. Lu 2012. Synthetic biology: An emerging engineering discipline. 155-178.

235. Naik, S. and S.J. Russell 2009. Engineering oncolytic viruses to exploit tumor specific defects in innate immune signaling pathways. Expert Opinion on Biological Therapy. 9, 1163-1176.

236. Russell, S. J. and K. -. Peng 2007. Viruses as anticancer drugs. 326-333.

237. Colina, R., M. Costa-Mattioli, R. J. O. Dowling, M. Jaramillo, L. -. Tai, C. J. Breitbach, Y. Martineau, O. Larsson, L. Rong, Y. V. Svitkin, A. P. Makrigiannis, J. C. Bell and N. Sonenberg 2008. Translational control of the innate immune response through IRF-7. 323-328.

238. Haralambieva, I., I. Iankov, K. Hasegawa, M. Harvey, S. J. Russell and K. -. Peng 2007. Engineering oncolytic measles virus to circumvent the intracellular innate immune response. 588-597.

239. Le Bœuf, F. and J.C. Bell 2010. United virus: The oncolytic tag-team against cancer! Cytokine and Growth Factor Reviews. 21, 205-211.

240. Wein, L. M., J.T. Wu and D.H. Kirn 2003. Validation and analysis of a mathematical model of a replication-competent oncolytic virus for cancer treatment: Implications for virus design and delivery. Cancer Res. 63, 1317-1324.

241. Tao, Y. and Q. Guo 2005. The competitive dynamics between tumor cells, a replication-competent virus and an immune response. J. Math. Biol. 51, 37-74.

242. Komarova, N. L. and D. Wodarz 2010. ODE models for oncolytic virus dynamics. J. Theor. Biol. 263, 530-543.

243. Breitbach, C. J., J. Burke, D. Jonker, J. Stephenson, A.R. Haas, L.Q.M. Chow, J. Nieva, T.-. Hwang, A. Moon, R. Patt, A. Pelusio, F. Le Boeuf, J. Burns, L. Evgin, N. De Silva, S. Cvancic, T. Robertson, J.-. Je, Y.-. Lee, K. Parato, J.-. Diallo, A. Fenster, M. Daneshmand, J.C. Bell and D.H. Kirn 2011. Intravenous delivery of a multi-mechanistic cancer-targeted oncolytic poxvirus in humans. Nature. 477, 99-104.

244. Breitbach, C. J., T. Reid, J. Burke, J.C. Bell and D.H. Kirn 2010. Navigating the clinical development landscape for oncolytic viruses and other cancer therapeutics: No shortcuts on the road to approval. Cytokine and Growth Factor Reviews. 21, 85-89.

245. Crompton, A. M. and D.H. Kirn 2007. From ONYX-015 to armed vaccinia viruses: The education and evolution of oncolytic virus development. Current Cancer Drug Targets. 7, 133-139.

246. Symons, J. A., A. Alcami and G.L. Smith 1995. Vaccinia virus encodes a soluble type I interferon receptor of novel structure and broad species specificity. Cell. 81, 551-560.

247. Buller, R. M. L., G.L. Smith, K. Cremer, A.L. Notkins and B. Moss 1985. Decreased virulence of recombinant vaccinia virus expression vectors is associated with a thymidine kinase-negative phenotype. Nature. 317, 813-815.

248. Guidotti, L. G., R. Rochford, J. Chung, M. Shapiro, R. Purcell and F.V. Chisari 1999. Viral clearance without destruction of infected cells during acute HBV infection. Science. 284(5415), 825-829.

249. Goujon, C. and M.H. Malim 2010. Characterization of the alpha interferon-induced postentry block to HIV-1 infection in primary human macrophages and T cells. J. Virol. 84, 9254-9266.

250. Burdeinick-Kerr, R., D. Govindarajan and D.E. Griffin 2009. Noncytolytic clearance of sindbis virus infection from neurons by gamma interferon is dependent on Jak/Stat signaling. J. Virol. 83, 3429-3435.

251. Power, A. T., J. Wang, T.J. Falls, J.M. Paterson, K.A. Parato, B.D. Lichty, D.F. Stojdl, P.A.J. Forsyth, H. Atkins and J.C. Bell 2007. Carrier cell-based delivery of an oncolytic virus circumvents antiviral immunity. Molecular Therapy. 15, 123-130.

252. Wu, Y., X. Lun, H. Zhou, L. Wang, B. Sun, J.C. Bell, J.W. Barrett, G. McFadden, J.A. Biegel, D.L. Senger and P.A. Forsyth 2008. Oncolytic efficacy of recombinant vesicular stomatitis virus and myxoma virus in experimental models of rhabdoid tumors. Clinical Cancer Research. 14, 1218-1227.

253. Ferrell Jr., J. E. and E.M. Machleder 1998. The biochemical basis of an all-or-none cell fate switch in xenopus oocytes. Science. 280, 895-898.

254. Alcami, A. and G.L. Smith 1995. Vaccinia, cowpox, and camelpox viruses encode soluble gamma interferon receptors with novel broad species specificity. J. Virol. 69, 4633-4639.

255. Alcami, A., J.A. Symons, P.D. Collins, T.J. Williams and G.L. Smith 1998. Blockade of chemokine activity by a soluble chemokine binding protein from vaccinia virus. Journal of Immunology. 160, 624-633.

256. Colamonici, O. R., P. Domanski, S.M. Sweitzer, A. Larner and R.M.L. Buller 1995. Vaccinia virus B18R gene encodes a type I interferon-binding protein that blocks interferon α transmembrane signaling. J. Biol. Chem. 270, 15974-15978.

257. Vančovâ, I., C. La Bonnardiere and P. Kontsek 1998. Vaccinia virus protein B18R inhibits the activity and cellular binding of the novel type interferon-δ. J. Gen. Virol. 79, 1647-1649.

258. Park, B. -., T. Hwang, T.-. Liu, D.Y. Sze, J.-. Kim, H.-. Kwon, S.Y. Oh, S.-. Han, J.-. Yoon, S.-. Hong, A. Moon, K. Speth, C. Park, Y.-. Ahn, M. Daneshmand, B.G. Rhee, H.M. Pinedo, J.C. Bell and D.H. Kirn 2008. Use of a targeted oncolytic poxvirus, JX-594, in patients with refractory primary or metastatic liver cancer: A phase I trial. The Lancet Oncology. 9, 533-542.

259. Mineta, T., S.D. Rabkin, T. Yazaki, W.D. Hunter and R.L. Martuza 1995. Attenuated multi-mutated herpes simplex virus-1 for the treatment of malignant gliomas. Nat. Med. 1, 938-943.

260. Lin, S. -., S.P. Gao, D.L. Price, S. Li, T.-. Chou, P. Singh, Y.-. Huang, Y. Fong and R.J. Wong 2008. Synergy of a herpes oncolytic virus and paclitaxel for anaplastic thyroid cancer. Clinical Cancer Research. 14, 1519-1528.

261. Kelly, K., S. Nawrocki, A. Mita, M. Coffey, F.J. Giles and M. Mita 2009. Reovirus-based therapy for cancer. Expert Opinion on Biological Therapy. 9, 817-830.

262. Halldén, G. and G. Portella 2012. Oncolytic virotherapy with modified adenoviruses and novel therapeutic targets. Expert Opinion on Therapeutic Targets. 16, 945-958.

263. Saloura, V., L.-.S. Wang, Z.G. Fridlender, J. Sun, G. Cheng, V. Kapoor, D.H. Sterman, R.N. Harty, A. Okumura, G.N. Barber, R.G. Vile, M.J. Federspiel, S.J. Russell, L. Litzky and S.M. Albelda 2010. Evaluation of an attenuated vesicular stomatitis virus vector expressing interferon-β for use in malignant pleural mesothelioma: Heterogeneity in interferon responsiveness defines potential efficacy. Hum. Gene Ther. 21, 51-64.

264. Emig, D., N. Salomonis, J. Baumbach, T. Lengauer, B.R. Conklin and M. Albrecht 2010. AltAnalyze and DomainGraph: Analyzing and visualizing exon expression data. Nucleic Acids Res. 38, W755-W762.

265. Eden, E., R. Navon, I. Steinfeld, D. Lipson and Z. Yakhini 2009. GOrilla: A tool for discovery and visualization of enriched GO terms in ranked gene lists. BMC Bioinformatics. 10.

266. Samarajiwa, S. A., S. Forster, K. Auchettl and P.J. Hertzog 2009. INTERFEROME: The database of interferon regulated genes. Nucleic Acids Res. 37, D852-D857.

267. Ilkow, C., J. Bell and J. Diallo 2013. From scourge to cure: Tumour-selective viral pathogenesis as a new strategy against cancer. PLoS Pathogens. (In press).

268. Ottolino-Perry, K., J.-. Diallo, B.D. Lichty, J.C. Bell and J. Andrea McCart 2010. Intelligent design: Combination therapy with oncolytic viruses. Molecular Therapy. 18, 251-263.

269. Obuchi, M., M. Fernandez and G.N. Barber 2003. Development of recombinant vesicular stomatitis viruses that exploit defects in host defense to augment specific oncolytic activity. J. Virol. 77, 8843-8856.

270. Le Bœuf, F., C. Batenchuk, M. Vähä-Koskela, S. Breton, D. Roy, C. Lemay, J. Cox, H. Abdelbary, T. Falls, G. Waghray, H. Atkins, D. Stojdl, J.-. Diallo, M. Kærn and J.C. Bell 2013. Model-based rational design of an oncolytic virus with improved therapeutic potential. Nature Communications. 4.

271. Chang, H. -., M. Paulson, M. Holko, C.M. Rice, B.R.G. Williams, I. Marié and D.E. Levy 2004. Induction of interferon-stimulated gene expression and antiviral responses require protein deacetylase activity. Proc. Natl. Acad. Sci. U. S. A. 101, 9578-9583.

272. Connolly, D. C., R. Bao, A.Y. Nikitin, K.C. Stephens, T.W. Poole, X. Hua, S.S. Harris, B.C. Vanderhyden and T.C. Hamilton 2003. Female mice chimeric for expression of the

simian virus 40 TAg under control of the MISIIR promoter develop epithelial ovarian cancer. Cancer Res. 63, 1389-1397.

273. Platanias, L. C. 2005. Mechanisms of type-I- and type-II-interferon-mediated signalling. Nature Reviews Immunology. 5, 375-386.

274. Havell, E. A. and J. Vilcek 1975. Inhibition of interferon secretion by vinblastine. J. Cell Biol. 64, 716-719.

275. Ito, Y., Y. Nishiyama, K. Shimokata, Y. Kimura, I. Nagata and A. Kunii 1976. The effects of cytochalasin and colchicine on interferon production. J. Gen. Virol. 33, 1-5.

276. Li, Z., G.S. Davis, C. Mohr, M. Nain and D. Gemsa 1996. Inhibition of LPS-induced tumor necrosis factor-a production by colchicine and other microtubule disrupting drugs. Immunobiology. 195, 624-639.

277. Lacy, P. E., S.L. Howell, D.A. Young and C.J. Fink 1968. New hypothesis of insulin secretion. Nature. 219, 1177-1179.

278. Le Marchand, Y., A. Singh, F. Assimacopoulos-Jeannet, L. Orci, C. Rouiller and B. Jeanrenaud 1973. A role for the microtubular system in the release of very low density lipoproteins by perfused mouse livers. J. Biol. Chem. 248, 6862-6870.

279. Zurier, R. B., S. Hoffstein and G. Weissmann 1973. Mechanisms of lysosomal enzyme release from human leukocytes. I. effect of cyclic nucleotides and colchicine. J. Cell Biol. 58, 27-41.

280. Williams, J. A. and J. Wolff 1972. Colchicine-binding protein and the secretion of thyroid hormone. J. Cell Biol. 54, 157-165.

281. Conrad, D. P., J. Tsang, M. Maclean, J.-. Diallo, F. Le Boeuf, C.G. Lemay, T.J. Falls, K.A. Parato, J.C. Bell and H.L. Atkins 2013. Leukemia cell-rhabdovirus vaccine: Personalized immunotherapy for acute lymphoblastic leukemia. Clinical Cancer Research. 19, 3832-3843.

282. Das, S. C., D. Nayak, Y. Zhou and A.K. Pattnaik 2006. Visualization of intracellular transport of vesicular stomatitis virus nucleocapsids in living cells. J. Virol. 80, 6368-6377.

283. Smith, G. L., A. Vanderplasschen and M. Law 2002. The formation and function of extracellular enveloped vaccinia virus. J. Gen. Virol. 83, 2915-2931.

284. Herrero-Martínez, E., K.L. Roberts, M. Hollinshead and G.L. Smith 2005. Vaccinia virus intracellular enveloped virions move to the cell periphery on microtubules in the absence of the A36R protein. J. Gen. Virol. 86, 2961-2968.

285. Passer, B. J., T. Cheema, S. Wu, C.-. Wu, S.D. Rabkin and R.L. Martuza 2013. Combination of vinblastine and oncolytic herpes simplex virus vector expressing IL-12 therapy increases antitumor and antiangiogenic effects in prostate cancer models. Cancer Gene Ther. 20, 17-24.

286. Pestka, S. 2007. The interferons: 50 years after their discovery, there is much more to learn. J. Biol. Chem. 282, 20047-20051.

287. Zhou, B. and M. Rabinovitch 1998. Microtubule involvement in translational regulation of fibronectin expression by light chain 3 of microtubule-associated protein 1 in vascular smooth muscle cells. Circ. Res. 83, 481-489.

288. Terkeltaub, R. A. 2009. Colchicine update: 2008. Semin. Arthritis Rheum. 38, 411-419.

289. Havercroft, J. C., R.A. Quinlan and K. Gull 1981. Binding of parbendazole to tubulin and its influence on microtubules in tissue-culture cells as revealed by immunofluorescence microscopy. J. Cell. Sci. Vol. 49, 195-204.

290. Verma, S., D. Miles, L. Gianni, I.E. Krop, M. Welslau, J. Baselga, M. Pegram, D.-. Oh, V. Diéras, E. Guardino, L. Fang, M.W. Lu, S. Olsen and K. Blackwell 2012. Trastuzumab emtansine for HER2-positive advanced breast cancer. N. Engl. J. Med. 367, 1783-1791.

291. Lemay, C. G., J.L. Rintoul, A. Kus, J.M. Paterson, V. Garcia, T.J. Falls, L. Ferreira, B.W. Bridle, D.P. Conrad, V.A. Tang, J.-. Diallo, R. Arulanandam, F. Le Boeuf, K. Garson, B.C. Vanderhyden, D.F. Stojdl, B.D. Lichty, H.L. Atkins, K.A. Parato, J.C. Bell and R.C. Auer 2012. Harnessing oncolytic virus-mediated antitumor immunity in an infected cell vaccine. Molecular Therapy. 20, 1791-1799.

292. Diallo, J. -., M. Vähä-Koskela, F. Le Boeuf and J. Bell 2012. Propagation, purification, and in vivo testing of oncolytic vesicular stomatitis virus strains. 127-140.

293. Vultur, A., J. Cao, R. Arulanandam, J. Turkson, R. Jove, P. Greer, A. Craig, B. Elliott and L. Raptis 2004. Cell-to-cell adhesion modulates Stat3 activity in normal and breast carcinoma cells. Oncogene. 23, 2600-2616.

294. Pfaffl, M. W. 2001. A new mathematical model for relative quantification in real-time RT-PCR. Nucleic Acids Res. 29.

295. Hanahan, D. and L. Coussens 2012. Accessories to the crime: Functions of cells recruited to the tumor microenvironment. Cancer Cell. 21, 309-322.

296. Cirri, P. and P. Chiarugi 2011. Cancer associated fibroblasts: The dark side of the coin. Am J Cancer Res. 1(4), 482-497.

297. Lisanti, M. P., U.E. Martinez-Outschoorn and F. Sotgia 2013. Oncogenes induce the cancer-associated fibroblast phenotype: Metabolic symbiosis and "fibroblast addiction" are new therapeutic targets for drug discovery. Cell Cycle. 12, 2723-2732.

298. Nakasone, E., H. Askautrud, T. Kees, J.-. Park, V. Plaks, A. Ewald, M. Fein, M. Rasch, Y.-. Tan, J. Qiu, J. Park, P. Sinha, M. Bissell, E. Frengen, Z. Werb and M. Egeblad 2012. Imaging tumor-stroma interactions during chemotherapy reveals contributions of the microenvironment to resistance. Cancer Cell. 21, 488-503.

299. Hwang, R. F., T. Moore, T. Arumugam, V. Ramachandran, K.D. Amos, A. Rivera, B. Ji, D.B. Evans and C.D. Logsdon 2008. Cancer-associated stromal fibroblasts promote pancreatic tumor progression. Cancer Res. 68, 918-926.

300. Straussman, R., T. Morikawa, K. Shee, M. Barzily-Rokni, Z.R. Qian, J. Du, A. Davis, M.M. Mongare, J. Gould, D.T. Frederick, Z.A. Cooper, P.B. Chapman, D.B. Solit, A. Ribas, R.S. Lo, K.T. Flaherty, S. Ogino, J.A. Wargo and T.R. Golub 2012. Tumour micro-environment elicits innate resistance to RAF inhibitors through HGF secretion. Nature. 487, 500-504.

301. Wilson, T. R., J. Fridlyand, Y. Yan, E. Penuel, L. Burton, E. Chan, J. Peng, E. Lin, Y. Wang, J. Sosman, A. Ribas, J. Li, J. Moffat, D.P. Sutherlin, H. Koeppen, M. Merchant, R. Neve and J. Settleman 2012. Widespread potential for growth-factor-driven resistance to anticancer kinase inhibitors. Nature. 487, 505-509.

302. Ronnov-Jessen, L. and O.W. Petersen 1993. Induction of alpha-smooth muscle actin by transforming growth factor-beta 1 in quiescent human breast gland fibroblasts. implications for myofibroblast generation in breast neoplasia. Lab Invest. 68(6), 696-707.

303. Tsukada, T., M.A. McNutt, R. Ross and A.M. Gown 1987. HHF35, a muscle actin-specific monoclonal antibody. II. reactivity in normal, reactive, and neoplastic human tissues. Am. J. Pathol. 127, 389-402.

304. Azzarone, B., M. Mareel, C. Billard, P. Scemama, C. Chaponnier and A. Macieira-Coelho 1984. Abnormal properties of skin fibroblasts from patients with breast cancer. International Journal of Cancer. 33, 759-764.

305. Brouty-Boye, D., H. Raux, B. Azzarone, A. Tamboise, E. Tamboise, S. Beranger, V. Magnien, I. Pihan, L. Zardi and L. Israel 1991. Fetal myofibroblast-like cells isolated from post-radiation fibrosis in human breast cancer. International Journal of Cancer. 47, 697-702.

306. Löhr, M., C. Schmidt, J. Ringel, M. Kluth, P. Müller, H. Nizze and R. Jesnowski 2001. Transforming growth factor-ß1 induces desmoplasia in an experimental model of human pancreatic carcinoma. Cancer Res. 61, 550-555.

307. Erez, N., M. Truitt, P. Olson and D. Hanahan 2010. Cancer-associated fibroblasts are activated in incipient neoplasia to orchestrate tumor-promoting inflammation in an NF-κB-dependent manner. 135-147.

308. Franco, O. E., A.K. Shaw, D.W. Strand and S.W. Hayward 2010. Cancer associated fibroblasts in cancer pathogenesis. Seminars in Cell and Developmental Biology. 21, 33-39.

309. Räsänen, K. and A. Vaheri 2010. Activation of fibroblasts in cancer stroma. Exp. Cell Res. 316, 2713-2722.

310. Spaeth, E. L., J.L. Dembinski, A.K. Sasser, K. Watson, A. Klopp, B. Hall, M. Andreeff and F. Marini 2009. Mesenchymal stem cell transition to tumor-associated fibroblasts contributes to fibrovascular network expansion and tumor progression. PLoS ONE. 4.

311. Ablasser, A., F. Bauernfeind, G. Hartmann, E. Latz, K.A. Fitzgerald and V. Hornung 2009. RIG-I-dependent sensing of poly(dA:DT) through the induction of an RNA polymerase III-transcribed RNA intermediate. Nat. Immunol. 10, 1065-1072.

312. Chiu, Y. -., J.B. MacMillan and Z.J. Chen 2009. RNA polymerase III detects cytosolic DNA and induces type I interferons through the RIG-I pathway. Cell. 138, 576-591.

313. Yoneyama, M., M. Kikuchi, T. Natsukawa, N. Shinobu, T. Imaizumi, M. Miyagishi, K. Taira, S. Akira and T. Fujita 2004. The RNA helicase RIG-I has an essential function in double-stranded RNA-induced innate antiviral responses. Nat. Immunol. 5, 730-737.

314. Hou, F., L. Sun, H. Zheng, B. Skaug, Q.-. Jiang and Z.J. Chen 2011. MAVS forms functional prion-like aggregates to activate and propagate antiviral innate immune response. Cell. 146, 448-461.

315. Sun, Q., L. Sun, H.-. Liu, X. Chen, R.B. Seth, J. Forman and Z.J. Chen 2006. The specific and essential role of MAVS in antiviral innate immune responses. Immunity. 24, 633-642.

316. Tamura, T., H. Yanai, D. Savitsky and T. Taniguchi 2008. The IRF family transcription factors in immunity and oncogenesis. 535-584.

317. Erkan, M., S. Hausmann, C.W. Michalski, A.A. Fingerle, M. Dobritz, J. Kleeff and H. Friess 2012. The role of stroma in pancreatic cancer: Diagnostic and therapeutic implications. Nature Reviews Gastroenterology and Hepatology. 9, 454-467.

318. Gonda, T. A., A. Varro, T.C. Wang and B. Tycko 2010. Molecular biology of cancer-associated fibroblasts: Can these cells be targeted in anti-cancer therapy? Seminars in Cell and Developmental Biology. 21, 2-10.

319. Ijichi, H., A. Chytil, A.E. Gorska, M.E. Aakre, B. Bierie, M. Tada, D. Mohri, K. Miyabayashi, Y. Asaoka, S. Maeda, T. Ikenoue, K. Tateishi, C.V.E. Wright, K. Koike, M.

Omata and H.L. Moses 2011. Inhibiting Cxcr2 disrupts tumor-stromal interactions and improves survival in a mouse model of pancreatic ductal adenocarcinoma. J. Clin. Invest. 121, 4106-4117.

320. Li, X., C.-. Liang, J.-. Song and X.-. Chen 2008. The ORF 113 of helicoverpa armigera single nucleopolyhedrovirus encodes a functional fibroblast growth factor. Virol. Sin. 23, 321-329.

321. Katsuma, S., S. Horie, T. Daimon, M. Iwanaga and T. Shimada 2006. In vivo and in vitro analyses of a bombyx mori nucleopolyhedrovirus mutant lacking functional vfgf. Virology. 355, 62-70.

322. Detvisitsakun, C., E.L. Hutfless, M.F. Berretta and A.L. Passarelli 2006. Analysis of a baculovirus lacking a functional viral fibroblast growth factor homolog. Virology. 346, 258-265.

323. Skevaki, C., S. Psarras, E. Volonaki, H. Pratsinis, I. Spyridaki, M. Gaga, V. Georgiou, S. Vittorakis, A. Telcian, P. Maggina, D. Kletsas, D. Gourgiotis, S. Johnston and N. Papadopoulos 2012. Rhinovirus-induced basic fibroblast growth factor release mediates airway remodeling features. Clin Transl Allergy. 2(1), e14.

324. Do, M. -. Q., T. Suzuki, B. Gerelt, Y. Sato, W. Mizunoya, M. Nakamura, Y. Ikeuchi, J.E. Anderson and R. Tatsumi 2012. Time-coordinated prevalence of extracellular HGF, FGF2 and TGF-B3 in crush-injured skeletal muscle. Animal Science Journal. 83, 712-717.

325. Tanaka, T., S. Saika, Y. Ohnishi, A. Ooshima, J.W. McAvoy, C.-. Liu, M. Azhar, T. Doetschman and W.W.-. Kao 2004. Fibroblast growth factor 2: Roles of regulation of lens cell proliferation and epithelial-mesenchymal transition in response to injury. Molecular Vision. 10, 462-467.

326. Bos, P. K., G.J.V.M. Van Osch, D.A. Frenz, J.A.N. Verhaar and H. Verwoerd-Verhoef 2001. Growth factor expression in cartilage wound healing: Temporal and spatial immunolocalization in a rabbit auricular cartilage wound model. Osteoarthritis and Cartilage. 9, 382-389.

327. Cowin, A. J., T.M. Holmes, P. Brosnan and M.W.J. Ferguson 2001. Expression of TGF-B2 and its receptors in murine fetal and adult dermal wounds. European Journal of Dermatology. 11, 424-431.

328. Li, D., C. Zhang, F. Song, I. Lubenec, Y. Tian and Q.H. Song 2009. VEGF regulates FGF-2 and TGF-B1 expression in injury endothelial cells and mediates smooth muscle cells proliferation and migration. Microvasc. Res. 77, 134-142.

329. Sanfilippo, C. M. and J.A. Blaho 2006. ICP0 gene expression is a herpes simplex virus type 1 apoptotic trigger. J. Virol. 80, 6810-6821.

330. Sobol, P. T., J.E. Boudreau, K. Stephenson, Y. Wan, B.D. Lichty and K.L. Mossman 2011. Adaptive antiviral immunity is a determinant of the therapeutic success of oncolytic virotherapy. Molecular Therapy. 19, 335-344.

331. Kim, J. H., J.Y. Oh, B.H. Park, D.E. Lee, J.S. Kim, H.E. Park, M.S. Roh, J.E. Je, J.H. Yoon, S.H. Thorne, D. Kirn and T.H. Hwang 2006. Systemic armed oncolytic and immunologic therapy for cancer with JX-594, a targeted poxvirus expressing GM-CSF. Molecular Therapy. 14, 361-370.

332. Lichty, B. D., D.F. Stojdl, R.A. Taylor, L. Miller, I. Frenkel, H. Atkins and J.C. Bell 2004. Vesicular stomatitis virus: A potential therapeutic virus for the treatment of hematologic malignancy. Human Gene Therapy. 15 (9), 821-831.

333. Willmon, C. L., V. Saloura, Z.G. Fridlender, P. Wongthida, R.M. Diaz, J. Thompson, T. Kottke, M. Federspiel, G. Barber, S.M. Albelda and R.G. Vile 2009. Expression of IFN-β enhances both efficacy and safety of oncolytic vesicular stomatitis virus for therapy of mesothelioma. Cancer Res. 69, 7713-7720.

334. Melcher, A., K. Parato, C.M. Rooney and J.C. Bell 2011. Thunder and lightning: Immunotherapy and oncolytic viruses collide. Molecular Therapy.

335. Barber, G. N. 2005. VSV-tumor selective replication and protein translation. Oncogene. 24, 7710-7719.

336. Bais, S., E. Bartee, M.M. Rahman, G. McFadden and C.R. Cogle 2012. Oncolytic virotherapy for hematological malignancies. Advances in Virology. 2012.

337. Zeyaullah, M., M. Patro, I. Ahmad, K. Ibraheem, P. Sultan, M. Nehal and A. Ali 2012. Oncolytic viruses in the treatment of cancer: A review of current strategies. Pathology and Oncology Research. 18, 771-781.

338. Wildner, O. 2003. Comparison of replication-selective, oncolytic viruses for the treatment of human cancers. Curr. Opin. Mol. Ther. 5, 351-361.

339. Hernández-Alcoceba, R. 2011. Recent advances in oncolytic virus design. Clinical and Translational Oncology. 13, 229-239.

340. Galivo, F., R.M. Diaz, P. Wongthida, J. Thompson, T. Kottke, G. Barber, A. Melcher and R. Vile 2010. Single-cycle viral gene expression, rather than progressive replication and oncolysis, is required for VSV therapy of B16 melanoma. Gene Ther. 17, 158-170.

341. Ebert, O., S. Harbaran, K. Shinozaki and S.L.C. Woo 2005. Systemic therapy of experimental breast cancer metastases by mutant vesicular stomatitis virus in immune-competent mice. Cancer Gene Ther. 12, 350-358.

342. Dinarello, C. A. 2007. Historical insights into cytokines. Eur. J. Immunol. 37, S34-S45.

343. Luther, S. A. and J.G. Cyster 2001. Chemokines as regulators of T cell differentiation. Nat. Immunol. 2, 102-107.

344. Metcalfe, S. M. 2011. LIF in the regulation of T-cell fate and as a potential therapeutic. Genes Immun. 12, 157-168.

345. Zitvogel, L., O. Kepp, L. Senovilla, L. Menger, N. Chaput and G. Kroemer 2010. Immunogenic tumor cell death for optimal anticancer therapy: The calreticulin exposure pathway. Clinical Cancer Research. 16, 3100-3104.

346. Finke, J. and A. Nagler 2007. Viewpoint: What is the role of allogeneic haematopoietic cell transplantation in the era of reduced-intensity conditioning - is there still an upper age limit? A focus on myeloid neoplasia. Leukemia. 21, 1357-1362.

347. Daenen, S., B. Van Der Holt, A.W. Dekker, R. Willemze, A.W. Rijneveld, B.J. Biemond, P. Muus, A.A. Van De Loosdrecht, H.C. Schouten, M. Van Marwijk Kooy, D.A. Breems, H. Demuynck, J. Maertens, P.W. Wijermans, S. Wittebol, E.W. De Klerk and J.J. Cornelissen 2012. Intensive chemotherapy to improve outcome in patients with acute lymphoblastic leukemia over the age of 40: A phase II study for efficacy and feasibility by HOVON. Leukemia. 26, 1726-1729.

348. Giles, F. J., M. O'Dwyer and R. Swords 2009. Class effects of tyrosine kinase inhibitors in the treatment of chronic myeloid leukemia. Leukemia. 23, 1698-1707.

349. Hehlmann, R. 2012. How I treat CML blast crisis. Blood. 120, 737-747.

350. Kepp, O., L. Senovilla, L. Galluzzi, T. Panaretakis, A. Tesniere, F. Schlemmer, F. Madeo, L. Zitvogel and G. Kroemer 2009. Viral subversion of immunogenic cell death. Cell Cycle. 8, 860-869.

351. Mahoney, D. J., C. Lefebvre, K. Allan, J. Brun, C. Sanaei, S. Baird, N. Pearce, S. Grönberg, B. Wilson, M. Prakesh, A. Aman, M. Isaac, A. Mamai, D. Uehling, R. Al-Awar, T. Falls, T. Alain and D. Stojdl 2011. Virus-tumor interactome screen reveals ER stress response can reprogram resistant cancers for oncolytic virus-triggered caspase-2 cell death. Cancer Cell. 20, 443-456.

352. Escobar-Zarate, D., Y.-. Liu, L. Suksanpaisan, S.J. Russell and K.-. Peng 2013. Overcoming cancer cell resistance to VSV oncolysis with JAK1/2 inhibitors. Cancer Gene Ther. 20, 582-589.

353. Jha, B. K., I. Polyakova, P. Kessler, B. Dong, B. Dickerman, G.C. Sen and R.H. Silverman 2011. Inhibition of RNase L and RNA-dependent protein kinase (PKR) by sunitinib impairs antiviral innate immunity. J. Biol. Chem. 286, 26319-26326.

354. Daubeuf, S., D. Singh, Y. Tan, H. Liu, H.J. Federoff, W.J. Bowers and K. Tolba 2009. HSVICP0 recruits USP7 to modulate TLR-mediated innate response. Blood. 113, 3264-3275.

355. Smith, E. J., I. Marie, A. Prakash, A. GarcÃa-Sastre and D.E. Levy 2001. IRF3 and IRF7 phosphorylation in virus-infected cells does not require double-stranded RNA-dependent protein kinase R or IkB kinase but is blocked by vaccinia virus E3L protein. J. Biol. Chem. 276, 8951-8957.

356. Fitzgerald-Bocarsly, P., J. Dai and S. Singh 2008. Plasmacytoid dendritic cells and type I IFN: 50 years of convergent history. Cytokine and Growth Factor Reviews. 19, 3-19.

357. Abraham, N., M.L. Jaramillo, P.I. Duncan, N. Methot, P.L. Icely, D.F. Stojdl, G.N. Barber and J.C. Bell 1998. The murine PKR tumor suppressor gene is rearranged in a lymphocytic leukemia. Exp. Cell Res. 244, 394-404.

358. Whitaker-Dowling, P. and J.S. Youngner 1988. Alteration of vesicular stomatitis virus L and NS proteins by uv irradiation: Implications for the mechanism of host cell shut-off. Virology. 164, 171-175.

359. Ahmed, M., L.M. Mitchell, S. Puckett, K.L. Brzoza-Lewis, D.S. Lyles and E.M. Hiltbold 2009. Vesicular stomatitis virus M protein mutant stimulates maturation of toll-like receptor 7 (TLR7)-positive dendritic cells through TLR-dependent and-independent mechanisms. J. Virol. 83, 2962-2975.

360. Kopecky, S. A. and D.S. Lyles 2003. Contrasting effects of matrix protein on apoptosis in HeLa and BHK cells infected with vesicular stomatitis virus are due to inhibition of host gene expression. J. Virol. 77, 4658-4669.

361. Chakraborty, P., J. Seemann, R.K. Mishra, J.-. Wei, L. Weil, D.R. Nussenzveig, J. Heiber, G.N. Barber, M. Dasso and B.M.A. Fontoura 2009. Vesicular stomatitis virus inhibits mitotic progression and triggers cell death. EMBO Rep. 10, 1154-1160.

362. Balachandran, S., P.C. Roberts, T. Kipperman, K.N. Bhalla, R.W. Compans, D.R. Archer and G.N. Barber 2000. Alpha/beta interferons potentiate virus-induced apoptosis through activation of the FADD/caspase-8 death signaling pathway. J. Virol. 74, 1513-1523.

363. Roscoe, D. M., K. Ishikawa and D.S. Lyles 1991. Role of de novo protein synthesis in target cells recognized by cytotoxic T lymphocytes specific for vesicular stomatitis virus. J. Virol. 65, 6856-6861.

364. Kelly, E. J., R. Nace, G.N. Barber and S.J. Russell 2010. Attenuation of vesicular stomatitis virus encephalitis through microRNA targeting. J. Virol. 84, 1550-1562.

365. Yarde, D. N., S. Naik, R.A. Nace, K.-. Peng, M.J. Federspiel and S.J. Russell 2013. Meningeal myeloma deposits adversely impact the therapeutic index of an oncolytic VSV. Cancer Gene Ther. 20, 616-621.

366. Heiber, J. F. and G.N. Barber 2011. Vesicular stomatitis virus expressing tumor suppressor p53 is a highly attenuated, potent oncolytic agent. J. Virol. 85, 10440-10450.

367. Jaks, E., M. Gavutis, G. Uzé, J. Martal and J. Piehler 2007. Differential receptor subunit affinities of type I interferons govern differential signal activation. J. Mol. Biol. 366, 525-539.

368. Levy, D. E., D.S. Kessler, R. Pine and J.E. Darnell Jr. 1989. Cytoplasmic activation of ISGF3, the positive regulator of interferon-alpha-stimulated transcription, reconstituted in vitro. Genes Dev. 3, 1362-1371.

369. Improta, T. and R. Pine 1997. Susceptibility to virus infection is determined by a stat-mediated response to the autocrine effect of virus-induced type I interferon. Cytokine. 9, 383-393.

370. Zee, Y. C., A.J. Hackett and L. Talens 1970. Vesicular stomatitis virus maturation sites in six different host cells. J. Gen. Virol. 7, 95-102.

371. Hoshino, M., H. Taira, S. Hattori and M. Kawakita 1987. The target reaction in the antiviral action of mouse interferon against vesicular stomatitis virus multiplication. J. Biochem. 101, 685-694.

372. Rostaing, L., E. Chatelut, J.-. Payen, J. Izopet, C. Thalamas, H. Ton-That, J.-. Pascal, D. Durand and P. Canal 1998. Pharmacokinetics of αIFN-2b in chronic hepatitis C virus patients undergoing chronic hemodialysis or with normal renal function: Clinical implications. Journal of the American Society of Nephrology. 9, 2344-2348.

373. McKenna, S. D., K. Vergilis, A.R.N. Arulanandam, W.Y. Weiser, R. Nabioullin and M.A. Tepper 2004. Formation of human IFN-β complex with the soluble type I interferon receptor IFNAR-2 leads to enhanced IFN stability, pharmacokinetics, and antitumor activity in xenografted SCID mice. Journal of Interferon and Cytokine Research. 24, 119-129.

374. Zhu, Y., A. Yongky and J. Yin 2009. Growth of an RNA virus in single cells reveals a broad fitness distribution. Virology. 385, 39-46.